

**Nieuwe technologieën voor elastische microsystemen:
ontwikkeling, karakterisering en toepassingen.**

**Novel Technologies for Elastic Microsystems:
Development, Characterization and Applications.**

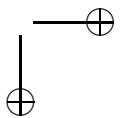
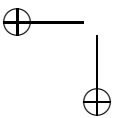
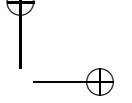
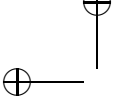
Frederick Bossuyt

Promotor: Prof. dr. ir. J. Vanfleteren

Proefschrift ingediend tot het behalen van de graad van
Doctor in de Ingenieurswetenschappen
Elektrotechniek

Vakgroep Elektronica en Informatiesystemen
Voorzitter: Prof. dr. ir. J. Van Campenhout
Faculteit Ingenieurswetenschappen
Academiejaar 2010–2011





**Nieuwe technologieën voor elastische microsystemen:
ontwikkeling, karakterisering en toepassingen.**

**Novel Technologies for Elastic Microsystems:
Development, Characterization and Applications.**

Frederick Bossuyt

Promotor: Prof. dr. ir. J. Vanfleteren

Proefschrift ingediend tot het behalen van de graad van
Doctor in de Ingenieurswetenschappen
Elektrotechniek

Vakgroep Elektronica en Informatiesystemen
Voorzitter: Prof. dr. ir. J. Van Campenhout
Faculteit Ingenieurswetenschappen
Academiejaar 2010–2011

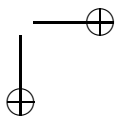
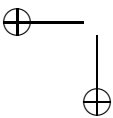
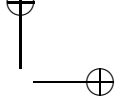
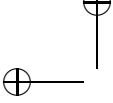


ISBN 978-90-8578-400-5
NUR 959
Wettelijk depot: D/2011/10.500/5

Promotor:

Prof. dr. ir. J. Vanfleteren

Onderzoeksgroep CMST Microsystems
Vakgroep Elektronica en Informatiesystemen
Technologiepark 914A
B-9052 Zwijnaarde



Dankwoord

Eindelijk. Het ligt er. Natuurlijk raakt het me.

Vier jaar lang zaten er puzzelstukken over 'Hoe elektronica uitrekbaar maken?' in m'n hoofd. Vier jaar lang probeerde ik met deze puzzelstukken een geheel te vormen. Een deel van de puzzel ligt hier voor je, een deel zal door enthousiaste mensen verder vervolledigd worden.

Vele mensen droegen, bewust of onbewust, een puzzelstukje aan deze grote puzzel bij...

Eerst en vooral wil ik mijn promotor Jan Vanfleteren bedanken. Voor de kans die hij me gegeven heeft om aan dit onderzoek te kunnen werken. Verder bedank ik hem ook voor de vrijheid die hij me in dit hele ontwikkelingsproces gaf, een vrijheid die ik enorm apprecieerde. Bedankt voor het vertrouwen!

Ook aan André Van Calster, leider van de CMST onderzoeksgroep, wil ik mijn dank betuigen. Eerst en vooral voor het ter beschikking stellen van de infrastructuur, de omkadering,.. Bedankt ook voor de leuke barbecues, de gezellige etentjes,..

Verder bedank ik het ganse CMST team om op de een of andere manier, rechtstreeks of onrechtstreeks bij te hebben gedragen aan wat ik de laatste 4 jaar verwezenlijkt heb. De lijst van mensen is lang, heel lang. Iedereen persoonlijk bedanken zou ons te ver leiden maar ik wil bij deze benadrukken: zonder jullie intellectuele, instrumentele, administratieve, motiverende steun was dit zeker niet gelukt. Bedankt!

Een speciale dank gaat uit naar Wim, voor het (tot 2 maal toe) nauwgezet nalezen van mijn proefschrift. De feedback heeft me enorm geholpen en vooral een gerust gevoel gegeven. Een dikke merci Wim, je hebt er nog (meer dan) ene te goed!

Ook wil ik mijn bureaugenoten persoonlijk bedanken, voor het geven van kleur aan de dagelijkse sleur van het doctoraatsbestaan. Bjorn, Lieven, Fabrice, Pietro, Tomas, bedankt om allen op jullie (eigenzinnige) wijze te hebben bijgedragen aan dit werk. Ook de vrouwelijke collega's die een tijdje geleden nog op onze buro vertoefden: Eva en Pritesh, het waren heel leuke momenten samen!

Buiten CMST zijn er nog mensen die op professioneel vlak bijgedragen hebben en een oprecht woord van dank verdienen:

De mensen binnen Stella waarmee ik samengewerkt heb. In het bijzonder de collega's (vrienden) van TU Berlijn - Thomas en Manuel. Ook Hans de Vries, voor de hele goeie samenwerking op het vlak van betrouwbaarheidstesten. Verder wil ik Mario Gonzalez en Hsu Yung-Yu bedanken voor het mechanische modelleer werk die ze verricht hebben, wat een zeer grote bijdrage betekent voor de (verdere) ontwikkeling van de voorgestelde technologieën.

Daarnaast zijn er nog een aantal mensen buiten het werk die natuurlijk een belangrijke bijdrage hebben geleverd tot wat ik verwezenlijkt heb en heb kunnen verwezenlijken, zowel voor als tijdens mijn doctoraat.

Mijn ouders, bedankt voor alle kansen die jullie me al gegeven hebben. Ik ben jullie heel erg dankbaar. Ook mijn zus Laurence en Jonas, voor de goede band die we al jaren hebben. En dan nog mijn rots in de branding, mijn allerliefste Adinda. Merci voor alle steun en gewoon, omdat je er altijd bent voor mij.

Ook mijn vrienden, in het bijzonder Thomas en Silvie en mijn nauw aan het hart liggende vrouwelijke kotgenoten, verdienen ook nog een plaatsje in deze ere galerij.

Soms vragen mensen: was je niet beter meteen gaan 'werken' in plaats van te doctoreren? Wel, ik wil eindigen met te vertellen wat ik, naast de intellectuele voldoening natuurlijk, aan het doctoreren te danken heb en wat me het meest is bijgebleven van de afgelopen 4 jaren...

De conferenties naar San Francisco. Ik ben nog steeds verliefd op deze stad.

De reis naar India was onvergetelijk... Dankzij Pritesh dit avontuur beleefd samen met enkele collega's en hun vriendin. Niet voor de hand liggend maar de hele reis was onvergetelijk!

Het CMST minivoetbal team. De kans gehad om een jaartje voorzitter te mogen zijn. Het enthousiasme van iedereen om mee te doen is onbeschrijflijk. Zelfs al gaan we regelmatig op onze bek.

De citytrip naar Barcelona, een weekend vol cava en tapas... en een beetje sport natuurlijk, maar niet door mij.

De gezellige barbecues die tot in de vroege uurtjes duurden, Duvelmomentjes inclusief.

Alle andere conferenties in binnen en buitenland: het eens gaan uitleggen voor een internationaal gezelschap geeft wel een kick. En door te doctoreren wordt de wereld toch plots een stukje kleiner.

De goeie buitenlandse contacten, vooral met de Duitsers. Ze hebben misschien wel een betere infrastructuur, wij hebben Gent met al zijn leuke plekjes, cafés waar tot in de vroege uren gefeest kan worden. Ze zijn er meermaals onder de indruk van geweest.

Nee, ik heb er zeker geen spijt van!

Contents

1	Introduction and research context	1
1.1	Elastic microsystems: approaches	1
1.1.1	Out-of-plane designs	2
1.1.2	In-plane designs	8
1.1.3	Combination of out-of-plane and in-plane designs	12
1.2	Elastic (opto)electronic devices	13
1.2.1	Elastic (opto)electronic components	13
1.2.2	Elastic interconnects between rigid components	15
1.2.3	Elastic integrated systems	23
1.2.4	Elastic power supplies	24
1.3	Scope of this PhD work	27
1.4	Research context	29
1.5	Research dissemination	32
2	Introduction to concepts related to elastic microsystems	40
2.1	System architecture and methodology	40
2.2	Polymers	41
2.2.1	Classification by chain structure	42
2.2.2	Classification by polymerization structure	43
2.2.3	Classification by thermal behaviour	43
2.2.4	Embedding material: silicone	44
2.2.5	Supporting material: polyimide	48
2.3	Mechanical aspects of elastic microsystems	50
2.3.1	Mechanical characterization of embedding materials	50
2.3.2	Mechanical design of stretchable metallic interconnects	53
2.4	Conclusions	64
3	Stretchable substrate technology	68
3.1	Introduction	68
3.2	General description of process flow	68
3.3	Application of polymer on copper substrate	71

3.4	Patterning of copper	73
3.5	Application of soldermask	74
3.6	Copper surface finish	75
3.7	Assembly of components	76
3.8	Embedding	77
3.9	Conclusions	78
4	Peelable technology	82
4.1	Introduction	82
4.2	General description of process flow	83
4.3	Lamination of copper on carrier with temporary adhesive	86
4.3.1	Copper type	86
4.3.2	Temporary adhesives	87
4.3.3	Temporary substrate	94
4.3.4	Lamination	95
4.3.5	Adhesion of copper on carrier	96
4.4	Patterning of copper	100
4.4.1	Micro-etching	100
4.4.2	Photoresist application	100
4.4.3	Copper spray etching	101
4.5	Application of soldermask	102
4.6	Copper surface finish	103
4.6.1	No finish	103
4.6.2	NiAu-finish	103
4.6.3	OSP-finish	104
4.7	Assembly of components	105
4.8	Testing and rework	106
4.9	Embedding	107
4.9.1	Casting of PDMS	107
4.9.2	Moulding using PDMS	108
4.10	Conclusions	109
5	Peelable technology with local polyimide support	112
5.1	Introduction	112
5.2	General description of process flow	113
5.3	Pattern definition of polyimide	116
5.3.1	Photodefinable polyimide	116
5.3.2	Screenprintable polyimide	121
5.4	Lamination of copper on carrier	128
5.5	Patterning of copper	128
5.6	Application of soldermask	129
5.7	Copper finish	130
5.8	Assembly of components	130

CONTENTS **v**

5.9	Embedding	130
5.9.1	Casting of PDMS	131
5.9.2	Moulding using PDMS	131
5.10	Double polyimide layer technology	133
5.10.1	Possible process flow	133
5.10.2	Process description and feasibility	133
5.11	Double conductor layer technology	136
5.11.1	Process description	136
5.11.2	Process feasibility	138
5.11.3	Characterization	139
5.11.4	Discussion	144
5.12	Conclusions	146
6	Reliability evaluation of the technologies	148
6.1	Introduction	148
6.2	Physics-of-failure	149
6.3	Performed reliability tests	150
6.4	Mechanical reliability test setup	151
6.5	Reliability tests of stretchable interconnects	151
6.5.1	Peelable technology	154
6.5.2	Stretchable substrate technology	156
6.5.3	Double polyimide layer technology	156
6.5.4	Cyclic endurance test results	157
6.5.5	Failure analysis	163
6.5.6	Discussion	166
6.6	Reliability tests on testvehicle with embedded interposer	166
6.6.1	Peelable technology: interposer testvehicle, 18 μm TW-YE copper	166
6.6.2	Peelable technology: improved interposer testvehicle, 18 μm TW-YE copper with photodefinable polyimide	168
6.7	Conclusions	171
7	Applications	174
7.1	Introduction	174
7.2	Stretchable substrate technology demonstrators	175
7.2.1	Technology analysis samples	175
7.2.2	Stretchable multi-electrode arrays	175
7.3	Peelable technology demonstrators	176
7.3.1	Temperature sensor demonstrator	176
7.3.2	Wireless power circuit	180
7.3.3	Stretchable high-frequency interconnects and antennas	181
7.3.4	Stretchable heater with built-in flexible display	185
7.4	Peelable technology with local polyimide support demonstrators	188

7.4.1	Baby respiration monitor	188
7.4.2	Fitness activitiy monitor	196
7.5	Conclusions	200
8	Conclusions and outlook	203
8.1	Main achievements	203
8.2	Future work	205

List of Tables

2.1	Equivalent plastic strain (in %) in the copper lines at different positions and for different elongations (Sylgard 186).	61
2.2	Equivalent plastic strain in the copper lines at different positions and for different elongations with Walopur TPU as embedding material. Mooney fit was used in this model.	61
2.3	Equivalent plastic strain in the copper lines at different positions and for different elongations for Sylgard 186 as embedding material. Neo-Hookean fit was used in this model.	62
2.4	Equivalent plastic strain in the copper lines at different positions and for different elongations. Both Mooney and neo-Hookean fit were used in this model.	64
3.1	Lithography parameters for AZ4562 photoresist.	74
4.1	Properties of TW-YE copper foil.	86
4.2	Properties of Aquabond ABS-85 water soluble wax.	92
4.3	Settings of roll laminator.	97
4.4	Peelstrength test results.	97
4.5	Parameters for lithography of peelable samples using AZ4562.	99
4.6	Properties of Sylgard 184 and Sylgard 186 silicone.	107
5.1	Cured film properties of PI2731 and HD4100 photodefinable polyimide.	117
5.2	Linewidths of photodefined HD4100 polyimide.	120
5.3	Properties of selected polyimides for screenprinting.	121
5.4	Dimensions of concentric circles on screenprinting screen.	123
5.5	Lithography parameters of AZ4562 photoresist.	134
5.6	Comparison between track widths defined and printed.	142
5.7	Comparison between track widths and spacing defined and printed.	142
5.8	Comparison between track widths defined and printed.	143

6.1	Characteristics of testsamples shown in Figure 6.3 and Figure 6.4. The geometrical parameters are defined in Figure 6.5.	153
6.2	Characteristic dimensions of testsample.	167
7.1	Transmission line horseshoe characteristics.	182
7.2	Rubbery ruler characteristics.	188

List of Figures

1.1	Schematic illustration of out-of-plane and in-plane design approach for stretchable electronics.	2
1.2	Schematic illustrations of different out-of-plane designs applied to stretchable inorganic materials.	3
1.3	(Left) Schematic illustration of the process for fabricating buckled, or wavy, single crystal Si ribbons on a PDMS substrate. (Right) Schematic illustration of a transfer approach using a rubber stamp to remove selected collections of semiconductor micro- and nanostructures from a wafer and to deliver them to a receiving substrate.	4
1.4	Optical images of the wave pattern formed in a 100-nm-thick gold film evaporated on a 1-mm-thick PDMS membrane (a) over the entire surface (b) of a stripe evaporated through a shadow mask. Dark margins are from the PDMS substrate.	5
1.5	Variation of the normalized change in electrical resistance of a 100-nm-thick Au stripe with applied tensile strain $\epsilon_{external}$ (right curve). The left curve represents the linear behavior of the normalized resistance with the applied external strain for $0 \leq \epsilon_{external} \leq 8\%$	6
1.6	Fabrication of gold interconnects on an elastomeric PDMS substrate. (a) PDMS substrate. (b) Prestretched PDMS. (c) Laminated Riston photoresist mask. (d) Evaporated metal films. (e) Lift-off. (f) Release from prestretch: the gold stripe buckles.	7
1.7	PDMS encapsulated gold micro-conductors patterned on a 3 inch diameter PDMS membrane. (a) The circle indicates the conductor design used on the stretchability test. (b) The patterned conductors on PDMS are highly conformable.	8
1.8	SEM images of a silicon structure etched into the shape of spirals surrounding central hubs after the DRIE step before (left) and after (right) the release step.	9

1.9	Optical images of a 71 node network before and after expansion. The surface ratio between both is 51.	10
1.10	The expandable monolithic networks are flexible and conformable to curved substrates making them suitable for curved focal-plane arrays.	10
1.11	Optical images of straight and serpentine metal lines (low- and high-amplitude structures) on an elastomeric substrate. The sequence of the images on the bottom shows the same structures after application of tensile strain in the direction indicated by the arrows. The discolored regions correspond to deformations at locations of peak strain.	11
1.12	(a) Fabrication process of a reversibly deformable dipole antenna. PDMS elastomer cured on a topographically patterned substrate produces two adjacent microfluidic channels (only one shown). After sealing the PDMS channels to another piece of PDMS, injection of liquid metal alloy into the microfluidic channels produces a dipole antenna. (b,c) Photographs of a prototype antenna being stretched and rolled. There is no hysteresis in the spectral properties of the antenna as it is returned to the 'relaxed' state. (d) The antenna self-heals in response to sharp cuts, such as those inflicted by a razor blade.	12
1.13	SEM images of a silicon integrated circuit composed of device islands that support transistors for CMOS inverters interconnected by non-coplanar serpentine structures consisting of trilayer stacks of polymer/metal/polymer.	13
1.14	(a) Optical images of a stretchable single crystal Si p-n diode on a PDMS substrate at - 11% (top), 0% (middle) and 11% (bottom) applied strains. The Al regions correspond to thin (20 nm) Al electrodes; the pink and green regions correspond to n (boron) and p (phosphorous) doped areas of the Si. (b) Current density as a function of bias voltage for stretchable Si p-n diodes, measured at various levels of applied strain. The curves labeled 'light' and 'dark' correspond to devices exposed to or shielded from ambient light, respectively. The solid curves show modeling results. (c) Current-voltage characteristics of a stretchable Schottky-barrier Si MOSFET, measured at - 9.9%, 0%, and 9.9% applied strains (the gate voltage varied from 0 V to 5 V, with a 1-V step).	14
1.15	Image of stretchable inverter composed of non-stretchable n-type amorphous silicon TFTs interconnected with stretchable metal lines.	15
1.16	Process flow for the fabrication of stretchable copper board (SCB) substrates ready for assembly.	17

LIST OF FIGURES **xi**

1.17	Stretchable copper board (SCB) substrates.	18
1.18	Maximum elongation till break for different meander configurations.	18
1.19	Total number of cycles to failure.	18
1.20	Stretchable polymer boards based on use of non-woven thermoplastic polyurethane.	19
1.21	Stretchable polymer board transformed into an arbitrary 3D shape.	19
1.22	Interconnect mesh concept for rectilinear, meandering and redundant meandering interconnects. The interconnects consist of a polymer substrate and two metal layers separated by a spin-on polyimide dielectric layer.	20
1.23	SEM micrographs of double-layer interconnects. Meandering interconnect designs with 10 μm line-width, meandering interconnect designs with 20 μm line-width, redundant interconnect designs with 40 μm line-width.	21
1.24	40 mm by 40 mm redundant sensor mesh fabricated using large-area seamless scanning techniques. The flexibility and conformability are demonstrated.	21
1.25	Stretchable organic transistor active matrix network of pressure and thermal sensors. Film device is stretchable upto 25%. The organic transistors are placed at the intersection areas.	22
1.26	Stretchable silicon circuit in a wavy geometry compressed in its center by a glass capillary tube (main) and wavy logic gate built with two transistors (top right inset).	23
1.27	Stretchable silicon circuit with a mesh design, wrapped onto a model of a fingertip.	24
1.28	Electronic eyeball camera that uses a hemispherically curved array of silicon photodetectors.	24
1.29	Picture collected with a similar camera that uses a paraboloid design.	24
1.30	Scheme of a compliant zinc carbon dry gel cell. The cell is based on pastes as electrodes, chemically active cells and an electrolyte gel to close the circuit. Intermixing of the chemicals and short-circuiting of the electrochemical power supply are prohibited by laterally separating the electrodes with an elastomer separator.	25
1.31	Realization of 2 dry gel cells in series for powering a SMD light emitting diode. a) Photo of the circuit prior to the stretch experiments b) At 100% strain.	25

1.32	(a) Self-discharge of an electrochemical cell by monitoring the open circuit voltage versus time. (b) Capacities of compliant power supplied without strain (black triangles) and with 50% strain (red squares). Following common notation, the capacity is determined when the cell voltage drops to 0.8V. (c) Load curves of the batteries at 0% strain (black triangles) and 50% strain (red squares), short circuit currents of 20-30 mA are achieved. (d) Open circuit voltage versus strain up to 100% (black triangles). Short circuit currents versus stretch for two stretch cycles. Blue filled squares: first cycle, red empty squares: second cycle.	26
2.1	Stretchable circuit system architecture.	41
2.2	Classification of polymers by their chain structure.	43
2.3	Graphical representation of PDMS.	45
2.4	Imide.	49
2.5	Polyimides usually come in two forms: aromatic heterocyclic polyimides (left) and linear polyimides (right).	49
2.6	Imidization process of aromatic polyimides.	50
2.7	Stress-strain curve at room temperature T_r for three different polymers. (I) Glassy polymer with $T_r < T_g$. (II) Elastomer with $T_r > T_g$. (III) Partially crystalline polymer with $T_g < T_r < T_m$	51
2.8	Tension test of 3 different substrate materials.	52
2.9	neo-Hookean fit of Sylgard 186.	53
2.10	Different conductor shapes.	54
2.11	Stress distribution in copper conductor line for three different conductor shapes.	54
2.12	Relation between the induced Von Mises stress and the wave amplitude for 3 different designs. (Left) Single track. (Right) Multi-track design.	55
2.13	Meander definition	56
2.14	Relation between the equivalent plastic strain and the scale factor (R/W) for a substrate with a Young's modulus of 0.7 MPa for a horseshoe design with $\theta=0$	57
2.15	Relation between the equivalent plastic strain and the scale factor (R/W) for a substrate with a Young's modulus of 0.7 MPa for a horseshoe design with $\theta=45$	57
2.16	Poisson effect observed during a uniaxial tension test for a single conductor line (dashed lines show the original dimensions of the substrate).	58
2.17	Equivalent plastic strain induced in copper as function of Young's modulus of the substrate.	59
2.18	Geometry and mesh density of test structure used for modeling.	60

LIST OF FIGURES

xiii

2.19	Model of equivalent plastic strain with Sylgard 186 as embedding material for 30% applied strain in X direction.	61
2.20	Model of equivalent plastic strain with Walopur TPU as embedding material for 30% applied strain in X direction.	62
2.21	Model of equivalent plastic strain with Sylgard 186 as embedding material for 30% applied strain in Y direction.	63
2.22	Model of equivalent plastic strain with Walopur TPU as embedding material for 30% applied strain in Y direction.	63
3.1	Stretchable substrate technology process flow - substrate fabrication	69
3.2	Stretchable substrate technology process flow - moulding	70
3.3	Sylgard 186: thickness vs. spinspeed	72
3.4	Alignment of soldermask is impossible due to shrinkage of the silicone substrate.	73
3.5	Perforated Cirlex polyimide foil with thickness of 300 μm is a good carrier for thin stretchable substrates during processing. . .	73
3.6	Stretchable substrate after copper etching and photoresist stripping.	74
3.7	Effect of plasma treatment of Sylgard 186 sample. With (left) and without (right) plasma treatment.	75
3.8	Stretchable substrate after application of soldermask.	75
3.9	Stretchable substrate after NiAu plating.	76
3.10	Stretchable substrate after assembly of SMD components.	77
3.11	Component with a high number of I/O connections (TQFP44 package, 0.8mm pitch) soldered on a gelly silicone substrate. . . .	77
3.12	Completely embedded stretchable electronic system.	78
3.13	Stretchable cables made on stretchable substrate.	79
4.1	Au-plating technology process flow for achieving stretchable electronic circuits.	83
4.2	Au-plated meanders on copper substrate. Typical feature size: 90 μm width, 4 μm height.	83
4.3	Peelable technology process flow - substrate fabrication.	84
4.4	Peelable technology process flow - substrate moulding.	85
4.5	FX Riston as adhesive/carrier and photoresist for copper etching: after etching copper.	90
4.6	FX Riston as adhesive/carrier and photoresist for copper etching: after stripping top photoresist.	90
4.7	FX Riston as adhesive/carrier and photoresist for copper etching: before (a) and after (b) vapour phase soldering.	90
4.8	AZ4562 photoresist as adhesive: before (a) and after (b) vapour phase soldering.	91

4.9	Application of Aquabond wax on copper sheet by doctorblading.	92
4.10	Result after copper etching: no delamination observed by use of Aquabond 85.	93
4.11	(a) Before vapour phase soldering, after application of solder-paste and TSSOP package. (b) After vapour phase soldering, well soldered TSSOP package. (c) After vapour phase soldering, Aquabond wax is burnt (brown color).	93
4.12	Temporary carriers: (a) flexible and (b) rigid.	95
4.13	Vacuum lamination profile.	96
4.14	Vacuum lamination of TW-YE copper samples on etched RO4003 substrate.	96
4.15	Peeltest sample in test setup.	97
4.16	Peelstrength test results.	98
4.17	Part of Cu wet etching adhesion test design.	99
4.18	Spray etch tests to measure adhesion performance: (a) Normal lithography temperatures. (b) Lowered lithography temperatures.	100
4.19	Spray etched sample containing meander tracks with different widths.	101
4.20	Profiles of different layers during copper patterning (dimensions in μm).	102
4.21	Substrate after NiAu-finish application. Cracks in the photoresist are observed and the quality of the finish is poor.	104
4.22	Vapour phase soldering temperature profile.	106
4.23	Tracks shift during reflow soldering and wax melting in absence of soldermask.	107
4.24	Soldermask preventing movement of tracks during reflow soldering and wax melting.	107
4.25	Application of PDMS by casting manually.	108
4.26	Application of PDMS by casting using a doctorblade.	108
5.1	Due to the polyimide supporting layer, mechanical stress during stretching will be shifted from the component connection pads and the straight tracks on the functional islands towards the border of the flexible islands.	113
5.2	Process flow of polyimide supported peelable technology.	114
5.3	Process flow of polyimide supported peelable technology.	115
5.4	Spinspeed vs. layer thickness of PI2731 (30 secs spintime).	117
5.5	Spinspeed vs. layer thickness of HD4100 (30 secs spintime).	117
5.6	Feasibility design for polyimide supported peelable technology: polyimide, copper and soldermask. Trackwidth = $100 \mu\text{m}$	118
5.7	Definition of HD4100 polyimide.	119
5.8	Alignment of polyimide relative to copper is important, achieved by laserdrilling alignment holes in the copperfoil.	119

LIST OF FIGURES

xv

5.9	HD4100 photodefinable polyimide profile after curing.	120
5.10	Dedicated screen for polyimide screenprinting purposes.	122
5.11	Definition of Q-Pilon polyimide by screenprinting: feature size ~150 μm , thickness ~40 μm	123
5.12	Definition of U-Varnish A polyimide by screenprinting.	124
5.13	Behaviour of Durimide 10 on screen.	125
5.14	Behaviour of Durimide 116 on screen.	126
5.15	Behaviour of Durimide 116 on ceramic substrate. The material flows too much when it is at rest. Picture taken at t=0 and t=2 mins.	126
5.16	Difference in behaviour between screenprinting paste (arrow) and Durimide 116.	127
5.17	Results after printing and curing Durimide 116H.	127
5.18	Results after printing and curing Durimide 116HC.	128
5.19	Copper pattern definition, resulting in well aligned copper pat- terns supported by HD4100 photodefinable polyimide.	129
5.20	Soldermask screenprinted on functional islands.	130
5.21	Assembly of 0402 SMD components by vapour phase soldering.	131
5.22	Dedicated mould design.	132
5.23	Samples after completely embedding in Sylgard 186 by using a dedicated mould.	132
5.24	Approach in order to have a polyimide sandwich around copper structures.	133
5.25	Current approach in order to have a polyimide sandwich around copper structures.	134
5.26	Realized double polyimide layer samples, not embedded, at dif- ferent strains.	135
5.27	Profile measurement of realized samples indicating the different layer thicknesses.	136
5.28	Processflow of double conductor layer stretchable technology.	137
5.29	Parts of feasibility mask: (a) Daisy chains for testing conducti- vity and minimum track width (b) Test of double sided meander structures (c) Vertical printing line pitch test (d) Horizontal prin- ting line pitch test.	140
5.30	Pattern definition of polyimide for double conductor layer stretch- able technology.	140
5.31	Photodefined vias.	141
5.32	Deposition by screenprinting of silver conductor Dupont 5025.	141
5.33	Closer view on printed tracks.	141
5.34	Closer view on parallel printed tracks.	142
5.35	Closer view on parallel printed tracks.	143
5.36	Profile of screenprinted conductor after hardbake.	143
5.37	Pattern definition of copper for double conductor layer stretch- able technology.	144

5.38	Pattern definition of copper for double conductor layer stretchable technology.	145
5.39	View on daisy chains: copper tracks on top side connected through vias to silver conductor on bottom side.	145
5.40	View on double sided meander tracks: silver conductor overprinting leads to shorts between top and bottom conductor. . . .	146
6.1	Schematic of physics-of-failure.	149
6.2	(Left) View on the electromechanical test system (Instron 5543). (Right) Sample mounted in a dedicated clamping tool.	152
6.3	Layout for single track using H45 ($\theta=45$) meander design, track-width= 100 μm	152
6.4	Layout for single track using H30 ($\theta=30$) meander design, track-width= 100 μm	152
6.5	Generic design of meander-shaped conductor.	153
6.6	Local stress reduction by introduction of fillet.	153
6.7	View on the fabrication of the testsamples before embedding: etched sample, sample with solderpaste applied, sample with flexible connector applied.	154
6.8	View on the fabrication of the testsamples after embedding: tapered, thicker silicone part at position of contact pads.	154
6.9	Testsample with 20 μm soldermask applied.	155
6.10	Testsample used for stretchable substrate reliability testing.	156
6.11	Double polyimide layer testsample using H30 design.	157
6.12	Resistance behavior of stretchable copper tracks without mechanical support layer during cyclic endurance tests (0-5% strain). . . .	158
6.13	Resistance behavior of stretchable copper tracks with photodefinable polyimide support layer during cyclic endurance tests (0-5% strain).	158
6.14	Cycles to failure for H45 horseshoe shape testvehicle and 1% strainrate for peelable technology.	159
6.15	Cycles to failure for H45 horseshoe shape testvehicle for peelable technology. 1% (diamonds) and 10% strainrate (s^{-1}) (squares). . . .	159
6.16	Cycles to failure for H45 horseshoe shape testvehicle, peelable technology covered with (squares) and without (diamonds) soldermask at 10% strainrate (s^{-1}).	160
6.17	Cycles to failure for H45 horseshoe shape testvehicle supported by HD4100 photodefinable polyimide (squares) and 10% strainrate. Non-supported samples' results (diamonds) are included for comparison.	161
6.18	Cycles to failure for H30 testsample for 1% strainrate (s^{-1}).	161

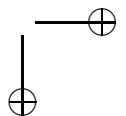
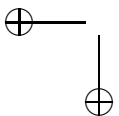
LIST OF FIGURES

6.19	Cycles to failure for H30 test sample fabricated in double layer polyimide technology (blue) in comparison with non-supported H30 design (red).	162
6.20	Complete breakdown and observed microcracks at top of meanders in pure copper sample after stretching 0-5%. Trace width is 100 μm	163
6.21	(A) Roughness of TW-YE copper (6 μm -8 μm). (B) Crack growth at rough copper surface after 100 cycles stretching at 30% strain. (C) Crack propagation through cross-section of meander, fibrillation initiation observation at edges of meander. (D) Transgranular fracture through electrodeposited TW-YE copper.	164
6.22	Complete breakdown and observed microcracks at top of meanders in soldermask covered copper interconnects after stretching 0-5%. Trace width is 100 μm	165
6.23	Complete breakdown and observed microcracks at top of meanders in photodefinable polyimide supported copper sample after stretching 0-5%. Trace width is 100 μm	165
6.24	Design of copper mask used for embedded meander tracks with interposer test vehicle. Trackwidth= 100 μm	167
6.25	Embedded meander tracks with interposer: realization in peelable technology.	167
6.26	Observed failures after cyclic stretching.	168
6.27	Improved interposer test vehicle.	169
6.28	Comparison between pure peelable design and peelable with polyimide support: integration of connectors, integration of interposer and moulding.	170
6.29	Modeling of interposer test vehicle before and after design optimization.	170
6.30	Failure modes at flex-stretch transition.	171
7.1	Stretchable multi electrode array cell cultivating device.	175
7.2	Stretchable multi electrode array: uniaxial stretching is realized by creating underpressure in the device.	176
7.3	Electronic design of stretchable temperature sensor: copper etch mask.	176
7.4	Production of stretchable temperature sensor: photodefined pattern on copper-wax-rigid carrier stack.	177
7.5	Production of stretchable temperature sensor: etched pattern on copper-wax-flexible carrier stack after soldermask application.	177
7.6	Production of stretchable temperature sensor: substrate after vapour phase soldering of components.	178
7.7	Production of stretchable temperature sensor: substrate placed in mold just before injection of Sylgard 186.	178

7.8	Production of stretchable temperature sensor: (Left) Completely embedded in Sylgard 186. (Right) Components are molded with a locally thicker layer of silicone in order to limit the stretching (components) and having a higher stretching in thinner silicone parts (stretchable interconnects).	179
7.9	(Left) Stretchable temperature sensor implemented in a head-band. (Right) Measurements of the body temperature demonstrating the functionality of the device.	179
7.10	Driving scheme for wireless powering inductive coil.	180
7.11	(Left) Realization of inductive link by use of 70 μm copper before embedding. (Right) Same circuit after embedding in Sylgard 186.	180
7.12	Inductive link in water environment.	181
7.13	Inductive link after 1 month emersion in water environment: increasing number of bubbles and oxidation of copper.	181
7.14	Coplanar waveguide with narrow reference conductors.	182
7.15	Transmission line realized in peelable technology by use of 9 μm copper.	182
7.16	Transmission and loss characteristics of transmission lines realized in different technologies including peelable technology.	183
7.17	Reflection and transmission characteristics of stretched transmission lines realized in peelable technology.	183
7.18	Design and realization in peelable technology of a fractal slot dipole antenna.	184
7.19	Reflection characteristics of realized fractal slot dipole antennas.	185
7.20	Antenna gain at 20 cm distance of realized fractal slot dipole antennas.	185
7.21	Stretchable heater: (Left) Detail of stretchable connections. (Right) Realization by use of Sylgard 184.	186
7.22	IR picture of heater when 3 A is applied.	186
7.23	Stretchable heater: detail of stretchable connections.	187
7.24	Stretchable heater: IR picture of heat distribution when applied to the human skin.	187
7.25	Rubbery ruler: capacitive sensor changing capacitance during elongation.	188
7.26	Sensitivity of the rubbery ruler sensors.	189
7.27	Stretchable respiratory monitor production: polyimide mask, copper mask and soldermask.	191
7.28	Stretchable respiratory monitor production: HD4100 polyimide support defined on copper.	191
7.29	Stretchable respiratory monitor production: after vapour phase soldering of components.	191
7.30	Stretchable respiratory monitor production: encapsulated by casting Sylgard 186.	192

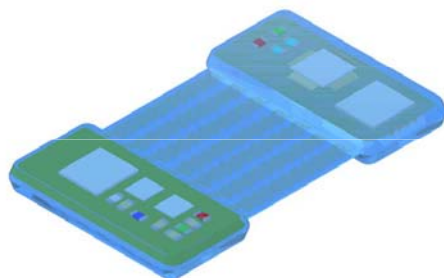
LIST OF FIGURES

7.31	Stretchable respiratory monitor production: dedicated moulds used for encapsulation indicating placement of rubbery rulers, buzzer and external connection (battery).	192
7.32	Stretchable respiratory monitor production: view on the dimensions of the dedicated moulds.	193
7.33	Stretchable respiratory monitor production: moulded Verhaert demonstrator using Sylgard 186.	193
7.34	Stretchable respiratory monitor production: moulded demonstrator attached to different textiles.	193
7.35	Stretchable respiratory monitor: mechanical baby model used for testing functionality of the demonstrator.	194
7.36	Stretchable respiratory monitor: reliability test sample mounted on Instron 5543 for uni-axial testing.	195
7.37	Stretchable respiratory monitor: reliability test results.	195
7.38	Scheme of the Philips Fitness monitor.	196
7.39	Interposer boards used in the Philips Fitness monitor.	197
7.40	Fitness activitiy monitor: polyimide mask, copper mask and solder mask.	198
7.41	Production of fitness activitiy monitor: after polyimide definition, lamination and copper definition.	198
7.42	Production of fitness activitiy monitor: after soldermask definition.	199
7.43	Production of fitness activitiy monitor: after soldering test interposers (left) and functional boards (right).	199
7.44	Philips activitiy monitor: X-Ray measurement after vapour phase soldering functional boards. Voids in the solderballs can be observed.	199
7.45	Production of fitness activity monitor: after moulding into Sylgard 186.	200



Samenvatting

In de electronica sector is een toenemende groei van de vraag naar flexibele elektronische substraten aan de gang. Een recente evolutie is de opkomst van vervormbare, elastische elektronische substraten. Elasticiteit is nog een uitdagendere eigenschap dan flexibiliteit. Deze uitrekbare, elastische elektronische microsystemen moeten in staat zijn om grote vervormingen ($\gg 1\%$) op te vangen zonder dat ze significant in elektronische functionaliteit degraderen of falen. De combinatie van mechanisch uitrekbaar zijn en de implementatie van elektronische componenten in een zacht, vervormbaar substraat maakt een hele waaier aan nieuwe toepassingen mogelijk voor healthcare, wellness en intelligente kledij.



Dit doctoraatswerk stelt enkele nieuwe technologieën voor om elastische microsystemen te realiseren. Nieuwe uitrekbare elektronische substraten werden ontwikkeld, gebruikmakend van conventionele gedrukte schakelingen proces technieken in combinatie met spuitgiettechnieken. Hierbij worden standaard, niet-vervormbare elektronische componenten gebruikt die gegroepeerd worden op functionele eilanden. Deze eilanden worden elektrisch met elkaar verbonden met elastische, metallische interconnecties die zorgen voor de uitrekbaarheid van het systeem. Het hoeft niet benadrukt te worden dat de betrouwbaarheid van deze verbindingen en overgangen met de functionele eilanden uiterst belangrijk is. Al deze aspecten zullen behandeld worden in dit werk: de ontwikkeling van de technologie, het karakteriseren ervan en de realisatie van een aantal elastische microsystemen.

In **Hoofdstuk 1** wordt een overzicht gegeven van verschillende technologische aanpakken voor het realiseren van uitrekbare elektronische systemen die momenteel onderwerp van onderzoek zijn aan verschillende onderzoeksinstellingen wereldwijd.

Een eerste methode om intrinsieke, niet-uitrekbare materialen uitrekbaar te maken is door gebruik te maken van vervormingen die plaatsvinden buiten het vlak van het materiaal. Deze manier wordt o.a. gebruikt bij het realiseren van elastische inorganische systemen waarbij golvend silicium selectief in of aan een reeds uitgerokken substraat gehecht wordt, en om uitrekbare verbindingen te maken door dunne film depositie van metalen op een reeds uitgerokken elastisch substraat. Geïntegreerde schakelingen die een elastische digitale camera vormen, uitrekbare TFT schakelingen,... zijn enkele resultaten van deze aanpak.

Een tweede methode is gebaseerd op het gebruik van hoefijzer-, meandervormde metalen interconnecties die in het vlak kunnen plooien en de uitgeoefende vervormingen kunnen opvangen. Deze methode wordt gebruikt voor het aanbrengen van op goud, koper, aluminium en zilverbasta gebaseerde interconnecties op elastische substraten. Hiermee kunnen uitrekbare circuits gemaakt worden voor grote oppervlakte applicaties (textiel, implantaten,..). De technologieën die in dit doctoraatswerk worden voorgesteld, zijn ook gebaseerd op deze methode.

Andere manieren zijn het realiseren van vervormbare antennes d.m.v. vloeibare metalen die in gesloten, 3 dimensionele microkanalen in een elastisch substraat gevangen zitten. D.m.v. DRIE geëtste silicium spiralen die eilanden met elektronica verbinden en een uitrekbaar systeem vormen na het afwikkelen van de spiralen. Geperforeerde metaal-polyimide substraten voor de realisatie van robothuiden. Geleidende pasta voor het maken van elastische batterijen. En veel, veel meer..

In **Hoofdstuk 2** wordt onze aanpak voor de realisatie van elastische microsystemen uitgelegd. Een elektronisch circuit ontwerp wordt omgevormd tot een uitrekbaar, elastisch design door het systeem op te splitsen in functionele eilanden die de niet-uitrekbare, elektronische componenten bevatten. Deze eilanden zijn elektrisch met elkaar verbonden d.m.v. uitrekbare interconnecties en het geheel is geëncapsuleerd in een uitrekbaar elastomeer.

Een korte inleiding wordt gegeven i.v.m. de eigenschappen van polymeren die gebruikt worden in onze technologie. Enerzijds de polymeren als encapsulatie materiaal (silicones) en anderzijds de polymeren als ondersteunend materiaal voor de uitrekbare interconnecties (polyimides).

Tenslotte wordt een samenvatting gegeven van de kennis rond mechanische aspecten die deels uitmaken bij het ontwerp van uitrekbare interconnecties, gebaseerd op kennis die voor en tijdens dit doctoraatsonderzoek werd ontwikkeld door werktuigbouwkundige ingenieurs. De mechanische performantie van de uitrekbare interconnecties wordt verduidelijkt in functie van encapsulatie materiaal

(hardheid, dikte) en het design ervan (breedte, vorm, straal).

In **Hoofdstuk 3** wordt een eerste technologie voorgesteld. We maken gebruik van gedrukte schakelingen technologie en spuitgiettechnieken om een elastisch microstelsel te realiseren door te starten vanaf een elastisch substraat. Deze aanpak is handig voor bepaalde applicaties maar heeft enkele nadelen in vergelijkbaar met de technologie in Hoofdstuk 4.

De verschillende processtappen worden in detail uitgelegd, waarbij de realiseerbaarheid en karakterisatie bestudeerd worden.

In **Hoofdstuk 4** wordt een tweede technologie voorgesteld voor het maken van uitrekbare, elastische microsystemen. Deze maakt gebruik van standaard gedrukte schakelingen technologie (laminatie, lithografie, etsen, zeefdrukken, vapour phase solderen) voor het realiseren van een elektronisch circuit die met een tijdelijke lijm aan een stijf substraat wordt vastgehecht. Het elektronische design werd aangepast om te functioneren als uitrekbaar stelsel, door het stelsel op te splitsen in functionele eilanden die de rigiede elektronische SMD componenten bevatten, en de uitrekbare koper interconnecties. D.m.v de tijdelijke lijm kan het elektronisch circuit getransfereerd worden in een elastomeer d.m.v een 2-staps spuitgiet proces, waarbij silicone als encapsuleer materiaal gebruikt wordt. De verschillende processtappen worden in detail uitgelegd, waarbij de realiseerbaarheid en karakterisatie bestudeerd worden.

In **Hoofdstuk 5** wordt een erg verbeterde versie van de technologie uit Hoofdstuk 4 voorgesteld. Deze maakt gebruik van polyimide als ondersteunend materiaal om de betrouwbaarheid van het stelsel te verhogen. Fotodefinieerbare polyimide wordt gebruikt om de uitrekbare interconnecties te ondersteunen alsook ter ondersteuning van de functionele eilanden die de elektronische componenten bevatten. Het effect van het toevoegen van polyimide als laag onder en boven de interconnecties wordt bestudeerd. De eerste stappen in het aanbrengen van het polyimide door andere technieken zoals zeefdrukken wordt bestudeerd.

Voorts laat het gebruik van polyimide toe om de technologie uit te breiden met een extra geleidende laag nl. gezeefdrukte zilverpasta, die de nood aan 0 Ohm weerstanden teruggedrijft. Deze worden normaal gebruikt om overbruggingen te realiseren van geleiders. Met de extra geleidende laag kan de complexiteit van het stelsel verhoogd worden.

De verschillende verbeterings processen worden in detail uitgelegd voor de polyimide ondersteunde, dubbele polyimide bedekte en dubbele geleider laag technologieën.

In **Hoofdstuk 6** wordt een overzicht gegeven van de bestaande betrouwbaarheidstesten die gebruikt worden bij het quantificeren van de performantie van

een product tijdens de onderzoeks en ontwikkelfase. De verschillende technologieën die in dit doctoraatswerk worden voorgesteld, worden onderworpen aan cyclische duurtesten voor elongaties tussen 0 en 20%. De performantie van 2 types testspecimens wordt bestudeerd: designs die enkel bestaan uit parallelle uittrekbare interconnecties en designs die naast parallelle uittrekbare interconnecties ook een componenteneiland bevatten.

Tijdens de levensduur van de uittrekbare interconnecties verandert de weerstand niet significant tijdens het uitvoeren van de cyclische duurtesten. De elastische interconnectie faalt door de opeenstapeling van plastische vervorming in het koper, wat leidt tot het ontstaan van defecten aan het ruwe oppervlakte van het koper. Deze defecten groeien aan en verplaatsen zich over de doorsnede van de koper interconnectie.

De elastische interconnecties vervaardigd uit koper en geëncapsuleerd in PDMS kunnen tot meer dan een miljoen keer uitgerokken worden bij een uitrek tussen 0-2.5%. Bij hogere rek, 0-5%, 0-10% en 0-20% vermindert het gemiddelde aantal cycli tot respectievelijk 17900, 2420 en 200.

Er werd geen verschil waargenomen in de levensduur van de uittrekbare interconnecties die aan verschillende reksnelheid werden onderhevig, dit bij 1% (s^{-1}) en 10% (s^{-1}). Het gebruik van 25 μm soldeermasker als bedekking voor de uittrekbare interconnecties verbetert de levensduur niet. Een laag fotodefinieerbare polyimide HD4100 daarentegen verhoogt de levensduur met een factor $\sim 2-3.6$, afhankelijk van de aangelegde rek. Dit is te wijten aan de bufferende werking en de vertraging van de propagatie van defecten door dit stijve, ondersteunende polyimide.

Een enorme toename in de levensduur werd vastgesteld bij de teststructuren vervaardigd in de dubbelzijdige polyimide technologie (meer dan 480 keer bij 30% rek) te wijten aan de volgende 3 factoren: het gebruik van een mechanisch beter polyimide, een breder polyimide die als buffer werkt en de bedekking aan beide kanten die een nog symmetrische buffer vormt en defect propagatie tegengaat.

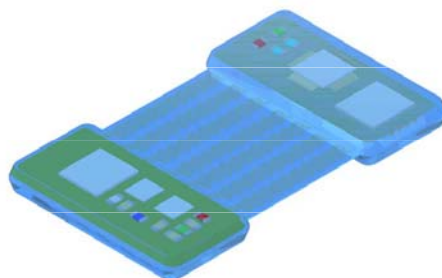
Het implementeren van een componenten eiland verbonden met de uittrekbare interconnecties leidt tot defecten aan de overgang tussen beiden. Een verbeterde versie van dit testsample wordt voorgesteld gebruikmakend van fotodefinieerbare polyimide. Mechanische simulaties en experimentele analyse hebben de verbeterde mechanische performantie van het design aangetoond. Dit in hoofdzaak door het vervangen van het rigiede componenteneiland door een flexibele versie, het optimaliseren van de vorm van het eiland, het aanpassen van de vorm van de encapsulatie. Een verbetering in levensduur van 400 tot 2500 cycli bij 10% elongatie werd waargenomen. Er werd wel vastgesteld dat de falingsmechnismen op willekeurige plaatsen voorkwamen en zich niet enkel beperkten tot de elastische interconnectie zone of de overgangszone.

In **Hoofdstuk 7** beëindigen we dit doctoraatswerk met een overzicht van de gerealiseerde technologie demonstratoren, gemaakt in de voorgestelde techno-

logieën. De demonstratoren zijn vooral draagbare elektronische applicaties. Een uitrekbare temperatuursensor, een uitrekbaar verwarmingselement, een uitrekbare ademhalingsensor voor baby's en een uitrekbare fitness activiteitsmonitor werden gerealiseerd. Voorts tonen we de mogelijkheid aan om een draadloos voedingscircuit te realiseren die door de encapsulatie enige waterbestendigheid vertoont. Uitrekbare hoog-frequente interconnecties en antennes voor draadloze applicaties werden gerealiseerd. Ook de eerste stappen in het realiseren van een uitrekbare multi-electrode matrix worden getoond.

Summary

In the world of electronics, an expanding growth in the market of flexible electronic substrates is being observed. An emerging topic and a step further is the realization of conformable, elastic microsystems. Elasticity is a more general, and more challenging characteristic than flexibility. Stretchable, elastic electronic circuits should have the capacity to absorb large levels of strain ($\gg 1\%$) without fracture or significant degradation in their electronic properties. The combination of mechanical stretchability and the presence of electronic functionality inside a soft, conformable substrate presents a promising new technology platform which combines the advantages of both and enables a wide range of new applications for use in healthcare, wellness and intelligent clothes.



This PhD dissertation presents novel technologies to realize such elastic microsystems. New stretchable substrates with stretchable interconnects have been developed, based on the use of printed circuit board (PCB) techniques in combination with liquid injection moulding steps. Off-the-shelf, rigid electronic components are used, grouped onto flexible islands. These islands are electrically interconnected by use of elastic metallic interconnects, giving the system its stretchability. It shouldn't be stressed that the reliability of these interconnections and the transitions to the islands is of major importance. All these aspects will be covered in this work: the technology development, characterization and realization of a number of elastic microsystems.

In **Chapter 1**, an overview is given of the different technological approaches leading to stretchable electronic devices, currently being topic of research at different institutions worldwide.

Making use of out-of-plane designs is a first method to make intrinsic, non-stretchable materials stretchable. This approach is used to make elastic inorganic systems where wavy silicon is selectively bonded to or embedded in prestretched elastomeric substrates, and to make stretchable interconnects by applying thin metal films on a prestretched elastomer. Integrated circuits forming a conformable digital camera, stretchable TFT circuits,.. are a few results of these approaches.

A second method is the use of in-plane designs, by specially horseshoe/meander shaped metal interconnects in which bending at the corners can accommodate the applied strains. This method has been used for the realization of gold, copper, aluminium, silverpaste conductors on elastomeric substrates forming large-area stretchable circuit boards. The technology presented in this PhD work is based on this method.

Other methods are the use of conductive liquid metal alloys filled into sealed, 3 dimensional microchannels in elastomeric substrates to achieve deformable antennas. Silicon spirals formed by DRIE connecting electronic islands, being unwinded to form an extensible system. Perforated metal-polyimide sheets forming stretchable robotic skins. Conductive polymer paste to form elastic batteries. And many, many more..

In **Chapter 2**, our philosophy on elastic microsystems is explained. An electronic circuit design is transformed into a stretchable design by dividing the system into functional, component islands connected with stretchable interconnects, fully encapsulated in a stretchable elastomer.

A brief introduction on the characteristics of polymers used in our technology as embedding material (silicones) and support material for the stretchable interconnects (polyimide) is included.

Finally, a resume is given of the mechanical aspects related to the design of stretchable interconnects, based on pre-existing knowledge and knowledge created by mechanical engineers during the period of this PhD. The mechanical performance of the stretchable interconnects is clarified in function of embedding material (stiffness, thickness) and mechanical design of meandered interconnects (width, shape, radius).

In **Chapter 3**, a first technology is presented. In a straightforward way, an elastic microsystem is realized by use of printed circuit board fabrication techniques and moulding techniques, by processing on an elastomeric substrate, PDMS. This is an approach suitable for certain applications but it has some disadvantages compared to the technology presented in Chapter 4.

The different process steps are in detail explained including a feasibility and characterization study of the technology.

In **Chapter 4**, a second technology is presented in order to realize a stretchable electronic system. It makes use of printed circuit board fabrication techniques (lamination, lithography, etching, screenprinting, vapour phase soldering) in order to produce an electronic circuit attached with a temporary adhesive on a carrier. The electronic design has been adapted to act as a stretchable device by splitting it up into functional islands, containing rigid SMD components, and stretchable copper interconnects. Due to the temporary adhesive, the electronic circuit can be transferred into an elastomer, done in a 2 step moulding process using PDMS as encapsulant.

The different process steps are in detail explained including a feasibility and characterization study of the technology.

In **Chapter 5**, a much improved version of the technology presented in Chapter 4 is described. It makes now use of polyimide as supporting material in order to improve the system's reliability. A photodefinable polyimide is used for this purpose in order to support the stretchable, metallic interconnections and the functional islands with electronic components. The effect of adding polyimide is studied, below and above the conductors. The first steps in finding other ways to apply the supporting polyimide are explored. Screenprinting tests of non-photodefinable polyimide have been performed.

Furthermore, the use of polyimide allows for an extension of this technology by adding an extra conductor layer, screenprinted silverpaste, reducing the need of zero-ohm resistors in order to realize cross-overs and increasing the possible complexity of such a system.

The different improvement process steps are in detail explained for the polyimide supported, the double polyimide layer and double conductor layer technologies including a feasibility and characterization study.

In **Chapter 6**, an overview is given of the existing reliability tests in order to quantify the performance of a product during the research and development phase. The technologies presented in this PhD work are subjected to cyclic endurance tests in the 0-20% strain range. The performance of 2 types of test samples is studied: designs containing only parallel meander tracks and designs containing parallel meander tracks and an interposer.

The resistivity behaviour of the parallel tracks during cyclic elongation has been observed, showing no significant increase during the lifetime of the track. The failure mode of the copper is due to accumulated plastic strain, leading to crack magnification at the rough side of the copper tracks, followed by a cross sectional crack propagation.

Copper, PDMS embedded meander tracks having a particular meander design, can be stretched upto more than a million cycles for 0-2.5% elongation. For higher strains, 0-5%, 0-10% and 0-20% the average number of cycles is around 17900, 2420 and 200 respectively.

No difference has been observed in the lifetime of the interconnects subjected to a strainrate of 1% (s^{-1}) and 10% (s^{-1}). Using a layer of 25 μm soldermask as coverlayer doesn't affect the lifetime. A layer of photodefinable polyimide HD4100 increases the lifetime by a factor $\sim 2-3.6$, depending on the applied strain. This due to the buffer effect of the stiff polyimide support and the crack propagation delay.

A huge increase in the lifetime has been observed by using the double layer polyimide technology (upto 480 times for 30% strain), due to 3 factors: the use of a mechanical better polyimide, a wider polyimide acting as a strain buffer and covering both sides resulting to a more symmetrical buffer and crack propagation protection.

Embedding of an interposer connected with the stretchable interconnects, leads to failures at the rigid-stretch transition. An improved version of this testvehicle has been proposed using photodefinable polyimide support. Mechanical simulation and experimental analysis have demonstrated the improved mechanical performance. This mainly due to the replacement of the rigid by a flexible interposer, optimizing the shape of the functional island and adjusting the mould design, an increase in lifetime from 400 upto 2500 cycles could be obtained for 10% strain. The failure modes occurred in a random way at different places, not only limited to the flex-stretch transition zone.

In **Chapter 7**, we conclude this PhD study with an overview of realized elastic microsystems by using the presented technologies. The demonstrators are mainly for wearable applications including a stretchable temperature sensor, a stretchable heater, a stretchable baby respiration monitor and a fitness activity monitor. Furthermore, the feasibility of having a fully encapsulated, to a certain degree water resistant, wireless power circuit is demonstrated. Stretchable high-frequency interconnects and antennas for wireless communication have been realized. The first steps in the realization of a stretchable multi-electrode array have been done.

Notations

Notation	Denotation
CTE	Coefficient of Thermal Expansion
FCB	Flexible Circuit Board
FE	Finite Element
FEA	Finite Element Analysis
FFC	Flexible Flat Connector
DRIE	Deep Reactive Ion Etching
HDI	High Density Interconnections
IC	Integrated Circuit
IPA	Iso Propanol Alcohol
LPCVD	Low-Pressure Chemical Vapour Deposition
MOSFET	Metal Oxide Field Effect Transistor
PCB	Printed Circuit Board
PDMS	Polydimethyl Siloxane
PE	PolyEthyleen
PP	PolyPropyleen
PSA	Pressure Sensitive Adhesives
PVC	PolyVinyl Chloride
PI	PolyImide
QFB	Quad Flat Package
RIE	Reactive Ion Etching
rpm	rotations per minute
SMI	Stretchable Moulded Interconnect
SCB	Stretchable Copper Board
sccm	standard cubic centimeters per minute
SEM	Scanning Electron Microscope
SMT	Surface Mount Technology
SMD	Surface Mount Device
SOI	Silicon On Insulator
SPB	Stretchable Polymer Board
TFT	Thin Film Transistor

TPU	Thermoplastic Polyurethane
UV	Ultra Violet
UVO	UV-induced Ozone

Chapter 1

Introduction and research context

The work described in this PhD thesis presents the development of different technologies for the realization of elastic microsystems. This chapter will picture the upcoming need for stretchable electronics and will discuss the added value of this PhD work to this technology field. In the world of electronics, an expanding growth in the market of flexible substrates is being observed. An emerging topic and a step further is the realization of elastic microsystems. Elasticity is a more general, and more challenging, characteristic than flexibility. Stretchable circuits should have the capacity to absorb large levels of strain ($\gg 1\%$) without fracture or significant degradation in their electronic properties; they are also flexible, due to this mechanics. The combination of mechanical stretchability and the presence of electronic functionality inside a soft, conformable substrate presents a promising new technology platform which combines the advantages of both and enables a wide range of new applications. Especially in the field of ambient, biomedical and intelligent textile applications.

1.1 Elastic microsystems: approaches

Worldwide, different research groups are active in the field of elastic, stretchable electronics. An overview of the most successful approaches will be given, including the materials, mechanical aspects, properties of the devices and stretchable circuits that can be achieved.

To make intrinsic, non-stretchable materials (e.g. silicon, metal conductors) stretchable, in-plane or out-of-plane designs are used to accommodate the applied strains. These materials are always used in combination with an elastomer e.g. polydimethylsiloxane (PDMS), thermoplastic polyurethane (TPU) acting as a

carrier or encapsulant for the stretchable system. In this literature overview, a division will be made between out-of-plane designs and in-plane designs. This criterion reflects to the position of the non-stretchable material structures relative to the strain plane (Figure 1.1).

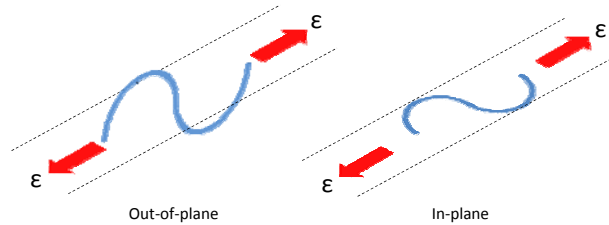


Figure 1.1: Schematic illustration of out-of-plane and in-plane design approach for stretchable electronics.

The pictures used in this chapter can be found in the cited references.

1.1.1 Out-of-plane designs

Specialized structural layouts and mechanical designs can be used in order to make brittle inorganic materials (e.g. single-crystal inorganic semiconductor materials) or metal films stretchable.

An approach found in literature ([1],[2],[3],[4],[5],[6],[7]) exploits out-of-plane motion in thin layers to accommodate strains applied in the plane. Structures of inorganics bonded to or embedded in elastomeric substrates exhibit reversible responses to large strain deformations that exceed, by orders of magnitude, the intrinsic fracture strains in the ribbon materials themselves. Broad ranges of stretchability are possible with significant strains only in the elastomer. Figure 1.2 illustrates this principle where in Figure 1.2 (top left), flat ribbons are bonded at all points on their bottom surfaces to an elastomeric substrate that is mechanically strained along the length of the ribbons. The substrate, mostly PDMS, has a Young's modulus (typically ~2MPa) that is nearly five orders of magnitude smaller than those of typical single-crystalline semiconductors (e.g. 130 GPa for Si, 85.5 GPa for GaAs). Releasing the prestrain induces compressive forces on the ribbons that lead to a non-linear buckling response. The resulting 'wavy' deformations have well-defined wavelengths and amplitudes being linearly proportional to the ribbon thickness and depending on the material properties and the level of prestrain. In this configuration, the hybrid system can be stretched or compressed reversibly with a linear elastic response to strain. In a related

1.1 Elastic microsystems: approaches

3

strategy, the ribbons can be designed to bond to the elastomer only at certain locations (Figure 1.2 (bottom left)). Here releasing the prestrain leads to large, out-of-plane bridge structures, due to delamination of the non-bonded regions from the substrate. The advantage of this layout is that the wavelengths can be defined precisely, in geometries that optimize the range of stretchability, with a level of engineering control that is absent from the case of Figure 1.2 (top left). In practical applications, both involve an elastomeric encapsulation layer applied on top. The same concepts can be applied to two dimensional membranes or interconnected mesh structures, as shown in Figure 1.2 (top right and bottom right).

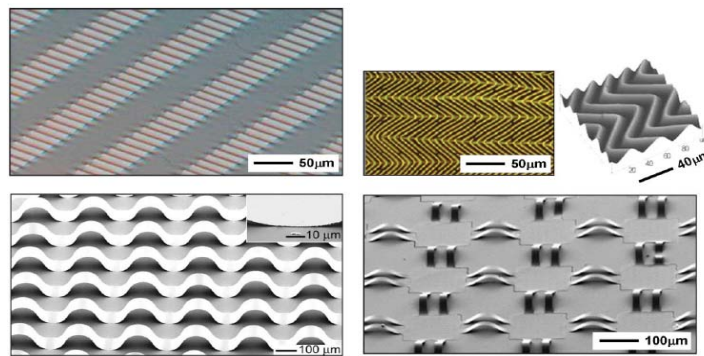


Figure 1.2: Schematic illustrations of different out-of-plane designs applied to stretchable inorganic materials.

The fabrication of these concepts is done by use of ultrathin structures of single crystalline silicon and gallium arsenide. For both, these materials are generated from high-quality bulk or layered wafers. As examples, silicon nanoribbons can be made with either silicon on insulator (SOI) wafers through undercut etching of the buried oxide, or with bulk silicon wafers (111 direction) through anisotropic etching with KOH or TMAH. Transfer printing such materials to a prestrained polydimethylsiloxane (PDMS) membrane followed by release leads to the desired buckled structures, via patterned or unpatterned bonding (Figure 1.3). The required adhesion between layers of SiO_2 on the nanoribbons and hydroxylated surfaces of the PDMS can be achieved by covalent chemical linkages between silanol (Si-OH) groups on the PDMS and similar groups on the SiO_2 . The required functionalization of PDMS is accomplished by exposure to ozone, either uniformly or in selective, lithographically defined regions. Oxidizing the PDMS surface by exposure to ozone, for example, produces a surface that can react with a wide range of materials to form strong chemical bonds, simply upon physical contact at room or slightly elevated temperatures.

For uniformly bonded systems, the strain advantage associated with the wavy shapes provides a 10-20x improvement in the stretchability for most inorganic semiconductors, compared to intrinsic values set by the fracture strains (~1%) of these materials. For example, wavy silicon structures can accommodate strain ranges of 15-20% before fracture.

On pre-stretched PDMS substrates where the surface is oxidized only in selected areas, the semiconductor ribbons form buckled structures that involve complete separations of the ribbons from the PDMS in the unoxidized regions. The example shown in Figure 1.2 (bottom left) has been made on a 60% prestretched PDMS substrate patterned with an UV induced ozone (UVO) mask to define parallel surface activated (oxidized) narrow stripes (widths of $10\mu\text{m}$) separated by wide, unactivated regions (widths of $400\mu\text{m}$). Contacting such a PDMS substrate with preformed ribbons on a mother wafer removing the substrate and then relaxing its prestrain leads to large buckled structures forming the ribbons. These selectively bonded systems can accommodate much larger strains. In optimized designs, strains of 100% or more, even to values approaching the fracture strain of the elastomer PDMS are possible [8].

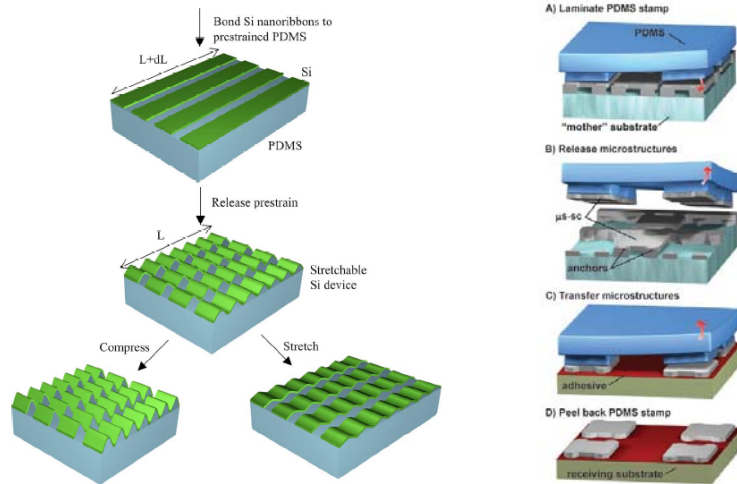


Figure 1.3: (Left) Schematic illustration of the process for fabricating buckled, or wavy, single crystal Si ribbons on a PDMS substrate. (Right) Schematic illustration of a transfer approach using a rubber stamp to remove selected collections of semiconductor micro- and nanostructures from a wafer and to deliver them to a receiving substrate.

Another approach found in literature ([9],[10],[11],[12],[13]) exploits the compressive stress that can be built into thin films of gold evaporated onto elastomeric membranes of PDMS. Thin metal films consisting of 100-nm-thick layers of gold

on top of a 5-nm-thick adhesion interlayer of chromium, are deposited in one run by successive electron beam evaporation onto elastomeric substrates of PDMS held at room temperature. Compressive stress in the gold films induces spontaneous wrinkling (Figure 1.4 a), which can shrink the net length of the thin-film conductors by several tenths of a percent.

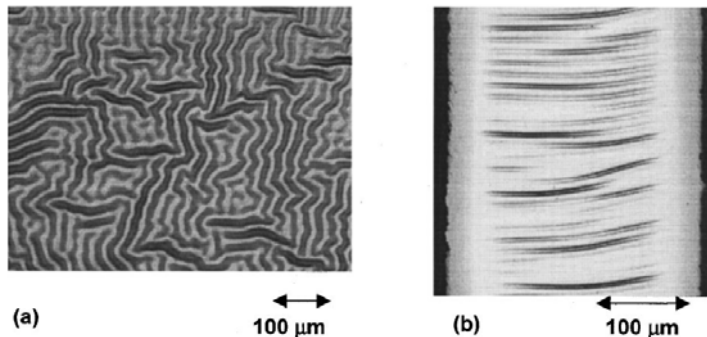


Figure 1.4: Optical images of the wave pattern formed in a 100-nm-thick gold film evaporated on a 1-mm-thick PDMS membrane (a) over the entire surface (b) of a stripe evaporated through a shadow mask. Dark margins are from the PDMS substrate.

The intention of this approach is to make use of this strain to raise the stretchability of the gold films above their fracture strain of typically 1%. It was discovered that the stripes can retain electrical continuity when stretched by as much as 22%. For the conductor stripes, Cr/Au is evaporated through a shadow mask made of polyimide foil. When the polyimide foil is taken off, the stress in the metal film is released and no longer is equiaxial. The structure relaxes laterally at the edges of the gold lines and a pattern of parallel waves develops with its crests aligned perpendicularly to the direction of the maximum compressive stress as shown in Figure 1.4 b. This pattern is a regular sinusoid with a wavelength similar to that of the random buckling ($\sim 10 \mu\text{m}$). The Au stripe is 100 nm thick, 28 mm long, and 0.25 mm wide. The electrical resistance as a function of uniaxial strain was measured in situ. Figure 1.5 presents the change in electrical resistance normalized to its initial value, with the tensile strain.

Figure 1.5 shows that, the Au line remains conducting under $\epsilon_{\text{external}}$ much above this typical fracture strain of a free-standing thin film. Figure 1.5 exhibits two regimes. At strains lower than 8%, the normalized resistivity is proportional to elongation. In this regime small cracks appear at the edges of the stripe. At higher strain, cracks extend across much of the width of the stripe, perpendicular to its longitudinal dimension. These longer cracks cause a pronounced rise of the

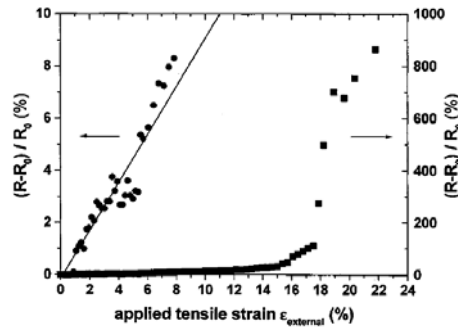


Figure 1.5: Variation of the normalized change in electrical resistance of a 100-nm-thick Au stripe with applied tensile strain $\epsilon_{external}$ (right curve). The left curve represents the linear behavior of the normalized resistance with the applied external strain for $0 \leq \epsilon_{external} \leq 8\%$.

electrical resistance. At strains above 15%, these cracks traverse the full width of the Au line. However, while the electrical resistance rises drastically, it remains finite. This observation suggests that the film is broken, but that a thin conductive layer remains at the bottom of the cracks [9]. From the crack dimensions it is estimated that this conducting remnant layer is one metal atom thick. So far, the material of this layer hasn't been detected. At $\epsilon_{external} = 23\%$, the resistance became infinite.

In follow up studies, an explanation has been found for the ability of the elastomeric substrate to be stretched repeatedly by tens of percent over hundreds of cycles without fatigue while remaining electrically conducting. After deposition of the metals on the PDMS layer, it was found through SEM that the surface of the metal-film is covered with tribranched microcracks being randomly distributed. The average spacing between these microcracks is a few tenths of a micrometer, forming a network that percolates the whole film but remaining the conductivity of the whole film. The microcrack pattern in the metal film allows the film to elongate by deflecting and twisting out-of-plane, so that a large applied strain only induces small and elastic strain in the film. The energy released at the crack tips is minimized, inhibiting crack growth across the metal film. Because the metal film only deforms elastically, finite and reproducible electrical conduction is maintained over repeated deformation.

In order to make the gold stripes reversibly stretchable with little change in electrical resistance, the metal can be preshaped to a wave on the elastomeric substrate [10] by use of the prestrain. Figure 1.6 shows the fabrication process where a 1 mm thick membrane of PDMS is 15% prestretched. 5nm/25nm thick Cr/Au metal stripes are patterned by a lift-off technique and deposited by electronbeam evaporation. When the PDMS substrate is released from its prestretched state,

1.1 Elastic microsystems: approaches

7

the metal stripes on the silicone substrate buckle together.

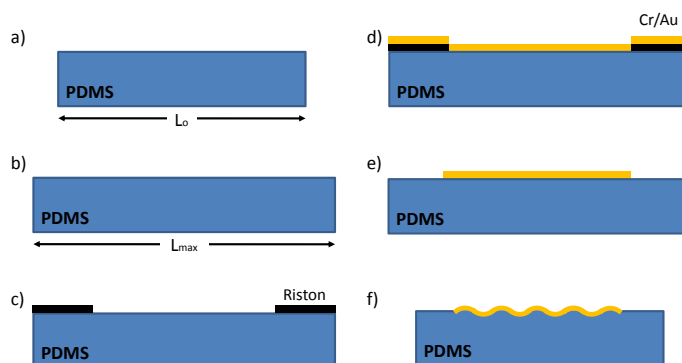


Figure 1.6: Fabrication of gold interconnects on an elastomeric PDMS substrate. (a) PDMS substrate. (b) Prestretched PDMS. (c) Laminated Riston photoresist mask. (d) Evaporated metal films. (e) Lift-off. (f) Release from prestretch: the gold stripe buckles.

Before release from an elongation of 15%, the Au stripes are $500\ \mu\text{m}$ wide and 4.6 mm long. The electrical resistance of a 25 nm thick gold stripe evaporated on glass is $7.5\ \Omega$. On the PDMS substrate, the resistance varies between this value and several megaohms. But, the electrical resistance of the Au conductor decreases by $\sim 30\%$ from prestretched to the relaxed state. It has been observed that the resistance first decreases with increasing strain ϵ up to 17% i.e. beyond the value of the prestretch of 15%. At higher strains the resistance keeps increasing until it rises suddenly to open circuit at $\sim 28\%$ strain. The highest strain that has been reached before electrical failure was 100%.

The possibility of patterning stretchable gold conductors by lithography into PDMS opens the possibility to fabricate stretchable microelectrodes [14]. They are fabricated by evaporating gold thin films ($< 100\text{nm}$ thick) by use of a metal adhesion layer (titanium or chromium) on a PDMS substrate. On top, another metal adhesion layer is applied, followed by lithographical patterning of the metals. On top, a thin layer ($\sim 6\ \mu\text{m}$) of PDMS is applied by spincoating and openings are foreseen by dry etching through an applied metal mask. The stretchable property of this technology has been demonstrated and relies on the percolation of the electrical current through the built-in network of gold-ligaments and micro-cracks. During stretching, the microcracks in-between the gold open while the gold tilts and twists out of the conductor plane, hence minimizing the strain on the metal.

Encapsulated (Figure 1.7), $50\ \mu\text{m}$ wide gold tracks were uni-axially stretched. It was found that the resistance response upto 20% strain was comparable for embedded and non-embedded gold tracks: the resistance increases nonlinearly with

the applied strain and recovers after a cycle. But, when stretched further upto 30% strain, several conductors failed and did not recover after unloading. An explanation for this difference has not been found yet. The strain values do not demonstrate the conductors' stretchability limit but demonstrate the technology.

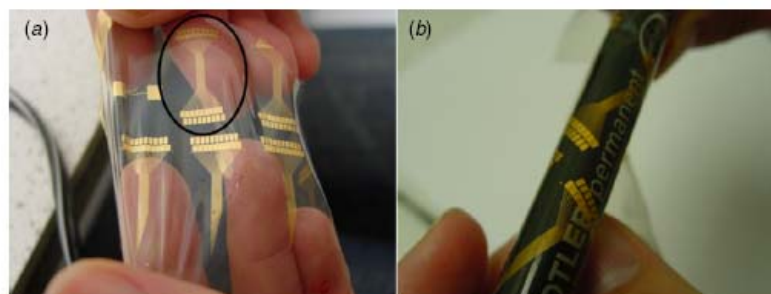


Figure 1.7: PDMS encapsulated gold micro-conductors patterned on a 3 inch diameter PDMS membrane. (a) The circle indicates the conductor design used on the stretchability test. (b) The patterned conductors on PDMS are highly conformable.

1.1.2 In-plane designs

Stretchable structures that do not use, or are not specifically designed to exploit out-of-plane motion are also possible.

One such approach [15],[16] realizes a large-area electronic system from monolithic silicon substrates by expanding a functional silicon die by several orders of magnitude by structuring the silicon die as a two-dimensional network of silicon islands and springs. The springs consist of $1.6\mu\text{m}$ thin spiral ribbons of silicon wrapped around a $200\mu\text{m}$ diameter circular silicon island. The islands contain electronics whereas the different springs connect the islands mechanically and electronically. By finite element analysis (FEA), it has been observed that the maximum strain is reached in the junction between the silicon node and the spiral. All the strain induced by the expansion process is contained in the spiral ribbons, the active device area remains strain free.

The fabrication process can start with a standard fabricated SOI substrate where the electronic islands and interconnects between the islands have been defined. Release of the stretchable membrane structures is achieved by under-etching the spiral ribbons and silicon islands using an isotropic XeF_2 vapour phase etch of the silicon substrate. The structures shown in Figure 1.8 are $30\mu\text{m}$ thick but stretchable membranes up to $100\mu\text{m}$ thick have been fabricated by tuning of the

1.1 Elastic microsystems: approaches

9

deep reactive ion etching (DRIE) step. To uncoil the spiral ribbons, the devices are transferred to an electrostatic chuck, where stainless-steel probes manipulate pads at the corner of the coiled structures to expand the devices into an array. As soon as the desired shape and size is obtained, the structures can be attached to a surface pre-coated with an adhesive.

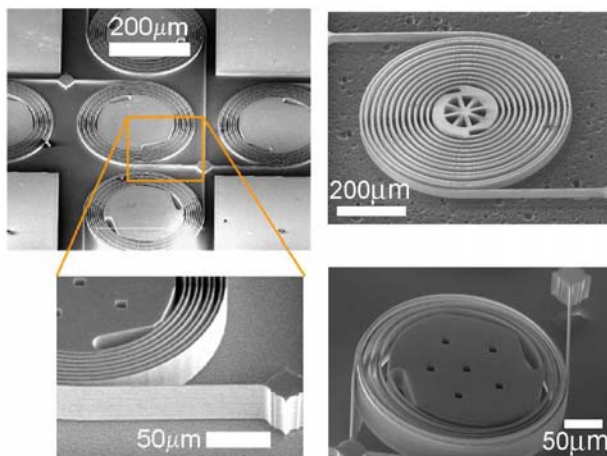


Figure 1.8: SEM images of a silicon structure etched into the shape of spirals surrounding central hubs after the DRIE step before (left) and after (right) the release step.

Unwinding of the coiled spirals yields an extensible system that could also achieve some degree of stretchability if bonded to an elastomeric substrate (Figure 1.9). Instead of out-of-plane motions, stretching is accomplished through a combination of bending of the coils of the spiral and rotation of the islands. The released structures can be cycled to full extension multiple times without breaking even when the spirals uncoil out of plane. No delamination of low-pressure chemical vapour deposited (LPCVD) and thermally grown SiO_2 or Al (sputtered or evaporated) films on the spiral ribbons was observed during stretching. The resistance of the 130nm thick Al interconnect on the spiral structures increased by 5% upon full extension.

In Figure 1.9, a 30 μm thick structure with 71 islands before and after stretching is shown. The ratio of stretched over unstretched area is 51. Longer spiral springs could even further extend this expandable network. In Figure 1.10, the possibility of applying these structures to curved substrates is demonstrated. This makes the technology suitable for curved focal-plane arrays that, by nature of their shape, eliminate many of the off-axis color mixing and image noise problems inherent in flat arrays. All these features allow to use this technology in applications where high performance large-area electronics are needed in a cost-effective way.

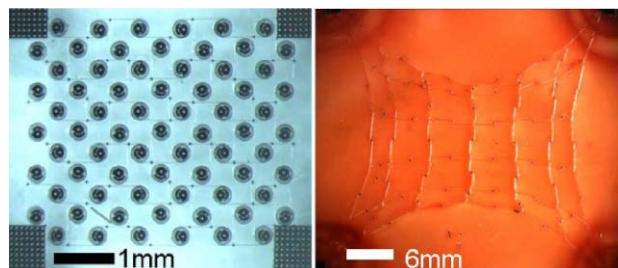


Figure 1.9: Optical images of a 71 node network before and after expansion. The surface ratio between both is 51.

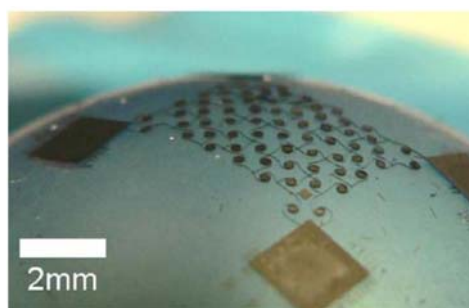


Figure 1.10: The expandable monolithic networks are flexible and conformable to curved substrates making them suitable for curved focal-plane arrays.

Another in-plane design involves planar S-shaped (i.e. serpentine, meander) structures in which bending at the corners can accommodate applied strains. Figure 1.11 shows some examples. The design is in-the-plane but during stretching, the motion can also involve out-of-plane deformations.

An approach using this design is based on the fact that many metals, despite being unable to stretch significantly, are able to bend if their cross sections are sufficiently small. By use of standard lithography techniques, the hypothesis has been tested that integrated circuits made of springs could form the basis of stretchable elastomeric electronics [17]. Figure 1.11 shows straight and spring-shaped metal wires on an elastomer. Gold was the chosen metal based on its high conductivity and chemical inertness. Polydimethylsiloxane (PDMS) was chosen to form the elastomeric circuit board mechanically protecting and electrically insulating the wires. PDMS is optically clear, and, in general is considered to be inert, non-toxic and non-flammable. Macroscopic fractures appeared when the straight wires were strained even minimally ($\sim 2.4\%$) interrupting the conductivity. The

1.1 Elastic microsystems: approaches

serpentine shaped structures containing a wave formed of linked half-ellipses with an amplitude of half the magnitude of the period, remained conductive at a much greater strain of ~14.2 %. The strain at electronic failure was further improved to ~27.2 % simply by doubling the amplitude-wavelength ratio. In all cases, conductivity recovered upon removal of the strain. These findings demonstrate that tortuosity increases the ability of wires to elongate because metal bends more readily than it stretches.

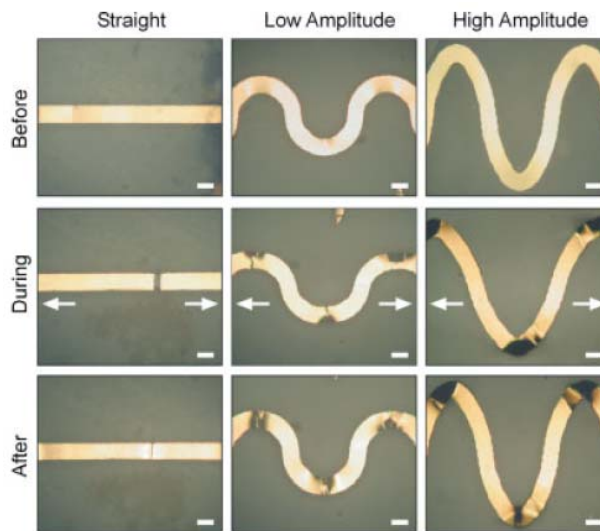


Figure 1.11: Optical images of straight and serpentine metal lines (low- and high-amplitude structures) on an elastomeric substrate. The sequence of the images on the bottom shows the same structures after application of tensile strain in the direction indicated by the arrows. The discolored regions correspond to deformations at locations of peak strain.

Another approach [18],[19] demonstrates the use of liquid metal alloys and materials with liquid/solid phase transitions near room temperature (e.g. Eutectic Gallium Indium (EGaIn) has a meltingpoint of 15.7°C), filled into sealed, 3 dimensional microchannels in elastomeric substrates such as PDMS. Typically, prefabricated channels are filled with liquid alloys using pressure induced flows. The liquid alloy has a thin, solidlike oxide skin on its surface that is well suited for microfluidics. Once the metal is in the channel, the skin reforms and provides mechanical stability to the otherwise low-viscosity and high-surface-tension liquid (in contrast, Hg withdraws from microchannels rapidly to minimize its surface area). The elasticity of PDMS combined with a reversible flow in the conductor,

yield a stretchable response. Unlike electrodeposited or sheet metals, the fluidic metal tracks resist permanent deformation and can thus be deformed reversibly without any hysteresis. Deformable antennas (Figure 1.12) and electrical connections to light emitting diodes have been demonstrated. The fluidic dipole antennas radiated with 90% efficiency, the shape was reconfigurable and the resonant frequency could be tuned mechanically by elongating the antenna via stretching without hysteresis upon relaxing.

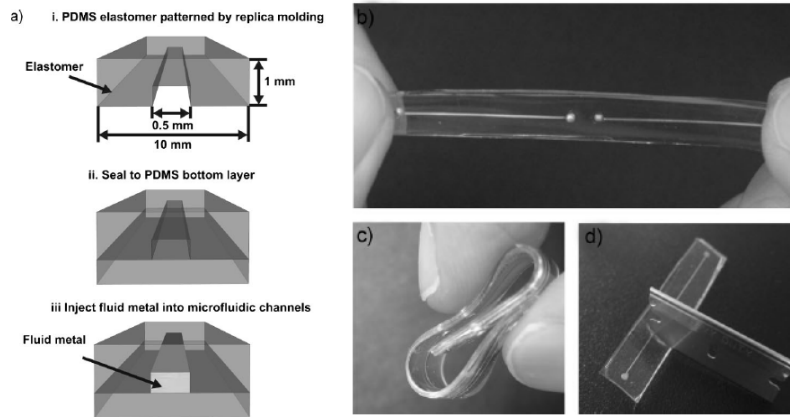


Figure 1.12: (a) Fabrication process of a reversibly deformable dipole antenna. PDMS elastomer cured on a topographically patterned substrate produces two adjacent microfluidic channels (only one shown). After sealing the PDMS channels to another piece of PDMS, injection of liquid metal alloy into the microfluidic channels produces a dipole antenna. (b,c) Photographs of a prototype antenna being stretched and rolled. There is no hysteresis in the spectral properties of the antenna as it is returned to the 'relaxed' state. (d) The antenna self-heals in response to sharp cuts, such as those inflicted by a razor blade.

1.1.3 Combination of out-of-plane and in-plane designs

Some approaches combine serpentine interconnects with out-of-plane geometries using prestraining techniques and patterned bonding [6], [20]. Figure 1.13 shows this principle where the bridge design has been optimized by using a serpentine interconnect. The integrated circuit is composed of silicon devices at bonded island locations and triple layer stacks of polymer and metal in non-coplanar, serpentine layouts as interconnects. In this way, the integrated circuit can accommodate strains larger than the pre-strain. This was not possible with the straight bridge designs [5].

In such systems, modeling indicates that strains in the active materials can be held

1.2 Elastic (opto)electronic devices

13

below $\sim 0.1\%$ even for applied strains larger than $\sim 100\%$. Decreasing the width of the lines, increasing the number of 'coils' in the serpentine while maintaining the amplitude-to-wavelength ratio are the factors leading to this low strain number. The interconnects accommodate these strains through combinations of bending, twisting, rotating and buckling, both in and out of the plane. Further reduction in the bridge thickness and longer serpentine interconnects can decrease the maximum strain.

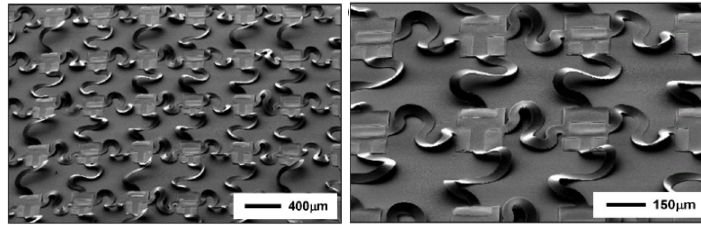


Figure 1.13: SEM images of a silicon integrated circuit composed of device islands that support transistors for CMOS inverters interconnected by non-coplanar serpentine structures consisting of trilayer stacks of polymer/metal/polymer.

In practice and especially for non-coplanar designs, electronic circuits require top surface encapsulation to provide mechanical and environmental protection. It has been found that non-encapsulated, prestrained devices can be stretched up to a level equal to the prestrain percentage without fracture. By contrast, encapsulated devices using PDMS showed a lower maximum elongation [20].

1.2 Elastic (opto)electronic devices

Based on the principles mentioned in Section 1.1, stretchable electronic devices can be realized. In the following sections, successfully implemented functional devices are discussed based on the use of a wide range of materials: from semiconductors to conductors and insulators, both organic and inorganic.

1.2.1 Elastic (opto)electronic components

By additional steps at the beginning of the fabrication sequence explained in the first approach of the out-of-plane design of Section 1.1.1, patterns of dopants in the Si, thin metal contacts and dielectric layers using conventional processing

techniques can be introduced. Two and three-terminal devices, diodes and transistors respectively, can be fabricated in this manner providing basic building blocks for circuits with advanced functionality. Figure 1.14 a and b show optical images and electrical responses of a stretchable p-n junction diode for various levels of strain applied to the PDMS. No systematic variation has been observed in the electrical properties of the devices when stretched or compressed [21]. The device properties do not change substantially, even after ~100 cycles of compressing, stretching, and releasing. Figure 1.14 b-c shows current/voltage characteristics of a stretchable, wavy Si Schottky-barrier metal oxide semiconductor fieldeffect transistor (MOSFET) formed with procedures similar to those used for the p-n diode and with an integrated thin layer (40 nm) of thermal SiO₂ as a gate dielectric. As with the p-n diodes, these wavy transistors can be reversibly stretched and compressed to large levels of strain without damaging the devices or substantially altering their electrical properties. Solar cells and light-emitting diodes (LED) can also be constructed in this manner. These examples illustrate that common and relatively simple underlying physics can be used with various devices and materials, as building blocks of more complex systems described.

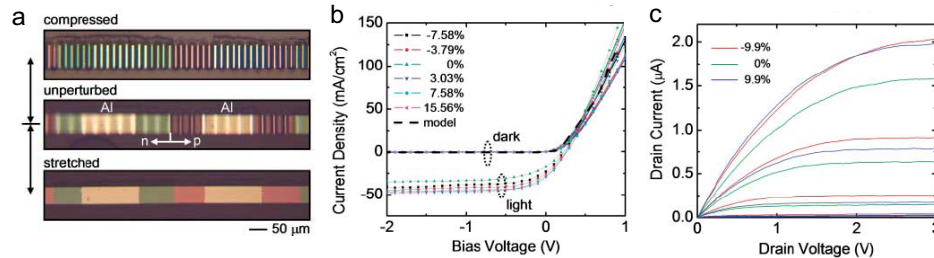


Figure 1.14: (a) Optical images of a stretchable single crystal Si p-n diode on a PDMS substrate at - 11% (top), 0% (middle) and 11% (bottom) applied strains. The Al regions correspond to thin (20 nm) Al electrodes; the pink and green regions correspond to n (boron) and p (phosphorous) doped areas of the Si. (b) Current density as a function of bias voltage for stretchable Si p-n diodes, measured at various levels of applied strain. The curves labeled 'light' and 'dark' correspond to devices exposed to or shielded from ambient light, respectively. The solid curves show modeling results. (c) Current-voltage characteristics of a stretchable Schottky-barrier Si MOSFET, measured at - 9.9%, 0%, and 9.9% applied strains (the gate voltage varied from 0 V to 5 V, with a 1-V step).

1.2.2 Elastic interconnects between rigid components

Stretchable interconnects, wavy out-of-plane or serpentine-like in-plane, can be used to define stretchable wiring between non-stretchable device islands. Stretch-

1.2 Elastic (opto)electronic devices

ability derives from the mechanics of such (metal) structures, which electrically interconnect rigid, active device regions that remain flat and non-stretched.

Wavy interconnects between non-stretchable islands, prepared with 25% pre-strain showed stretchability upto 100% with only slight increase of the electrical resistance. Serpentine interconnects, optimized in curvature, amplitude and shape of the edges, showed stretchability up to 70%.

An example of wavy, out-of-plane metal interconnects, connecting rigid active device components is shown in Figure 1.15. An amorphous silicon inverter with stretching capability upto 12% strain is shown ([22], [23]). Thin wavy metal lines are deposited and directly patterned on the PDMS providing interconnects between separately fabricated and assembled devices.

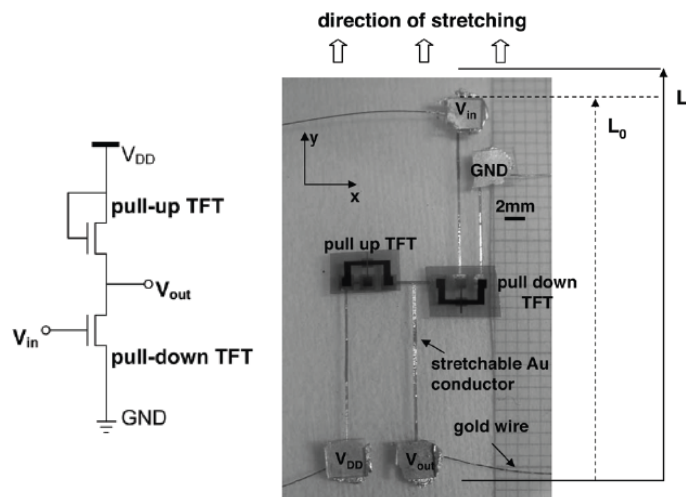


Figure 1.15: Image of stretchable inverter composed of non-stretchable n-type amorphous silicon TFTs interconnected with stretchable metal lines.

Amorphous silicon (a-Si:H) TFTs in the bottom-gate, back-channel etch geometry were fabricated on $50 \mu\text{m}$ thick polyimide foil. After fabrication the TFT/polyimide structure is flat. The TFTs channel is $40 \mu\text{m}$ long and $370 \mu\text{m}$ wide. The TFTs were provided with 0.85 by 0.85 mm contact pads, made large to stabilize the electrical contacts between the gold pads on the TFTs and the elastomer against shear generated by the stretching of the elastomeric substrate. The device characteristics were typical of a-Si:H TFTs prepared on polyimide foil at a 150°C process temperature [24]. It has been observed that the dc response of the transistor is slightly affected by the uni-axial mechanical deformation. Furthermore, the

ac response does not change substantially when the circuit is stretched by 12%. These results show that a simple transistor circuit that is fully elastic, electrically as well as mechanically, is enabled by elastic interconnects on an elastomeric substrate.

Serpentine-like in-plane interconnects between non-stretchable device islands is the technology approach covered in this work. It will be described in the following chapters.

The same principle is used in the technology described in [25],[26],[27],[28]. This Stretchable Copper Board technology (SCB) is very similar to the fabrication of a single sided rigid or flexible printed circuit board. The main difference to conventional printed circuit technology is the organic substrate material, which is thermoplastic polyurethane (TPU) instead of polyimide (flex) or epoxy (rigid). Copper is used as conducting material and by a lamination process, it is laminated on the polyurethane. The succeeding steps are the patterning of the copper into stretchable interconnections and contacts to the electronic components, by use of lithography and wet etching. Other steps involved are application of soldermask, copper finish and reflow soldering of surface mounted device (SMD) components. In this way, a stretchable circuit board is obtained consisting of SMD components connected by stretchable copper interconnections laying on a polyurethane sheet. In Figure 1.16, the process steps are depicted and in Figure 1.17 a realization is shown.

Limits of stretchability and fatigue behavior of the meandering Cu interconnects (Cu thickness $35\ \mu\text{m}$, line width $100\ \mu\text{m}$) on TPU ($100\ \mu\text{m}$) were tested for different meander layouts and dimensions. The various designs were classified according to the wavelength and amplitude of the undulations. The prevalent failure is the line fracture in the apex of the meanders. As depicted in Figure 1.18 the smaller the wavelength of the meander the higher elongation is possible.

This finding is attributed to the distribution of stress over a larger number of weak points per length in the smaller wavelength meander. For technical applications not only a single elongation of the lines, but also the repeated cyclic stretching is of general interest. In Figure 1.18 results of cyclic elongation tests are depicted. The acquired data points can be fitted to a Coffin-Manson type potential equation and display a typical fatigue behavior of the Cu interconnects due to the cyclic stretching (Figure 1.19).

Another in-plane approach uses classical screenprinting to structure the circuit by applying a printable and conductive paste onto a stretchable base material (Evolon Polyurethane micro fibre non-woven). In this technology [29], the Stretchable Polymer Board technology, both the conductor and the base material

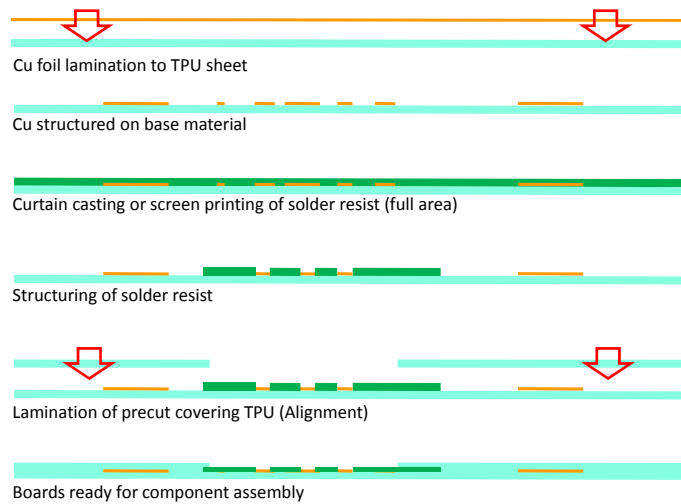


Figure 1.16: Process flow for the fabrication of stretchable copper board (SCB) substrates ready for assembly.

have stretchability as intrinsic properties. As discussed before, stretchability can be achieved using geometrical designs that allow even for non-stretchable materials like Cu a significant stretching. For SPB a specific paste has been developed that allows also a primary stretching of the printed conductors. For this purpose, thermoplastic polyurethane is used as polymer matrix. As conducting particles Ag-coated flakes have been selected and a water based paste has been developed that allows a variation of the fraction of the conductive filler and by thus a variety of pastes in terms of the resistance per square. After printing the conductive layer, a drying and thermosetting process is performed. This is different from classical screenprinting where a curing process is the only process step to finalize the flexible printed boards.

In Figure 1.20, an example is shown of such a stretchable polymer board. This technology is not the best option for repetitive stretching, but could very well be used in applications where no periodic stretching is needed, but instead one asks for contour shaping of an electronic circuit board. Such an application might be cladding the interior of a car compartment, which will be done only once. The resistance of the conductors can be adapted to different requirements through the conductive paste. In Figure 1.21, the feasibility is shown of transforming the stretchable polymer board in an arbitrary shape.

The latter 2 technologies have been developed within the European Stella project together with the technologies that will be described in the upcoming chapters.

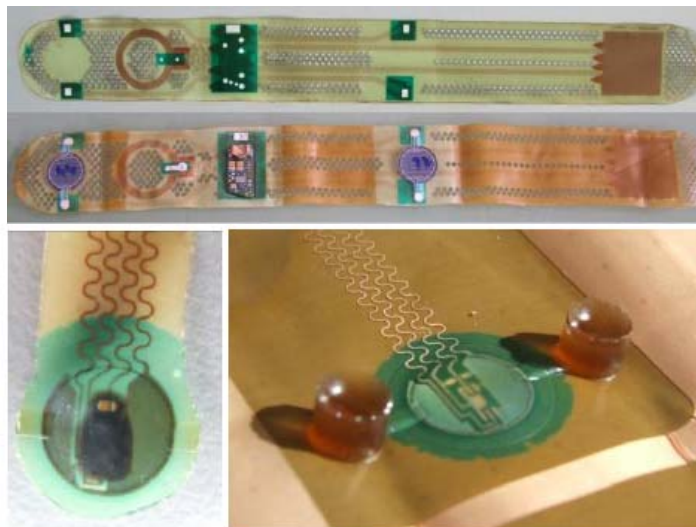


Figure 1.17: Stretchable copper board (SCB) substrates.

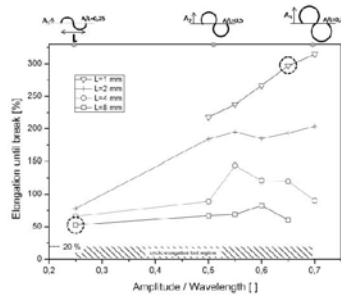


Figure 1.18: Maximum elongation till break for different meander configurations.

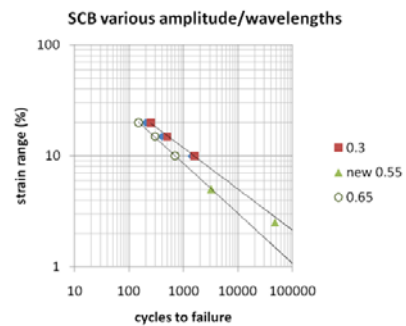


Figure 1.19: Total number of cycles to failure.

A novel in-plane approach for stretchable interconnects on polymer substrates connecting nodes containing active devices and sensors for sensor skins is described in [30],[31]. These stretchable metal interconnect layers are fabricated on polyimide by use of excimer laser photoablation.

Interconnect meshes contain two layers of metal layers aligned perpendicularly

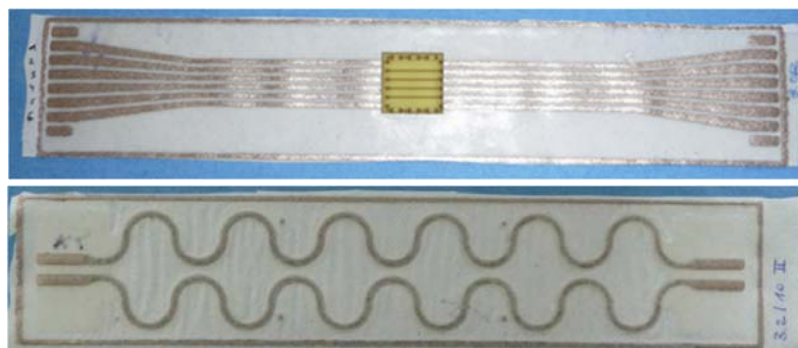


Figure 1.20: Stretchable polymer boards based on use of non-woven thermoplastic polyurethane.

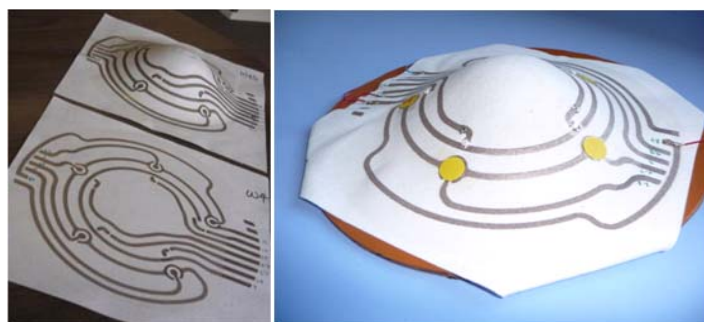


Figure 1.21: Stretchable polymer board transformed into an arbitrary 3D shape.

to form row and column lines such that nodes are formed at the intersection of the two interconnect layers, as shown in Figure 1.22.

The metal layers ($\sim 1\mu\text{m}$ Al) of the interconnect mesh are fabricated on a $25\mu\text{m}$ -thick Kapton-E polyimide substrate and separated by a polymer dielectric layer, consisting of a sputtered $0.35\mu\text{m}$ -thick film of SiO_2 or a $5\text{-}\mu\text{m}$ -thick spin-on polyimide (SiO_2 has been used as a thermal barrier to increase the ablation damage threshold of aluminum). While the polymer substrate provides structural rigidity to the design, it limits the stretchability of the interconnect mesh. Therefore, areas of the substrate that are not beneath the interconnects are strategically patterned and removed by excimer laser photoablation using the metal patterns as in situ masks. This is possible due to the fact that the fluences for photoablation of polymers are in general much lower than the threshold fluence for removal or damage of high-thermally-conductive metals. For many polymers, the threshold fluence (the lowest fluence at which material can be effectively patterned or

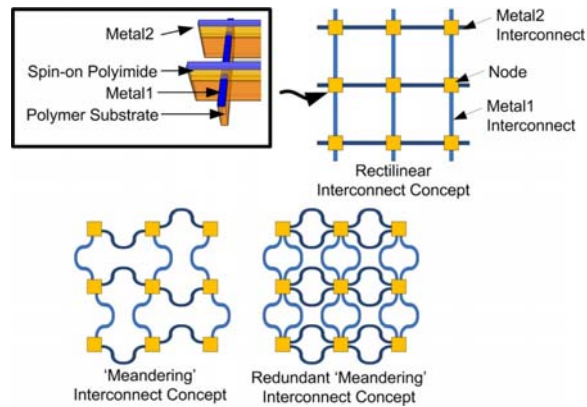


Figure 1.22: Interconnect mesh concept for rectilinear, meandering and redundant meandering interconnects. The interconnects consist of a polymer substrate and two metal layers separated by a spin-on polyimide dielectric layer.

etched) is known to be less than 50 mJ/cm^2 [32], [33].

Meandering interconnect structures are patterned to maximize stretchability. Redundant interconnect designs may also be patterned to maximize robustness without sacrificing the stretchability of the substrate. Realizations of single-layer interconnects, double layer interconnects and redundant interconnect meshes are respectively shown in Figure 1.23 using a scanning electron microscope (SEM). Patterns with line-widths of $10 \mu\text{m}$, $20 \mu\text{m}$ and $40 \mu\text{m}$ have been successfully obtained. The SEM images reveal that the sidewalls are sloped (20%) what shouldn't influence the stretchability of the substrates. Furthermore, conical defects have been observed formed in those regions that are difficult to ablate or originating from ablated debris being redeposited on the sample causing a 'shadow mask' resulting in these defects.

Various single-layer and double-layer interconnect designs have been modeled, fabricated and tested. It has been observed that meandering interconnects have a maximum stretchability of more than 50% with a change in resistivity of only 5%. Redundant interconnect meshes showed a maximum stretchability of almost 30%. Redundant designs will increase the robustness and viability of interconnects without sacrificing stretchability. In Figure 1.24, a 40 mm by 40 mm prototype is shown, containing redundant structures similar as shown in Figure 1.23 (right). It demonstrates the stretchability and conformability of the mesh-like structure to spherical objects whereas conventional flexible structures fabricated on a polymer film have a limited conformability to spherical objects.

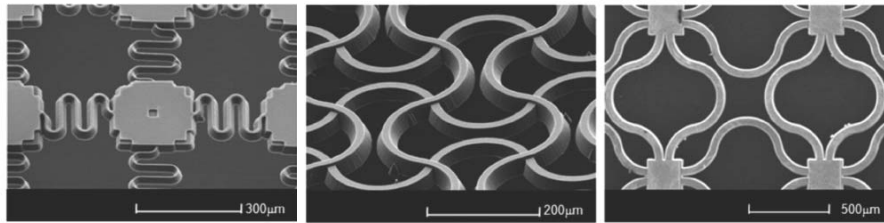


Figure 1.23: SEM micrographs of double-layer interconnects. Meandering interconnect designs with 10 μm line-width, meandering interconnect designs with 20 μm line-width, redundant interconnect designs with 40 μm line-width.

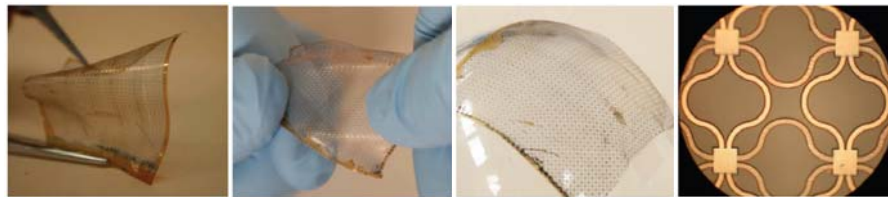


Figure 1.24: 40 mm by 40 mm redundant sensor mesh fabricated using large-area seamless scanning techniques. The flexibility and conformability are demonstrated.

Another approach found in literature [34], [35], [36] achieves stretchable, large-area sensors by perforating plastic films where organic transistors have been processed on. In this way, large-area sensor networks that detect distributions of pressure and temperature can be realized for electrical artificial skin applications. Skin-like sensitivity will be a crucial property for future robots to enable them to work in an unstructured environment. Such flexible and bendable E-skins have been developed [37], [38] but placing the E-skin on curved surfaces or joints of arms, requires stretchability. Such a manufactured film contains islands with multiple thermal and pressure sensors which are read out with active matrices of organic transistors. The fabrication starts with a base substrate of 75 μm-thick polyimide film where the transistor gate electrodes are formed on by using a shadow mask and evaporation of a 50 nm-thick Au layer on a 5 nm-thick Cr adhesion layer. Polyimide is used to form 750 nm-thick gate dielectric layers. Pentacene is used to form a 50 nm-thick channel layer and the buildup is finished by forming the source and drain electrodes by shadow mask evaporation of a 60 nm-thick Au layer. The obtained channel length and width are respectively 50 μm and 1800 μm. The periodicity of the transistors is 4 mm. Parylene is used as a passivation layer in order to protect the circuit mechanically and for intrusion

of gasses. The electrodes are kept open by a locally removal of the $2\ \mu\text{m}$ parylene layer by CO_2 -laser ablation. The flexible sheet is made stretchable by mechanically processing using a numerically controlled cutting plotter or a drilling machine in order to make the net-shaped structures. The width of the bridges between the different transistor islands is $0.3\text{-}0.5\ \text{mm}$. This net-shaped sheet forms the basis of a pressure or thermal sensor sheet, where the pressure or thermal capturing possibility is achieved by laminating of a net-shaped pressure sensitive rubbersheet or a net-shaped PEN film based thermal sensor array respectively. The realization of these concepts is shown in Figure 1.25.

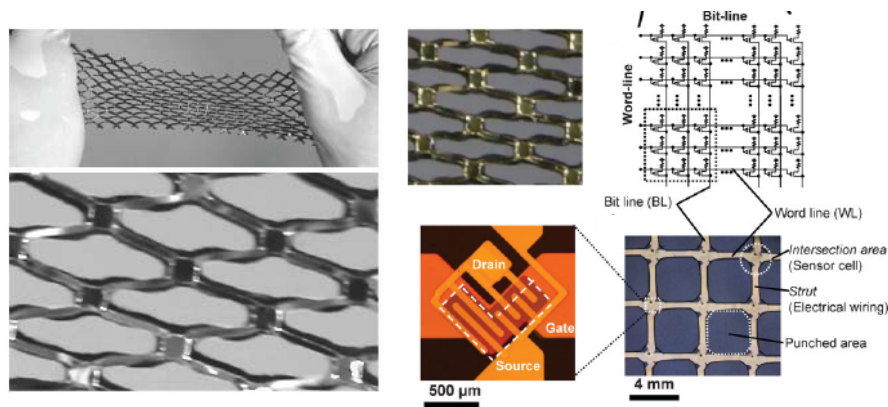


Figure 1.25: Stretchable organic transistor active matrix network of pressure and thermal sensors. Film device is stretchable upto 25%. The organic transistors are placed at the intersection areas.

When such a device is stretched, the many small square-holes of the net are deformed into diamonds (Figure 1.25). The mechanical properties of such structures have been investigated by uniformly coating such a plastic surface by a $100\ \text{nm}$ -thick gold layer and mechanically processing it to form a net-shaped structure. It has been observed that the resistance of this structure remained unchanged upon 1.5N with 25% stretching. Furthermore, a cyclic test has been performed by repeatedly performing a 20% extension and release of the stress. It was found that the device didn't show a significant degradation of electronic performance after 1000 cycles. The major part of the strain occurs at the bases of the bridges while it is small in the transistor regions.

1.2.3 Elastic integrated systems

The principles described in the first out-of-plane approach in Section 1.1.1 can be used to make integrated circuits including silicon transistors, logic gates and ring oscillators. The main image shown in Figure 1.26 shows such a circuit deformed in its center with a glass pipette to illustrate the soft elastic nature. A pair of transistors in an inverter appears in the upper inset.

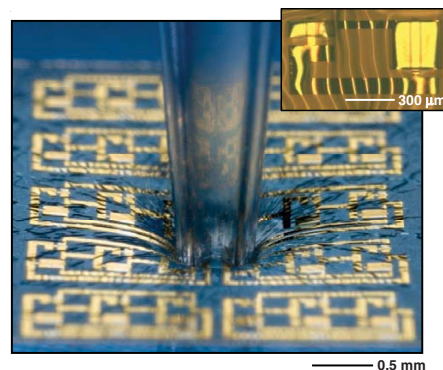


Figure 1.26: Stretchable silicon circuit in a wavy geometry compressed in its center by a glass capillary tube (main) and wavy logic gate built with two transistors (top right inset).

An example of a selectively bonded integrated circuit is shown in Figure 1.27 containing ribbon cables of metal and plastic interconnecting silicon devices. The circuit is conformally integrated onto a model of a fingertip as an example of a surface whose nonzero Gaussian curvature would be impossible to wrap with a system that is only flexible.

By use of these techniques, integrated circuits forming a digital camera based on arrays of silicon photodetectors can be achieved. They can be as small and adjusted to the shape of the human retina. Such a design offers enhanced field of view and uniformity in illumination compared to a comparable planar detector. These ideas create new engineering options in imaging devices where the geometry of the detector array can be optimized together with the lens configuration (Figure 1.28). Ultimately such devices might be used as retinal implants or as active components on the eye to restore or enhance vision (Figure 1.29).

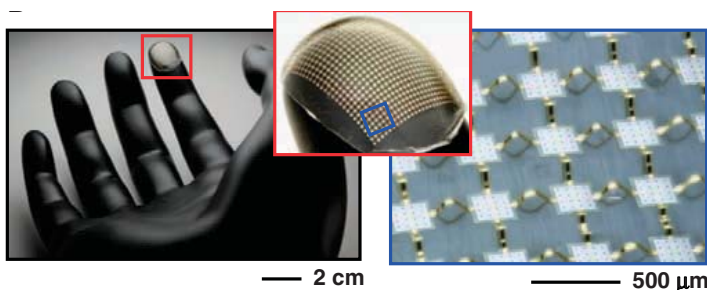


Figure 1.27: Stretchable silicon circuit with a mesh design, wrapped onto a model of a fingertip.

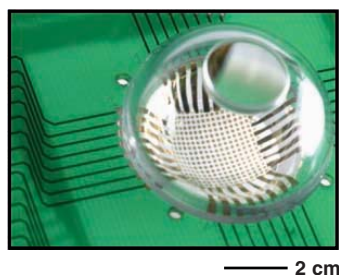


Figure 1.28: Electronic eyeball camera that uses a hemispherically curved array of silicon photodetectors.

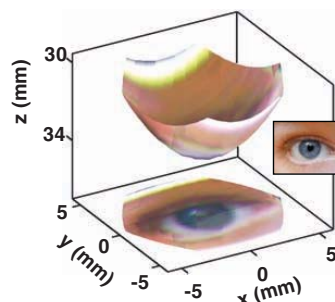


Figure 1.29: Picture collected with a similar camera that uses a paraboloid design.

1.2.4 Elastic power supplies

In [39], a solution for integrating a stretchable power supply is presented. Dry gel cells are demonstrated withstanding stretch ratios up to 100% before failure.

These cells deliver open circuit voltages close to 1.5 V and short circuit currents up to 30 mA, a lifetime of more than 1000 h and capacities of 3.5 mAh cm^{-2} active area. Making these cells ultra-compliant is not a trivial task since the batteries are not allowed to be internally short-circuited upon mechanical stretching. Therefore, the concept is based on the integration of highly elastic carbon black silicon oil paste electrodes into a stretchable acrylic elastomer. In Figure 1.30, a scheme of the cell is shown where the anode consists of a printed paste consisting of 33% Zn, 9% carbon black and 58% xanthan gel (0.1% xanthan dissolved in purified water), whereas the printed cathode consists of a 24% MnO_2 , 8% carbon black

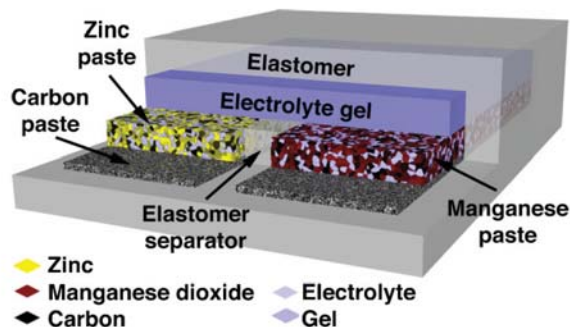


Figure 1.30: Scheme of a compliant zinc carbon dry gel cell. The cell is based on pastes as electrodes, chemically active cells and an electrolyte gel to close the circuit. Intermixing of the chemicals and short-circuiting of the electrochemical power supply are prohibited by laterally separating the electrodes with an elastomer separator.

and 68% electrolyte paste. To avoid the mixing of the chemicals upon stretching it, it is crucial to laterally separate the two 1 cm^2 Zn and MnO_2 containing electrodes by a distance of 0.3 cm. During uniaxially stretching the device to an extent of 20% the batteries were functional after as much of 100 cycles. These batteries can be easily arranged in arrays, with stretchable interconnections they can be connected in parallel to enhance the output current or in series to enhance the voltage. Figure 1.31 shows such a realization of 2 dry gel cells in series for powering a SMD light emitting diode.

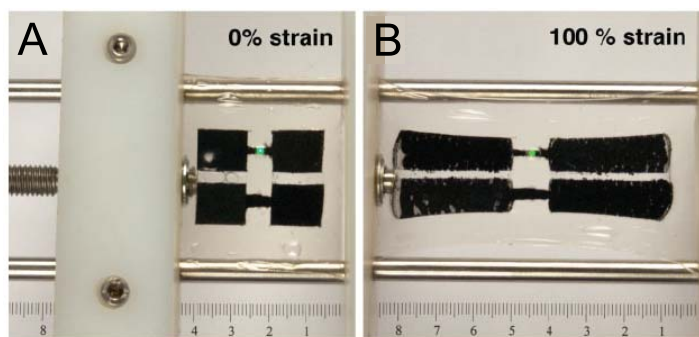


Figure 1.31: Realization of 2 dry gel cells in series for powering a SMD light emitting diode. a) Photo of the circuit prior to the stretch experiments b) At 100% strain.

The performance of these ultra-compliant batteries has been characterized. In Fi-

Figure 1.32 a the self-discharge of a gel cell as decay of the open circuit voltage is shown. Extrapolation suggests that such cells can work up to much more than 1000h. The capacity of the power supply is shown in Figure 1.32 b where the decay of the output voltage is recorded for a constant current load of 1mA. Following current practice the capacity is recorded when the battery voltage drops to 0.8V, which results in a typical capacity of 7 mAh for a Zn and MnO₂ electrode area of 2 cm² at 0% strain (black triangles). A reduced capacity of 3.1 mAh is found for a 50% strained battery (red squares), most likely caused by conductive losses within the permanently stretched electrodes of the element. Figure 1.32 c shows the load curves of 2 batteries at 0% and 50% strain. Short circuit currents of 20-30 mA are easily feasible. Figure 1.32 b shows the open circuit voltage of a battery versus stretch ratio (up to 100% of the initial length). Open circuit voltage is insensitive to stretching. The diagram for the short circuit current shows an irreversible decrease in the first cycle from 25 to around 10 mA. This is due to depercolation effects in the electrodes at high strain levels. Such irreversible effects are much less pronounced at strain levels below 50%.

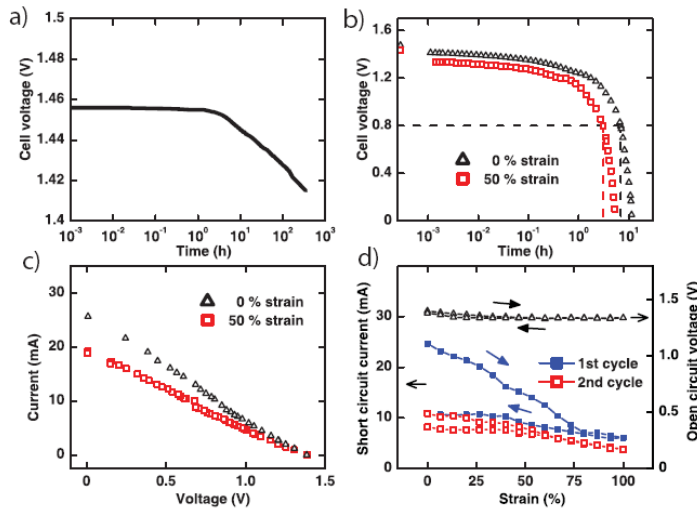


Figure 1.32: (a) Self-discharge of an electrochemical cell by monitoring the open circuit voltage versus time. (b) Capacities of compliant power supplied without strain (black triangles) and with 50% strain (red squares). Following common notation, the capacity is determined when the cell voltage drops to 0.8V. (c) Load curves of the batteries at 0% strain (black triangles) and 50% strain (red squares), short circuit currents of 20-30 mA are achieved. (d) Open circuit voltage versus strain up to 100% (black triangles). Short circuit currents versus stretch for two stretch cycles. Blue filled squares: first cycle, red empty squares: second cycle.

1.3 Scope of this PhD work

The objective of this PhD is the development of stretchable electronics technologies for large area applications for use in health care, wellness and functional clothes, and for integrated electronics in stretchable parts and products. Stretchable electronics include the integration of electronic components, energy supply, sensors, actuators or display and switches on a stretchable substrate with stretchable conductors.

In case of wearable electronics on the human body, the electronic circuit must be thin and flexible, but even more stretchable and pliable in order to follow the shape and the movement of the human body for optimal mobility and comfort. In washable functional clothes an integrated stretchable electronic system has to withstand several cleaning processes.

Apart from consumer's needs for 'on-the-body' applications, a stretchable electronic technology can also serve many other applications where the ability to stretch is an asset. The need for miniaturization due to restriction of installation space in industrial and automotive applications opens up the market for mechatronic systems. In mechatronic parts mechanical functions are combined with electronic functions. This approach saves space and increases performance significantly. The scope of elastomeric mechanical products, which up to now cannot be properly designed as a mechatronic system with the electronics as an integral part, is almost endless. Products like rubber seals and vibration dampers with rubber body cannot properly be designed as a true mechatronic system due to the missing of stretchable electronics. Motion detection (person and vehicle tracking) and illumination in rubber flooring or failure recognition on rubber membranes are other possible applications for stretchable substrates.

In this PhD, the following challenges will be tackled:

- A new stretchable flex substrate with stretchable conductors
- Assembling technology adapted for stretchable substrates
- Integration methods for stretchable electronics in elastomeric parts
- Manufacturing methods for stretchable electronic systems

The purpose is to use existing base substrate materials that are new for the electronic interconnection technology. On these base materials, stretchable conductors will be somehow deposited. The ability to stretch conductors will be achieved by choosing suitable thicknesses and layouts of 'classic' metallic conductors that can be stretched to a certain degree. Examples are very narrow tracks (compared to wires) and serpentine-like tracks. By embedding the tracks into a stretchable material, better reliability will be achieved, and this will also

offer the possibility of multilayer interconnection. Adequate patterning or structuring of the conductors, and (laser) via technology will allow complex electronic systems to be made on stretchable substrates. Lines and spaces of $125\mu\text{m}$ are envisaged. Compared to state-of-the-art printed circuits (rigid and especially flex), this is not a very high density interconnection, but taken into account the very special substrate materials and stretchability requirements, this target certainly is challenging.

Another important issue will be the development of an assembly technology for electronic components (bare dies, packaged dies, sensors, connectors, passives) onto the substrate. Minimum connector pitch would be 0.5 mm and minimum component I/O pitch is 0.5 mm. These values are state-of-the-art in rigid and flex assemblies, and hence especially challenging on stretchable substrates. But as rather small components of max. 5×5 mm (but preferably smaller) are considered (in order to facilitate conformal shaping to the body or other irregular forms), the assembly on these small pitches should be feasible.

The system solution to realize such conformable systems by use of standard, rigid electronic components will be based on a hybrid design of small rigid or less stretchable and/or flexible parts (islands) with stretchable interconnections between them. The size of the islands should of course not lower the comfort of wearing or using the stretchable electronic system. A methodology for this system approach, depending on complexity of the system and of the available technology, will be handled. Special attention must be given to the compliance between the islands and the stretchable substrate to ensure robust and long lasting interconnections.

The technology developments in this PhD have been supported by modeling activities (mechanical). Models are essential for stretchable design, technology validation, and for evaluation and testing (especially reliability testing). Results from these modeling activities will be mentioned in this PhD work as support and insight in the mechanical aspects of stretchable electronic systems. More detailed and elaborated descriptions and explanations can be found in published papers of Mario Gonzalez and most of the findings will be covered in the PhD work of Hsu Yung Yu.

Throughout the technology platform development, the manufacturability and cost will be the leading themes, as these are essential for future exploitation of the technology and wide spread use in the consumer, professional and disposables market, which all demand low prices.

The technology platform for stretchable substrates and systems will be demonstrated by realizing some functional demonstrators in different application areas: wellness, healthcare, sports,...

1.4 Research context

The research which formed the base of this dissertation was carried out within the framework of following projects:

STELLA (Stretchable Electronics for Large Area Applications)

European IST-Project, Framework 6, 4th call

Starting date: February 1, 2006

Finishing date: January 31, 2010

Project coordinator: Dr. Christopher Klatt (Freudenberg, Germany)

Partners: Freudenberg, IMEC, TU Berlin, CEA, Philips, QPI, BESI, Verhaert, Urgo, Fundico, NXP, TNO.

Innovations from the proposed STELLA project include:

- New stretchable substrates with stretchable conductor pattern.
- Assembly technology on stretchable substrates, based on lead-free reflow soldering.
- Integration methods for electronics in stretchable products.

BIOFlex (BIOcompatible Flexible Electronic Circuits)

Strategic Basic Research Proposal IWT 040101, Call 2004

Starting date: October 1, 2004

Finishing date: September 7, 2010

Project coordinator: Prof. Dr. ir. Jan Vanfleteren (IMEC/UGent/CMST, Belgium)

Partners: IMEC, PMRG UGent, MICAS ESAT KULeuven.

Innovations from the proposed BIOFlex project include:

- Development of stretchable flex interconnection circuits with metal and/or polymer conductors.
- Development of embedding and assembly technologies for a wide range of components, in/on the stretchable flex, giving the circuit a high functionality and reliability, combined with a high compactness.

Place-It (Platform for Large Area Conformable Electronics by Integration)

European IST-Project, Framework 7, 4th call

Starting date: February 1, 2010

Finishing date: January 31, 2013

Project coordinator: Dr. Liesbeth van Pieteron (Philips Research, The Netherlands)

Partners: Philips Research, TNO, TU Berlin, IMEC, Centexbel, TITV Greiz, Philips Lighting, Grupo Antolin, Zentrum für Medizinische Forschung, RZTH Aachen, Ohmatex.

Innovations from the proposed Place-It project include:

- A technology platform, offering foil based, stretch based and fabric based building blocks that can be connected to form a system.
- Building blocks in foil, stretch and fabric technologies will be adapted so that they fit the technology platform and the interfacing with other building blocks.

Pasta (Integrating Platform for Advanced Smart Textile Applications)

European IST-Project, Framework 7, 5th call

Starting date: October 1, 2010

Finishing date: September 30, 2014

Project coordinator: ir. Johan De Baets (IMEC/UGent/CMST, Belgium)

Partners: IMEC, CEA-LETI, Fraunhofer-Gesellschaft, STFI, CSEM, PEP, ETTLIN, CTX, SPS.

Innovations from the proposed Pasta project include:

- Development of a stretchable interposer package for implementation in textiles.

Integrated Elastic Microsystems for Cerebral Electromodulation

FWO Project

Starting date: September 1, 2007

Finishing date: August 31, 2010

Project coordinator: Prof. Dr. ir. Jan Vanfleteren (IMEC/UGent/CMST, Belgium)

Innovation from the proposed Integrated Elastic Microsystems for Cerebral Electromodulation project include:

- Development of stretchable flex interconnection circuits with metal and/or polymer conductors.

1.5 Research dissemination

Journal papers

- F. Bossuyt, T. Vervust, J. Vanfleteren. Stretchable Electronics Technology For Large Area Applications: Fabrication and Mechanical Characterization. Submitted for publication in *IEEE Transactions on Advanced Packaging*.
- F. Bossuyt, J. Günther, T. Löher, M. Seckel, T. Sterken, J. de Vries. Cyclic endurance reliability of stretchable electronic substrates. Accepted for publication in *Microelectronics Reliability*.
- Y. Hsu, M. Gonzalez, F. Bossuyt, F. Axisa, J. Vanfleteren, I. De Wolf. The effects of Encapsulation on Deformation Behavior and Failure Mechanisms of Stretchable Interconnects. Accepted for publication in *Thin Solid Films*.
- Y. Hsu, M. Gonzalez, F. Bossuyt, F. Axisa, J. Vanfleteren, I. De Wolf. Pitch Effect on Deformation Behavior and Stretching-Induced Failure of Polymer-Encapsulated Stretchable Circuit. *Journal of Micromechanics and Microengineering*, vol. 20, no. 7, 2010.
- Y. Hsu, M. Gonzalez, F. Bossuyt, F. Axisa, J. Vanfleteren, B. Vandeveld, I. De Wolf. Design and analysis of a novel fine pitch and highly stretchable interconnect. *Microelectronics International*, vol. 27, no. 1, pp. 33-38, 2010.
- M. Gonzalez, F. Axisa, F. Bossuyt, Y. Hsu, B. Vandeveld, J. Vanfleteren. Design and performance of metal conductors for stretchable electronic circuits. *Circuit world*, vol. 35, no. 1, pp. 22-29, 2009.
- Y. Hsu, M. Gonzalez, F. Bossuyt, F. Asixa, J. Vanfleteren, I. De Wolf. A novel interconnect design with high stretchability and fine pitch capability for applications in stretchable electronics. *Applied Physics Letters*, 2009.
- Y. Hsu, M. Gonzalez, F. Bossuyt, F. Asixa, J. Vanfleteren, I. De Wolf. In situ observations on deformation behaviour and stretching-induced failure of fine pitch stretchable interconnect. *Journal of Materials Research*, 2009.
- J. Govaerts, J. Robbelein, M. Gonzalez, I. Gordon, K. Baert, I. De Wolf, F. Bossuyt, S. Van Put and J. Vanfleteren. Developing an advanced module for back-contact solar cells. Submitted to *IEEE Transactions on Advanced Packaging*.

Proceedings of International Conferences

- Y. Hsu, B. Dimcic, M. Gonzalez, F. Bossuyt, J. Vanfleteren, I. De Wolf, Reliability Assessment of Stretchable Interconnect. *Proceedings of the International*

Microsystems, Packaging, Assembly and Circuits technology conference, (Taipei, Taiwan), October 2010.

- J. Govaerts, J. Robbelein, C. Gong, B. Pawlak, F. Bossuyt, S. Van Put, I. Gordon, K. Baert, J. Vanfleteren. Performance of a New Type of Module Based on Back-Contact Solar Cells. *Proceedings of the SPIE Optics+Photonics Conference*, San Diego, USA, August 2010
- F. Bossuyt, T. Vervust, F.Axisa, J. Vanfleteren. Improved Stretchable Electronics Technology for Large Area Applications. *Proceedings of MRS Spring meeting*, Symposium JJ, (San Francisco, USA), April 2010.
- F. Bossuyt, T. Vervust, F.Axisa, J. Vanfleteren. From Single Conductive Layer to Double Conductive Layer Stretchable Electronics. *Proceedings of MRS Spring meeting 2010*, Symposium JJ, (San Francisco, USA), April 2010.
- T. Sterken, F. Bossuyt, R. Verplancke, T. Vervust, F.Axisa, J. Vanfleteren. Lifetime of Stretchable Meander-Shaped Copper Conductors in PDMS Subjected to Cyclic Elongation. *Proceedings of MRS Spring meeting 2010*, Symposium JJ, (San Francisco, USA), April 2010.
- R. Verplancke, F. Bossuyt, T. Sterken, J. Vanfleteren. Thin-film Interconnection Technology for Use in a Stretchable Cell Culture Platform. *Proceedings of MRS Spring meeting 2010*, Symposium JJ, (San Francisco, USA), April 2010.
- M. Gonzalez, B. Vandeveld, W. Christiaens, Y. Hsu, F. Iker, F. Bossuyt, J. Vanfleteren, O. Van der Sluis, P.H.M. Timmermans. Thermo-Mechanical Analysis of Flexible and Stretchable Systems. *Proceedings of the 11th Annual IEEE EUROSIME Conference*, Bordeaux, France, April 2010
- D. Brosteaux, E. Lippens, R. Cornelissen, E. Schacht, R. Carta, P. Jourand, R. Puers, F. Axisa, T. Vervust, F. Bossuyt, J. Vanfleteren. In vitro cytotoxicity testing and the application of elastic interconnection technology for short-term implantable electronics. *31th Int. Conf of the IEEE Eng. in Medicine and Biology Society (IEEE EMBC 2009)*, (Minneapolis, Minnesota, USA), September 2009.
- F. Bossuyt, T. Vervust, F. Axisa, J. Vanfleteren. A new low cost, elastic and conformable electronics technology for soft and stretchable electronic devices by use of a stretchable substrate. *Proceedings of the European Microelectronics and Packaging Conference (EMPC 2009)*, (Rimini, Italy), June 2009.
- Y. Hsu, M. Gonzalez, F. Bossuyt, F. Axisa, J. Vanfleteren, I. De Wolf. A novel interconnect design with high stretchability and fine pitch capability for applications in stretchable electronics. *Proceedings of MRS Spring meeting*, Symposium PP, (San Francisco, USA), April 2009.

- M. Gonzalez, F. Axisa, F. Bossuyt, Y. Hsu, B. Vandeveldel, J. Vanfleteren. Design and performance of metal conductors for stretchable electronic circuits. *Proceedings of the 2nd Electronics System Integration Technology Conference (ESTC 2008)*, (Greenwich, UK), pp. 371-376, September 2008.
- F. Axisa, F. Bossuyt, T. Vervust, J. Vanfleteren. Laser based fast prototyping methodology of producing stretchable and conformable electronic systems. *Proceedings of the 2nd Electronics System Integration Technology Conference (ESTC 2008)*, (Greenwich, UK), pp. 1387-1390, September 2008.
- F. Axisa, F. Bossuyt, J. Missinne, R. Verplancke, T. Vervust, J. Vanfleteren. Stretchable engineering technologies for the development of advanced stretchable polymeric system. *Proceedings of the 7th International IEEE Conference on Polymers and Adhesives in Microelectronics and Photonics (Polytronic)*, (Garmisch-Partenkirchen, Germany), August 2008.
- B. Kuyken, W. Verstichel, F. Bossuyt, J. Vanfleteren, M. Demey, M. Leman. The HOP sensor: wireless motion sensor. *Proceedings of the 8th International Conference on new interfaces for musical expression (NIME)*, (Genova, Italy), June 2008.
- M. Demey, M. Leman, L. De Bruyn, F. Bossuyt, J. Vanfleteren. The musical synchrotron: using wireless motion sensors to study how social interaction affects synchronization with musical tempo. *Proceedings of the 8th International Conference on new interfaces for musical expression (NIME)*, (Genova, Italy), June 2008.
- F. Axisa, D. Brosteaux, E. De Leersnyder, F. Bossuyt, J. Vanfleteren, B. Hermans, R. Puers. Biomedical stretchable systems using MID based stretchable electronics technology. *Proceedings of the 29th Annual International Conference of the IEEE Engineering in Medicine and Biology Society*, (Lyon, France), pp. 5687-5690, August 2007.
- F. Axisa, D. Brosteaux, E. De Leersnyder, F. Bossuyt, M. Gonzalez, N. De Smet, J. Vanfleteren. Low cost, biocompatible elastic and conformable electronic technologies using MID in stretchable polymer. *Proceedings of the 29th Annual International Conference of the IEEE Engineering in Medicine and Biology Society*, (Lyon, France), pp. 6592-6595, August 2007.
- F. Axisa, D. Brosteaux, E. De Leersnyder, F. Bossuyt, M. Gonzalez, M. Vanden Bulcke, and J. Vanfleteren. Low cost elastic and conformable electronic circuits and assemblies using MID in stretchable polymer. *Proceedings of the 16th European Microelectronics and Packaging Conference (EMPC)*, (Oulu, Finland), pp. 691-696, June 2007.

- F. Axisa, D. Brosteaux, E. De Leersnyder, F. Bossuyt, M. Gonzalez, M. Vanden Bulcke, J. Vanfleteren, Elastic and conformable electronic circuits and assemblies using MID in polymer. *Proceedings of the 6th International IEEE Conference on Polymers and Adhesives in Microelectronics and Photonics*, (Tokio, Japan), pp. 280-286, January 2007.

Proceedings of National Conferences

- F. Bossuyt, T. Vervust, F. Axisa, J. Vanfleteren. Stretchable electronics for ambient applications. *2nd Flex- and Stretch workshop*, (Ghent, Belgium), October 2009.
- F. Bossuyt, T. Vervust, F. Axisa, J. Vanfleteren. Stretchable electronics for ambient applications. *8th Belgian Day on Biomedical Engineering*, (Brussels, Belgium), October 2009.

The following patents have been filed

- F. Axisa, J. Vanfleteren, F. Bossuyt. Semi-stretchable connection between stretchable and flexible circuitry, US Provisional Application, IMEC reference number 2008/017, filed February, 2009.
- F. Axisa, J. Vanfleteren, F. Bossuyt. Stretchable electronic device, PCT application number PCT/EP2009/054353, filed April 10, 2009.
- J. Vanfleteren, F. Bossuyt, F. Axisa. Elastic electrical interconnections through conductor support and stretch stop integration, US Provisional Application, IMEC reference number 2008/100, filed February, 2009.

References

- [1] H. Lee D. Khang, J. Rogers. Mechanical Buckling: Mechanics, Metrology, and Stretchable Electronics. *Advanced Functional Materials*, 19(10):1526–1536, May 22 2009.
- [2] A. Baca, J. Ahn, Y. Sun, M. Meitl, E. Menard, H. Kim, W. Choi, D. Kim, , Y. Huang, J. Rogers. Semiconductor wires and ribbons for high-performance flexible electronics. *Angewandte Chemie-International Edition*, 47(30):5524–5542, 2008.
- [3] J. Rogers D. Kim. Stretchable Electronics: Materials Strategies and Devices. *Advanced Materials*, 20(24):4887–4892, Dec 17 2008.
- [4] D. Kim, J. Xiao, J. Song, Y. Huang, J. Rogers. Stretchable, Curvilinear Electronics Based on Inorganic Materials. *Advanced Materials*, 22(19):2108–2124, May 18 2010.
- [5] J. Rogers, T. Someya, Y. Huang. Materials and Mechanics for Stretchable Electronics. *Science*, 327(5973):1603–1607, Mar 26 2010.
- [6] D. Kim, Y. Kim, J. Wu, Z. Liu, J. Song, H. Kim, Y. Huang, K. Hwang, J. Rogers. Ultrathin Silicon Circuits With Strain-isolation Layers and Mesh Layouts for High-Performance Electronics on Fabric, Vinyl, Leather, and Paper. *Advanced Materials*, 21(36):3703+, Sep 25 2009.
- [7] D. Khang, J. Rogers, H. Lee. Mechanical Buckling: Mechanics, Metrology, and Stretchable Electronics. *Advanced Functional Materials*, 19(10):1526–1536, May 22 2009.
- [8] J. Rogers Y. Sun. Structural forms of single crystal semiconductor nanoribbons for high-performance stretchable electronics. *Journal Of Materials Chemistry*, 17(9):832–840, Mar 7 2007.
- [9] S.P. Lacour, S. Wagner, Z.Y. Huang, Z. Suo. Stretchable gold conductors on elastomeric substrates. *Applied Physics Letters*, 82(15):2404–2406, Apr 14 2003.

REFERENCES

37

- [10] S.P. Lacour, J. Jones, Z. Suo, S. Wagner. Design and performance of thin metal film interconnects for skin-like electronic circuits. *IEEE Electron Device Letters*, 25(4):179–181, Apr 2004.
- [11] S.P. Lacour, J. Jones, S. Wagner, T. Li, Z.G. Suo. Stretchable interconnects for elastic electronic surfaces. *Proceedings of the IEEE*, 93(8):1459–1467, Aug 2005.
- [12] P. Mandlik, S.P. Lacour, J. Li, S. Chou, S. Wagner. Fully elastic interconnects on nanopatterned elastomeric substrates. *IEEE Electron Device Letters*, 27(8):650–652, Aug 2006.
- [13] I.M. Graz, D.P.J. Cotton, S.P. Lacour. Extended cyclic uniaxial loading of stretchable gold thin-films on elastomeric substrates. *Applied Physics Letters*, 94(7):071902 (3 pp.), 16 February 2009.
- [14] T. Adrega, S.P. Lacour. Stretchable gold conductors embedded in PDMS and patterned by photolithography: fabrication and electromechanical characterization. *Journal Of Micromechanics And Microengineering*, 20(5), May 2010.
- [15] H. Kevin, R. Dinyari, G. Lanzara, K. Jong Yon, F. Jianmin, C. Vancura, C. Fu-Kuo, P. Peumans. An approach to cost-effective, robust, large-area electronics using monolithic silicon. In *2007 IEEE International Electron Devices Meeting - IEDM '07*, pages 217–20, 2007 2007.
- [16] R. Dinyari, S. Rim, K. Huang, P. Catrysse, P. Peumans. Curving monolithic silicon for nonplanar focal plane array applications. *Applied Physics Letters*, 92(9), Mar 3 2008.
- [17] D.S. Gray, J. Tien, C.S. Chen. High-conductivity elastomeric electronics. *Advanced Materials*, 16(5):393+, Mar 5 2004.
- [18] J. So, J. Thelen, A. Qusba, G. Hayes, G. Lazzi, M. Dickey. Reversibly Deformable and Mechanically Tunable Fluidic Antennas. *Advanced Functional Materials*, 19(22):3632–3637, Nov 23 2009.
- [19] S. Cheng, Z. Wu, P. Hallbjorner, K. Hjort, A. Rydberg. Foldable and Stretchable Liquid Metal Planar Inverted Cone Antenna. *IEEE Transactions On Antennas And Propagation*, 57(12):3765–3771, Dec 2009.
- [20] D. Kim, Z. Liu, Y. Kim, J. Wu, J. Song, H. Kim, Y. Huang, K. Hwang, Y. Zhang, J. Rogers. Optimized Structural Designs for Stretchable Silicon Integrated Circuits. *Small*, 5(24):2841–2847, Dec 4 2009.
- [21] K. Dahl-Young, J. Hanqing, H. Young, J. Rogers. A stretchable form of single-crystal silicon for high-performance electronics on rubber substrates. *Science*, 311(5758):208–12, 13 January 2006.

- [22] S.P. Lacour, C. Tsay, S. Wagner. An elastically stretchable TFT circuit. *IEEE Electron Device Letters*, 25(12):792–794, Dec 2004.
- [23] S.P. Lacour, S. Wagner. Thin film transistor circuits integrated onto elastomeric substrates for elastically stretchable electronics. In *International Electron Devices Meeting 2005 (IEEE Cat. No.05CH37703C)*, page 4 pp., 2005 2005.
- [24] H. Gleskova, S. Wagner. Amorphous silicon thin-film transistors on compliant polyimide foil substrates. *IEEE Electron Device Letters*, 20(9):473–475, Sep 1999.
- [25] A. Ostmann, R. Viero, M. Seckel, T. Löher, H. Reichl. Stretchable circuit board technology in textile applications. In *2009 4th International Microsystems, Packaging, Assembly and Circuits Technology Conference (IMPACT)*, pages 216–19, 2009 2009.
- [26] T. Löher, M. Seckel, R. Viero, C. Dils, C. Kallmayer, A. Ostmann, R. Aschenbrenner, H. Reichl. Stretchable electronic systems: realization and applications. In *2009 11th Electronics Packaging Technology Conference (EPTC 2009)*, pages 893–8, 2009 2009.
- [27] R. Viero, T. Löher, M. Seckel, C. Dils, C. Kallmayer, A. Ostmann, H. Reichl. Stretchable Circuit Board Technology and Application. In *2009 International Symposium On Wearable Computers, Proceedings*, IEEE International Symposium on Wearable Computers, pages 33–36, 2009. 13th International Symposium on Wearable Computers, Linz, AUSTRIA, SEP 04-07, 2009.
- [28] T. Löher, R. Viero, M. Seckel, A. Ostmann, H. Reichl. Stretchable electronic systems for wearable and textile applications. In *2008 IEEE 9th VLSI Packaging Workshop in Japan*, pages 9–12, 2008 2008.
- [29] B. Schmied, J. Guenther, C. Klatt, H. Kober, E. Raemaekers. STELLA - STretchable ELEctronics for Large Area applications - A new technology for smart textiles. volume 60, pages 67–73, 2009. 3rd International Conference on Smart Materials, Structures and Systems, Acireale, ITALY, JUN 08-13, 2008.
- [30] K.L. Lin, K. Jain. Design and Fabrication of Stretchable Multilayer Self-Aligned Interconnects for flexible Electronics and Large-Area Sensor Arrays Using Excimer Laser Photoablation. *IEEE Electron Device Letters*, 30(1):14–17, Jan 2009.
- [31] K.L. Lin, K. Jain. Stretchable multilayer self-aligned interconnects fabricated using excimer laser photoablation and in situ masking. In *Proceedings of the SPIE - The International Society for Optical Engineering*, volume 7204, page 720409 (12 pp.), 2009 2009.

REFERENCES

39

- [32] J. Siegel, K. Ettrich, E. Welsch, E. Matthias. UV-laser ablation of ductile and brittle metal films. *Applied Physics A-Materials Science & Processing*, 64(2):213–218, Feb 1997.
- [33] R. Srinivasan, R.R. Hall, W.D. Löhle, W.D. Wilson, D.C. Allbee. Chemical-Transformations Of The Polyimide Kapton Brought About By Ultraviolet-Laser Radiation. *Journal of Applied Physics*, 78(8):4881–4887, OCT 15 1995.
- [34] T. Sekitani, T. Someya. Stretchable, Large-area Organic Electronics. *Advanced Materials*, 22(20):2228–2246, MAY 25 2010.
- [35] T. Sekitani, T. Someya. Large-area stretchable organic transistor integrated circuits for sensor and display applications. In *Proceedings of the SPIE - The International Society for Optical Engineering*, volume 7418, page 74180Q (15 pp.), 2009 2009.
- [36] T. Sekitani, T. Someya. Stretchable, printable organic transistor integrated circuits for large-area sensors and displays. In *LEOS 2008 - 21st Annual Meeting of the IEEE Lasers and Electro-Optics Society (LEOS 2008)*, pages 198–9, 2008 2008.
- [37] T. Someya, T. Sakurai, T. Sekitani. Flexible, large-area sensors and actuators with organic transistor integrated circuits. In *International Electron Devices Meeting 2005 (IEEE Cat. No.05CH37703C)*, page 4 pp., 2005 2005.
- [38] T. Someya, T. Sakurai, T. Sekitani. Flexible, large-area sensors and actuators with organic transistor integrated circuits. In *IEEE International Electron Devices Meeting 2005, Technical Digest*, International Electron Devices Meeting, pages 455–458, 2005. IEEE International Electron Devices Meeting, Washington, DC, DEC 05-07, 2005.
- [39] M. Kaltenbrunner, G. Kettlgruber, C. Siket, R. Schwoediauer, S. Bauer. Arrays of Ultracompliant Electrochemical Dry Gel Cells for Stretchable Electronics. *Advanced Materials*, 22(18):2065+, May 11 2010.

Chapter 2

Introduction to concepts related to elastic microsystems

Before we start with presenting the developed technologies, the reader gets an overview of the architecture and design methodology we used in order to create these stretchable electronic systems. These systems will be embedded in a stretchable polymer. Therefore, an introduction on polymers is given including the characterization of PDMS. In order to have an idea of the basic mechanical aspects related to stretchable electronics, an overview is given of knowledge that has been developed before and during this PhD work, based on the developed technologies.

2.1 System architecture and methodology

A picture says more than thousands words. We cannot better start the description of the architecture of a stretchable electronic system by showing a picture (Figure 2.1) of a typical stretchable device we have in mind. An electronic system will be split up into some functional islands which are spread over a large surface. The functional islands contain the sensors, micro-electronic devices,... which are made from standard, off-the-shelf components, mainly SMD components. The system can include batteries, switches, buttons,... all concentrated on the islands. They are connected with stretchable interconnections acting as electrical signal and power paths.

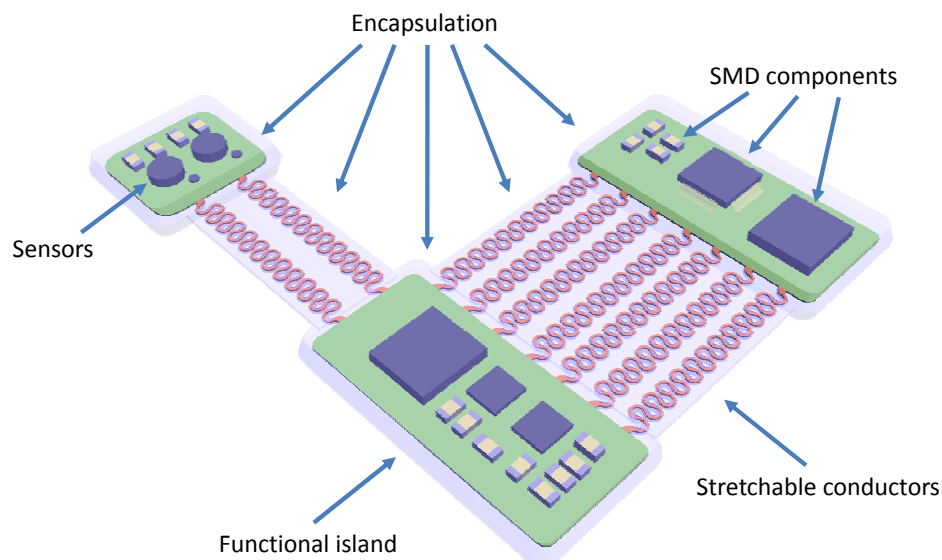


Figure 2.1: Stretchable circuit system architecture.

The developing methodology of the different technologies described in this PhD work, was setup having the following things in mind:

- Use of pre-existing PCB manufacturing technologies in order to make the transfer to an industrial environment easier.
- Trying to make the process flow as much as possible independent of the embedding material. The elastomer should be involved at the end of the process.
- A stretchable electronics technology for applications with elasticity upto 10-15%.
- Possibility to use the technology in textile and biomedical applications.

2.2 Polymers

The main difference between a standard printed circuit board (PCB) or a flexible circuit board (FCB) and the stretchable electronics technologies presented, is that everything will be embedded in a stretchable polymer in order to achieve the required stretchability (10-15%). Besides inducing stretchability of the system,

42 Introduction to concepts related to elastic microsystems

depending on the application the embedding polymer will also serve as protection of the electronic components against moisture, body fluids (blood, sweat,...), etc. The choice of this polymer will have a big impact on the durability of the system. Furthermore, due to processability and system reliability reasons, we will use a flexible polymer in order to mechanically support the electronic structures and components. The necessity will become clear during the presentation of the different technologies.

A polymer is a substance, having molecules which consist of a large number of low molecular monomer residues being connected by primary bonds. If A is a monomer molecule, then a polymer molecule is represented by:



where n is an integer, called the degree of polymerization of this polymer molecule, and -A- is also called the repeating unit. Monomers are low molecular weight compounds that can react with each other and with another monomer molecule, i.e. they polymerize to a polymer molecule. In this section, we will first give some of the main basic characteristics of polymers concerning their build-up, the polymerization mechanism and the main physical properties.

Polymers can be classified by chain structure, by polymerization mechanism or by thermal behaviour [1].

2.2.1 Classification by chain structure

If we classify polymers by chain structure, we can distinguish four different groups, which are schematically shown in Figure 2.2:

- Linear polymers: the structural unit is chainwise bonded. The molecular chains of a linear polymer may be intertwined, but the forces tending to hold the molecules together are physical rather than chemical and thus can be weakened by energy applied in the form of heat. They are thermoplastics like PVC, nylon.
- Branched polymers: the polymer is built-up of branched macromolecules.
- Polymer networks: the polymer chains are bonded to each other, forming a 3D network.
- Ladder polymers: there is a repetition of crosslinks between two chains.

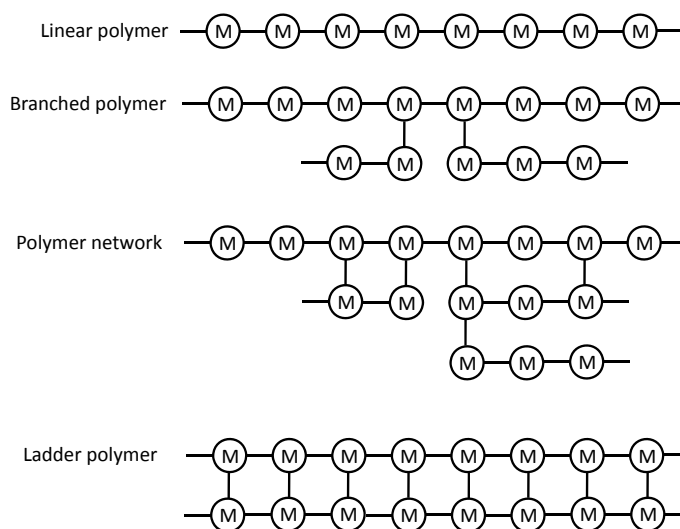


Figure 2.2: Classification of polymers by their chain structure.

2.2.2 Classification by polymerization structure

The original classification involves condensation polymerization, during which a low molecular weight molecule (e.g. H_2O) is split off, and addition polymerization, in which case this doesn't happen. A good way to distinguish the two mechanisms is to consider the polymerization mechanism as such: at the beginning of a condensation polymerization the whole system gradually transforms into a mixture of short chains (monomer, dimer, trimer, etc.) whereas at the beginning of the addition polymerization only a few, but very long, chains are formed. Besides these long chains only unreacted monomer is present. In later stages of the reaction, newly formed chains cannot attain the same length, so that the overall average degree of polymerization of the formed polymer gradually decreases during the addition polymerization.

2.2.3 Classification by thermal behaviour

In view of processing of polymers for consumer products, this is an important classification. Polymers can be subdivided in thermosets and thermoplastics.

A thermoset is a type of plastic that undergoes a chemical change during production that cannot be repeated or reversed. The way this happens is called cross-linking. This process results in permanent chemical bonding of the individual polymer chains to one another. These materials can never be reshaped

44 Introduction to concepts related to elastic microsystems

into a new form with the same chemical composition by heating and mixing as the other type of polymers can. Some examples of materials made of thermosets are fiberglass boats or showers, foam insulation and epoxy glues.

A thermoplastic is a material that can be processed many times without a chemical change in or bonding between the chains of the polymer. Because there is no chemical change, these materials can be melted again and again and reformed as many times as desired. (There is one flaw in this statement: many polymers degrade during processing because of the high temperatures used in the process. This degradation is a chemical process that cannot be reversed and is guarded against by the use of stabilizers.) Because they can be processed many times, these materials are the backbone of the plastics recycling industry. 90 weight percent of the processed polymers are thermoplastics. Examples are polyethylene (PE), polyvinylchloride (PVC) and polypropylene (PP).

2.2.4 Embedding material: silicone

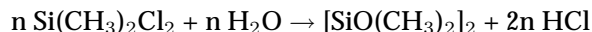
Chemical structure

The basic raw material for the silicone industry is silica - a plentiful, naturally occurring resource in the form of sand. The name 'silicone' was given in 1901 by Kipping to describe new compounds of the formula R_2SiO . These were rapidly identified as being polymeric and actually corresponding to polydialkylsiloxanes. Among them, the most common are polydimethylsiloxanes (PDMS), trimethylsilyloxy terminated. The chemical formula for PDMS is

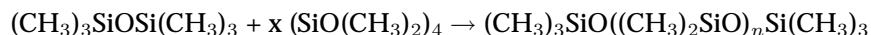


and being graphically shown in Figure 2.3, where n is the number of repeating monomer $[SiO(CH_3)_2]$ units.

In summary, PDMS is industrially synthesised from the hydrolysis of dimethyl dichlorosilane Me_2SiCl_2 , which leads to a mixture of linear and cyclic oligomers:



The synthesis of siloxanes has been described in [2], [3], [4], [5]. Higher molecular weight PDMS is obtained after polymerisation, for example, of the above cyclics in the presence of an end-blocker such as hexamethyldisiloxane and catalysed by a strong acid or strong base according to:



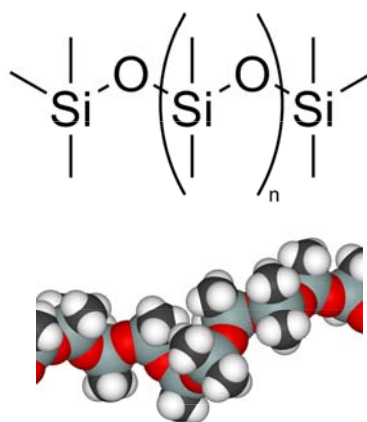


Figure 2.3: Graphical representation of PDMS.

The methyl groups along the chain can be substituted by many other groups (e.g., phenyl, vinyl or trifluoropropyl). The simultaneous presence of 'organic' groups attached to an 'inorganic' backbone gives silicones a combination of unique properties:

- A highly open, flexible, and mobile siloxane backbone leading to the ability to orient toward particular surfaces and bend without breaking.
- High bond strength stable in many different environments and under harsh conditions.
- The ability to form extremely long polymer chains and still remain fluid.
- The ability to bond with both organic and inorganic materials, creating a bridge between them.

Using other chlorosilanes, different end-blockers and/or different cyclics leads to many structures including polymers with various functional groups grafted on the polymer chain and/or at the polymer ends (e.g., vinyl, hydrogen, phenyl, amino alkyl). These can be formulated into solvent-based, emulsion or solvent-less products.

Reactive polymers can be cross-linked into elastomers (=elastic polymers) using:

- A peroxide-initiated reaction; in particular, if the silicone polymer carries some vinyl groups.
- A condensation reaction; for example, between a hydroxy end-blocked PDMS and an alkoxy silane, in presence of tin salt or titanium alkoxide as catalyst.

46 Introduction to concepts related to elastic microsystems

- An addition reaction; for example, between a vinyl-functional PDMS and an hydrogenomethyl dimethyl siloxane oligomer, in presence of a organic platinum complex.

Such polymers, cross-linkers and catalysts are formulated with various additives as one-part, ready-to-use products or two-part products to be mixed prior to use and to cure at room temperature or only at elevated temperatures.

Physical properties

The surface activity of silicones is perceived in many circumstances [6]:

- Polydimethylsiloxanes have a low surface tension (20.4 mN/m) and are capable of wetting most surfaces. With the methyl groups pointing to the outside, this gives very hydrophobic films and a surface with good release properties, particularly if the film is cured after application. Silicone surface tension is also in the most promising range considered for biocompatible elastomers (20 to 30 mN/m).
- Silicones have a critical surface tension of wetting (24 mN/m), which is higher than their own surface tension. This means that silicones are capable of wetting themselves, a property that promotes good film formation and good surface covering.
- Silicone organic copolymers can be prepared with surfactant properties, with the silicone as the hydrophobic part (e.g., in silicone polyether copolymers).

The low intermolecular interactions in silicones have other consequences [6]:

- Glass transition temperatures are very low (e.g., 146 K for a polydimethylsiloxane compared to 200 K for polyisobutylene, the analogue hydrocarbon); cross-linked PDMS will be elastomeric at RT in the absence of any plasticizers.
- The presence of a high free volume compared to hydrocarbons explains the high solubility and high diffusion coefficient of gas into silicones. Silicones have a high permeability to oxygen, nitrogen and water vapour, even if in this case liquid water is not capable of wetting a silicone surface. As expected, silicone compressibility is also high.
- In silicone, the activation energy to the viscous movement is very low, and viscosity is less dependent on temperature compared to hydrocarbon polymers. Moreover, chain entanglements are involved at higher temperature and contribute to limit the viscosity reduction.

2.2 Polymers

47

Siloxane polymers occur in a variety of common forms - fluids, gels, elastomers, and resins - for a wide variety of applications, mainly differing in their cross-linkage. When different chains are chemically linked with each other, they are crosslinked. In a fully crosslinked polymer each chain segment is chemically linked, directly or indirectly to every other chain segment. Rubbers, epoxies, polyester, polyethylene are crosslinked polymers. Crosslinked polymers are typically tougher than their linear counterparts and exhibit dimensional stability and elastic recovery at temperatures above their crystalline melting temperature or glass transition temperature. The distribution of crosslinks and the relative lengths of the connections control the properties of the crosslinked polymer.

Silicone gels are lightly cross-linked PDMS fluids, where the cross-link is introduced either through a trifunctional silane - such as CH_3SiCl_3 giving a "T-branched" silicone structure - or through a chemical reaction between a Si-vinyl group on one polymer chain with a hydrogen bonded to silicon in another. This chemical "tying" of siloxane chains produces a three-dimensional network that can be swollen with PDMS fluids to give a sticky, cohesive mass without form.

Silicone elastomers are cross-linked fluids whose three-dimensional structure is much more intricate than a gel. In addition, there is very little free fluid in the matrix. Fillers, such as amorphous silica, are frequently added to the matrix to give greater reinforcement to the network and thereby increase the strength of the product.

Silicone resins are more heavily cross-linked polymer networks that are formed by the introduction of a predominance of tri- and tetra-functional monomers, such as CH_3SiCl_3 . The physical properties of the finished silicone resin can be tailored to suit many applications by varying the ratio of branched and linear siloxanes and also the functional groups attached to the silicon.

The polymer can be manufactured in multiple viscosities, ranging from a thin pourable liquid (when n is very low), to a thick rubbery semi-solid (when n is very high). PDMS molecules have quite flexible polymer backbones (or chains) due to their siloxane linkages, which are analogous to the ether linkages used to impart rubberiness to polyurethanes. Such flexible chains become loosely entangled when molecular weight is high, which results in PDMS' unusually high level of viscoelasticity.

PDMS is viscoelastic, meaning that at long flow times (or high temperatures), it acts like a viscous liquid, similar to honey. However, at short flow times (or low temperatures), it acts like an elastic solid, similar to rubber. In other words, if some PDMS is left on a surface overnight (long flow time), it will flow to cover the surface and mold to any surface imperfections. However, if the same PDMS is rolled into a sphere and thrown onto the same surface (short flow time), it will bounce like a rubber ball.

48 Introduction to concepts related to elastic microsystems

The high density of methyl groups (CH_3) at the surface leads to the hydrophobicity of the PDMS material.

Sylgard 184 [7] and Sylgard 186 [8] are 2 types of PDMS, provided in 2-component form, including a base and curing agent. These comprised primarily the components of a reaction mixture having vinyl endcapped oligomeric dimethyl siloxane, a methyl hydrosiloxane as crosslinking agent, and a platinum complex as a catalyst for the hydrosilation reaction. The polymerisation is based on an addition cure system, no by-products are generated.

Both types of PDMS will be the most used through this PhD-work because of the following properties:

- Lab environment processability: viscosities make spincoating, casting and liquid injection moulding possible.
- Room temperature cure or rapid heat cure (e.g. 1 hour at 100°C).
- Pot life is 2 hours for the catalysed silicones at room temperature.
- Addition cure systems: no cure by-products.
- Translucent/transparent: the embedded parts can be analyzed during development of the different technologies. Failure mechanisms can be detected in this way.
- Appropriate mechanical properties, elongation till break of $\sim 400\%$.

2.2.5 Supporting material: polyimide

Polyimide is a material standard being used in flexible circuit board technologies. The reasons are obvious because the material is lightweight, flexible, resistant to heat and chemicals. For example, in a laptop computer, the cable that connects the main logic board to the display (which must flex every time the laptop is opened or closed) is often a polyimide base foil with copper conductors.

Polyimide (sometimes abbreviated PI) is a polymer of imide monomers. The structure of imide is shown in Figure 2.4. Polyimides usually take one of two forms. The first of these is a linear structure where the atoms of the imide group are part of a linear chain. The second of these structures is a heterocyclic structure where the imide group is part of a cyclic unit in the polymer chain (Figure 2.5).

Most commercial polyimides are typically aromatic heterocyclic polyimides, such as Ultem and DuPont's Kapton. This kind of polymers have very good mechanical and thermal properties that they are used in place of metals and glass in many high performance applications in the electronics, automotive, and the aerospace industries. These properties come from strong intermolecular forces between the

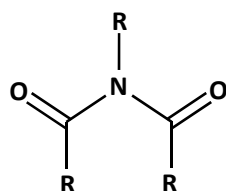


Figure 2.4: Imide.

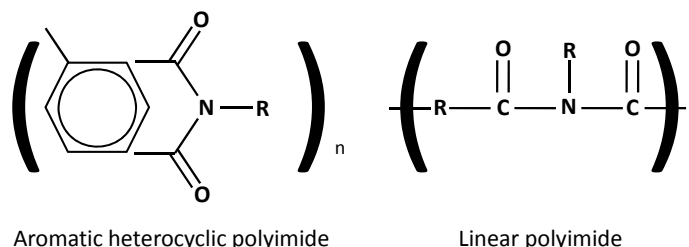


Figure 2.5: Polyimides usually come in two forms: aromatic heterocyclic polyimides (left) and linear polyimides (right).

polymer chains. The subtle variations in the structures of the dianhydride and diamine components have a tremendous effect on the properties of the final polyimide.

The most widely practiced procedure in polyimide synthesis is the two-step poly(amic acid) process [9]. It involves reacting a dianhydride and a diamine at ambient conditions in a dipolar aprotic solvent such as N,N-dimethylacetamide (DMAc) or N-methyl-pyrrolidone (NMP) to yield the corresponding poly(amic acid), which is then cyclized into the final polyimide. The intermediate poly(amic acid) is usually converted to the final polyimide by the thermal imidization route. This process is especially useful when the final product is desired in a film or a coating form. Films are first cast on a substrate and then undertaken through a thermal cycle with temperatures ranging from 100°C to 350°C. This process is shown in Figure 2.6.

Dramatic changes in the mechanical properties occur as the poly(amic acid) sample is converted to the final polyimide. Polyimide has excellent flexibility over a wide range of temperatures, good electrical properties, excellent chemical resistance, very good tear resistance, highest tensile strength. Disadvantages are that it has a high moisture uptake and is relative expensive. As will be discovered in the following chapters, we will use this material as mechanical support for the functional islands and stretchable interconnections, to improve the reliability of the process and the system. More details about the used polyimides are found in

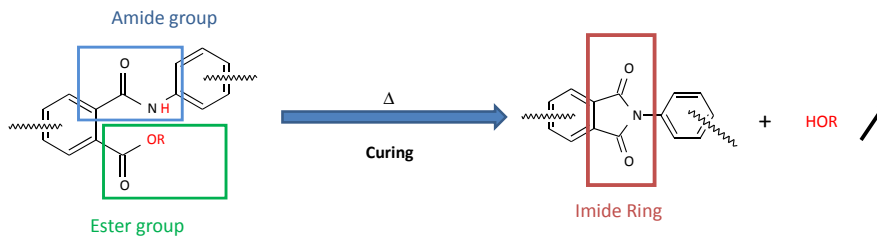


Figure 2.6: Imidization process of aromatic polyimides.

Chapter 5.

2.3 Mechanical aspects of elastic microsystems

We want to develop a technology for elastic microsystems being capable of absorbing strains upto 10 - 15%. Therefore, the mechanical reliability of these systems is a major concern. Insights in the mechanical aspects are necessary and will give us clues about the performance of the realized systems, in order to guarantee the functionality of the system. In this section, an introduction will be given to the mechanical knowledge related to stretchable electronics. It is mentioned before presenting the different technologies because it gives the reader already a feeling with some important aspects that are crucial related to the development of a stretchable electronic system. During the presentation of the different technologies, some more modeling and experimental results will be mentioned as clarification. Most of these findings are the results of modeling activities performed by mechanical engineers and experimental analysis based on samples made in the different stretchable electronic technologies presented in this PhD. The rationale behind the shape of the metal interconnects, the selection of materials, the system's architecture,... will be explained here, as this is just an introduction; elaborate findings and results are described in articles published by Mario Gonzalez and Hsu Yung Yu and will be described in the PhD work of Hsu Yung Yu. Their findings are based on samples realized in the presented technologies.

2.3.1 Mechanical characterization of embedding materials

From a materials science point of view, three basic types of stress-strain curves can be distinguished for polymers as shown in Figure 2.7. Amorphous or crystalline polymers (I) below T_g (glass transition temperature) exhibit a steep curve i.e. a large modulus E and a large stiffness, and often a small strain at the brittle fracture. This picture holds for thermoset polymers, but elastomers and rubbery

2.3 Mechanical aspects of elastic microsystems

materials above T_g (II) possess a low E-value which means that they are soft and show a tough fracture at high strain. However, partially crystalline polymers show a rather high E-value between T_g and T_m (melting temperature) (III). Furthermore, they show cold drawing beyond a maximum called the yield point. This process involves plastic deformation. It results in large ultimate stress and strain and therefore in a very high fracture energy. Such materials are tough and strong.

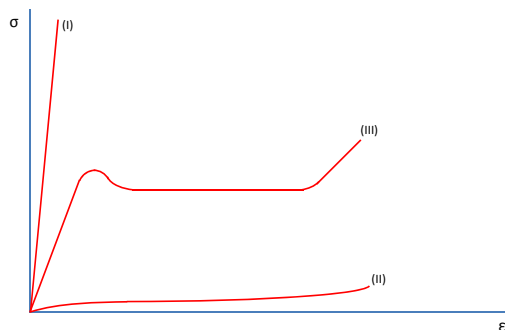


Figure 2.7: Stress-strain curve at room temperature T_r for three different polymers. (I) Glassy polymer with $T_r < T_g$. (II) Elastomer with $T_r > T_g$. (III) Partially crystalline polymer with $T_g < T_r < T_m$.

For the modeling activities, in the frame of the Stella project, three materials were investigated: Sylgard 186, Walopur and Permacol TPU shore A30. Stress-strain measurements were performed with a drawing machine on a specimen with a special shape, clamped at both sides. The force and extension can be measured continuously for a given extension rate. When dividing the observed force by the original cross-section the nominal stress is found, while the quotient of the extension and the original length gives the nominal strain. Since the cross-section diminishes during extension, the actual stress is larger. In the case of large extensions the specimen could sometimes deform inhomogeneously and the only local values of stress and strain would be significant. Most of the modeling work was and will further be based on the use of Sylgard 186 [10] as embedding material, used for the reasons mentioned in 2.2.4. The 3 materials mentioned are included here in order to give the reader an idea about the impact of different material types on the induced mechanical strains thus onto the mechanical reliability of a stretchable electronic system.

The mechanical characterization of PDMS Sylgard 186, Walopur 4201 TPU and Permacol TPU shore A30 was done at Philips AppTech. Figure 2.8 depicts the results of a uniaxial tension test for the 3 materials. In all cases, there were no fractures observed at the strains range shown in the figure. The behaviour of the substrates at higher deformations is not presented because we are mainly

52 Introduction to concepts related to elastic microsystems

interested in the region between 0% and 30% deformation. It can be seen that Permacol shore A30 and the silicone Sylgard 186 present similar stiffness for deformations up to 100%. The Walopur 4201 TPU is several times more rigid.

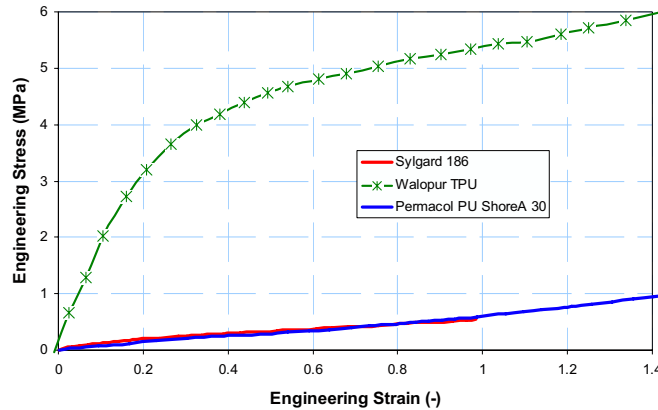


Figure 2.8: Tension test of 3 different substrate materials.

Unlike most metals, elastomers present a non-linear elastic behaviour. In other words, elastomer materials are fully non-linear in the displacement and strains. In finite element (FE) calculations, there is a big influence of the definition of the hyperelastic non-linear material behavior on the results. Therefore, a good fitting with the stress-strain curves is important. The material behavior of PDMS Sylgard 186 is described satisfactorily using a neo-Hookean fitting.

A neo-Hookean solid is a hyperelastic material model, similar to Hooke's law, that can be used for predicting the stress-strain behavior of materials undergoing large deformations [11], [12],[13]. The relationship between applied stress and strain is initially linear, but at a certain point the stress-strain curve will plateau. The neo-Hookean model is based on the thermodynamics of cross-linked polymer chains and is usable for plastics and rubber-like substances. Cross-linked polymers will act in a neo-Hookean manner because initially the polymer chains can move relative to each other when a stress is applied. However, at a certain point the polymer chains will be stretched to the maximum point that the covalent cross links will allow, and this will cause a dramatic increase in the elastic modulus of the material. The neo-Hookean material model does not predict that increase in modulus at large strains and is typically accurate only for strains less than 20%.

The mechanical characteristics of the polyurethane (Walopur 4201 TPU) are not described adequately by the neoHookean fit for large deformations. Due to the relatively high stiffness of this material, the stretchable metallic interconnections will fail at nominal strains below 10%. Within this PhD, no polyurethane will be

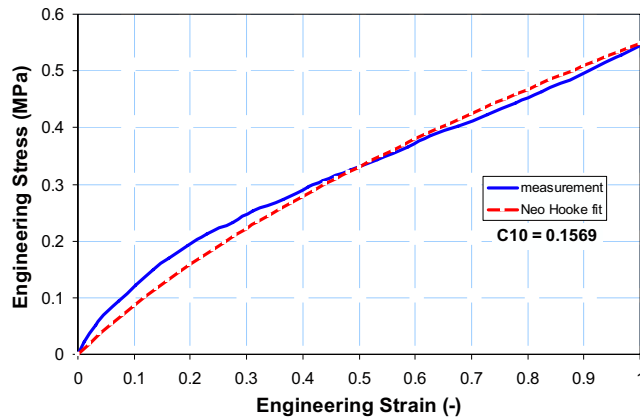


Figure 2.9: neo-Hookean fit of Sylgard 186.

used as embedding material. We only remember that the stiffer the embedding material, the more stress there will be exerted on the metallic interconnections, the lower the maximum elongation till break and the lower the lifetime of interconnects during cyclic stretching.

2.3.2 Mechanical design of stretchable metallic interconnects

Before and during this PhD work, finite element modeling was performed using the commercial finite element code, MSC MARC, in order to determine the ideal, stretchable conductor shape of the embedded metal tracks. In [14],[15],[16], the first results concerning the shape of the meander are discussed. We will sum up the most important thoughts about the ideal conductor design. Based on these results, meander designs will be used in the technologies in the upcoming chapters.

Shape of the conductor

In order to determine the ideal horseshoe, meander-like design, a 2D plane-stress model has been made [16]. The objective of this preliminary study was to compare the stresses induced in the copper conductors when a 20% deformation is applied in the axial direction of the meander. The effect of the substrate was neglected in a first instance. The conductor used for these models is copper with a thickness of 15 μm and a trace width of 90 μm . An amplitude of 700 μm and a period of 500 μm was used for 3 configurations (Figure 2.10). The mechanical

54 Introduction to concepts related to elastic microsystems

behaviour of the copper was modeled as being isotropic, linear-elastic and temperature independent. In a 3D simulation of these configurations an out of plane deformation is observed when a load or displacement is applied in the X direction. However, in an actual configuration the copper conductor is embedded into a stretchable substrate and the out of plane deformation is constrained. Therefore, even if a 2D plane stress (in plane deformation) model is not an accurate method because the effects of substrate and copper thickness and although out of plane deformation are not taken into account, it gives a good first insight in the stresses induced in the structure.

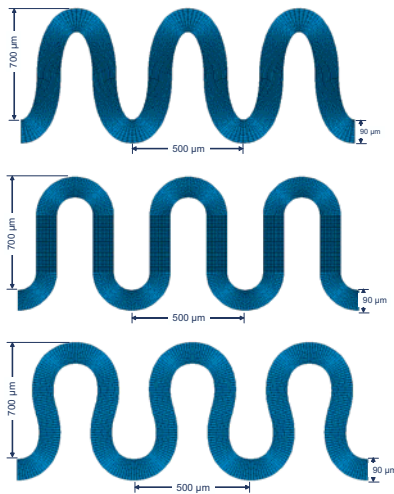


Figure 2.10: Different conductor shapes.

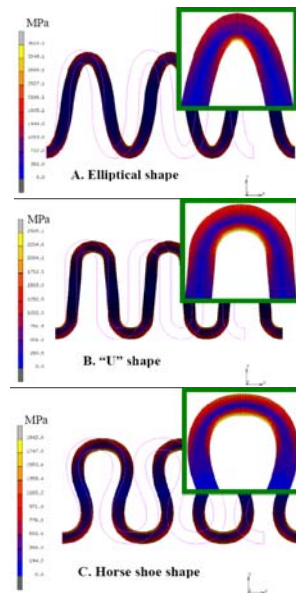


Figure 2.11: Stress distribution in copper conductor line for three different conductor shapes.

Three different conductor shapes were analyzed and compared. In all cases, a total deformation of 20% was applied in the X direction of the meander. Results of these models are presented graphically in Figure 2.11. In the case of an elliptical shape (Figure 2.11 top), a high stress concentration is observed in the crest and through of the line. In order to avoid this concentration of stresses, a rounded design is preferred. The U-shape (Figure 2.11 middle) offers a better stress distribution but is still limited by a reduced radius of curvature. Furthermore the straight vertical lines limit the deformation perpendicular to the axis of the meander when a biaxial deformation is needed. In the optimal shape (Figure 2.11

2.3 Mechanical aspects of elastic microsystems

bottom), the stress is distributed in an extended part of the conductor. A reduction of 46% in the stress is obtained with this shape compared to the elliptical one. As a first step, FEM simulations were developed considering linear behaviour of the materials, this explains the high values of calculated stress. Nevertheless, looking for trends, an 'A to B' stress comparison is enough for choosing the conductor shape. Predominant failures are expected in regions where the highest concentration of stress is located.

Width and radius of the conductor meander design

From modeling results [14],[15],[16] it is found that by keeping the same amplitude and period of the meander but reducing its width, it is possible to reduce considerably the stresses induced during the stretching of the substrate. If the technology allows it to make thin traces, a conductor line can be subdivided in several lines of smaller width. In this way, the electrical performance and the same amplitude/period of the meander can be maintained. In an idealized case (without substrate) for the geometry proposed in Figure 2.11 c, the stresses are reduced by a factor of 10 if the copper line width is reduced from 90 μm to 15 μm (Figure 2.12). However these small features won't be possible to realize in the presented technologies, this theoretical case is mentioned to show the impact on performance of a narrow conductor line. In the case of etched copper tracks (what will be the technology used in this work for patterning the copper), 5 μm large local defects will have a much higher impact on the reliability of the system for 30 μm defined tracks than for for 100 μm defined tracks.

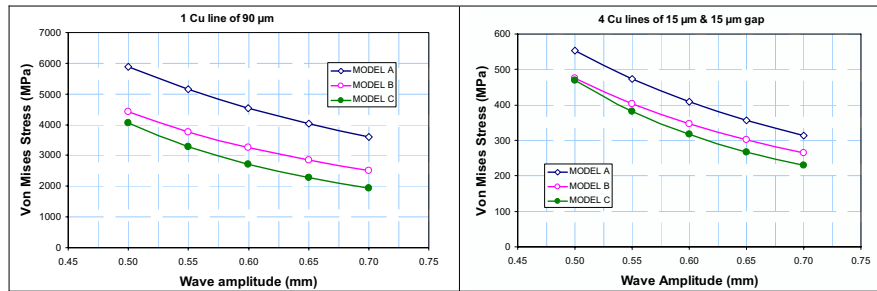


Figure 2.12: Relation between the induced Von Mises stress and the wave amplitude for 3 different designs. (Left) Single track. (Right) Multi-track design.

The presented horseshoe pattern presented is created by joining a series of circular arcs as shown in Figure 2.13, where R is the radius, W is the width of the copper trace and theta (θ) is the angle, measured clockwise, where the two arc

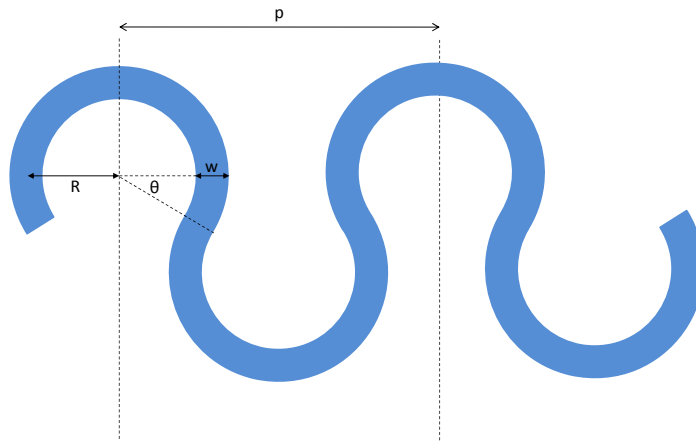


Figure 2.13: Meander definition

of circles intersect. When $\theta = 0^\circ$, we have a semicircle design, if $\theta > 0^\circ$, we obtain the horseshoe design. If the possible delamination and buckling problems are neglected, from a mechanical point of view it is possible to define a geometry parameter as the ratio R/W . The stress and strain induced in the copper are constant if the ratio R/W is kept constant, independently of the amplitude of the horseshoe design. A series of 250 models were simulated with different R , W , θ and Young's moduli of the substrate in order to find a relation between the damage parameter (plastic strain) and the scale factor R/W . The images shown in Figure 2.14 and 2.15 give a picture of the relation between plastic strain and the ratio R/W . The different percentages presented in the plots represent the total deformation applied to the structure, this for $\theta = 0^\circ$ and $\theta = 45^\circ$ horseshoe designs. The plots presented show a clear trend. An increase of the scale factor is translated into a reduction of the induced strain. Therefore a narrow copper trace or a large radius of curvature is preferred for these configurations. In the case of stiffer substrates (i.e. $E=20$ MPa), it is not easy to find a clear trend. A high scatter of the results mainly for deformations above 15% is observed. This scatter can be explained by the fact that the maximum strain point is shifted from the top region in case of small deformations to the center of the horseshoe for larger deformation. This shift is not systematic; combinations of factors such as the scale factor, the stiffness of the substrate and the applied deformation affect the location and the magnitude of the strains. Out of these plots, a recommended value for the scale factor is between 10 and 15.

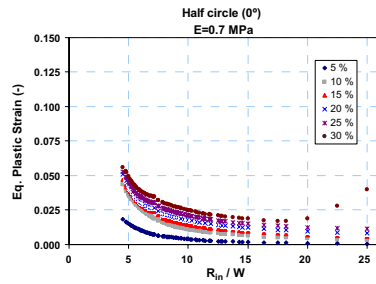


Figure 2.14: Relation between the equivalent plastic strain and the scale factor (R/W) for a substrate with a Young's modulus of 0.7 MPa for a horseshoe design with $\theta=0$.

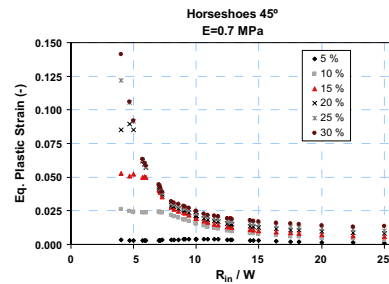


Figure 2.15: Relation between the equivalent plastic strain and the scale factor (R/W) for a substrate with a Young's modulus of 0.7 MPa for a horseshoe design with $\theta=45$.

Effect of embedding material characteristics

In order to quantify the strains in the copper meander, the substrate has to be included. When the substrate is stretched in the axial direction, due to the Poisson's effect, the structure is always accompanied by a lateral contraction as shown in Figure 2.16. During an uniaxial stretching, copper conductor is under tension in the crest and trough and in compression in the medium of the design. Yellow and red colors in the Figure 2.16 represent a concentration of strains when the structure is stretched 20%. Globally, the copper conductor is under tension when the line is parallel to the stretching direction and is under compression when the copper trace is perpendicular to the stretching direction. Locally, the inner part of the copper trace is in tension and the outer part in compression.

The meander shown in Figure 2.16 has been optimized in shape for a uniaxial deformation in the direction of the conductor. Other complex deformations like biaxial and torsion are not taken into account. A qualitative comparison between modeling and experiments showed that the calculated regions with a high concentration of plastic strain (ϵ^{pl}_{max}) corresponded to the observed failures. Cracks are observed in the crests and troughs of the meander at about 25% of total deformation.

Stiffness of embedding material

The magnitude of the strains caused by the local or global deformation depends on the stiffness of the substrate and the thickness of the copper trace. The deformation of the patterned copper line is, in a certain manner, controlled by the deformation of the embedding material. If the conductor is embedded in a stiff

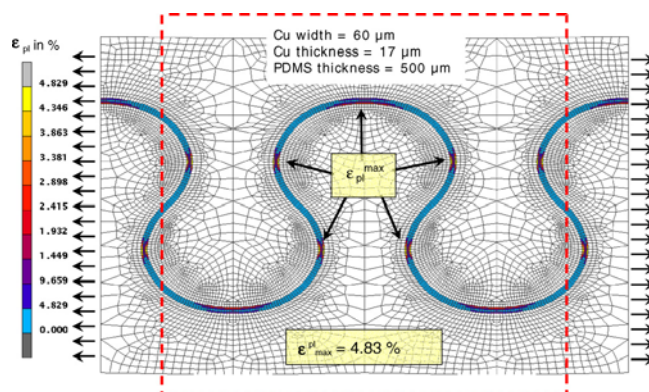


Figure 2.16: Poisson effect observed during a uniaxial tension test for a single conductor line (dashed lines show the original dimensions of the substrate).

substrate, the deformation of the conductor will be the same as the one of the substrate. On the other hand, if a very soft substrate is used, the conductor has some freedom to move inside the substrate, reducing in this way the Poisson effect and in consequence, reducing the accumulated plastic strain (compressive stresses are reduced). When a material is compressed in one direction, it usually tends to expand in the other two directions perpendicular to the direction of compression (=Poisson effect). In order to quantify the maximum strain in the conductor as a function of the stiffness of the substrate, the meander design presented in Figure 2.16 was modeled with different Young's modulus of the substrate. Thickness of copper and substrate and the total deformation were kept constant. Results of this study are presented in Figure 2.17. For this configuration, when the Young's Modulus of the substrate is about 120 MPa, the plastic strain in the copper is practically the same as the total strain applied to the substrate. This means, that increasing the stiffness of the substrate will decrease the maximum allowable stretchability of the structure.

Thickness of embedding material

The total thickness of the substrate, into which the copper interconnections are embedded, and its mechanical properties have a direct influence on the performance of the stretchable circuit. For instance, a soft and thin substrate will allow the copper to deform out-of-plane during stretching. This out-of-plane deformation is considered unfavorable during usage because of creating wavy/non-planar surface. However, in terms of plastic strain in metal, this out-of-plane deformation allows more degree of freedom in deformation and thus, reduces plastic strain in metal while stretching. The substrate thickness and the position

2.3 Mechanical aspects of elastic microsystems

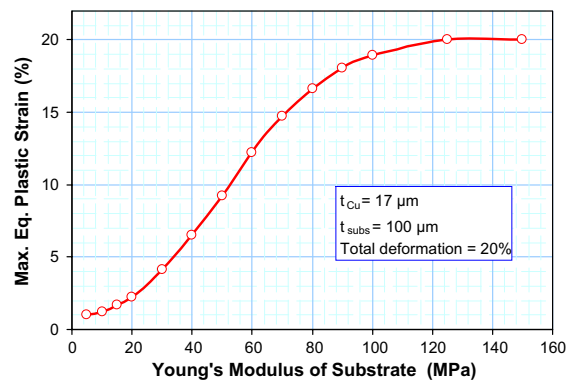


Figure 2.17: Equivalent plastic strain induced in copper as function of Young's modulus of the substrate.

of the copper line (in the thickness direction) can cause an out-of-plane deformation during stretching. In an experiment, a PDMS substrate was used. The first layer of PDMS was fixed at 0.5 mm. By reducing the thickness of the encapsulation layer, more out-of-plane deformation is observed when stretching. It is suggested to have the encapsulation layer the same thickness as the substrate to minimize the unfavorable out-of-plane deformation. The stiffness of the substrate can be increased either by increasing the total thickness or by increasing the elastic modulus (or both). Furthermore, it is preferable to keep a symmetry, in other words, the thickness of the substrate layer (below the copper) and the encapsulation layer (above the copper) has to be the same. In terms of plastic strain on metal, the thinner and softer the substrate, the smaller plastic strain on metal when stretching. The stiffness of the substrate influences the mechanical behavior of the copper interconnection, independently of its design. When the stiffness of copper interconnection is higher than the stiffness of the substrate, the metal deforms out-of-plane and smaller permanent deformation is induced. In the opposite case, the substrate constrains the copper to deform and higher plastic deformation is observed. The thinner the encapsulation layer, the longer the ultimate elongation (electrical failure). However, the interfacial delamination should also be taken into consideration even though it is still electrical functional. In certain applications, the electrical connection is the sole consideration. Considering the unfavorable environmental effect such as moisture, chemical corrosion, etc., it is recommended to limit elongations to avoid interfacial delamination. In the case of PDMS, delamination is observed at around 60% elongation. This value is higher for TPU's.

To conclude this introduction, results are shown of some specific test structures being modeled without optimizing their shape for the different substrate materi-

60 Introduction to concepts related to elastic microsystems

als. The objective was to test basic technology components in combination with different substrate materials. The test sample that has been used for modeling is presented in Figure 2.18. It consists of a strip with a length of 7 cm, a width of 1 cm and a total thickness of 500 μm . The meandering used is a horseshoe design with a radius of 750 μm , a joining angle of 30° and a line width of 100 μm . The thickness used for the copper is always 18 μm . In all cases presented, a uniform thickness was used for the substrate in order to compare results among them. In practice, the thickness of the substrate will be controlled by the technology and the final application. Moreover, the substrate material can present different thicknesses over the whole electronic circuit to restrain the displacement locally where the circuit will be more sensitive to deformations.

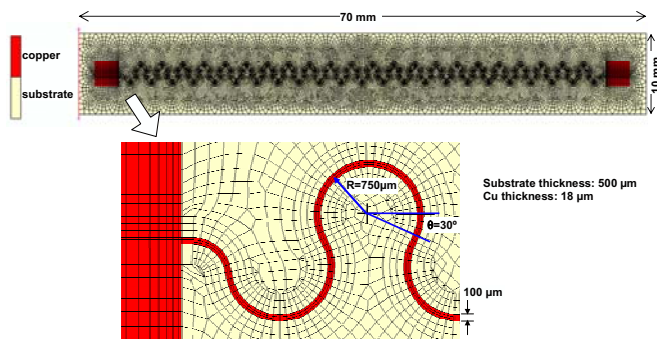


Figure 2.18: Geometry and mesh density of test structure used for modeling.

Uniaxial test, parallel to meander direction

Half symmetry is applied in the model. A total nominal strain of 30% is applied to the structure and is reported by increments of 5%. The accumulated plastic strain was used as damage criterion. As can be seen in Figure 2.19 and Table 2.1, the maximum plastic strain is observed in a region close to the metal pads, where the transition from rigid to stretchable section is present. This transition region can be redesigned to allow a smoother transition. As a direct comparison between different models and substrates is considered, a local optimization of the metal meandering is not necessary. Table 2.1 gives an idea about the evolution of the plastic strain in different regions of the meander. The statistic median is also given (considering only strains in the crest and trough of the meander). If a local meander optimization is used in the transition rigid/stretchable zone, the maximum plastic strain observed has to be similar to the median value reported. As it was observed in the materials characterization, Walopur TPU material is more rigid than the silicone Sylgard 186, therefore a more important damage is

2.3 Mechanical aspects of elastic microsystems

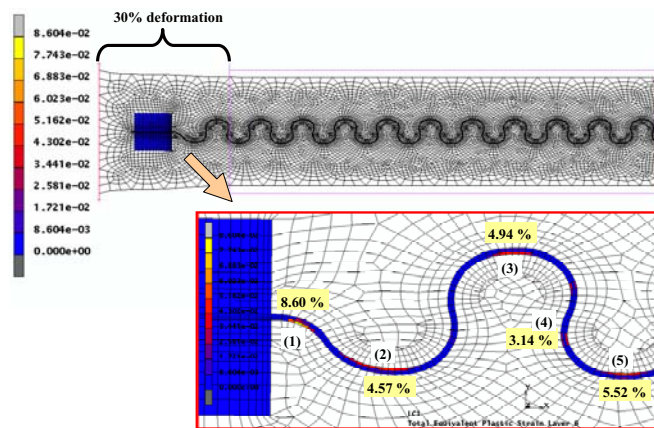


Figure 2.19: Model of equivalent plastic strain with Sylgard 186 as embedding material for 30% applied strain in X direction.

Strain zone	5%	10%	15%	20%	25%	30%
1	0.465	2.12	3.84	5.42	6.95	8.60
2	0.821	2.14	2.99	3.52	4.06	4.57
3	0.309	1.58	2.93	3.99	4.53	4.94
4	0	0.078	0.636	1.54	2.42	3.14
5	0.402	2.01	3.57	4.57	5.07	5.52
Median	0.289	1.70	3.05	4.17	4.77	5.22

Table 2.1: Equivalent plastic strain (in %) in the copper lines at different positions and for different elongations (Sylgard 186).

observed in the copper meandering, even at low deformations. For modeling purposes, the maximum deformation was fixed at 10% for this polyurethane. Figure 2.20 and Table 2.2 summarize the results for this material.

Strain zone	2%	4%	6%	8%	10%
1	0.22	2.25	5.24	7.89	10.47
2	0.56	3.09	6.44	9.67	13.16
3	0.45	1.72	5.04	8.03	11.10
4	0.48	1.68	5.03	7.91	10.84
5	0.42	1.42	4.60	7.40	10.19
6	0.156	0.775	1.56	2.30	3.09
7	0.41	1.36	4.49	7.24	9.95
Median	0.377	0.377	1.25	4.20	9.53

Table 2.2: Equivalent plastic strain in the copper lines at different positions and for different elongations with Walopur TPU as embedding material. Mooney fit was used in this model.

Taking into account that the same geometry (copper meandering and substrate dimensions) was used; the plastic strain in the copper conductor line embedded

62 Introduction to concepts related to elastic microsystems

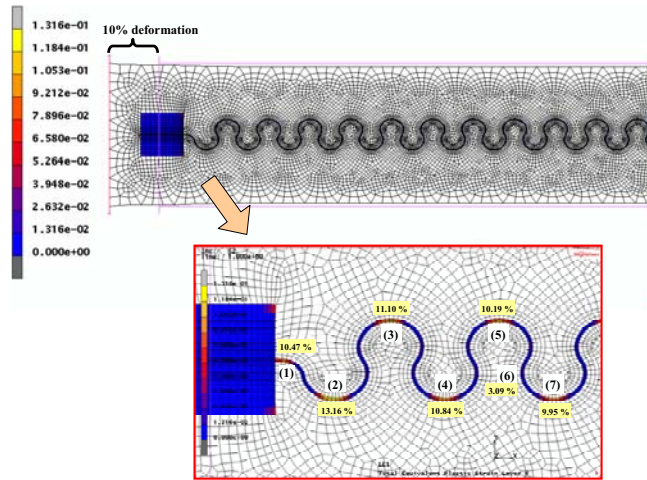


Figure 2.20: Model of equivalent plastic strain with Walopur TPU as embedding material for 30% applied strain in X direction.

into Sylgard 186 for 30% nominal deformation has the same order of magnitude than the copper embedded into Walopur TPU for deformations between 7 and 8%. This proves that softer materials are preferred for allowing large elongations without permanent damage in the conductor line.

Uniaxial test, perpendicular to the meander direction

The horseshoe design is optimised for deformations in the same axis as the conductor line. Nevertheless, to make an elastic circuit most of the time it will be necessary to have conductor lines perpendicular to the deformation axis. In order to model the behaviour of the metal line the same test sample is deformed in the Y axis, as a laminar tension test.

Strain zone	5%	10%	15%	20%	25%	30%
1	0.026	0.59	1.05	1.47	2.22	2.87
2	0.029	1.04	1.81	2.41	3.79	4.91
3	0.011	0.68	1.46	2.05	3.49	4.73
4	0.010	0.59	1.28	1.97	3.29	4.38
5	0.010	0.60	1.28	1.96	3.27	4.39
6	0.005	0.34	0.85	1.39	2.59	3.71
7	0.005	0.44	1.02	1.72	3.01	4.11
Median	0.001	0.29	0.85	1.35	2.49	3.52

Table 2.3: Equivalent plastic strain in the copper lines at different positions and for different elongations for Sylgard 186 as embedding material. Neo-Hookean fit was used in this model.

2.3 Mechanical aspects of elastic microsystems

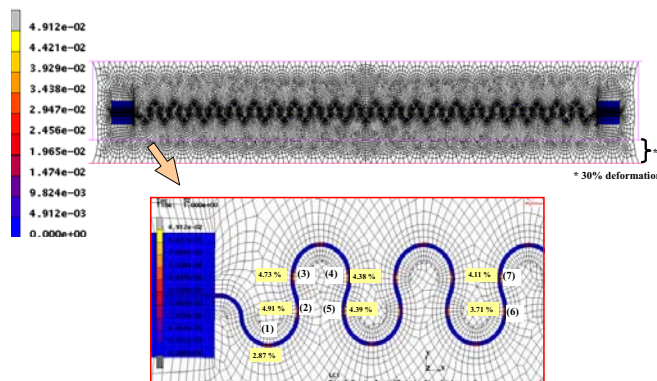


Figure 2.21: Model of equivalent plastic strain with Sylgard 186 as embedding material for 30% applied strain in Y direction.

Opposite to expected, plastic strain values in the copper meander for laminar test does not differ much from the tension test, even, they are smaller (Figure 2.21 and Table 2.3). The reason of this is due to the low stiffness of the substrate, compared with the one of the copper. By applying 30% nominal deformation in the substrate, the actual change in the meandering amplitude is only 6.6%. The rest of the elongation was done on the silicone surrounding the copper.

The same analysis was performed for Walopur TPU material. In this case, the stiffness of the polyurethane is closer to the one of the copper; therefore, copper was deformed more. By applying 10% total deformation, the meandering amplitude was increased by 7.8%. The equivalent plastic strain in the copper meander is summarized in Figure 2.22 and Table 2.4.

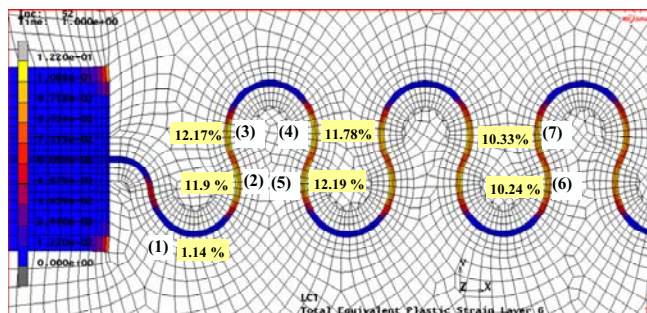


Figure 2.22: Model of equivalent plastic strain with Walopur TPU as embedding material for 30% applied strain in Y direction.

As can be observed in Table 2.4, the equivalent plastic strain obtained in the cop-

64 Introduction to concepts related to elastic microsystems

Strain zone	2%	4%	6%	8%	10%	10% (neo-Hooke)
1	0.022	0.187	0.442	0.72	1.14	0.67
2	0.49	2.88	5.69	8.67	11.9	10.73
3	0.65	3.03	5.86	8.81	12.17	10.95
4	0.42	2.86	5.64	8.59	11.78	10.74
5	0.68	3.13	5.94	8.94	12.19	11.09
6	0.56	2.81	5.32	7.99	10.84	10.24
7	0.62	2.88	5.41	8.11	10.99	10.33
Median	0.43	2.56	4.95	7.45	10.10	9.79

Table 2.4: Equivalent plastic strain in the copper lines at different positions and for different elongations. Both Mooney and neo-Hookean fit were used in this model.

per meander is slightly smaller if the neo-Hookean fit is used. However the difference is less than 10% in most of the cases.

Bi-axial test

Stretchable electronic circuits must also be capable of being subjected to multiaxial deformations. For this reason, in-plane biaxial testing is important for deriving the permanent deformation in the copper line and helps us to understand and improve the design of the meandering. Characterization of substrates for deriving the mechanical properties under biaxial test have not been performed, however, for modeling purposes, the neo-Hookean and Mooney approximations described previously have been used. In these simulations, a square sample of 7x7 cm² was deformed in both directions at the same time.

The permanent deformation in the copper is lower than the case of tension test or laminar test. The reason could be that during a tension test, the top and bottom part of the meandering is subjected to tensile stresses (opening of the meandering). During the laminar test, the top and bottom part of the conductor line is subjected to compressive stresses (closing of the meander). In this biaxial test, and due to the soft nature of the silicone Sylgard 186, tensile and compressive stresses are balanced, therefore, low strains are observed in the copper, with an exception in the region close to the copper pad, there only tensile stresses are present.

Similar simulations were done for the case of the polyurethane Walopur. As expected, due to its relatively high stiffness, permanent deformation in the copper is very high. For this configuration, early failures are expected between 4 and 6% of nominal deformation ($\epsilon^{pl} = 5\%$ approximately).

2.4 Conclusions

As an introduction to the technologies, we have given an overview of the aspects that come in to play when designing a stretchable electronic system.

2.4 Conclusions

65

The architecture and design methodology have been explained. The electronic system is spread over a surface by dividing it into functional islands connected with stretchable interconnections, encapsulated in a polymer resulting in a system capable of absorbing strains upto 10-15%. The fabrication of such a system will be done by standard PCB production techniques while keeping the freedom of the encapsulant to be used by introducing it at the end of the fabrication process.

The subject related important knowledge about polymers has been given including basic fundamentals on silicones and polyimides. Sylgard 184 and 186 have been selected as encapsulant for their lab environment use and mechanical properties. Polyimides will be used to improve the reliability of the system and the process.

Finally, to have an idea about the mechanical aspects that come up during the design of an electronic system that can be exerted to strains typically upto 10-15%. An introduction about the mechanical pre-knowledge and knowledge has been given. Based on mechanical simulations and models realized by mechanical engineers and experimental tests and analysis performed on fabricated technology samples, design related conclusions can be drawn related to the ideal shape of the stretchable interconnect, influence of properties of embedding material,.. Further findings will be introduced in the following chapters.

We are ready now to dive into the technology chapters.

References

- [1] Challa. *Polymer Chemistry - An introduction*. Ellis Horwood Limited, 1993.
- [2] B. Hardman. *Encyclopedia of Polymer Science*. 1989.
- [3] Rochow. *Silicone and silicones*. Springer-Verlag: Berlin, Heidelberg, New York, 1987.
- [4] Noll. *Chemistry and Technology of Silicones*. Academic Press: New York, 1968.
- [5] M. Gleria R. De Jaeger. *Silicones in Industrial Applications*. Nova Science Publishers, 2007.
- [6] M.J. Owen. *Chemie Nouvelle*. Chemtech, 2004.
- [7] Dow Corning. Technical datasheet - Sylgard 184.
- [8] Dow Corning. Technical datasheet - Sylgard 186.
- [9] V. Ratta. *Crystallization, Morphology, Thermal Stability and Adhesive Properties of Novel High Performance Semicrystalline Polyimides*. PhD thesis, Faculty of Virginia Polytechnic Institute and State University, 1999.
- [10] Dow Corning. <http://www.dowcorning.com>.
- [11] R.W. Ogden. *Nonlinear Elastic Deformations*. Dover, 1998.
- [12] C.W. Macosko. *Rheology: principles, measurement and applications*. VCH Publishers, 1994.
- [13] A.N. Gent. *Engineering with Rubber - How to Design Rubber Components*. Hanser Publishers, 2001.
- [14] M. Gonzalez, F. Axisa, F. Bossuyt, Y. Hsu, B. Vandeveldel, J. Vanfleteren. Design and performance of metal conductors for stretchable electronic circuits. *Circuit World*, 35(1):22–29, 2009.

REFERENCES

67

- [15] M. Gonzalez, F. Axisa, F. Bossuyt, Y. Hsu, B. Vandeveldel, J. Vanfleteren. Design and performance of metal conductors for stretchable electronic circuits. In *2008 2nd Electronics Systemintegration Technology Conference*, number vol.2, pages 371–6, 2008 2008.
- [16] M. Gonzalez, F. Axisa, M. Vanden Bulcke, D. Brosteaux, B. Vandeveldel, J. Vanfleteren. Design of metal interconnects for stretchable electronic circuits using finite element analysis. In *2007 International Conference on Thermal, Mechanical and Multi-Physics Simulation Experiments in Microelectronics and Micro-Systems. EuroSime 2007*, pages 346–51, 2007 2007.

Chapter 3

Stretchable substrate technology

This chapter describes a technology for the realization of stretchable electronic circuits by building it up onto a stretchable substrate. In the end, it is completely embedded into a stretchable polymer.

3.1 Introduction

Building up the stretchable electronic circuit directly on a stretchable polymer seems to be a straightforward way to realize an elastic microsystem. It's an approach being used by many other research groups ([1], [2], [3], [4], [5], [6], [7], [8]). In some cases, it's the best choice. Unfortunately, there are also some disadvantages related to this approach, especially for realizing elastic microsystems using soldered SMD electronic components. We propose our variant on this technology and discuss the advantages/disadvantages.

3.2 General description of process flow

The process flow is depicted in Figure 3.1 and 3.2 and will be in detail explained in the following sections. A layer of PDMS (e.g. Sylgard 186 [9]) is spincoated or casted on the backside of an adhesion promotor treated copperfoil, followed by a curing step. The sample is turned upside-down, attached to a temporary polyimide substrate (Cirlex [10]) and by lithography and etching, copper patterns are formed realizing the stretchable interconnections. Soldermask is applied on

3.2 General description of process flow

the areas where components are mounted and the copper is foreseen of a finish. Components are mounted and soldered leading to a functional circuit.

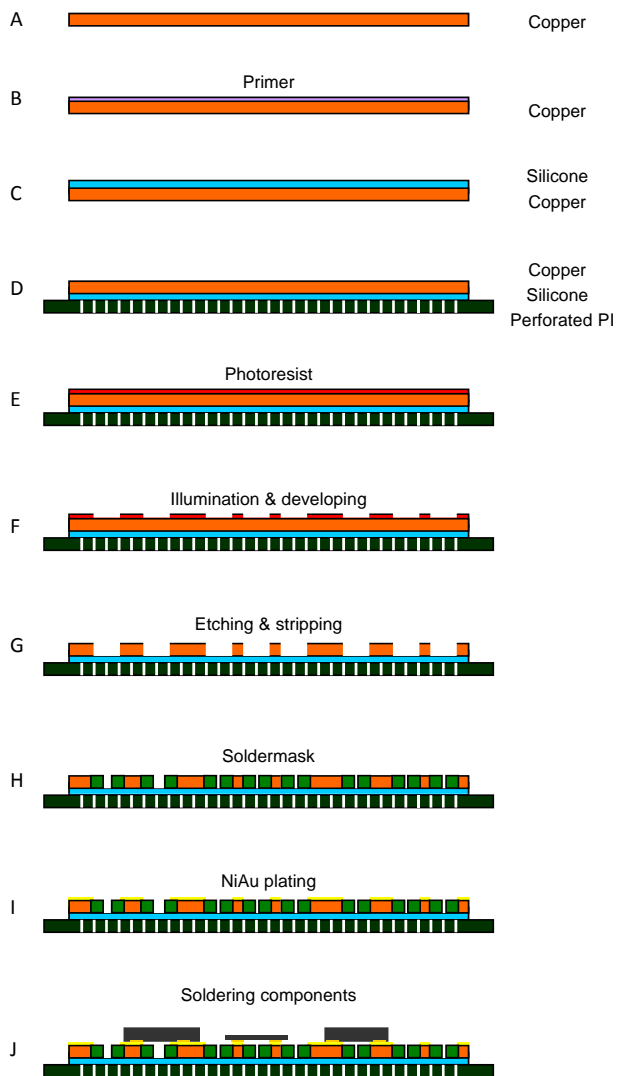


Figure 3.1: Stretchable substrate technology process flow - substrate fabrication

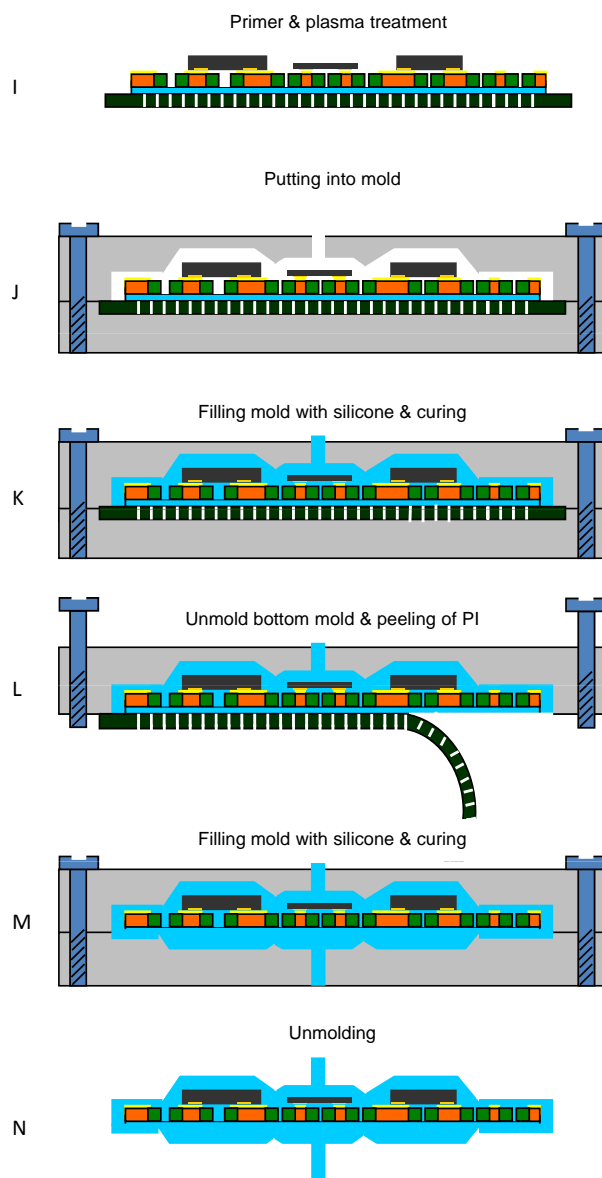


Figure 3.2: Stretchable substrate technology process flow - moulding

3.3 Application of polymer on copper substrate

71

Before embedding the top part, an adhesion promotor is applied to ensure good adhesion between the components, tracks, soldermask and the embedding polymer. This top polymer is typically another layer of PDMS, deposited on top by casting or moulding. For moulding, the substrate will be put into a mould into which the polymer is injected on top of the circuit by liquid injection moulding. After heatcuring the polymer, the bottom mould is removed. Finally, the temporary carrier is removed by just peeling it off. In case a thicker, shaped or different backside encapsulant is needed, a second moulding step takes place. This by application of adhesion promotor, placing the bottom mould and injecting the polymer. After fully curing, the mould is opened resulting in a completely polymer embedded stretchable electronic circuit.

3.3 Application of polymer on copper substrate

For developing this technology, an 18 μm TW/YE copperfoil (Circuitfoil [11]) was selected as base material. Proper adhesion can be enhanced both physically and chemically: by selecting a rough copper base material ($T_a \sim 5 \mu\text{m}$) good physical adhesion with the polymer will be obtained. Chemical adhesion can be achieved by applying dedicated adhesion promotor. In our case, using PDMS as embedding polymer we obtain good chemical adhesion by application of adhesion promotor OS1200 (Dow Corning [12]). Depending on the desired thickness of the PDMS, it can be spincoated or casted. In cases where electronic components are involved in the final system, being soldered at high temperatures (260°), a thin PDMS layer is preferred in order to minimize the undesired effect of thermal expansion, shifting the components during vapour phase soldering. For applications where the stretchable substrate doesn't have embedded components (stretchable cables, samples for reliability testing), a thick layer can be casted.

Application by spincoating

A thin layers of silicone can be obtained by spincoating liquid Sylgard 186 on the backside of a copper substrate. The spincoat curve of Sylgard 186 is shown in Figure 3.3. Typical thickness of the silicone used in the technology is $\sim 100 \mu\text{m}$. This is achieved by spinning during 1 min at 3000 rpm. In this step, it's crucial to avoid deposition of silicone at the backside of the copper substrate, in order to prevent problems during patterning of this thin Cu layer. This can be achieved by protecting that side by attaching a thin foil on it by tape.

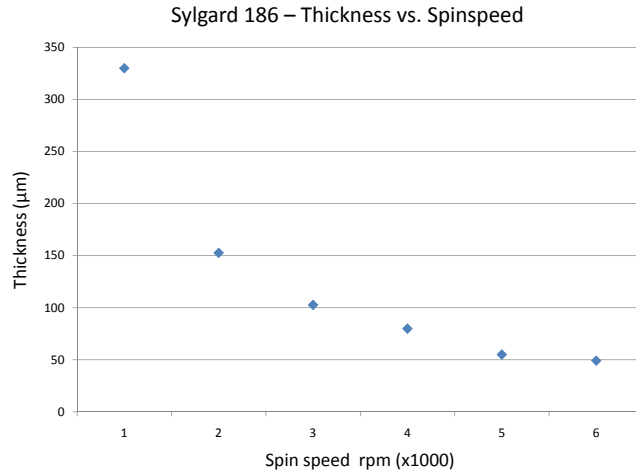


Figure 3.3: Sylgard 186: thickness vs. spinspeed

Application by casting

Thicker layers can be applied by casting using an aluminium frame or a teflon frame. By doctor blading, thin and thick layers ($50\text{-}1000\mu\text{m}$) can be achieved. For both application methods, curing the Sylgard 186 is done typically at 50°C . For thin layers, 2 hours is sufficient. For thicker layers, curing time increases up to 3 hours. The low curing temperature is needed to avoid thermal stress gradients between the copper and the PDMS. These cause problems after etching the copper: once the copper is patterned, silicone cured at higher temperatures will shrink and curl, making it impossible to align e.g. the soldermask on it. This is illustrated in Figure 3.4.

After curing, the substrate is also placed on a carrier. For the thin PDMS substrates, it's placed, with the copper on top, on a (perforated) Cirlex polyimide foil (Dupont [10]) having a thickness of $300\mu\text{m}$. Perforation holes (Figure 3.5) are recommended in order to avoid entrapment of air between the temporary PI carrier and the silicone: air bubbles cause problems because of thermal expansion during reflow soldering at elevated temperatures. The physical adhesion between the silicone and the polyimide keeps our stretchable substrate on the polyimide temporary carrier during processing; no temporary adhesive is needed here. For thick PDMS substrates, the carrier can be a FR4 or ceramic substrate foreseen with double-sided tape (Nitto Denko 64390 [13]) because in this case, no electronic components will be assembled.

3.4 Patterning of copper

73

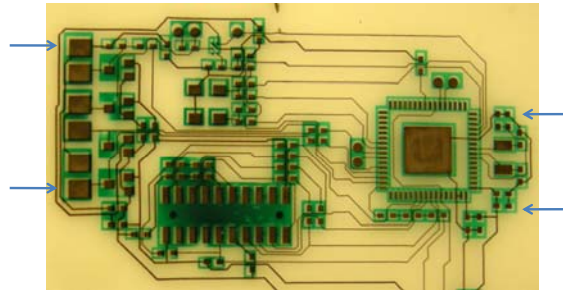


Figure 3.4: Alignment of soldermask is impossible due to shrinkage of the silicone substrate.

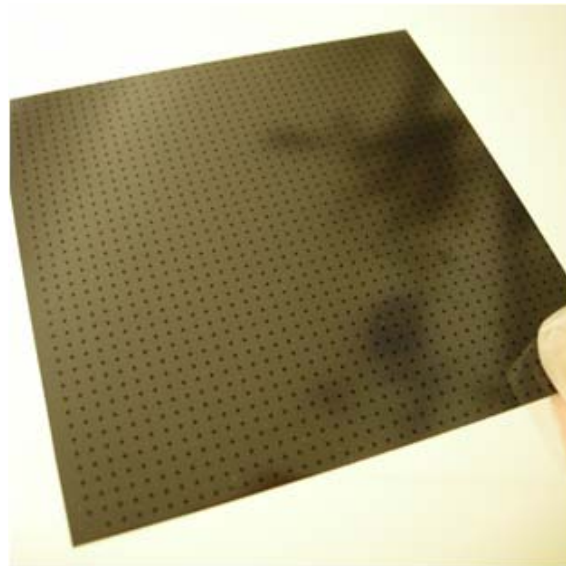


Figure 3.5: Perforated Cirlex polyimide foil with thickness of $300 \mu\text{m}$ is a good carrier for thin stretchable substrates during processing.

3.4 Patterning of copper

Before application of a photoresist, the surface of copper has to be pretreated for ensuring cleanliness and good adhesion. Preposit-Etch E25/29 (Rohm and Haas [14]) is used as a micro-etchant for our surface preparation. The sample is emersed in this solution during 1 minute in order to etch $1 \mu\text{m}$ off the surface. This surface treatment involves also a 60 secs cleaning step in a 10% HCl solution,

followed by a rinse in DI water.

Next, photoresist AZ4562 [15] is spun and a lithography step takes place in order to define the copper tracks. The lithography parameters are shown in Table 3.1

Parameter	Value
Spintime	1 min
Spinspeed	2000 rpm
Prebake time on hotplate	90 sec
Prebake temperature on hotplate	100°C
Development time in Microdev developer	2 min
Postbake time in convection oven	30 min
Postbake temperature in convection oven	120°

Table 3.1: Lithography parameters for AZ4562 photoresist.

Etching is done by use of a spray-etcher in an etch solution based on CuCl_2 , H_2O_2 , HCl (32%) and DI water, resulting in defined copper tracks attached to the silicone substrate. The achievable pitches for an 18 μm copper foil go down to 100 μm . Finally, the photoresist is stripped, the results of the etching steps are illustrated in Figure 3.6.

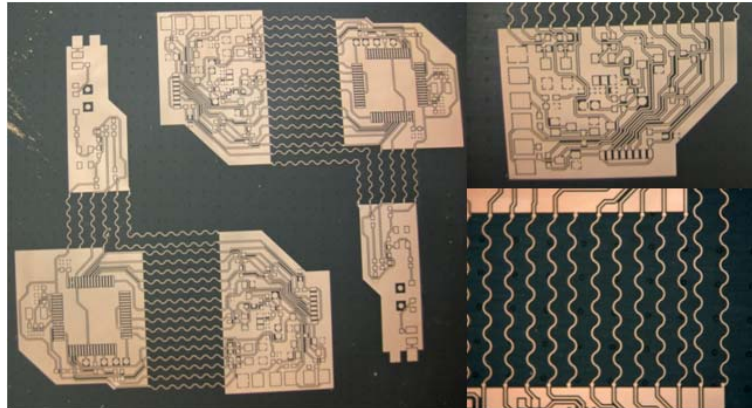


Figure 3.6: Stretchable substrate after copper etching and photoresist stripping.

3.5 Application of soldermask

Before application of soldermask, the silicone is treated with an air-based plasma, in order to make the surface hydrophilic: Figure 3.8 demonstrates the qualitative difference in printing on a non-treated and a treated Sylgard 186 sample.

A 20 μm layer of soldermask ELPIMER SD2463 FLEX HF is applied on the substrate by screenprinting, as demonstrated in Figure 3.8.

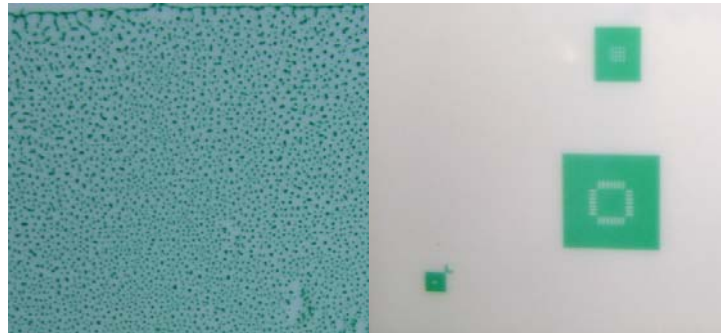


Figure 3.7: Effect of plasma treatment of Sylgard 186 sample. With (left) and without (right) plasma treatment.

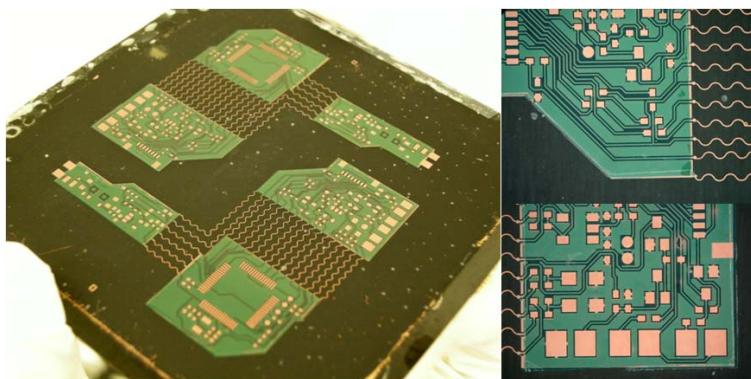


Figure 3.8: Stretchable substrate after application of soldermask.

3.6 Copper surface finish

Different copper finishes are possible (No finish, NiAu finish, OSP finish,..). We will cover these in section 4.6. Due to the high heat resistant nature of the PDMS, NiAu plating is possible (max. processing temperature = 90°C). An electroless Ni, finished with an electroless Au flash can be deposited on the copper, to improve the solder connection reliability. Typical thickness for the Ni deposition is a few 2-3 μm ; thickness of the Au is 150 nm. The result of the deposition is depicted in Figure 3.9.

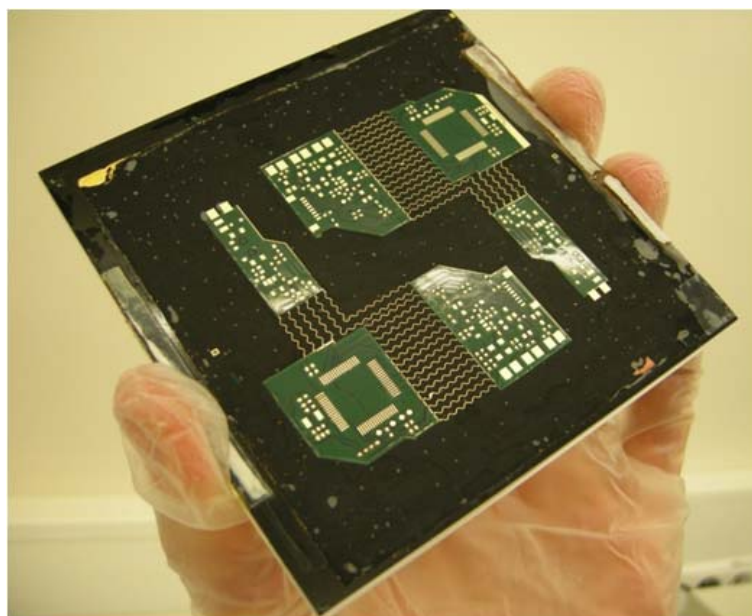


Figure 3.9: Stretchable substrate after NiAu plating.

3.7 Assembly of components

Components are soldered by vapour phase soldering using SAC305 alloy. Due to the high soldering temperature of 260°C , the silicone Sylgard 186 expands: since the linear coefficient of thermal expansion is $330 \text{ ppm}/^{\circ}\text{C}$. As can be seen in Figure 3.10, due to the high temperature during vapour phase soldering, the Sylgard 186 has expanded and some air bubbles are created under the substrate. This can lead to soldering problems, especially for components with a lot of I/O pins. We have noticed that an air bubble can lift a component, leading to a badly soldered component.

This problem can be solved by using a silicone with a lower Young's modulus and a lower CTE, leading to less deformation during soldering at high temperatures. Some tests were performed with Sylgard 527 (Dow Corning) which is a silicone gel and hasn't a noticeable expansion during vapour phase soldering (Figure 3.11). In the end, a different encapsulating silicone material has to be used to embed the whole stretchable circuit.

Furthermore, the use of low temperature soldering pastes (based on Sn, Bi and In which have melting temperatures less than 183°C) is another option or conductive epoxy glues can also overcome the problem of thermal expansion at 260°C .

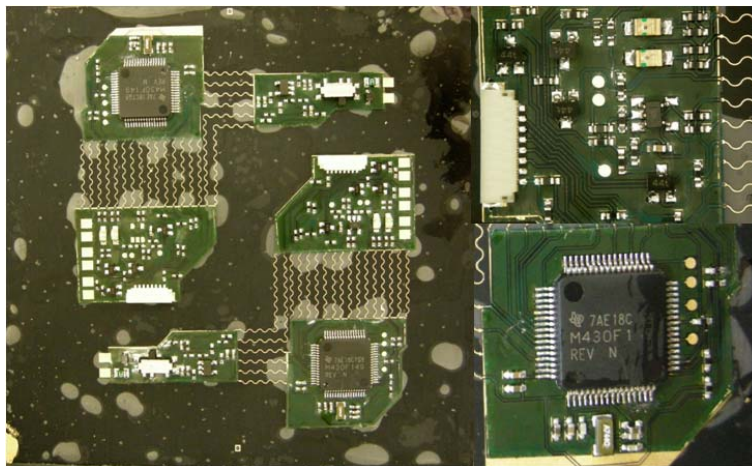


Figure 3.10: Stretchable substrate after assembly of SMD components.

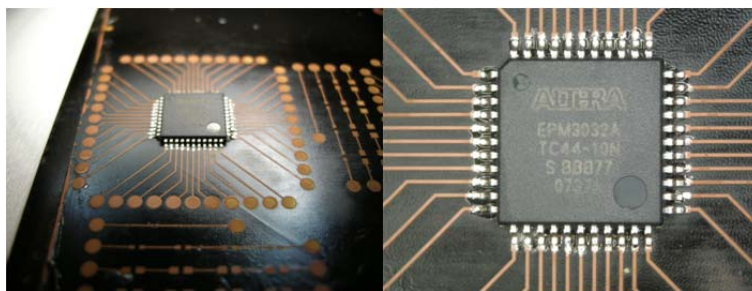


Figure 3.11: Component with a high number of I/O connections (TQFP44 package, 0.8mm pitch) soldered on a gelly silicone substrate.

Before embedding in a polymer, the functionality of the circuit can be tested. Components can be replaced and resoldered if necessary.

3.8 Embedding

Adhesion of the metal tracks, soldermask and components to the embedding elastic material is improved by using the adhesion primer OS1200 (Dow Corning). Finally, the substrate is embedded using the same elastic material (Sylgard 186) as the base material. In case that a gelly, low Young's modulus silicone is used as base substrate (e.g. Sylgard 527), the encapsulation should be done by a different elastic material. The gelly silicone is not suitable as encapsulant, due to

its tackiness and low tearstrength. Encapsulation is done by casting or by moulding. For the moulding steps, we refer to Chapter 4 and 5 where the moulding steps are explained in much more detail. In Figure 3.12, a completely embedded stretchable electronic circuit is shown. Not all components have been implemented and the embedding was done by casting a layer of Sylgard 186 on top, curing it and removing the temporary polyimide carrier and adding another Sylgard 186 layer at the back. The overall thickness is ~3mm.

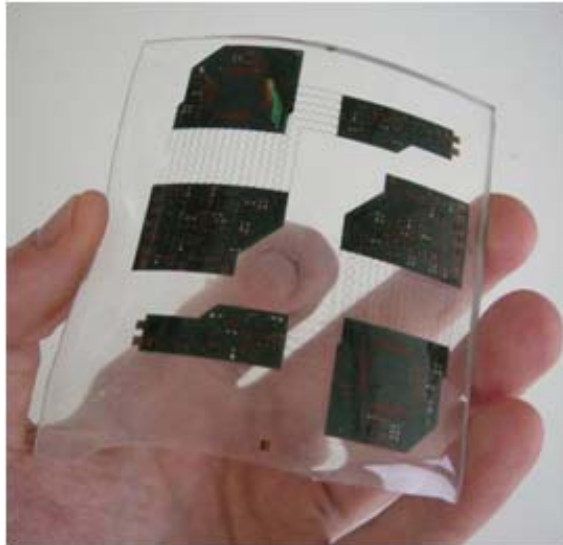


Figure 3.12: Completely embedded stretchable electronic system.

In Figure 3.13 copper meanders are shown produced on Sylgard 186 as base material. They can be used as stretchable cables between 2 non-stretchable circuits and can be soldered by use of SAC or glued by use of a conductive glue.

3.9 Conclusions

We have described a technology for realizing stretchable electronic circuits: by processing on an elastic substrate where the electronic circuit is being built up on. The material selection, the followed technology steps and the characterization of the steps have been presented into detail. As we have noticed, the reflow soldering of components at high temperatures is an issue due to the deformation of the elastomeric substrate. Due to its thermal expansion, the yield after soldering components is low. In the following chapters, we will cover a better approach.

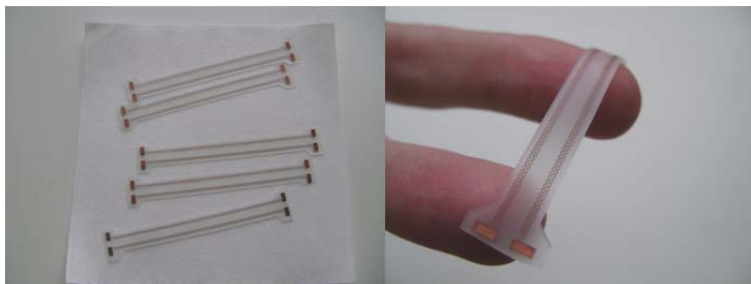


Figure 3.13: Stretchable cables made on stretchable substrate.

References

- [1] D. Kim, J. Xiao, J. Song, Y. Huang, J. Rogers. Stretchable, Curvilinear Electronics Based on Inorganic Materials. *Advanced Materials*, 22(19):2108–2124, May 18 2010.
- [2] I.M. Graz, D.P.J. Cotton, S.P. Lacour. Extended cyclic uniaxial loading of stretchable gold thin-films on elastomeric substrates. *Applied Physics Letters*, 94(7):071902 (3 pp.), 16 February 2009.
- [3] S.P. Lacour, J. Jones, Z. Suo, S. Wagner. Design and performance of thin metal film interconnects for skin-like electronic circuits. *IEEE Electron Device Letters*, 25(4):179–181, Apr 2004.
- [4] P. Mandlik, S.P. Lacour, J. Li, S. Chou, S. Wagner. Fully elastic interconnects on nanopatterned elastomeric substrates. *IEEE Electron Device Letters*, 27(8):650–652, Aug 2006.
- [5] T. Löher, R. Viero, M. Seckel, A. Ostmann, H. Reichl. Stretchable electronic systems for wearable and textile applications. In *2008 IEEE 9th VLSI Packaging Workshop in Japan*, pages 9–12, 2008 2008.
- [6] T. Löher, M. Seckel, R. Viero, C. Dils, C. Kallmayer, A. Ostmann, R. Aschenbrenner, H. Reichl. Stretchable electronic systems: realization and applications. In *2009 11th Electronics Packaging Technology Conference (EPTC 2009)*, pages 893–8, 2009 2009.
- [7] D. Khang, J. Rogers, H. Lee. Mechanical Buckling: Mechanics, Metrology, and Stretchable Electronics. *Advanced Functional Materials*, 19(10):1526–1536, May 22 2009.
- [8] B. Schmied, J. Guenther, C. Klatt, H. Kober, E. Raemaekers. STELLA - Stretchable Electronics for Large Area applications - A new technology for smart textiles. volume 60, pages 67–73, 2009. 3rd International Conference on Smart Materials, Structures and Systems, Acireale, ITALY, JUN 08-13, 2008.

REFERENCES

81

- [9] Dow Corning. Technical datasheet - Sylgard 186.
- [10] FRALOCK. Technical datasheet - Cirlex.
- [11] Circuitfoil. <http://www.circuitfoil.com>.
- [12] Dow Corning. Technical datasheet - OS1200 adhesion promoter.
- [13] Nitto Denko. Technical datasheet - Differential DC/T 64390.
- [14] Rohm and Haas. <http://www.rohmhaas.com>.
- [15] AZ Electronic Materials. Technical datasheet - AZ 4500 Series Photoresists.

Chapter 4

Peelable technology

This chapter describes a technology for the realization of stretchable electronic circuits by use of a temporary carrier where the electronic circuit is being built up on. In the end, it is embedded into a stretchable polymer. The first section gives a general overview of the optimized process flow and the following sections describe the choices made and the optimization of the individual processing steps in more detail.

4.1 Introduction

The initial technology for achieving a stretchable electronics circuit being developed at CMST was based on electroplating gold meander tracks on a copper foil [1]. The gold metal tracks are embedded into a stretchable polymer by partly embedding the sample with PDMS, etching the supporting copper and embedding the exposed side, resulting in a stretchable electronics substrate (Figure 4.1). Thin, typically $4\ \mu\text{m}$, fine-pitch, typically (starting from) $15\ \mu\text{m}$ wide meandered traces are possible due to the additive nature of the processflow (electroplating) leading to very dense electronic circuits (Figure 4.2). Elastic interconnections were developed which could be stretched between 50% and 100% in the longitudinal direction without influencing their resistance. This technology is very suitable for applications where biocompatibility is of major importance (Au is inert to all chemicals it encounters inside the body). Besides these features, the approach has some drawbacks. While processing, all metal tracks are short circuited. This can give problems when embedding batteries. Furthermore, the copper substrate used as temporary carrier needs to be etched completely in the end, lowering down the environmental friendliness of this process. These problems can be solved by the approach presented in this chapter.

4.2 General description of process flow

83

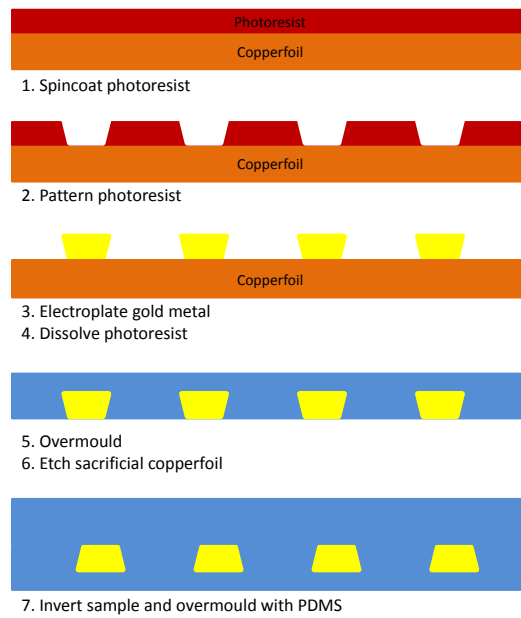


Figure 4.1: Au-plating technology process flow for achieving stretchable electronic circuits.

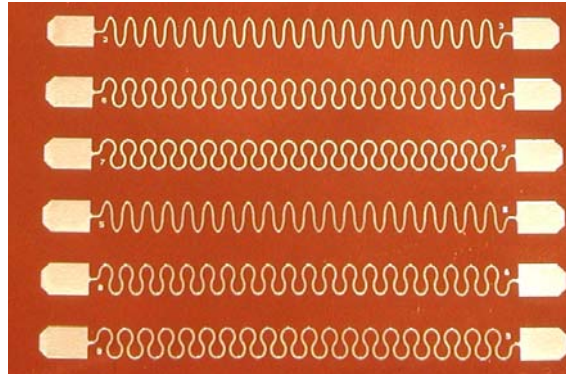


Figure 4.2: Au-plated meanders on copper substrate. Typical feature size: $90 \mu\text{m}$ width, $4 \mu\text{m}$ height.

4.2 General description of process flow

A general overview of the process flow developed during this PhD study is shown in Figure 4.3 and 4.4. A copper foil is laminated on a rigid/flexible carrier

by use of a temporary adhesive. By lithography and etching, the copper patterns are formed realizing the stretchable interconnections. Soldermask is applied on the areas where components are mounted and the copper is foreseen of a finish to enhance solderability. Components are mounted and soldered leading to a functional circuit. At this stage, after testing and eventually reparation, the circuit is ready to be transferred into a polymer.

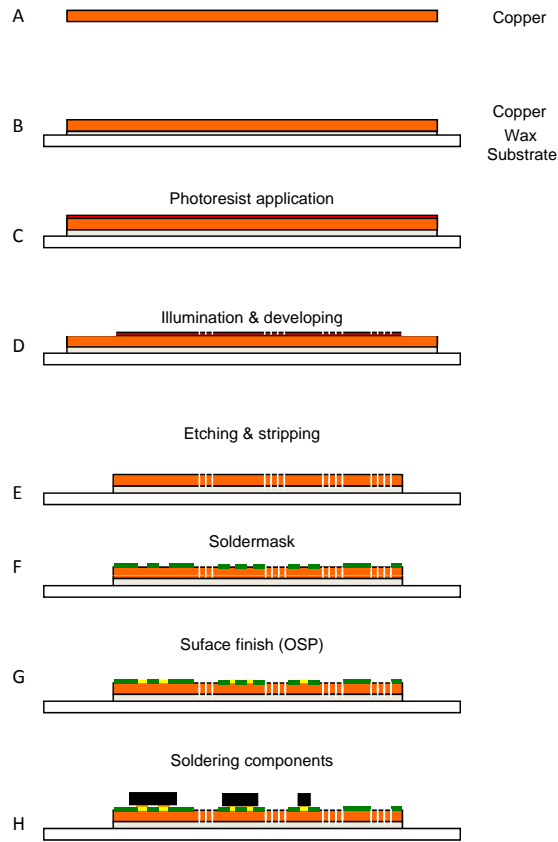


Figure 4.3: Peelable technology process flow - substrate fabrication.

4.2 General description of process flow

85

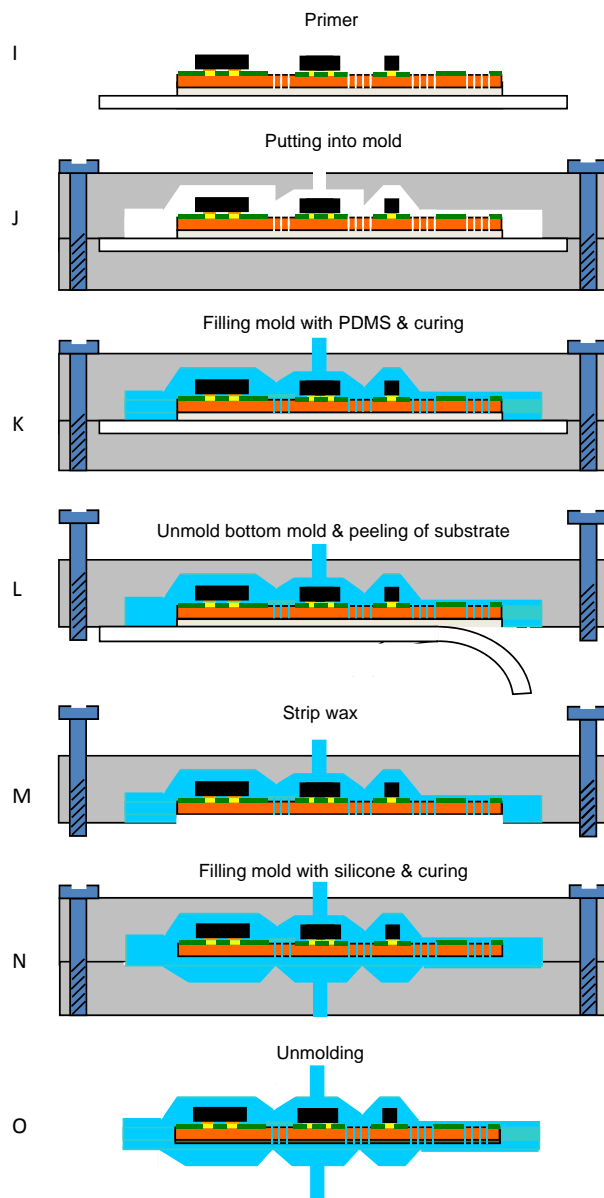


Figure 4.4: Peelable technology process flow - substrate moulding.

Before embedding, an adhesion promotor is applied. This in order to have a good adhesion between the components, tracks, soldermask and the polymer. In the case moulding is used, the substrate is put into a mould where PDMS is injected on top of the circuit by liquid injection moulding. After heatcuring the polymer, the bottom mould is removed. The temporary carrier can then be removed by dissolving/melting the temporary adhesive followed by a cleaning step to remove this temporary adhesive. Adhesion promotor is applied on the back side, the bottom mould is replaced and PDMS is injected. After fully curing, the mould is opened and the completely PDMS embedded stretchable electronic circuit can be removed. More details about this process flow and its optimization will be in detail explained in the following sections.

4.3 Lamination of copper on carrier with temporary adhesive

4.3.1 Copper type

The used copper foil in Figure 4.3(A) has been selected in order to have a good adhesion between the copper foil and the rigid/flexible carrier by use of the temporary adhesive. The good adhesion should be maintained during all the process steps. This is achieved by selecting a copper sheet, used for the fabrication of laminates for rigid composite and conventional multi-layer/mass lamination applications. This means, a copper sheet with a certain roughness at the interface side and a rather smooth surface at the patterning side. Furthermore, the mechanical properties of the copper foil are important, this because the copper will be subjected to mechanical forces. For these reasons, a TW-YE 18 μm copper foil (Circuitfoil [2]) has been used to demonstrate the feasibility and characterize the process flow. The properties of the copper foil are shown in Table 4.1. The untreated side of the copper has a roughness between 0.2-0.4 μm (=the side we will use for photodefinition), on the treated side it's between 6 μm -8 μm (the side we will use for having a good mechanical adhesion to the temporary substrate). The inorganic, so-called YE protection on the shiny surface of the foil offers superior resistance to oxidation in warm and humid environments.

Parameter	Value
Untreated side roughness	0.20 μm - 0.40 μm
Treated side roughness	6 μm - 8 μm
Tensile strength transverse at RT	276 MPa
Elongation transverse at RT	6%

Table 4.1: Properties of TW-YE copper foil.

4.3 Lamination of copper on carrier with temporary adhesive

87

4.3.2 Temporary adhesives

The copperfoil is laminated by use of a temporary adhesive on the rigid/flexible substrate 4.3(B, C).

The desired properties of the temporary adhesive include:

- Good adhesion between carrier and circuit upto 60°C (= temperature of Cu wet-etching process).
- Being non tacky when exposed in order to avoid dust collection, adherence to screen during screenprinting,...
- Compatible with acid etching, base developing/stripping, solvents,.. thus all chemicals involved in the process.
- Non-burning and removable after a temperature step of 260°C.
- Having a bad adhesion to PDMS when its surface is treated with PDMS primer. Otherwise the temporary carrier won't be removable anymore after the first moulding step.

We come back to these issues during the following sections. To find a temporary adhesive fullfilling all these needs was not easy. Different kinds of materials have been studied. The feasibility of every solution is discussed in the following paragraphs:

Pressure sensitive adhesives

To form a permanent bond, structural adhesives harden via processes such as evaporation of solvent, reaction with UV radiation, chemical reaction (such as two part epoxies), or cooling (as in hot melts). In contrast, pressure sensitive adhesives (PSAs) form a bond simply by the application of light pressure to marry the adhesive with the adherend. Pressure sensitive adhesives are designed with a balance between flow and resistance to flow. The bond forms because the adhesive is soft enough to flow, or wet the adherend. The bond has strength because the adhesive is hard enough to resist flow when stress is applied to the bond. PSAs are usually based on an elastomer compounded with a suitable tackifier. The strength of the bond, for PSAs expressed as the shear holding power, is determined by the type and ratio of the base polymer and tackifier and the level of cross-linking of the polymer [3],[4],[5]. The idea behind this option was to use an adhesive that shouldn't be removed by using a solvent rinse after moulding the top part of the circuit. With the other solutions that will be proposed, you always have a cleaning step in order to remove it completely. By use of a pressure

sensitive silicone, no residues are left after removing the temporary carrier. This offers a great advantage.

Gel silicones Sylgard 527 and Sylgard 4150

Sylgard 527 [6] and Sylgard 4150 [7] are primerless silicone dielectric gels. They are two component, transparent silicone encapsulants specially designed to seal, protect and preserve the electrical characteristics of delicate electronic circuits in severe environments. The products cure in place to form a cushioning, self-healing, resilient gel-like mass. They both exhibit a reformable, pressure-sensitive adhesive bond to many compatible substrates. These materials are typically uncross-linked or slightly cross-linked mixtures of a high molecular weight polymer with a tackifier resin, though in some systems the tackifier resin is omitted. The adhesive normally has a glass transition temperature of 20°C to 50°C below the temperature of usage, so is essentially a rubbery liquid. Both silicones have been applied on a substrate and cured. The main disadvantage is that the surface remains somehow tacky, this will give problems in terms of dust collection and adhesion to the screen during screenprinting soldermask, solderpaste. Furthermore, the adhesion itself of the copper structures to the gel-silicone interface was not high enough.

Flex fixer board

A flexfixer board [8] is used as carrier for flexible substrates. It is suitable for surface mount technology (SMT), solder paste printing, encapsulation or underfill dispensing and during reflow and curing processes. The base of the board can be ordered in various thicknesses. Usually, standard thickness is 1.6mm and base substrates can be manufactured from FR4, G-10, magnesium, aluminium. The resin is a film applied to the base and is used to hold the flexible circuits in place and flat. The resin will hold the flex circuit during the entire assembly process. At the end of the process the circuits can be peeled off, no residue will be left on the circuits. A copper foil has been laminated but it was immediately clear that the adhesion of the copper structures to the board was not high enough: delamination was observed during copper etching.

Double sided tape Nitto Denko

This tape Nitto 64390 is a differential pressure sensitive tape [9] been developed for application of flexible substrates on carriers during processing and has been optimized to be able to withstand reflow soldering temperatures. It consists of a pressure sensitive acrylic adhesive (38 μm) on the permanent side and a pressure sensitive acrylic adhesive (25 μm) on the removable side. In between, there is a PET carrier (12 μm). It serves for temporary bonding of various substrates who need to be removed from each other without leaving any residue. A drawback of this tape is that it sticks, thus during processing it will give problems in terms of dust collection and adhesion to the screen during screenprinting soldermask or

4.3 Lamination of copper on carrier with temporary adhesive

89

solderpaste. Furthermore, the adhesion itself of the copper structures to the tape was not high enough.

Photoresists as adhesion layer

Another idea was to use a photoresist layer as adhesive layer between the copper and another substrate. Photoresist has been optimized to have a good adhesion with copper, can be easily stripped in a stripper solution and doesn't stick during processing. Attention should be paid to the fact that the photoresist acting as the adhesive layer doesn't dissolve during developing or stripping the photoresist used for the pattern definition of the copper. Another issue needed to be tested was the possibility of stripping the photoresist adhesion layer after vapour phase soldering.

Dry film photoresist FX Riston 930

FX Riston 930 [10] is a negative working, aqueous processable dry film photoresist suitable for print-and-etch and tent-and-etch applications with acid and alkaline etchants. It has a very high resolution capability with wide processing latitude. The thickness is 30 μm and is applied by lamination using a roll laminator. A micro-etched 18 μm TW-YE copper sheet has been used where the rough side was foreseen of 3 layers of FX Riston 930 photoresist by roll laminating at a temperature of 120°C. 3 layers are used in order to reach a thickness giving enough mechanical strength to act as supporting layer. The photoresist has a protective sheet and is removed before every new laminating step. In this way, a final photoresist thickness of 90 μm has been achieved. On the smooth side of the copper, 1 layer of FX Riston 930 was foreseen, being used to pattern the copper. This side was photo-illuminated and patterned through a glass mask. Also the backside was illuminated in order to make it resistant to the 1% Ca_2CO_3 developer solution. Nitto 64390 double sided tape is used to attach the sample to a ceramic for the subsequent wet processing steps. The copper has been etched and the top photoresist stripped by use of 0.8% NaOH solution. The result of these process steps is shown in Figure 4.5 and 4.6. The photoresist at the backside is also attacked by the stripper solution but due to the thickness (60 μm) this is not a problem.

A similar sample was made for testing the vapour phase soldering resistance. The same design has been used as shown in Figure 4.11. It was observed that the photoresist didn't withstand the vapour phase temperature and started to deform. Furthermore, delamination of the copper structures was observed as depicted in Figure 4.7.

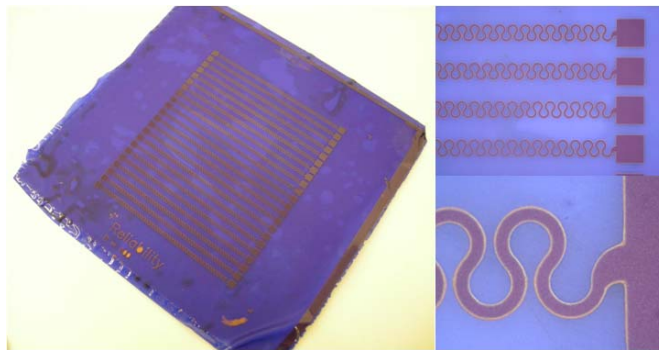


Figure 4.5: FX Riston as adhesive/carrier and photoresist for copper etching: after etching copper.

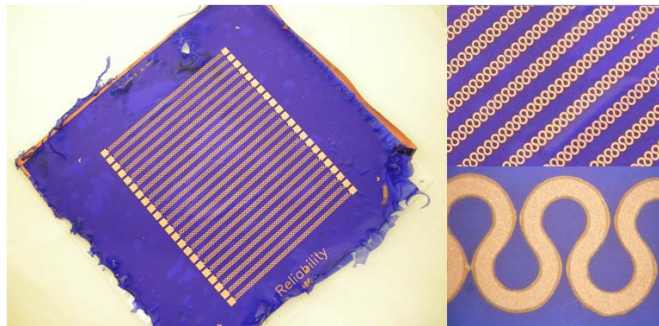


Figure 4.6: FX Riston as adhesive/carrier and photoresist for copper etching: after stripping top photoresist.

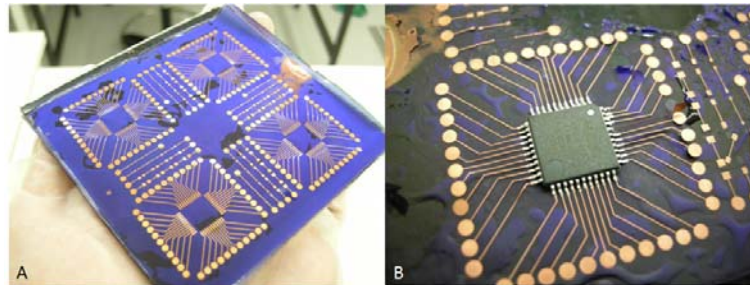


Figure 4.7: FX Riston as adhesive/carrier and photoresist for copper etching: before (a) and after (b) vapour phase soldering.

4.3 Lamination of copper on carrier with temporary adhesive

91

Spin-on photoresist AZ4562

AZ4562 [11] is a thick positive photoresist, intended for applications where coating thicknesses above $3\ \mu\text{m}$ are required. We applied it by spincoating on the rough side of a $18\ \mu\text{m}$ TW-YE copper sample at 2000 rpm, resulting in a layer thickness of $\sim 10\ \mu\text{m}$. A hardbake step was performed in a convection oven at 120°C during 30 minutes. Copper patterning was done using the dry film photoresist FX Riston 930 and wet etching. After application of the photoresist by roll lamination, the sample was placed on a ceramic with the Nitto 64390 double sided tape. The AZ4562 photoresist is not strong enough to act as a carrier during the wet processing steps. After etching, it was already observed that the strength of the AZ4562 photoresist was not high enough and some parts of it already delaminated (Figure 4.8 a). Vapour phase soldering was performed (Figure 4.8 b) but the quality of the sample was already too low before so this option was discarded.

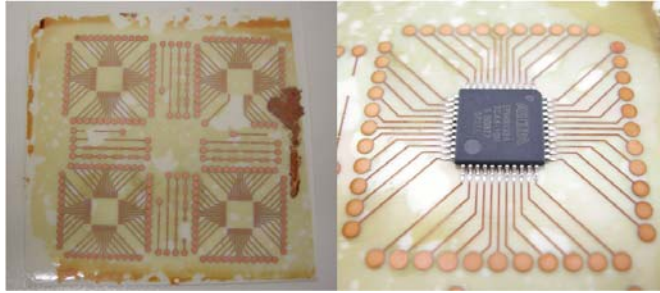


Figure 4.8: AZ4562 photoresist as adhesive: before (a) and after (b) vapour phase soldering.

Waxes

Waxes can be characterized by the following properties [12]:

- Solid at room temperature (soft and flexible to brittle and hard).
- Melting point above 40°C .
- Low viscosity just above melting point.
- Natural or synthetic origin.
- Consistency and solubility are strongly dependent on temperature.
- Can be polished under slight pressure.

The fact that they are solid at room temperature, especially non-tacky, make them ideal for our application. When they are melted, they can be applied and used as adhesive, as long as they aren't subjected to temperatures above the melting point and emersed in mediums that dissolve them. Different types of waxes are compared below.

Aquabond water soluble wax

Aquabond's water soluble thermoplastic [13] is designed for temporary mounting of hard materials for slicing, dicing, grinding, lapping and polishing, and works well as a chemical etch barrier. Aquabond comes in 3 different bonding temperatures. ABS-85 has been tried, having the highest melting temperature of 85-105°C. The other properties are listed in Table 4.2. It has been applied on the rough side of a 18µm TW-YE copper sheet. This by heating up the copper on the hotplate of a doctorblade upto 120°C and applying a layer of this wax by casting using the blade (Figure 4.9).

Parameter	Value
Tacking temperature	50-60°C
Softening temperature	60-85°C
Melting temperature	85-105°C
Bonding temperature	85-105°C
Viscosity (75°C)	<3000 cps
Water Solubility (80°C)	100%
Debond/Cleanup	Hot DI Water

Table 4.2: Properties of Aquabond ABS-85 water soluble wax.

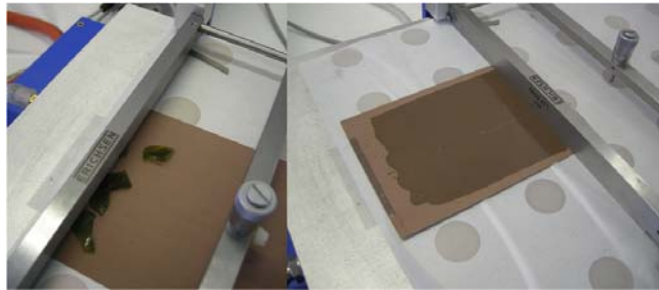


Figure 4.9: Application of Aquabond wax on copper sheet by doctorblading.

A thickness of 100 µm has been chosen. The sample has been manually applied on an etched RO4003 ([14]) substrate by pressing such a substrate on the heated copper sheet with molten wax. When the sample is back at room temperature, the wax hardens again. The copper has been patterned by use of a dry film photoresist (FX Riston 930 [10]) and wet etching. During wet etching of the copper at 65°C, no delamination has been observed of the patterns (Figure 4.10). Next,

4.3 Lamination of copper on carrier with temporary adhesive

the sample was put into the vapour phase soldering station resulting in a good soldered thin small-outline package (TSSOP) (Figure 4.11 a) but during soldering, it has been observed that the wax started to burn (Figure 4.11 c). It was not removable anymore and PDMS Sylgard 186 didn't cure anymore on it. Therefore, this option has been discarded.

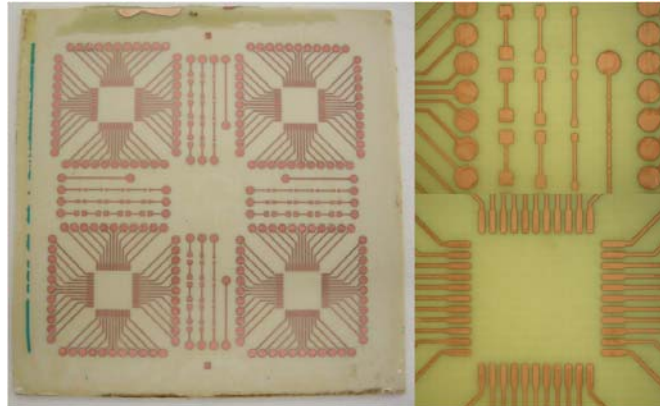


Figure 4.10: Result after copper etching: no delamination observed by use of Aquabond 85.

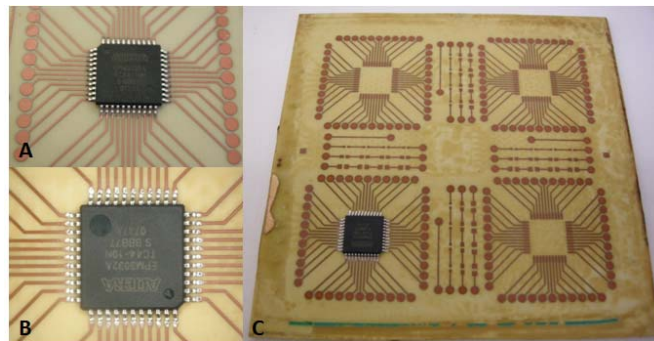


Figure 4.11: (a) Before vapour phase soldering, after application of solderpaste and TSSOP package. (b) After vapour phase soldering, well soldered TSSOP package. (c) After vapour phase soldering, Aquabond wax is burnt (brown color).

Quickstick T135 wax

This is a crystal clear wax [15] and has a high hardness and strength. This temporary mounting wax is used in a variety of applications to bond samples during processing. It has been developed for diamond wheel cutting, wire saw cutting, abrasive slurry cutting, ultrasonic cutting, lapping and polishing, etc. This wax is soluble in acetone and methylene chloride, but resists most other common solvents. It's a thermoplastic polymer with a softening point of 71°C and flow point of 135°C. The viscosity at flow point is 6000 cps. It has been tested in a similar way as the Aquabond wax. This wax resisted all chemicals used during processing and was removable after vapour phase soldering! This wax will be further described in the following sections and is the main option for use in the stretchable circuit technologies.

To conclude this section, several materials have been tested and compared, some with more success than others. In the technologies that will be presented, Quickstick 135 is the best option and will be used because it gives good adhesion during processing, even during wet etching at 65°C. It's compatible with all the chemicals used and it doesn't stick at room temperature, a necessity for screenprinting soldermask or solderpaste. It also doesn't stick with the adhesion promotor we use in order to get good adhesion between the PDMS and the circuit structures. A drawback is the way of application and the needed removal rinse in the end of the process. By use of alternative process techniques, the issues we have with some materials could be solved. E.g. by laminating soldermask and dispense solderpaste, the tackiness of the surface becomes less critical. Concerning adherence to the embedding elastomer after application of the primer on the adhesive, if one would use other embedding materials than silicone (e.g. polyurethane), this issue would disappear. During this work, we will focus on the use of Quickstick 135 wax.

4.3.3 Temporary substrate

In the beginning, a flexible substrate has been used as carrier. A flexible substrate offers the advantage of being compatible with roll-to-roll processes. Also, peeling off the temporary carrier after the first moulding step (see further) is easier compared to a rigid carrier. A copper etched Upisel SE1410 foil [16] has been used for these purposes: adhesion experiments showed that the adhesion between a smooth polyimide film, Quickstick T135 and a copper sheet was not high enough. Therefore, an etched Upisel SE1410 foil has been used, having a certain roughness at the interface and allowing a good physical adhesion. In Figure 4.12 a, the peeling off of such a substrate is shown at the end of the fabrication process. Due to impractical reasons, mainly because of handling, the change was made to a rigid carrier. This makes the manual processing much easier during the PCB

4.3 Lamination of copper on carrier with temporary adhesive

95

process steps. In this way, the production of our stretchable circuit technology comes closer to standard, rigid PCB production steps what is favorable. An etched RO4003 substrate (Rogers [14]) was chosen, having a glass transition temperature of 260°C and thus, able to withstand a vapour phase reflow soldering process. In a later stage of the process development, an etched FR4 board has been used. In Figure 4.12 b, the RO4003 carrier (Rogers [17]) is shown.

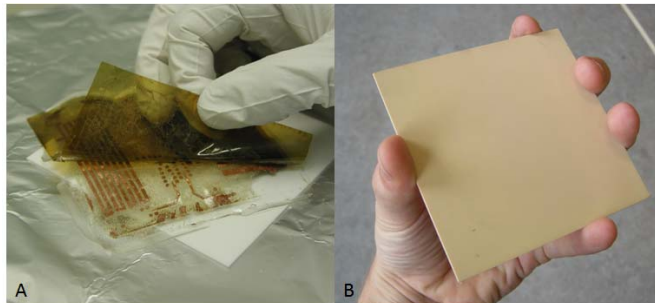


Figure 4.12: Temporary carriers: (a) flexible and (b) rigid.

4.3.4 Lamination

The wax is deposited on the roughest side of the copper, to ensure maximum adhesion of the copper to the temporary substrate. The wax is used as a temporary adhesive which loses its adhesion when heated (melting point is 135°C) or when dissolved in acetone. The wax is applied by dissolving one Quickstick (13.5 g) in 30 ml of acetone and spin coating it on the copper and the temporary substrate. Spinning is done at 1000 rpm during 30 secs. The copper is then laminated on the flexible substrate in a Lauffer vacuum lamination press. The temperature and pressure profile for vacuum lamination is shown in Figure 4.13. The temperature is increased from 50°C upto 75°C . In this way, the wax starts to melt. After 10 minutes, when the wax has become tacky, pressure is applied followed by lowering the temperature.

In this way, laminated samples are obtained as illustrated in Figure 4.14.

These rigid samples can be handled as conventional PCB substrates ready for further processing. $18\ \mu\text{m}$ TW-YE copper has been chosen resulting in achievable linespacing/trackwidth of $50\ \mu\text{m}/50\ \mu\text{m}$. The sheet can easily be replaced by another, thinner/thicker copper foil depending on the application (see Wireless Power Circuit demonstrator in Chapter 7). The minimal copper thickness we used was $9\ \mu\text{m}$, to obtain small features for e.g. high-density electronic circuits.

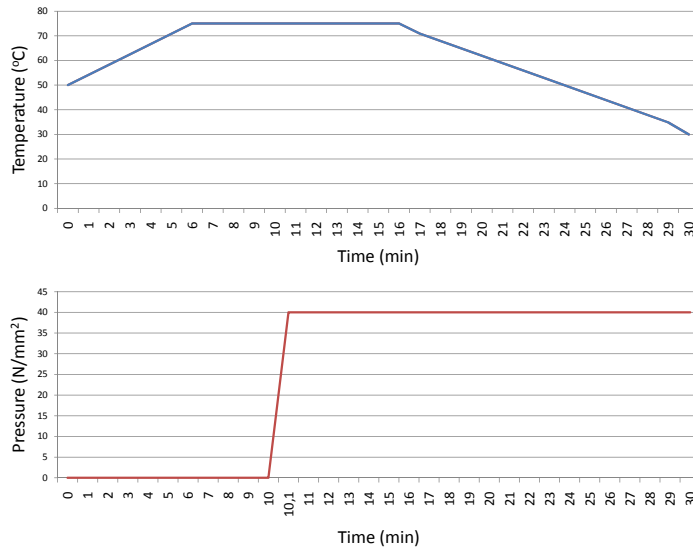


Figure 4.13: Vacuum lamination profile.

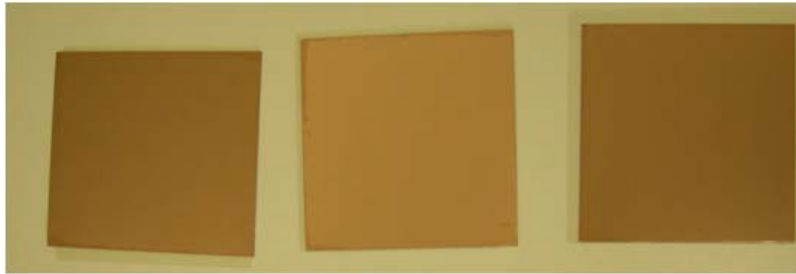


Figure 4.14: Vacuum lamination of TW-YE copper samples on etched RO4003 substrate.

4.3.5 Adhesion of copper on carrier

To determine the effect of certain process parameters on the adhesion of the copper on the temporary carrier, peeltests on different samples have been performed. 2 types of copper have been used, having a different roughness. For TW-YE, it is $6\mu\text{m} - 8\mu\text{m}$, for plain copper it is $\sim 2\mu\text{m}$. This to have a clue of the importance of the roughness of the copper on the adhesion. 2 ways of lamination of the copper on the sample have been used. A first way by spinning wax on the copper and on

4.3 Lamination of copper on carrier with temporary adhesive 97

the substrate and vacuum lamination during 30 minutes according to the profile as shown in Figure 4.13. A second way by spinning wax on the substrate and roll lamination the copper onto it by use of a roll laminator. The configuration of the roll laminator is depicted in Table 4.3. 3 different wax solutions have been made: 15 ml, 30 ml and 60 ml acetone per Quickstick (13.5g). This in order to determine the effect of wax concentration on the adhesion.

Parameter	Value
Laminator type	MegaElectronics Photopolymer Dry Film Laminator
Temperature	140°C
Lamination speed	0.15 meters / min.
Pressure setting	1/16th inch thick panels to 3/32nd inch thick panels.

Table 4.3: Settings of roll laminator.

For all the samples, peelstrength tests have been performed. This by lasercutting 3 mm wide strips after lamination of the copper on the substrate. A sample is shown in Figure 4.15 mounted into the peelstrength test setup.

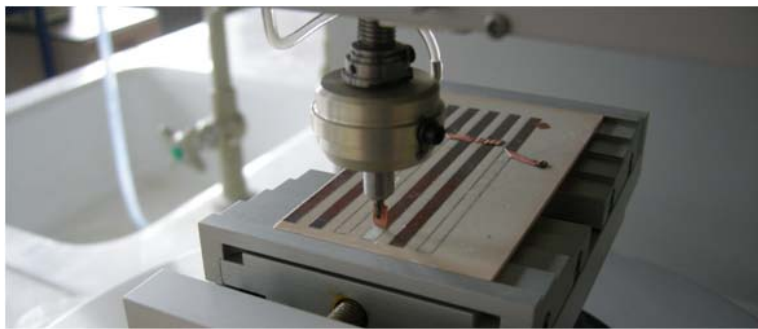


Figure 4.15: Peelttest sample in test setup.

The results of these tests are shown in Table 4.4 and Figure 4.16 where the peelstrength is expressed in N/mm.

	15 ml	30 ml	60 ml
TW-YE copper	0.57 N/mm	0.64 N/mm	0.34 N/mm
Plain copper	0.78 N/mm	0.69 N/mm	0.35 N/mm
TW-YE copper, roll laminated	0.47 N/mm	0.32 N/mm	0 N/mm

Table 4.4: Peelstrength test results.

For the value of 0 N/mm, the adhesion was too low to do proper peelstrength measurements.

Adhesion copper - wax - substrate

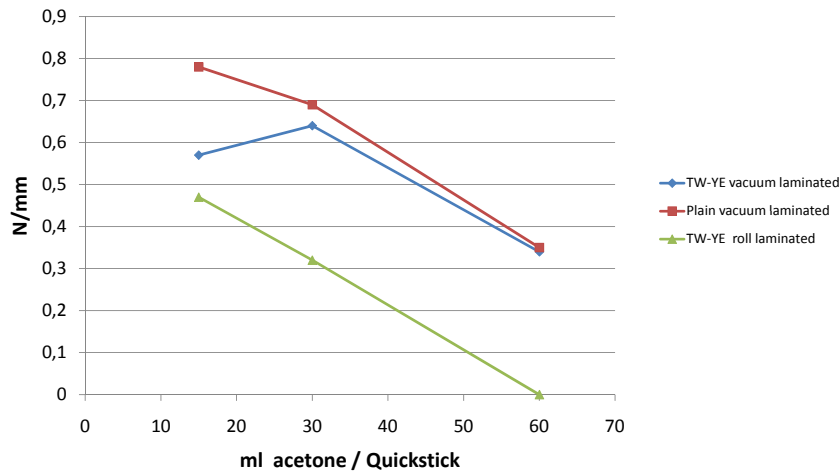


Figure 4.16: Peelstrength test results.

The following conclusions can be made out of the data:

- Adhesion of wax solution based on 30 ml acetone is twice as good than for a 60 ml solution. The effect on adhesion is much more expressed between the 30 ml and 60 ml based solution than between the 15 ml and 30 ml based solution.
- No big difference in adhesion between TW-YE and plain copper: roughness is less important than expected.
- The adhesion of the roll laminated samples is half the adhesion strength of the vacuum press laminated samples in the case of a 30 ml based solution.
- The adhesion of the roll laminated samples by use of the 60 ml solution, is not sufficient to perform peelstrength tests.

Out of these experiments, we concluded to work further with the TW-YE type of copper foil. The roughness of the copper on the backside will play an important role in the technologies presented in the upcoming chapters where adhesion to the supporting polymer is of major importance. A wax solution of 1 stick per 30 ml is used giving more or less the same adhesion compared to the 15 ml solution. Furthermore, dissolving the stick in 30 ml is easier, as is the spincoating of a less viscous material. The presented vacuum lamination cycle will be further used,

4.3 Lamination of copper on carrier with temporary adhesive **99**

due to its proven functionality.

After lamination of the copper on the carrier, a lithography step takes place. The temperatures of the soft- and postbake steps mentioned in the datasheet of AZ4562, are quite high and we risk the loss of adhesion between the copper and substrate (due to wax melting). In order to verify this, copper laminated base substrates were compared by processing a number of samples at the recommended lithography temperatures and at lowered lithography temperatures. Part of the used copper mask design is shown in Figure 4.17, consisting of parallel rows of meanders varying in width from 56 μm upto 136 μm . The remaining of the mask contains a repetition of these structures. The parameters of the process steps are listed up in Table 4.5.

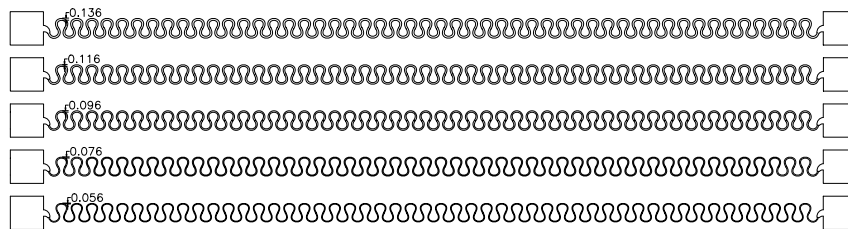


Figure 4.17: Part of Cu wet etching adhesion test design.

	Normal temperature	Lowered temperature
Prebake	90 °, 2 minutes on hotplate	60 °, 15 minutes on hotplate
Postbake	120 °, 30 minutes in convection oven	60 °, 15 minutes on hotplate

Table 4.5: Parameters for lithography of peelable samples using AZ4562.

Spray etching tests were performed to see the effect of the temperature steps during the lithography on the adhesion of patterned meanders.

The samples were etched by use of a spray etcher and an etch solution based on CuCl_2 , H_2O_2 , HCl (32%) and DI water. In Figure 4.18 the results are shown from TW-YE copper samples being processed at normal lithography temperatures (Figure 4.18 a) and TW-YE copper samples being processed at lowered temperatures (Figure 4.18 b). Qualitatively, we see a clear difference between the samples. Lowering the lithography temperatures is necessary in order to keep the good adhesion between the tracks and the substrate. Non of the samples with lowered processing temperatures didn't show any delamination.

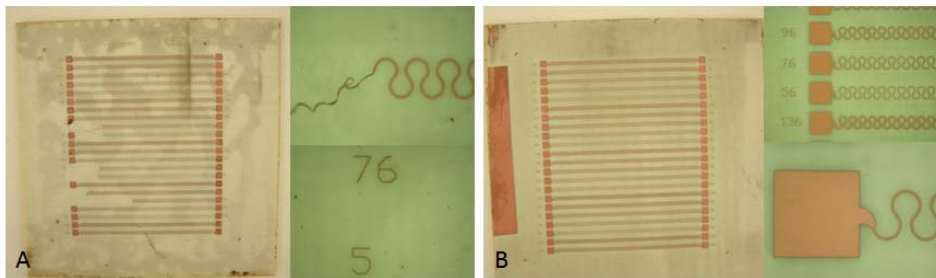


Figure 4.18: Spray etch tests to measure adhesion performance: (a) Normal lithography temperatures. (b) Lowered lithography temperatures.

4.4 Patterning of copper

4.4.1 Micro-etching

Before the application of a photoresist, the surface of copper has to be prepared for cleanliness and good adhesion. Inadequate adhesion may result in resist delamination during spray etching of the copper. Preposit-Etch E25/29 (Shipley) is used as a micro-etchant for our surface preparation. The etch rate is $0.5 \mu\text{m}/\text{min}$. After 2 minutes of Preposit Etch E25/29, substrates are rinsed immediately in 10% HCl solution during 1 minute, followed by a 1 minute rinse in DI water. The HCl rinse is mandatory as there are always Cu^+ and Cu^{2+} ions left on the foil surfaces after the microetch, which cannot be removed by immediate rinsing in DI water.

4.4.2 Photoresist application

Photoresist AZ4562 [11] (AZ-Electronic Materials [18]) is spun onto the copper and pattern definition is done by standard lithography. The spin speed is 2000 rpm, resulting in a $\sim 10 \mu\text{m}$ thick photoresist layer. After a softbake at 60°C during 15 mins, the photoresist is illuminated during 22,5 secs under a $8 \text{ mW}/\text{cm}^2$ UV lamp, using a dedicated glass mask. We develop the samples in a 1:1 solution of Microposit Developer and DI water. Developing time is 2 mins. After development, the photoresist is hard baked on a hotplate during 15 mins at 60°C . The softbake temperature has been lowered from 90°C mentioned in the datasheet to 60°C . The hardbake temperature has also been lowered from a recommended 120°C in a convection oven to 60°C on a hotplate. This is necessary in order to avoid melting of the wax resulting in a bad adhesion of the copper (see previous section). The parameters were shown in Table 4.5.

4.4.3 Copper spray etching

An etching step takes place to define the copper tracks of the electronic circuit. For stripping the photoresist, non-diluted AZ400K [19](AZ-Electronic Materials [18]) developer is used being compatible with the wax. In this way, copper tracks are obtained being attached with the wax to the temporary substrate. Iso-Propanol Alcohol (IPA) has also been tested for stripping the photoresist, but the time to strip the photoresist was too long and the result was not always satisfying. The photoresist was not completely removed even after several minutes of emersion.

Also, a characterization of the copper etching of the TW-YE copper laminated samples, was performed. This in order to determine the minimal feature sizes and underetch. Samples were prepared by use of the parameters mentioned in the previous sections. A dedicated mask design was used containing meanders varying in width. In Figure 4.19, part of the design is shown after etching showing the meander tracks going from 56 μm upto 136 μm width defined on the mask. Samples were made and processed while measuring the features after every process step. The dimensions of the patterns on the glass mask were compared with the dimensions of the photoresist after development and the dimensions of the copper tracks after spray-etching. On one of the samples made, the variance in width of the tracks within a sample was studied in order to get an average width of the different tracks. To minimize the amount of measurements, for the other samples only a few measurements were done to check if the track widths are in the same range as the other measured samples. This was confined.



Figure 4.19: Spray etched sample containing meander tracks with different widths.

The conclusions we could draw out of the measurements are:

- The average difference in width between the track width definition on the mask and the track definition of the photoresist for a first sample is $6,2 \mu\text{m}$.
- The average difference in width between the track width definition on the mask and the track definition for a second sample is $6,6 \mu\text{m}$.
- The average underetch for that first sample is $12,7 \mu\text{m}$ (underetch = difference between photoresist width and copper track width).
- The average underetch for that second sample is $10,3 \mu\text{m}$.
- The average difference in track width between mask and copper pattern definition is $18,8 \mu\text{m}$ for that first sample ($12,7 \mu\text{m} + 6,2 \mu\text{m}$).
- The average difference in track width between mask and copper pattern definition is $16,94 \mu\text{m}$ for that second sample ($10,3 \mu\text{m} + 6,6 \mu\text{m}$).

In Figure 4.20, it is shown what happens with the profiles of the different layers (copper, photoresist) during the different process steps.

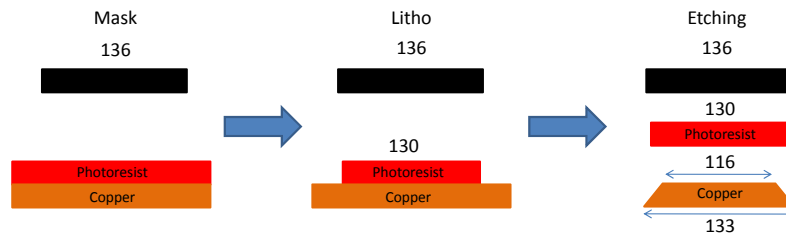


Figure 4.20: Profiles of different layers during copper patterning (dimensions in μm).

In this way, the underetch can be taken into account during the mask designs.

4.5 Application of soldermask

Similar to conventional PCB or FCB substrate processing, soldermask can be applied. This soldermask forms a permanent protective coating and prevents bridging between conductors by solder. This is done by screenprinting ELPIMER SD2463 FLEX HF on the samples. Curing temperatures and time were optimized to avoid melting of the wax and mixing with the soldermask. Prebake was done

at 60°C during 120 mins. Postbake was done at 150°C during 60 mins. In between, illumination (250 mJ/cm²) takes place through a glass mask and developing in a 1 % Na₂CO₃ solution. The result is a cured soldermask layer with thickness ~20µm.

4.6 Copper surface finish

In order to have a reliable connection between the copper pads and the leads of components, several finishes have been examined.

4.6.1 No finish

Chemically clean copper is the easiest material to solder; it can be soldered with even the mildest fluxes [20]. Unless it is protected with a protective coating, its solderability will rapidly degenerate because of oxides (caused by oxygen in air) and tarnishes (mainly caused by chemicals in the air e.g sulfur dioxide). This option has sometimes been successfully used in cases where the soldering happened immediately after dipping the substrates in a 10% HCl solution in order to remove the oxides on the copper due to oxidation of the copper during the curing step of the soldermask (150°C).

4.6.2 NiAu-finish

Copper metal pads can be coated with a NiAu finish. The Ni prevents the diffusion of the copper atoms through the gold layer, causing tarnishing of its surface and formation of an oxide and/or sulfide layer [20]. Au is a highly solderable material but is extremely expensive and it rapidly dissolves in the molten solder. The main function is again protecting the copper from oxidation and it improves the wear resistance. The use of higher gold thicknesses can reduce solder joint reliability due to the formation of tin-gold intermetallics. In the used technology, an electroless Ni finish with an electroless Au flash is deposited on the copper. Typical thickness for the Ni deposition is a few (2-3) microns; thickness of the Au is 150nm. Ni plating happens at 90° C which leads to delamination of the copper tracks from the temporary substrate, due to the melting of the wax. To avoid this, attempts have been made to fix this by putting a photoresist layer on the sample, in order to counteract the delamination of the patterned structures. Places which need to be plated are left open. In this way, a NiAu finish can be obtained. Photoresist cracking was observed and the quality of the NiAu finish was not optimal. Therefore, the conclusion has been made that this finish is not applicable for our technology.

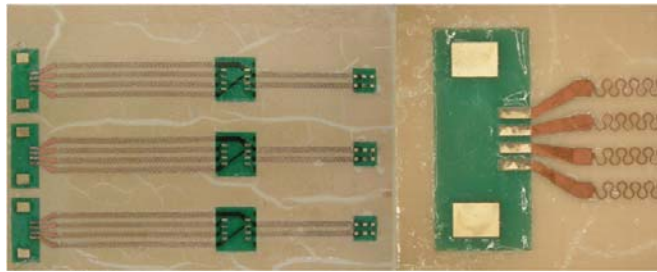


Figure 4.21: Substrate after NiAu-finish application. Cracks in the photoresist are observed and the quality of the finish is poor.

4.6.3 OSP-finish

For applications that do not require a long shelf life, an economical solution is the use of an organic protective coating. Organic protective coatings must be easily removable and they must be compatible with the fluxes used in the printed circuit board industry. An organic surface protection (OSP) from MEC has been tested and successfully applied to the technology. It involves the following products, a microetchant and the OSP itself.

MECBRITE CA-92 [21] is an acidic micro-etch cleaner specifically formulated to remove organic and inorganic soils such as fingerprints, light oils and oxides from copper surfaces. It is versatile and particularly useful for copper cleaning applications where it is essential to remove a thin layer metallic copper together with oxides and organic contaminants.

MECSEAL CL-5018 [22] is a heat-resistant water soluble preflux. Compared with conventional alkylimidazole type preflux, CL-5018 is less foamy and offers superior heat-resistance, solder wettability and spreadability. Even in short processing time, CL-5018 effectively forms a heat-resistant anti-tarnish coating only on the copper surface. Since CL-5018 is easy to control, it offers excellent workability and safety.

The process steps to apply this OSP are:

- Emersion of substrate in MECBRITE CA-92 solution at room temperature in order to have an micro-etched surface of 1 μm .
- Water rinse of 30 seconds.
- Water removal by warm air.
- Emersion of substrate in MECSEAL CL-5018 for 20 seconds and more at 20°C - 40°C.

- Water rinse of 30 seconds.
- Water removal by warm air.

4.7 Assembly of components

Soldering, both wave and reflow, are currently by far the most standard ways of automated assembly of electronic components onto substrates. It is our chosen way in order to make electrical contact between the defined stretchable copper interconnections and the SMD components. In the past, most component assembly was done by soldering with Pb-Sn-alloys. However, European regulation states that lead (Pb) must be banned from all processes, also in the electronics industry. Alternatives have been developed and are typically Sn-Ag-Cu-alloys (SAC). They have the disadvantage that they still require higher reflow temperatures, over 250°C instead of approximately 180°C.

We have used Interflux Delphine SAC305 solderpaste alloy, consisting of a mixture of flux and metal solder particles. This solderpaste is lead-free and also free of halogens, guaranteeing a high reliability. This paste has a high resistance to the elevated temperatures inherent to lead-free processes.

The solder paste can be dispensed manually or automatically on the contact pads of the substrate, before aligning and placing the components. A common problem in soldering is tombstoning. This term refers to surface mounted components, mostly small passives (resistors and capacitors), that rise up during soldering leaving one end soldered to the board and the other end free. It is caused by an unbalanced force due to non-uniform melting during reflow, mostly coming from different amounts of solder at opposite ends of the component. Therefore, automatic application by screenprinting or dispensing is preferred in order to have equal amounts of solderpaste. The wax is a plane, non-sticky surface making screenprinting solderpaste not an issue in terms of adherence to the screen during printing.

A considerable advantage of soldering as compared to current adhesive assembly, is its self-alignment ability: during reflow, the solder makes sure the components contacts (pins) are aligned optimally to the corresponding substrate pads. This is especially the case when a soldermask is applied next to the contact pads: the soldermask repels the solder, so that it is forced onto the pads. On the downside, soldering requires relatively high temperatures.

We have used a vapour phase reflow station because of its availability at the lab facilities of CMST. By this soldering technique, the board is placed with solderpaste and components into the reflow chamber where it is exposed to the vapour phase of a boiling liquid. This liquid is inert with respect to the solder and the board. The hot vapours begin to condense on the cooler printed circuit board, thus heating it. As the process progresses sufficient energy for sustained solder

reflow results. The solder wets to lead and pad and, as the board is removed from the hot vapour, the molten solder solidifies, bonding component leads to circuit board pads. An advantage of this process is that the reflow happens in an inert atmosphere, resulting in an excellent joint quality.

Figure 4.22 shows the temperature profile of the used vapour phase soldering process. This profile is based on the profile recommended in the datasheet of the SAC305 alloy.

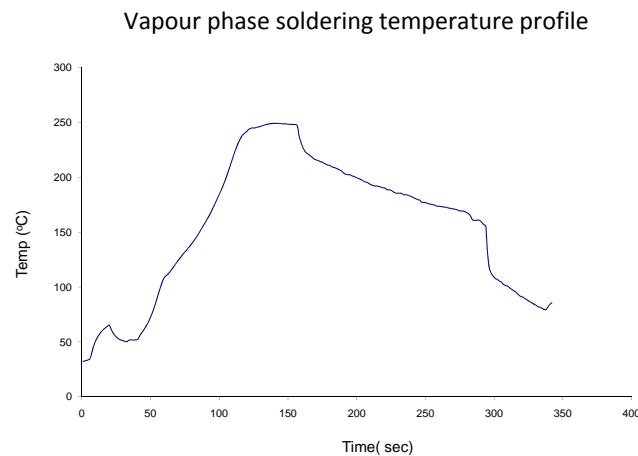


Figure 4.22: Vapour phase soldering temperature profile.

The wax melts during soldering but hardens again after soldering. The circuit is temporarily laying free on the carrier. The total wax thickness is important here. When it is too thick, it's easier for the tracks to start to float. Figure 4.23 shows the effect of melting of the wax during soldering. Due to forces appearing during the hardening of the solderpaste, the tracks are shifted. This is an effect that we certainly want to avoid. Luckily, this can be solved by use of soldermask, which holds the tracks in their place, see Figure 4.24.

4.8 Testing and rework

A major advantage of this technology compared to technologies where the process steps take place on the elastomer, is that the electronic circuit can be tested before embedding. Although we try to keep up processing yields as high as possible, component replacement might be necessary. Resoldering and replacement is possible without deteriorating the final stretchable circuit performance.

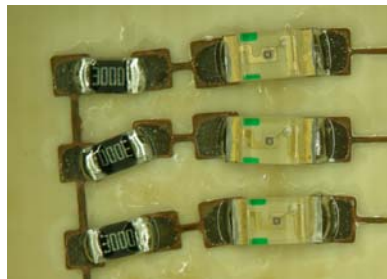


Figure 4.23: Tracks shift during reflow soldering and wax melting in absence of soldermask.

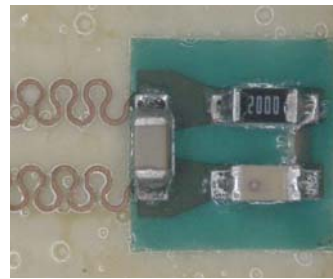


Figure 4.24: Soldermask preventing movement of tracks during reflow soldering and wax melting.

4.9 Embedding

The substrate carrying the electronic circuit is embedded by use of an elastic material. For feasibility studies we have chosen for Sylgard 184 and Sylgard 186 from Dow Corning. The properties of these silicones are mentioned in Table 4.6.

Parameter	Sylgard 184	Sylgard 186
Young's modulus	0.6-2.3 MPa	N/A
Viscosity	3900 mPa.sec	65000 mPa.sec
Appearance	Transparent	Translucent
Refractive index (589nm)	1.41	N/A
Linear CTE	310 ppm/°C	330 ppm/°C
Hardness (durometer)	A50	A24

Table 4.6: Properties of Sylgard 184 and Sylgard 186 silicone.

Embedding of the circuit in a polymer can be done by casting (doctor blading) or by moulding. Before PDMS is applied, an adhesion promotor is applied for use with Sylgard 184 and 186. OS1200 primer from Dow Corning is applied by dipping with a wipe on the substrate. It is important to limit the applied amount of primer.

4.9.1 Casting of PDMS

In cases where a simple, flat encapsulation is needed or a very thin encapsulation layer, casting PDMS can be the option to embed the stretchable electronic circuit. Well controlled layers can be applied by hand (Figure 4.25) or by use of a doctorblade (Figure 4.26). After casting the PDMS has to be cured, but this curing should be limited in temperature. A temperature higher than 70°C will lead to wax melting, resulting in an incurable wax-PDMS mixture. After curing

the PDMS at 50°C during 4 hours, the temporary carrier is removed. This process will be described in the following section concerning moulding. In the end, the backside can be casted with another layer of PDMS, again by first applying the adhesion promotor followed by another casting step.

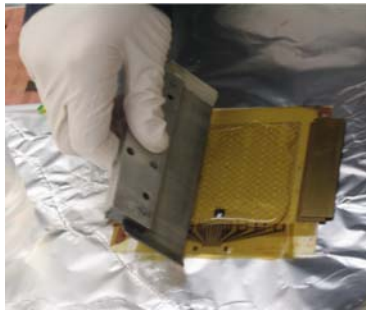


Figure 4.25: Application of PDMS by casting manually.



Figure 4.26: Application of PDMS by casting using a doctorblade.

4.9.2 Moulding using PDMS

The moulding process steps are shown in Figure 4.4. First, the temporary substrate supporting the functional electronic circuit is put into the mould. The upper layer of PDMS is then injected and cured. Optimal curing is done at 50°C preventing the wax of melting and mixing with the uncured PDMS resulting in an incurable mix. Secondly, the supporting mould is removed and the temporary substrate is removed by heating the temporary substrate up to 200°C. In this way, the wax melts and allows us to peel off the substrate. After release, wax residues should be removed by rinsing in an acetone bath. Next, the backside mould is mounted in order to inject the final layer of PDMS. After curing this layer at 50°C during 4 hours, the system is unmounted. The material chosen for the moulds can be PMMA, polyetherimide ULTEM or aluminium. Each of these materials have advantages/disadvantages compared to each other. PMMA and ULTEM are transparent, making them very suitable for silicone flow analysis. PMMA and aluminium are cheap compared to ULTEM. PMMA is not resistant to acetone, what leads to cracks in the mould when the emersion time is too long. ULTEM has a broad chemical resistance, high heat resistance and high mechanical strength and rigidity. We come back to the moulding steps in Chapter 5, where in more detail the mould design, the moulding and unmounting steps will be explained.

4.10 Conclusions

We have described a technology for realizing stretchable electronic circuits by use of a temporary carrier where the electronic circuit is being built up on. The choice of the materials, the different technology steps and the optimization of each step has been presented. A number of demonstrators will be presented in Chapter 7 including a stretchable temperature sensor, an inductive link protected by PDMS, stretchable transmission lines and antennas and a stretchable heater. These will demonstrate the feasibility of our technology process. In the following chapters, we will come back to this technology by presenting reliability results and by presenting an improved version of this technology.

References

- [1] D. Brosteaux, F. Axisa, M. Gonzalez, J. Vanfleteren. Design and fabrication of elastic interconnections for stretchable electronic circuits. *IEEE Electron Device Letters*, 28(7):552–554, Jul 2007.
- [2] Circuitfoil. <http://www.circuitfoil.com>.
- [3] I. Benedek. *Pressure-Sensitive Adhesives and Applications*. Taylor and Francis Inc, 2004.
- [4] J. Johnston. *Pressure Sensitive Adhesive Tapes*. PSTC, 2003.
- [5] I. Benedek. *Pressure Sensitive Formulation*. VSP, 2000.
- [6] Dow Corning. Technical datasheet - Sylgard 527 Technical Datasheet.
- [7] Dow Corning. Technical datasheet - Sylgard 4150 Technical Datasheet.
- [8] Micronsult. Technical datasheet - FlexFixer.
- [9] Nitto Denko. Technical datasheet - Differential DC/T 64390.
- [10] Dupont. Technical datasheet - Riston FX900 Series Dry Film Photoresist.
- [11] AZ Electronic Materials. Technical datasheet - AZ 4500 Series Photoresists.
- [12] C. Fillion. Shamrock Technologies - Presentation on surface modifiers.
- [13] Aquabond Technologies. Technical datasheet - ABS-85.
- [14] Rogers. Technical datasheet - RO4003- Woven Glass Reinforced Ceramic Filled Thermoset Materials.
- [15] South Bay Technologies. Technical datasheet - Quickstick MWH135 Mounting Wax.
- [16] UBE America Inc. Technical datasheet - Polyimide Base Copper Clad Laminate (Adhesiveless).

REFERENCES

111

- [17] Rogers. <http://www.rogerscorp.com/>.
- [18] AZ Electronic Materials. <http://www.az-em.com/>.
- [19] AZ Electronic Materials. Technical datasheet - AZ 400K Developer for AZ 4500 series.
- [20] Jr. C.F. Coombs. *Printed Circuits Handbook, 4th edition*. McGraw-Hill, 1996.
- [21] MEC. CA-92 Micro-etch cleaner technical datasheet.
- [22] MEC. Technical datasheet - CL-5018 Heat-resistant water soluble preflux.

Chapter 5

Peelable technology with local polyimide support

An optimized version of the technology in Chapter 4 is presented. A layer of polyimide is introduced as support for the stretchable conductors and the functional islands. The first section gives a general overview of the optimized process flow and the following sections describe the choices made and the optimization of the individual processing steps in more detail. Some side steps of this technology are presented including the extension to double conductor layer circuits, reliability improvement by polyimide sandwiched metal structures,..

5.1 Introduction

In Chapter 4, the peelable technology was presented. Some issues were reported that during reflow soldering, the patterns started floating onto the melted temporary adhesive and soldermask had to be used for holding the structures.

In order to solve this, a layer of polyimide is introduced in the technology stack: the polyimide is patterned in a way that it supports the functional islands and the stretchable interconnections. This layer prevents floating of the different pads of the components. Furthermore, the stress during stretching is shifted to the border of the flexible islands. The polyimide is not able to stretch and will mechanically protect the soldered component connections and the straight tracks on the component islands. This principle is shown in Figure 5.1, and enhanced reliability with this technology will be discussed in detail in Chapter 6.

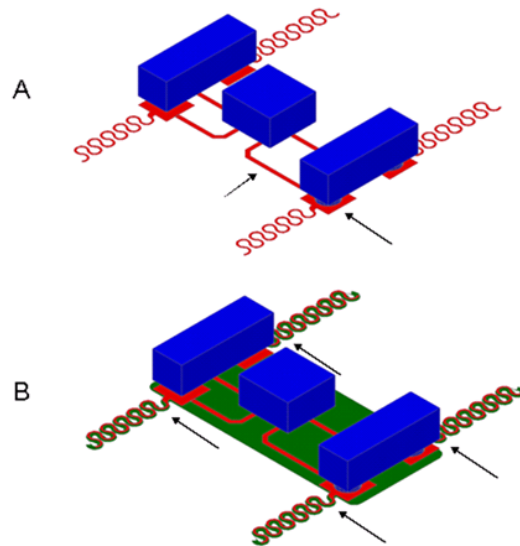


Figure 5.1: Due to the polyimide supporting layer, mechanical stress during stretching will be shifted from the component connection pads and the straight tracks on the functional islands towards the border of the flexible islands.

5.2 General description of process flow

The process flow is depicted in Figure 5.2 and 5.3 and will be in detail explained in the following sections. In comparison with Figure 4.3, the copper foil is now first foreseen by patterned polyimide structures. This can be achieved by use of photodefinable polyimide or screenprinting a non-photodefinable polyimide. A curing step is needed in order to imidize the polyimide to achieve its flexibility and strength. The polyimide structured copper foil is then laminated on a rigid/flexible carrier by use of the temporary adhesive, Quickstick 135 wax. By lithography and etching, the copper patterns are formed realizing the stretchable interconnections, soldermask is applied and the copper is foreseen of a finish to enhance solderability. Components are mounted and soldered leading to a functional circuit. At this stage, after testing and eventually reparation, the circuit is ready to be transferred into a polymer. Before embedding, an adhesion promotor is applied. This in order to have a good adhesion between the components, tracks, soldermask and the polymer. In the case moulding is used, the substrate is put into a mould where PDMS is injected on top of the circuit by liquid injection moulding. After heatcuring the polymer, the bottom mould is removed. The temporary carrier is removed by dissolving/melting the temporary adhesive fol-

114 **Peelable technology with local polyimide support**

lowed by a cleaning step to remove the temporary adhesive. Adhesion promotor is applied on the back side, the bottom mould is replaced and PDMS is injected. After fully curing, the result is a completely PDMS embedded stretchable electronic circuit.

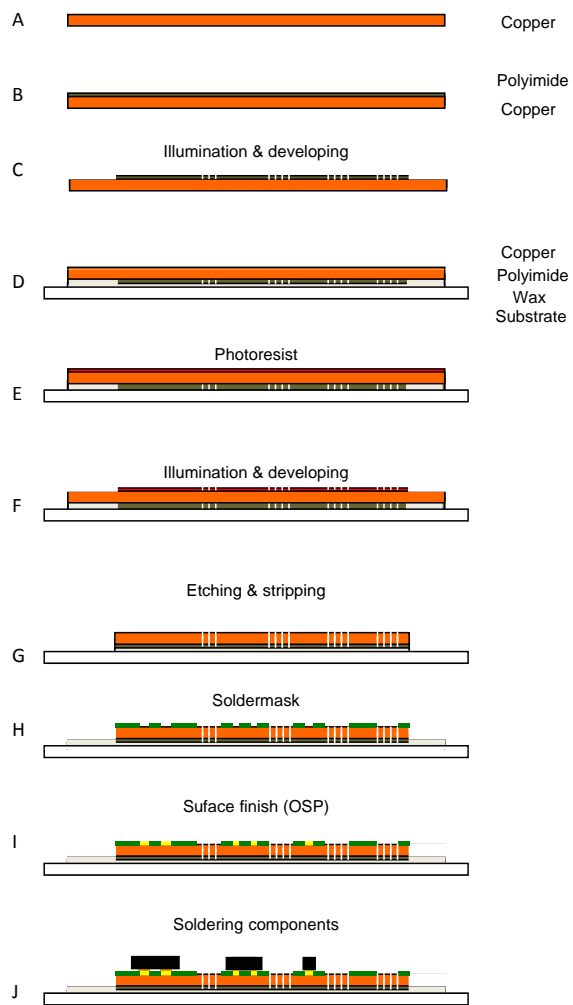


Figure 5.2: Process flow of polyimide supported peelable technology.

5.2 General description of process flow

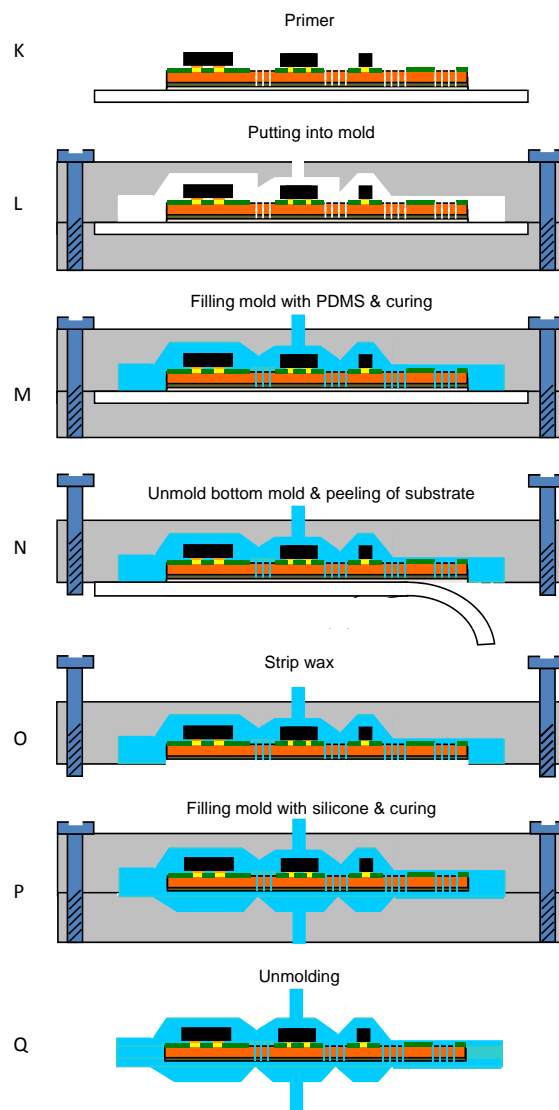


Figure 5.3: Process flow of polyimide supported peelable technology.

5.3 Pattern definition of polyimide

The main goals of the polyimide are to prevent the islands from flowing on the wax during reflow soldering and to improve the mechanical robustness of the stretchable circuit. Having a flexible material below the stretchable copper interconnections will improve the lifetime of these connections by withholding crack propagation in the copper. The polyimide will serve as a buffer for the stresses applied by the PDMS on the copper during stretching and the lateral stresses of the PDMS on the copper due to the Poisson effect. Polyimide is a suitable supporting material having a high Young's modulus, being able to plastically deform over a wide elongation and being non-brittle. Furthermore at the level of the islands, the polyimide will improve the robustness by protecting the straight copper tracks and components assembled on the islands from deforming. In order to have a support material below the copper, 2 ways of applying the polyimide have been investigated: lithographically and screenprinting.

5.3.1 Photodefinable polyimide

By using photodefinable polyimide, islands and meander support can be obtained by lithographical patterning of the polyimide. 2 types have been investigated: PI2730 and HD4100, both from HD Microsystems [1].

The **Pyralin PI 2730** [2] series have been specially developed for use as a passivation layer for semiconductors and as an interlayer dielectric layer for high density interconnection (HDI) applications. Pyralin PI 2730 series polyamic esters contain a negative-working photopackage making them sensitive to broadband exposure from a mercury lamp in the range of 350 to 435 nm. The materials are supplied as viscous solutions suitable for spin or roller coating applications. Cured film thicknesses can be achieved from 2,5 μm to 15 μm . These products are self-priming, thus eliminating the need for an additional adhesion promoter except in extreme cases. The cured polyimide film offers a low dielectric constant, low coefficient of thermal expansion and good mechanical properties.

The **HD-4100 Series** of products [3] are new negative-tone, solvent developed, photodefinable polyimides for stress buffer and flip chip bonding applications. These polyimides were developed as self-priming, i-line sensitive, photodefinable polyimide precursors that can be patterned to cleanly resolve micron scale relief patterns with controlled size and wall profiles without the need for photoresists. HD-4100 Series products have found their greatest applicability in packaging applications. They have excellent mechanical properties to handle the thermal and chemical extremes of post application processing, excellent elongation to prevent cracking, good adhesion (to underfill, UBMs, metal runners,

5.3 Pattern definition of polyimide

etc.), smooth sloping via sidewalls and compatibility with copper (no copper migration). They may also be used in traditional stress buffer applications.

As can be seen in Table 5.1, the CTE of PI2731 was much closer to the CTE of copper (~16 ppm/°C) than the CTE of HD4100. The larger CTE mismatch will result in some residual stress in the polyimide layers patterned on the copper by use of the HD4100 polyimide.

Parameter	PI2731	HD4100
Tensile strength	180 MPa	200 MPa
Elongation	>10%	45%
Modulus	6.18 GPa	6.18 GPa
Coefficient of thermal expansion	13 ppm/°C	35 ppm/°C
Dielectric Constant	2.9 (1 KHz)	3.36 (1 MHz)

Table 5.1: Cured film properties of PI2731 and HD4100 photodefinable polyimide.

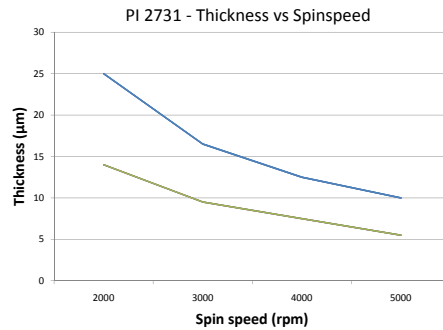


Figure 5.4: Spinspeed vs. layer thickness of PI2731 (30 secs spintime).

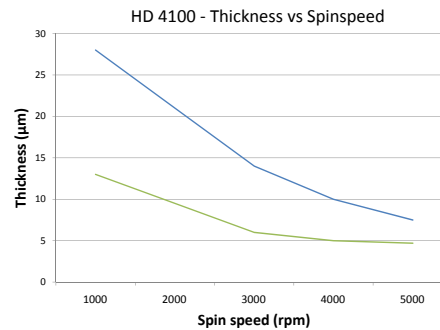


Figure 5.5: Spinspeed vs. layer thickness of HD4100 (30 secs spintime).

The spin vs. thickness curves of both polyimides are shown in Figure 5.4 and 5.5. During first process development for this technology, PI2731 was used, due to the CTE match with copper. Unfortunately, HD Microsystems stopped the production of this 'preferred' photodefinable polyimide and we had to shift to another variant, HD4100. Therefore, we will report the development of the technology by use of HD4100. To demonstrate the feasibility of the use of the HD4100 in the proposed process flow, as shown in Figure 5.6. It consists of 3 flexible islands connected with each other through stretchable interconnections. The islands and stretchable interconnections are supported by the photodefined polyimide layer. On places where components are, soldermask is foreseen. The design encompasses 3 layers: for patterning polyimide, copper and soldermask.

The size of the substrate is 10 by 10 cm and the processing of the polyimide will be done starting from TW-YE copperfoil (Circuitfoil [4]). The properties of the

118 **Peelable technology with local polyimide support**

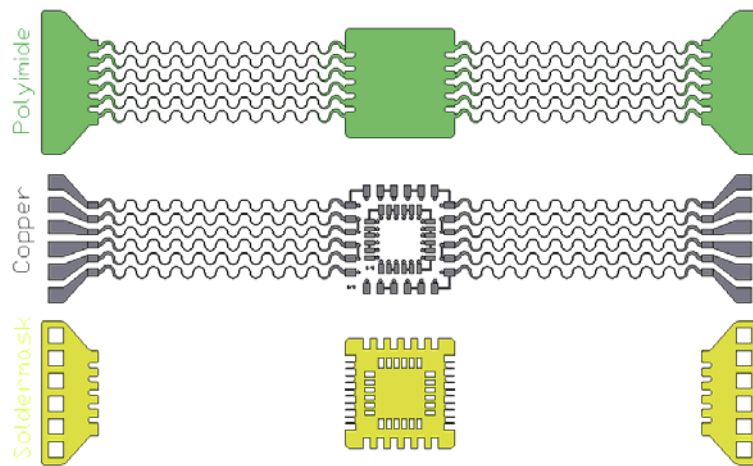


Figure 5.6: Feasibility design for polyimide supported peelable technology: polyimide, copper and soldermask. Trackwidth = 100 μm .

copper foil were shown in Table 4.1. The polyimide is for enhanced adhesion applied on the rough side of the copper, having a roughness between 6 μm -8 μm . Spinning is done during 10 secs at 500 rpm and 30 secs at 1500 rpm, targeting a cured layer thickness of 20 μm . We softbake the polyimide on a hotplate during 5 minutes at 90°C followed by 5 minutes at 110°C. To pattern the polyimide, illumination is done through a TiW patterned glass mask during 40 secs by use of an UV lamp (8 mW/cm²). Next, the polyimide is developed by use of PA400D and PA400R (HD Microsystems). The development parameters are as follows:

- 3 minutes in PA400D
- 2 minutes in a PA400D/PA400R 1:1 solution
- 3 minutes in PA400R
- rinse with DI water brush

Full cure of the polyimide is done in a nitrogen oven with the following curing temperature:

- heating from room temperature to 200°C, with a ramp rate of 4°C per minute
- 30 minutes at 200°C
- heating from 200°C to 375°C, with a ramp rate of 2,5°C per minute

5.3 Pattern definition of polyimide

- 60 minutes at 375°C
- cooling down to room temperature

The processing parameters have been deduced from the recommendations mentioned in the datasheet of the polyimide. In this way, a layer of $\sim 20 \mu\text{m}$ polyimide on the copper is obtained. Figure 5.7 shows a sample with patterned HD4100 polyimide on.



Figure 5.7: Definition of HD4100 polyimide.

Also alignment marks are defined on this polyimide layer and based on these marks, holes are drilled by a laser through the polyimide and copper. These holes are needed for alignment during copper definition at the other side. It is important that the copper layer definition is well aligned relative to the polyimide layer in order that the supporting polyimide meanders are well aligned compared to the copper meanders (Figure 5.8).

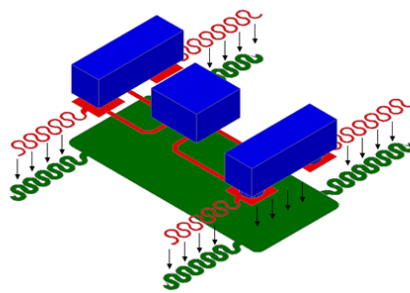


Figure 5.8: Alignment of polyimide relative to copper is important, achieved by laser-drilling alignment holes in the copper foil.

To check the reproducibility of the parameters for photodefinition of the polyimide, 3 samples were fully characterized, being processed as described. The samples consist of different meanders with a defined mask width of 100 μm . After development, the widths were measured. Table 5.2 shows for every sample the different measurements along the sample. The average track width for the different samples is respectively 102.69 μm ($\sigma=2.20 \mu\text{m}$), 104.66 μm ($\sigma= 2.20 \mu\text{m}$), 100.57 μm ($\sigma= 1.78 \mu\text{m}$). The last sample has been agitated more in the 1st developer solution than the others. It can be concluded that the uniformity of the definition across the sample is good. A profile measurement of a defined polyimide track after curing is depicted in Figure 5.9.

Sample 1 (width in μm)	Sample 2 (width in μm)	Sample 3 (width in μm)
101,42	104,8	102,54
105,92	107,05	101,42
101,42	104,8	96,91
101,42	101,42	100,29
104,8	107,05	101,42
99,16	104,8	101,42
103,67	101,42	99,16
103,67	105,92	101,42

Table 5.2: Linewidths of photodefined HD4100 polyimide.

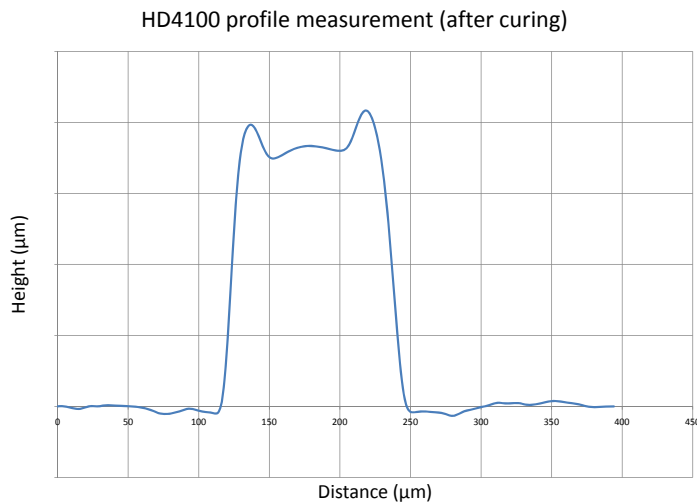


Figure 5.9: HD4100 photodefinable polyimide profile after curing.

5.3 Pattern definition of polyimide

5.3.2 Screenprintable polyimide

As an alternative for photodefinition of polyimide, screenprinting of polyimide was studied. In this way, the used material doesn't need to be photodefinable. Furthermore, less material is used because of the additive nature of screenprinting. So far, polyimide is not so common available in screenprintable format. Most of the commercial available polyimides are for spincoating, typically used as passivation layers for wafers or casted polyimide on copper clads. For a material to be screenprintable, it has to have the suitable rheology. The paste has to be a non-Newtonian fluid with thixotropic properties. This means that the idealiter viscosity of the paste has to change in time with applied shear rate. The change of the viscosity is usually described by a thixotropy index. It represents the change of viscosity between two different shear rates, usually different by a factor of 10. An example of a thixotropic material is e.g. ketchup or mayonese: in the equilibrium state they do not change their shape but when agitated their viscosity changes rapidly. This is the reason why a paste has to roll in front of the squeegee during printing - rolling causes the change of the viscosity of the paste. The most important properties of the different polyimides investigated for their screenprinting capability, are listed in Table 5.3. Most of the time, the thixotropy index is not mentioned in the datasheet. By just the viscosity index, it's hard to predict if a material will be screenprintable or not. For that purpose, several materials have been ordered and tested to check the capability to be screenprinted.

Property/Polyimide	PI2611	Q-Pilon	U-Varnish A	Durimide 10	Durimide 116
Main solvent	NMP	GBA	NMP	NMP	NMP
Solid contents (%)	13.50	27	18	N/A	11-15.5
Glass transition temperature	400°C	245°C	N/A	N/A	371°C
Coefficient of thermal expansion	3 ppm/°C	46 ppm/°C	16 ppm/°C	52 ppm/°C	32 ppm/°C
Elongation	25%	9.5%	100%	74%	80%
Elasticity	N/A	3200 MPa	3730 MPa	3500 MPa	3300 MPa
Tensile strength	350 MPa	N/A	196 MPa	N/A	260 MPa

Table 5.3: Properties of selected polyimides for screenprinting.

A dedicated screen has been developed for the screenprinting tests, showed in Figure 5.10. It's a stainless steel screen with the following characteristics:

- 400 mesh screen: 400 openings per inch
- 20 μm emulsion for NMP resistant emulsion / 60 μm for non-NMP resistant emulsion
- Angle of mesh: 45°
- Dek260 frame (23 inch by 23 inch)

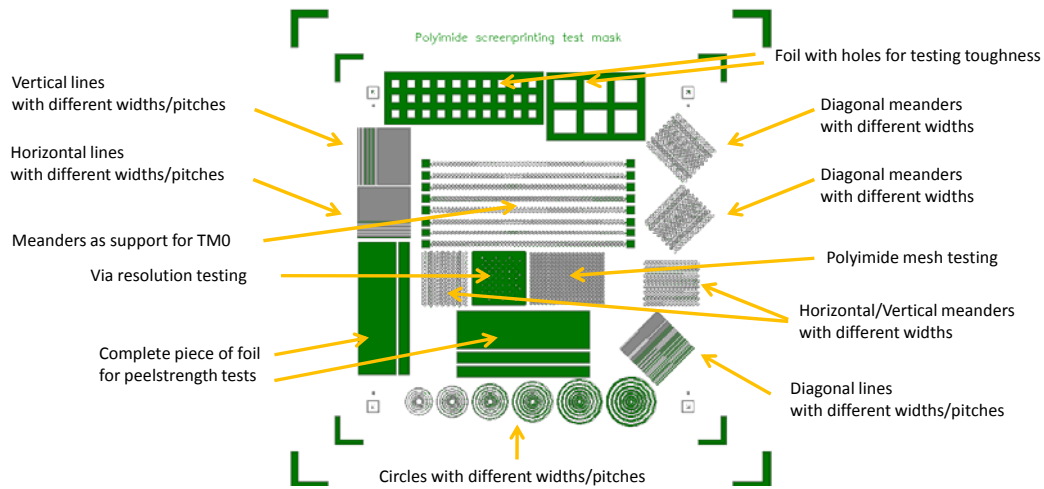


Figure 5.10: Dedicated screen for polyimide screenprinting purposes.

The squeegee had the following properties:

- Polyurethane 80-85 shore hardness
- Trailing edge 45° angle

N-Methyl-Pyrrolidone (NMP) resistant screens with emulsions thicker than 20 μm were not available. NMP is a very aggressive solvent, attacking the standard emulsions used for covering screenprint masks.

The dedicated screen contains the following test blocks:

- Vertical and horizontal lines with width of 250 μm , 200 μm , 150 μm , 100 μm .
- Vertical, horizontal and diagonal meanders with width of 100 μm , 150 μm , 200 μm , 275 μm .
- Full areas and areas with square holes.
- Concentric circles with different widths and pitches (Dimensions in Table 5.4).
- Full area with vias having diameters of 75 μm , 100 μm , 125 μm , 150 μm , 175 μm , 200 μm .
- Mesh of circles with 136 μm width and innerradius 282 μm .

In the following sections, the trials with the different polyimides will be discussed.

5.3 Pattern definition of polyimide

Circle width (μm)	Pitches (μm)
100	200, 300, 400, 500, 600, 700
200	300, 400, 500, 600, 700, 800
300	400, 500, 600, 700, 800, 900
400	500, 600, 700, 800, 900, 1000
500	600, 700, 800, 900, 1000, 1100
600	700, 800, 900, 1000, 1100, 1200

Table 5.4: Dimensions of concentric circles on screenprinting screen.

PI2611

PI2611 [1] has a viscosity of 110-135 Poise, which is quite low. It is based on N-Methyl-2-Pyrrolidone. Screenprinting tests showed that the polyimide was dropping through the screen and stuck the screen on the backside. This polyimide, made for spincoating applications, is not an option. Only modifications at the level of the material could make it screenprintable.

Q-Pilon Q-IP-GWK123

Q-Pilon Q-IP-GWK123 (PI-R&D) has a high heat resistance and good insulation properties. The datasheet claims that a fine pattern can be directly formed by a screenprinting method. It has been designed for application on printed circuit boards and as insulation layer film on wafers. The datasheet claims fine process ability. The product has a viscosity of 40000-50000 mPa.s and is based on γ -Butyrolactone.

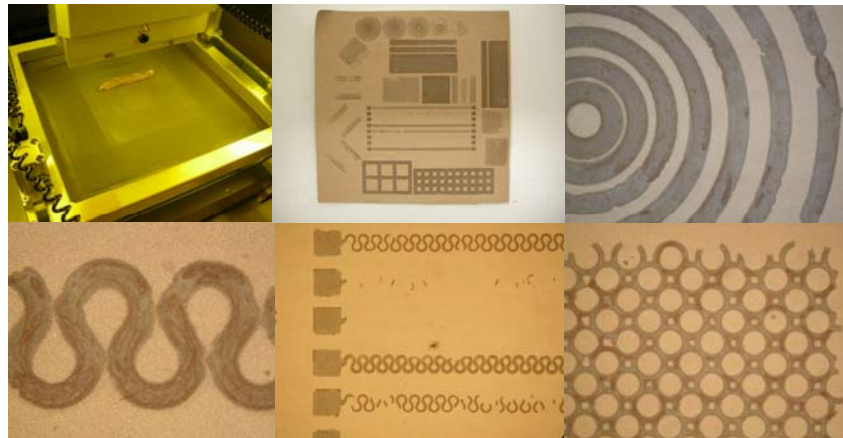


Figure 5.11: Definition of Q-Pilon polyimide by screenprinting: feature size $\sim 150 \mu\text{m}$, thickness $\sim 40 \mu\text{m}$.

For the experiments, the squeegee was first mounted under a 60° angle but we changed it to 45° . The reason: too little material was printed. As snap off distance, we started with 0.75 and moved to 1.25 mm. There was an effect but hard to describe quantitatively. Printing speed was 10 mm/second.

As can be seen in the upright picture of Figure 5.11, the material has a very high viscosity and behave like a thick paste. In the picture next to it, the results of printing are shown. The smallest features are not printed well, the uniformity of the deposition is very small, the pattern definition is poor and the thickness after curing is around $40\ \mu\text{m}$ (the emulsion thickness of the screen was $60\ \mu\text{m}$). The material doesn't have the property of settling after printing and the mesh patterns remain in the printed material. We concluded that this material doesn't have the capabilities for being screenprinted in a good way forming the support for the stretchable interconnects.

U-Varnish

U-Varnish (UBE [5]) is a solution of polyimide precursor/polyamic acid. It comes in two forms, U-VARNISH-A (Normal heat resistant type) and U-VARNISH-S (High heat resistant type). For our purpose, we experimented with U-VARNISH-A and performed some screenprinting tests. Some pictures are depicted in Figure 5.12.

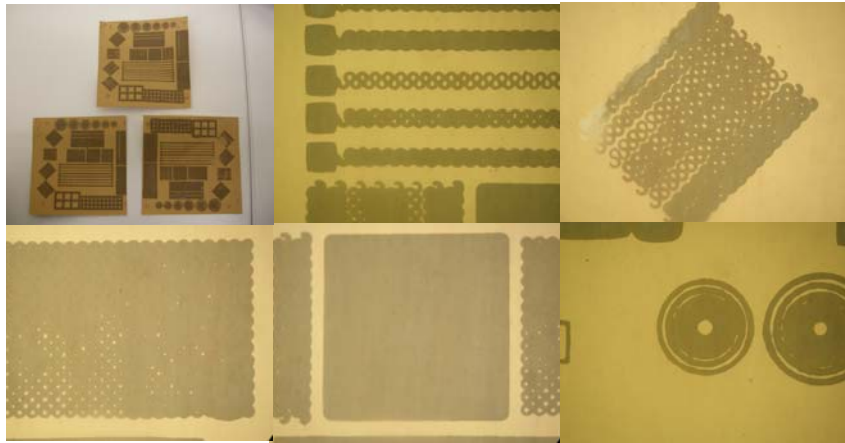


Figure 5.12: Definition of U-Varnish A polyimide by screenprinting.

As can be seen in the pictures, the viscosity of the material is too low: the material starts to flow after deposition, what makes it difficult to define good patterns. This material turned out to be not suitable for the fine pattern definition of meanders and islands. Only modifications at the level of the material could make it

5.3 Pattern definition of polyimide

125

screenprintable.

Fuji polyimides

Also some polyimides from Fuji were tested. Fuji was willing to change the material properties of some materials in order to make it suitable for our applications. We started with two materials, Durimide 10 and Durimide 116.

Durimide 10 is a non-photosensitive, pre-imidized polyamide-imide system. It has a low shrinkage upon bake, no high temperature cure (starting from 275 °C), good mechanical properties, patternable using dry etch processes, reworkable and solvent soluble (NMP). The main applications for this polyimide are junction coating for discrete devices, glob top applications, general passivation and for LCD alignment layers.

Durimide 116 is part of the Durimide 100 series, being non-photosensitive polyamic acid formulations which become fully stable polyimide coatings after thermal curing. They are self-priming, no pretreatment with adhesion promoter is required, have high thermal stability, have improved resistance to stress cracking and are reworkable.

The behaviour of both materials on a screen is compared in 5.13 and Figure 5.14.



Figure 5.13: Behaviour of Durimide 10 on screen.

For Durimide 10, the material flows through the screen without any shear stress. Controlled deposition of the material via screenprinting is impossible due to this phenomenon. The thixotropy index of Durimide 10 is unknown and it seems that it is 1.0 or close to it (Newtonian liquid). For successful screenprinting, the thixotropy index should be definitely higher than 1.0, preferably above 5.

The viscosity of Durimide 116 is higher, but also this type exhibits the same behavior as Durimide 10 (see also Figure 5.14). Figure 5.15 also demonstrates the



Figure 5.14: Behaviour of Durimide 116 on screen.

flow of the material even at rest: it's clear that it's not suitable for screenprinting purposes.

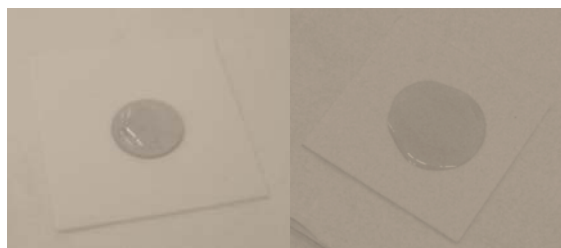


Figure 5.15: Behaviour of Durimide 116 on ceramic substrate. The material flows too much when it is at rest. Picture taken at $t=0$ and $t=2$ mins.

In Figure 5.16, the difference in flow behaviour is shown between a typical paste made for screenprinting on the screen (see pointer) and Durimide 116. The difference between the polyimide behavior and the paste can clearly be seen: the paste doesn't flow through the screen. The viscosity of the paste is quite low, comparable to the Durimide 116, but the thixotropy is much higher. The viscosity of the paste is 20-30 Pa.s compared to the viscosity of the polyimides: Durimide 116, 10.000-16.000 cSt (15 - 24 Pa.s) and Durimide 10, 2550-3550 cSt.

In order to make the polyimides screenprintable, the thixotropy of the material should be increased. Which means, the tendency for the viscosity of the material to decrease when subjected to shear, should be increased. The material at rest shouldn't start to flow because after being printed, it should stay on the sample where it is and during printing, it shouldn't flow through the screen.

The Durimide 116 material has been adjusted by Fuji by use of thixotropic fillers



Figure 5.16: Difference in behaviour between screenprinting paste (arrow) and Durimide 116.

in order to make it somehow screenprintable. Not much details can be given about these procedures because of the confidentiality. 2 versions were tested, Durimide 116 H and Durimide 116 HC. The same screen design has been used as shown in Figure 5.10.

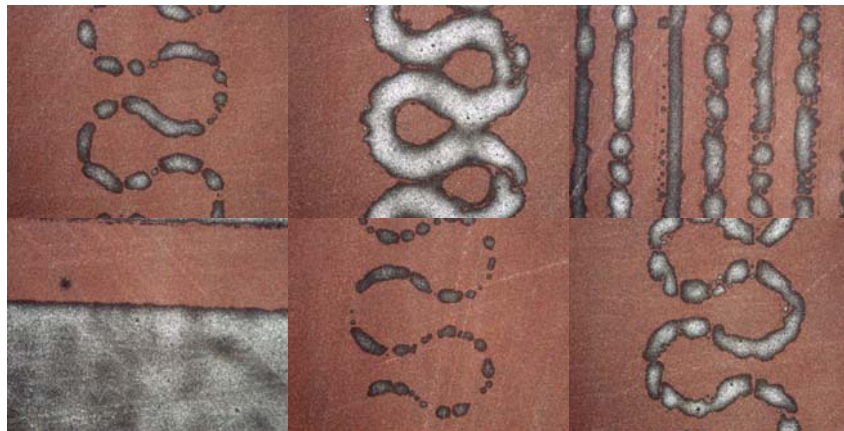


Figure 5.17: Results after printing and curing Durimide 116H.

The pattern definition of the Durimide 116HC (Figure 5.18) is much better compared to Durimide 116H (Figure 5.17). The thickness of both polyimides after curing is in the range of a few μm (1 - 3 μm) and the uniformity is low. The screen emulsion thickness is 20 μm , resulting in a thickness of only a few μm . For thicker layers, we would need several prints or a material with different properties.

We can conclude that these modified materials don't fulfill yet the requested pro-

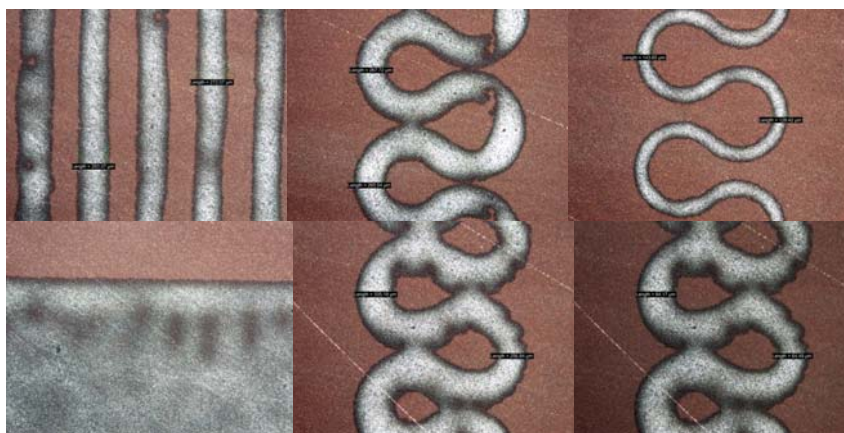


Figure 5.18: Results after printing and curing Durimide 116HC.

properties for our application. There is still a lot of work ahead on finetuning the flow properties of the polyimides for screenprintable purposes. This won't be covered anymore in this PhD work, the presented technology will make use of photodefinable polyimides. In terms of industrialization of the process, screenprinting is preferred but further material modifications and experiments are needed in order to get a printable, fine patternable, flexible and strong polyimide as supporting layer.

5.4 Lamination of copper on carrier

After pattern definition of HD4100 photodefinable polyimide, the copper sheet is laminated on a rigid carrier. This is done by spinning a layer of Quickstick 135 wax on the polyimide side of the copper, see section 4.3. The stick is dissolved in 30 ml of acetone and spinning is done during 30 secs at 1000 rpm. On an etched RO4003 substrate, we spin the same layer of wax. The substrate is used as a temporary carrier during the different process steps. Both substrates are then laminated to obtain a carrier-wax-polyimide-copper stack.

5.5 Patterning of copper

Before the application of a photoresist, the surface of the copper has to be pre-treated for cleanliness and good adhesion. Inadequate adhesion may result in resist delamination during spray etching of the copper. Preposit-Etch E25/29

5.6 Application of soldermask

129

(Shipley) is used as a micro-etchant for our surface preparation. After the Preposit Etch E25/29 substrates are rinsed immediately in 10% HCl solution followed by a rinse in DI water.

Photoresist AZ4562 (Shipley) is spun during 1 min at 2000 rpm. The softbake is done on a hotplate during 15 min at 60°C followed by the illumination during 22,5 secs under a 8 mW/cm² UV lamp. Good alignment is obtained by 50 μm laserdrilled holes. We develop the samples in a 1:1 solution of Microposit Developer and DI water. Developing time is 2 mins. The photoresist is hardbaked during 15 mins on a hotplate at 60°C. This low temperature is chosen to avoid the wax from melting, leading to a bad adhesion of the polyimide-copper layer to the substrate (see Section 4.3.5). Next, etching of copper is done in a HCl/CuCl solution at 55°C by use of a spray etcher. Rinsing and stripping the photoresist in a non-diluted AZ 400K solution bath is done next, followed by a DI water rinse: because the wax dissolves in acetone, we don't use acetone to strip the photoresist in order to avoid delamination of the polyimide-copper from the carrier. Figure 5.19 shows the samples after copper etching including some more detailed pictures.

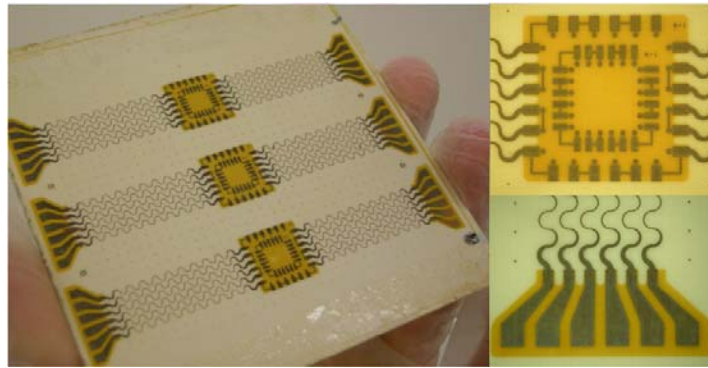


Figure 5.19: Copper pattern definition, resulting in well aligned copper patterns supported by HD4100 photodefinable polyimide.

5.6 Application of soldermask

In the next step, soldermask is applied. This is done by screenprinting ELPEMER SD2463 FLEX HF soldermask on the samples. A prebake is done during 45 mins at 60°C. Illumination of the samples is done by use of an 8 mW/cm² UV-lamp during 25 secs. Developing is done in a 1% Na₂CO₃ solution. A final hardbake of the sample is done during 60 mins at 150°C resulting in a cured soldermask layer with thickness ~20 μm.

130 Peelable technology with local polyimide support

In Figure 5.20, the samples are shown after application of soldermask. Some more detailed pictures are shown in Figure 5.20.

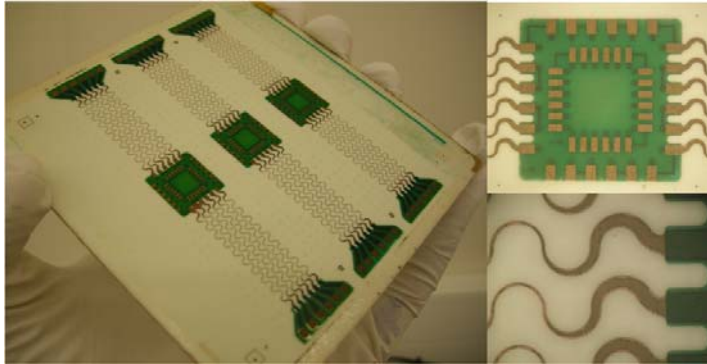


Figure 5.20: Soldermask screenprinted on functional islands.

5.7 Copper finish

As described in Section 4.6, different copper finishes are possible (No finish, OSP finish,..). For the reasons mentioned there, NiAu-finish is not possible due to wax melting.

5.8 Assembly of components

Components are mounted by use of SAC solderpaste and put in a vapour phase oven. Soldering happens at 250 °C. The result from reflow soldering some SMD components (0402 capacitors and resistors) on the flexible island is shown in Figure 5.21.

As can be observed, no pad floating occurs anymore compared to the non polyimide enhanced samples. Some residual stress in the polyimide foil can be observed, this due to the CTE mismatch between the polyimide and the copper.

5.9 Embedding

After soldering, adhesion promoter OS1200 primer (Dow Corning) is applied. This is done in order to improve the adhesion between components, soldermask, copper and polyimide to the stretchable molding material. The substrate carrying

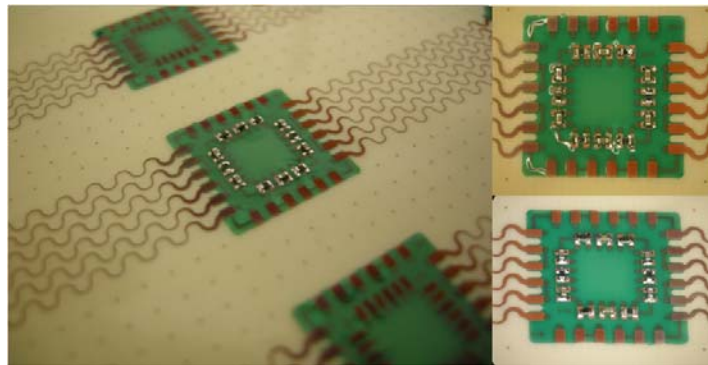


Figure 5.21: Assembly of 0402 SMD components by vapour phase soldering.

the electronic circuit is embedded by use of an elastic material. For feasibility studies we have chosen for Sylgard 184 and 186 from Dow Corning. More information about these polymers in Chapter 4. Embedding of the circuit in a polymer can be done by casting (doctor blading) or by moulding. Before PDMS is applied, an adhesion promotor is applied for use with Sylgard 184 and 186. OS1200 primer from Dow Corning is applied by dipping with a wipe on the substrate. A critical point is to limit the deposited amount of primer.

5.9.1 Casting of PDMS

For a detailed explanation of the casting steps, we refer to Section 5.9.1. By casting, thin and thick layers (0 - 1000 μm) of PDMS can be precisely applied by manual or doctorblade deposition.

5.9.2 Moulding using PDMS

The moulding process steps are shown in Figure 4.4 and are similar to the steps explained in Section 4.9.2. First, the temporary substrate supporting the functional electronic circuit is put into the mould. The upper layer of PDMS is then injected and cured. Curing is done at 50°C preventing the wax of melting and mixing with the uncured PDMS resulting in an incurable mix. Secondly, the supporting mold is removed and the temporary substrate is removed by heating the temporary substrate up to 200°C. In this way, the wax melts and allows us to peel off the substrate. Wax residues are removed by rinsing in an acetone bath. Next, the backside mould is mounted in order to inject the final layer of PDMS. After curing this layer at 50° C during 4 hours, the system is unmounted. The mate-

132 **Peelable technology with local polyimide support**

rial chosen for the moulds can be PMMA, polyetherimide ULTEM or aluminium. The dedicated mould design for our test structure is shown in Figure 5.22.

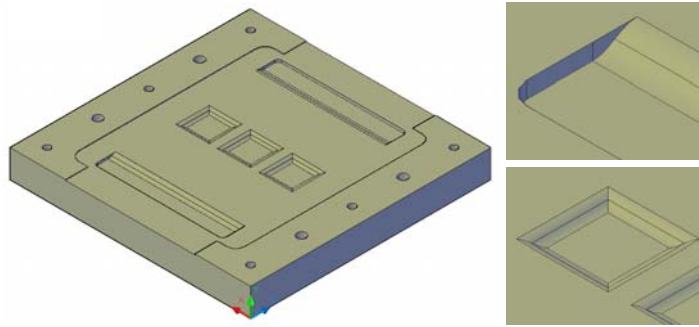


Figure 5.22: Dedicated mould design.

As can be observed, the transition between the thicker and thinner parts is done gradually, in order to prevent a stress concentration during stretching. The result of the molding is shown in Figure 5.23. On the right side of Figure 5.23, a detailed view on the molding showing the fluent transitions between thinner silicone parts and thicker silicone parts is shown. The reason behind this approach will be explained in Chapter 6 on reliability.

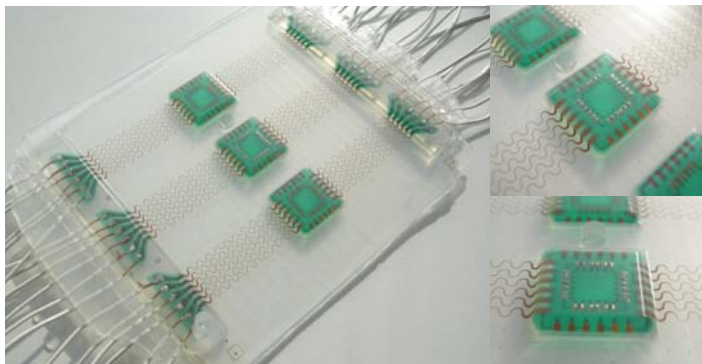


Figure 5.23: Samples after completely embedding in Sylgard 186 by using a dedicated mould.

The thicker silicone parts are situated in regions with flexible islands containing the mounted components. The thinner silicone parts are there in the regions where meanders are defined. In this way, we will make stretching more easily in the thinner parts where the conductors are especially designed to be stretchable and we will limit the stretching of the thicker parts, consisting of non-stretchable

components.

5.10 Double polyimide layer technology

5.10.1 Possible process flow

The difference between only one supporting layer of polyimide for the copper and a completely embedded approach has been investigated.

To achieve this with photodefinable polyimide is not possible at the moment. A possible process flow (Figure 5.24) would be patterning the supporting layer of polyimide, putting this on a carrier, etching the copper and then spincoating another layer of polyimide. For this approach, you need a carrier being able to hold the structures during the covering polyimide hardbake. This hardbake happens at 350°, at this moment we don't have a carrier fulfilling this criterion.

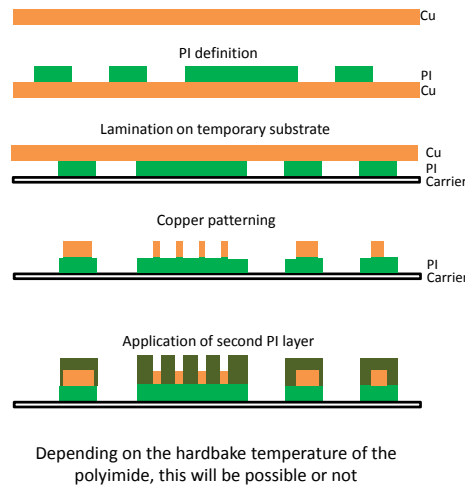


Figure 5.24: Approach in order to have a polyimide sandwich around copper structures.

But, in order to get an idea of the influence of a second polyimide layer in terms of improved reliability, we used another approach by use of a flex foil being lasercut.

5.10.2 Process description and feasibility

In [6], an approach is described of how to make such stretchable lasercut meanders. In that technology, an Upisel SE1410 [7] polyimide-copper foil is used as starting point, being laminated on a carrier with a temporary adhesive. Stretchable patterns are obtained by lasercutting through the copper and polyimide. The

approach we present here is better in terms of quality of the definition of the copper structures. In [6], the copper is cut by the laser itself. We will first pattern the copper in a lithographical way and then lasercut the supporting polyimide layer. The process flow is shown in Figure 5.25. It also starts from a temporary carrier where a flex foil is laminated on by use of Quickstick 135 wax in the same way as described previously. The flex foil, Upisel SE1410, is an adhesiveless copperclad consisting of 9 μm copper and 25 μm polyimide. The copper is patterned, using the process parameters depicted in Table 5.5. After the copper patterning, the foil is removed from the carrier and a layer of PI2611 polyimide is spincoated onto the substrate and hardbaked, this in order to cover the copper structures completely with a $\sim 25 \mu\text{m}$ polyimide layer.

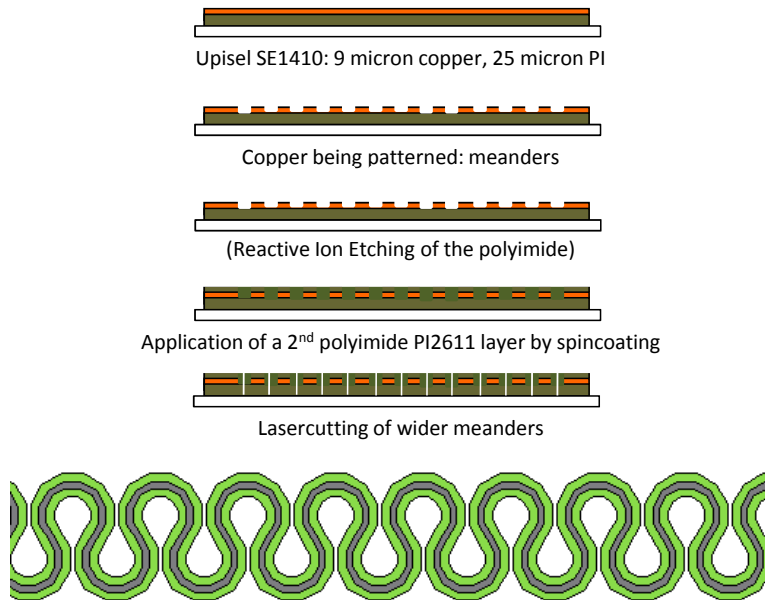


Figure 5.25: Current approach in order to have a polyimide sandwich around copper structures.

Parameter	Value
Spintime	1 min
Spinspeed	2000 rpm
Prebake time on hotplate	90 sec
Prebake temperature on hotplate	90°C
Development time in Microdev developer	2 min
Postbake time in convection oven	30 min
Postbake temperature in convection oven	120°

Table 5.5: Lithography parameters of AZ4562 photoresist.

5.10 Double polyimide layer technology

135

Spincoating is done at 1000 rpm, in order to obtain a symmetrical polyimide sandwich. The polyimide is cured with the same curing parameters as for the photodefinable polyimide. Because of the quite thick layer of polyimide, the substrates are curled when taken out of the oven. This due to a CTE mismatch between the supporting polyimide and the covering polyimide. For our investigation it's not a problem, but for future applications, this should be solved by using a polyimide that is better matched in terms of CTE. The samples are laminated on a RO4003 substrate by use of the same lamination profile and wax solution as described in Section 4.3. By use of a Nd:YAG-laser, the polyimide is lasercut in meander shapes being wider than the copper. The excess polyimide is peeled off and the samples are foreseen with wires and moulded in the mould used for reliability testing. In Figure 5.26, an example is shown of meanders fabricated in this way. They are not embedded and shown at different strains, upto 50%. It has been observed that these structures are very flexible and strong.

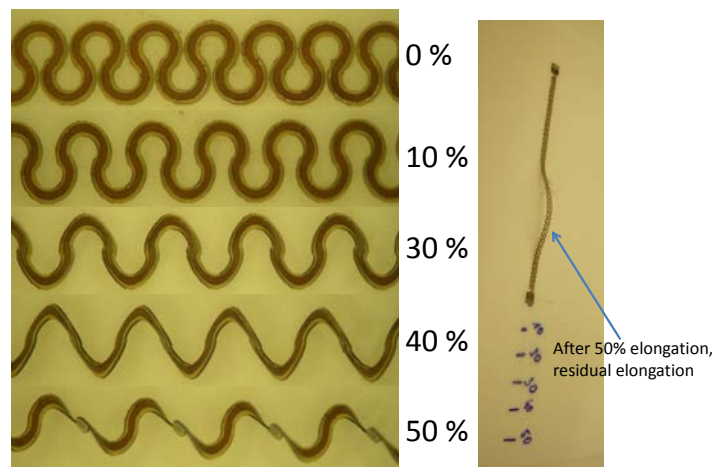


Figure 5.26: Realized double polyimide layer samples, not embedded, at different strains.

The profile of these meanders have been measured (Figure 5.27) in order to have an idea of the stack composition. Because the thickness of the base polyimide and the copper are known, being respectively $25\mu\text{m}$ and $9\mu\text{m}$, the thickness of the spincoated polyimide can be determined, being $\sim 22\mu\text{m}$.

Reliability results will be covered in Chapter 6.

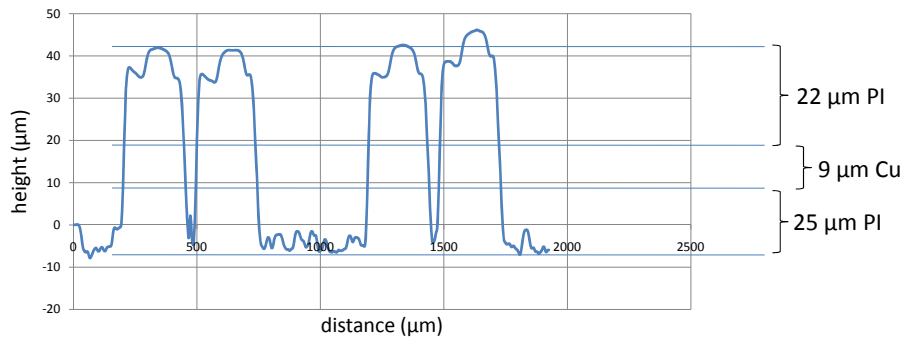


Figure 5.27: Profile measurement of realized samples indicating the different layer thicknesses.

5.11 Double conductor layer technology

5.11.1 Process description

This process is an extension to the peelable technology with local polyimide support, where a flexible supporting layer is used to support the meandered conductors and the flexible component islands. An extra conductor layer is added to the buildup stack. The processflow is shown in Figure 5.28.

It can be shortly described as follows:

1. A copper sheet is used as starting point for processing and will be 1 of the 2 conductors.
2. The flexible supporting/isolation material is patterned on the copper sheet by a photolithographic process. Photodefinable polyimide HD4100 will be used for this purpose. The flexible material is used as support for the meandered conductors defined in the copper and support for the flexible functional islands where straight conductor tracks are defined and SMD components are mounted. It is also used as insulating layer between the 2 conductors. Because of the possibility to pattern it, vias can be defined on places where a connection is needed between the upper conductor layer and the lower conductor layer.
3. The second conductor, a conductive polymer (Dupont 5025 Polymer Silver Conductor) is applied by screenprinting. By printing the second conductor, meandered conductors can be defined on places where flexible support is foreseen, straight conductors between components can be defined on places where the flexible support is foreseen, bridges can be made making contact

5.11 Double conductor layer technology

137

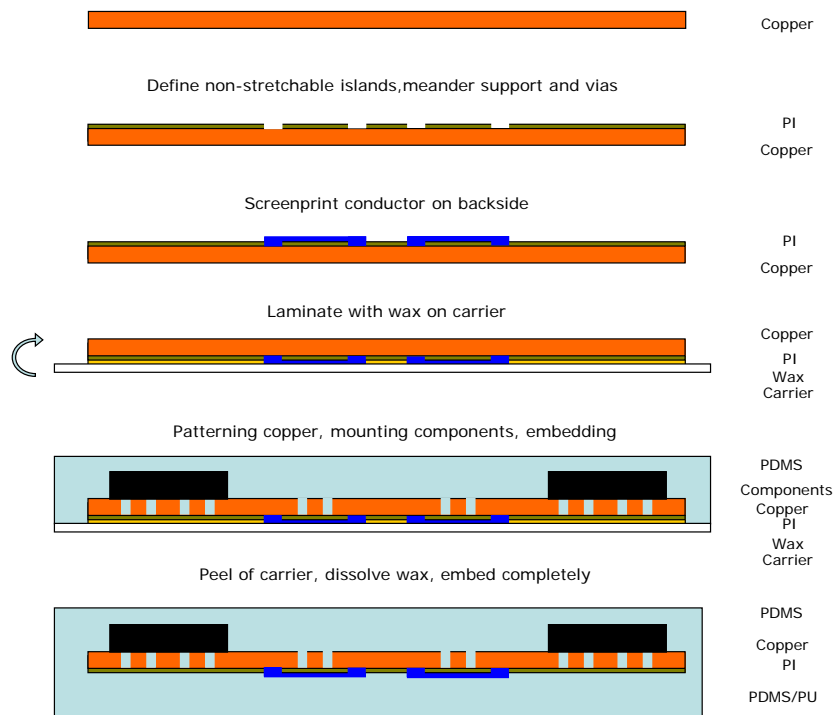


Figure 5.28: Processflow of double conductor layer stretchable technology.

through vias defined in the flexible material with the copper conductor on the other side.

4. The substrate is laminated by use of temporary glue (e.g. wax, Quickstick 135) on a temporary rigid/flexible carrier with the side of the copper on top, in order to be able to pattern the copper sheet by wet-etching it. In this way, the copper meandered conductors are defined and the tracks on the functional flexible islands are defined.
5. Soldermask is applied, a copper finish is applied (OSP), components are mounted by reflow soldering using SAC.
6. The top part is moulded using an elastomer e.g. Sylgard 186.
7. The temporary carrier is removed; the temporary glue (Quickstick 135) is removed.
8. The back part is moulded using the same elastomer (Sylgard 186).

138 Peelable technology with local polyimide support

9. The final result is a completely embedded, double conductor layer stretchable electronic circuit.

For more details about step 4-9, we refer to the previous sections.

5.11.2 Process feasibility

We start with a 10 cm by 10 cm 18 μm TW-YE grade copperfoil (Circuitfoil). We spin photodefinable polyimide HD4100 (HD Microsystems) on the rough side of the copperfoil. Spinning is done during 10 secs at 500 rpm and 30 secs at 1500 rpm. We softbake the polyimide on a hotplate during 5 minutes at 90°C followed by 5 minutes at 110°C. To pattern the polyimide, illumination is done through a TiW patterned glass mask during 40 seconds by use of an UV lamp (8mW/cm²). Next, the polyimide is developed by use of PA400D and PA400R (HD Microsystems).

The development parameters are as follows:

- 3 minutes in PA400D
- 2 minutes in a PA400D/PA400R 1:1 solution
- 3 minutes in PA400R
- rinse with DI water brush

Curing is done in a nitrogen oven, with the following temperature profile:

- heating from room temperature to 200°C, with a ramp rate of 4°C per minute
- 30 minutes at 200°C
- heating from 200°C to 375°C, with a ramp rate of 2,5°C per minute
- 60 minutes at 375°C
- cooling down to room temperature

In this way, a layer of 20 μm polyimide on the copper is obtained.

Alignment marks are defined in the polyimide layer for laserdrilling holes to be able to align the copper on the backside. These alignment marks are also used now for the correct placement of the extra conductor layer.

After curing the polyimide, the conductor layer is applied. We use Dupont 5025 silver conductor [?], being used to fabricate low voltage circuitry especially on

5.11 Double conductor layer technology

139

flexible substrates. The conductor has a sheet resistivity of $8-15 \Omega/\square/25\mu\text{m}$ (e.g. a track of $100\mu\text{m}$ width, 10 cm long has a resistivity of $8-15\Omega$) and resistivity after flex $< 50 \Omega/\square/25\mu\text{m}$ and this 15 sec after a 180° crease.

The conductor is screenprinted by use of a screen with a stainless steel mesh with the following characteristics: angle = 45° , mesh size = 400 and emulsion thickness = $20 \mu\text{m}$.

When the conductor layer is applied, it is cured in a convection oven during 5 mins at 120°C .

After the application, we spin a layer of Quickstick 135 wax (South Bay Technology Inc.) on the side where the silver conductor is. A Quickstick of 17,5g is dissolved in 30ml of acetone and spinning is done during 30 sec. at 1000 rpm. On an etched RO4003 substrate, we spin the same layer of wax. This substrate is used as a temporary carrier during the different process steps. Both substrates are then laminated to obtain a carrier-wax-silver polymer conductor-polyimide-copper stack.

After the lamination, the copper is patterned. This is done by use of a standard photoresist AZ4562, etching the copper in a HCl/CuCl solution and stripping the photoresist in AZ 400K. The silver filled polymer conductor is not attacked by the solution because it is protected by the polyimide layer and the wax. After these steps, the circuitry is being defined. Soldermask can be applied on the flexible functional islands and components can be soldered by use of a reflow soldering step.

5.11.3 Characterization

To show the feasibility of this process flow, a dedicated design was made to characterize the capabilities of this process in terms of minimum line width of the silver filled conductor, minimum spacing between 2 conductor lines, conductivity, via definition in the polyimide, etc.

In Figure 5.29, the different parts of the test mask are shown. Figure 5.29 a depicts the design of different daisy chains. There it is the purpose to determine the feasible width of the silver filled polymer tracks and the feasible size of the vias made in the polyimide layer. In Figure 5.29 b, the design is shown where the feasibility of double layer meanders with varying width is investigated. In Figure 5.29 c and d, the design is shown where the feasible line spacing is investigated between 2 printed silver filled polymer lines. In Figure 5.30, the result after the first process step is shown. The polyimide has been defined on the copper sheet. The most important is the definition of the vias, making contact possible between the upper copper layer and the lower silver filled conductor layer. Vias with a diameter from $300 \mu\text{m}$ down to $75 \mu\text{m}$ where defined in the polyimide mask. The vias shown in Figure 5.31 and being defined as $75 \mu\text{m}$ on the mask have

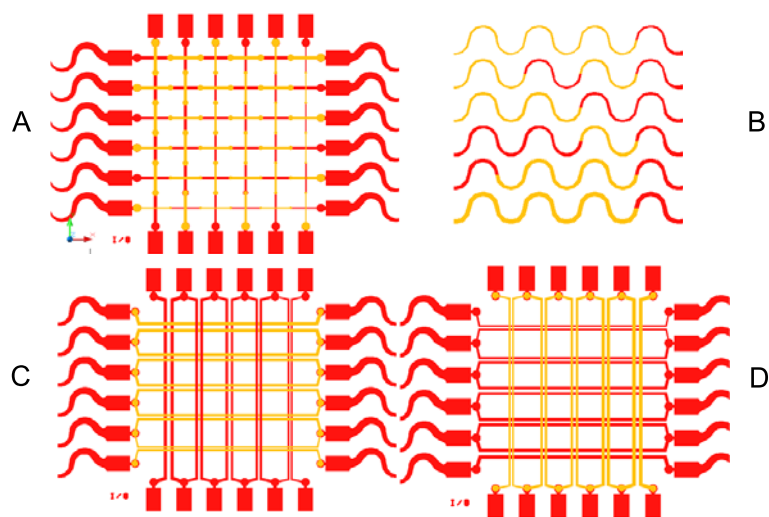


Figure 5.29: Parts of feasibility mask: (a) Daisy chains for testing conductivity and minimum track width (b) Test of double sided meander structures (c) Vertical printing line pitch test (d) Horizontal printing line pitch test.

become $95 \mu\text{m}$ in diameter. This is not a problem because the copper and silver filled conductor have been oversized at the place where the contact with the via is made.

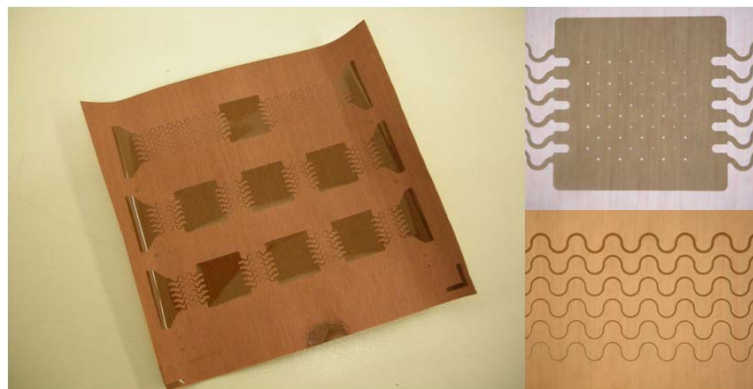


Figure 5.30: Pattern definition of polyimide for double conductor layer stretchable technology.

In Figure 5.32, the result of screenprinting the conductor paste on the sample is

5.11 Double conductor layer technology

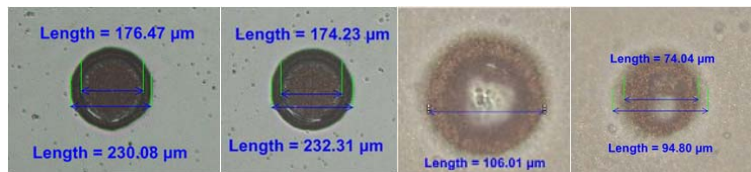


Figure 5.31: Photodefined vias.

shown. Curing was done during 5 mins at 120°C. Figure 5.33 illustrates printed tracks with different predefined widths.

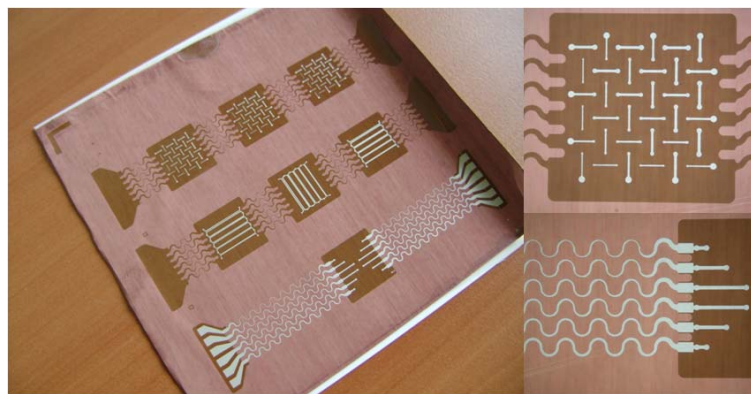


Figure 5.32: Deposition by screenprinting of silver conductor Dupont 5025.



Figure 5.33: Closer view on printed tracks.

Table 5.6 gives an overview of the defined and the printed track widths. The tracks being defined as 75 μm are on the edge of being printed properly, resulting in a track width between 61 μm and 86 μm , and resulting from time to time in an open track, thus non-conducting. The tracks being defined as 75 μm have a

142 **Peelable technology with local polyimide support**

typical resistivity of 5Ω , while all the other tracks have a resistivity in the range of 1-2 Ω .

Defined track width (μm)	Printed track width (μm)
150	163,3
100	119,2
75	61,8;68,4;86,1

Table 5.6: Comparison between track widths defined and printed.

Figure 5.34 shows the test patterns for testing the minimal line width and spacing. Table 5.7 shows the defined and the printed track widths: only the parallel lines of $200\ \mu\text{m}$ with a distance of $200\ \mu\text{m}$ in between were not short-circuited.

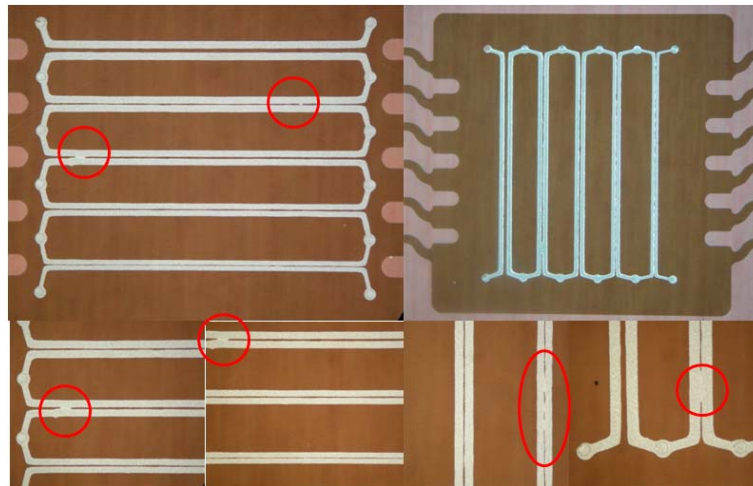


Figure 5.34: Closer view on parallel printed tracks.

Defined track width (μm) - spacing (μm) - track width (μm)	Printed track width (μm) - spacing (μm) - track width (μm)
200 μm - 200 μm - 200 μm	238,4 μm - 130,2 μm - 240,6 μm
200 μm - 200 μm - 200 μm	234,0 μm - 154,5 μm - 247,3 μm
200 μm - 125 μm - 200 μm	236,2 μm - 48,6 μm - 238,4 μm
200 μm - 125 μm - 200 μm	231,8 μm - 39,7 μm - 238,4 μm

Table 5.7: Comparison between track widths and spacing defined and printed.

In Figure 5.35, a closer view of the printed meander tracks are shown. In Table 5.8, the defined and the printed track widths are shown. As can be seen in the picture, sometimes the conductor is flowing out making contact with the copper. This can result in a short between the copper conductor on the other side of the polyimide layer, what is not the purpose. In this design, the polyimide has been

5.11 Double conductor layer technology

Defined track width (μm)	Printed track width (μm)
100 m	92.7 μm ; 110.4 μm ; 97.1 μm
125 m	125.8 μm ; 141.3 μm ; 128.1 μm
150 m	152.3 μm ; 165.5 μm ; 150.1 μm
175 m	163.4 μm ; 194.2 μm ; 181.0 μm
200 m	204.3 μm ; 211.6 μm ; 200.6 μm
250 m	248.5 μm ; 246.6 μm ; 248.5 μm

Table 5.8: Comparison between track widths defined and printed.

designed as wide as the conductor tracks and as wide as the copper tracks. In fact, it is better if the polyimide is defined wider, making contact between the 2 conductor layers not possible.

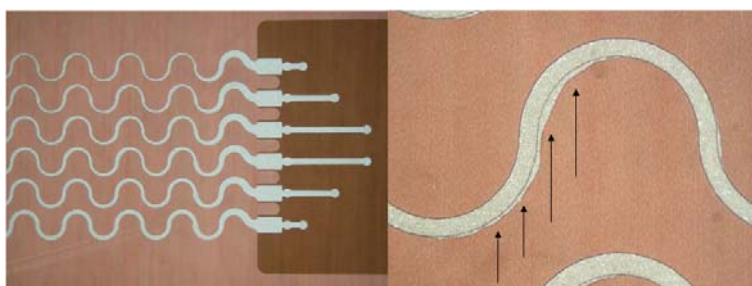


Figure 5.35: Closer view on parallel printed tracks.

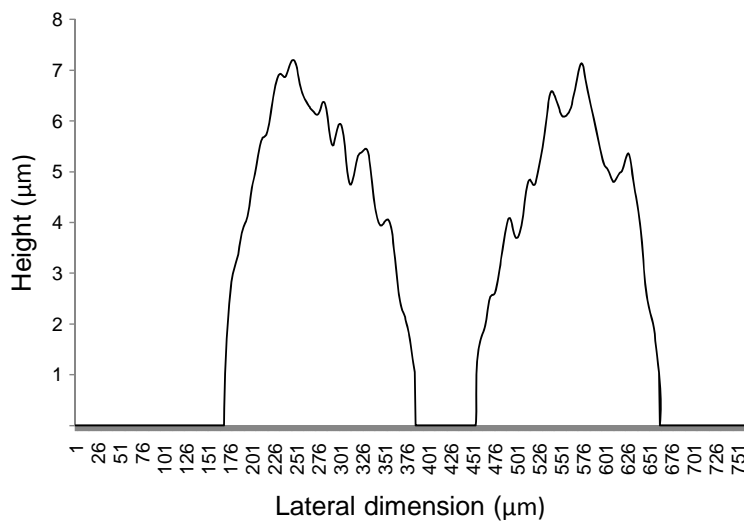


Figure 5.36: Profile of screenprinted conductor after hardbake.

In Figure 5.36, the profile of the printed silver conductor is shown after curing it at 120°C during 5 mins in a convection oven. The height of the tracks is around $7\ \mu\text{m}$. In Figure 5.37, the substrate is shown after the copper definition. In Figure 5.39, a closer view is shown where you can clearly see the realized daisy chains, with on one side the copper and on the other side the silver filled polymer. The daisy chains are conducting from the left side of the island to the right side of the island, and from top to bottom. In Figure 5.38, the parallel tracks are shown being realized in the copper and silver filled conductive polymer.

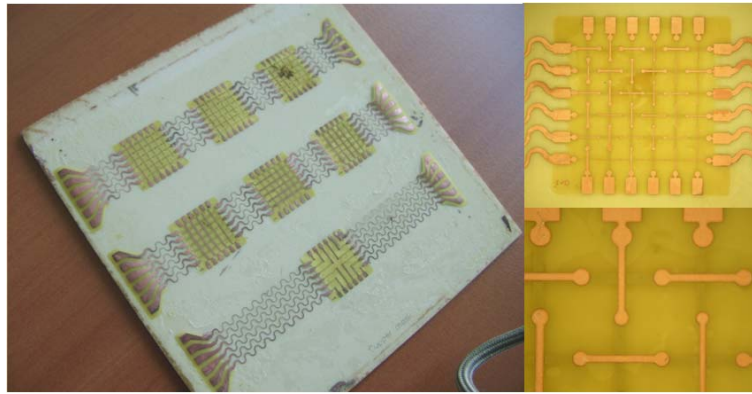


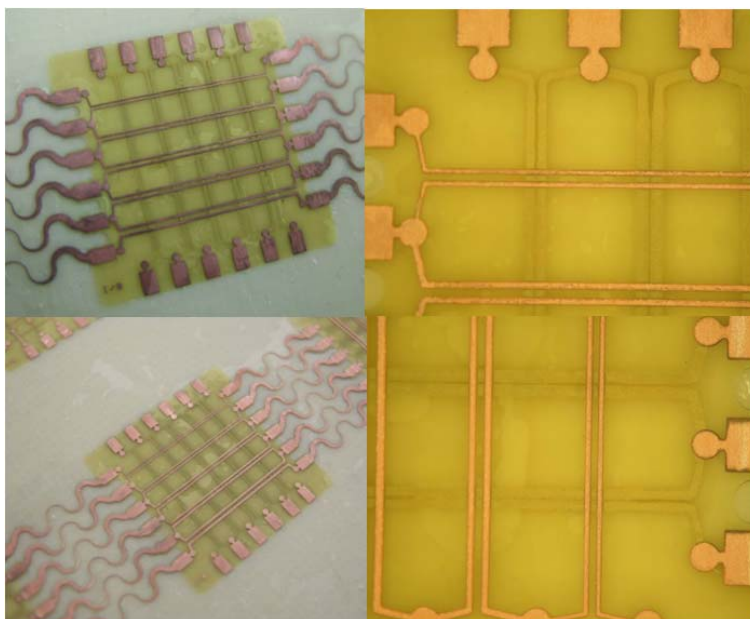
Figure 5.37: Pattern definition of copper for double conductor layer stretchable technology.

5.11.4 Discussion

The extra conductor layer is a big improvement to the standard single layer peelable polyimide supported technology. Having only 1 conductor layer puts some restrictions to the realizable electronic circuits. To cope with that, $0\ \Omega$ resistors were used to make cross-overs. In cases where a lot of crossovers are needed e.g. in the case of wearable signage applications, where a matrix of LEDs makes up a stretchable display, and where the LED matrix is driven by a set of crossing conductors. A 2-layer interconnect reduces the number of components by roughly a factor of 2, because no $0\ \Omega$ cross-over resistors are necessary anymore. The feasibility study has demonstrated that by using a stainless steel screen with the mentioned parameters, silver filled polymer defined tracks of $100\ \mu\text{m}$ are possible leading to tracks of $\sim 120\ \mu\text{m}$. Vias can be made down to $100\ \mu\text{m}$ in the photodefinable polyimide, ensuring contact between the copper above and the conductor below the polyimide. Of course, the via landing size dimensions should be bigger than the defined via dimensions, compensating the polyimide overdevelopment. Track pitches should be defined further away than $200\ \mu\text{m}$ from each other, to

5.11 Double conductor layer technology

145



— **Figure 5.38:** Pattern definition of copper for double conductor layer stretchable technology. —

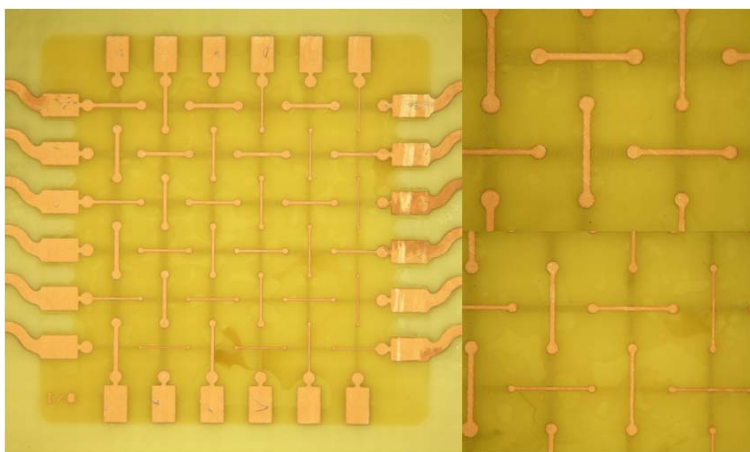


Figure 5.39: View on daisy chains: copper tracks on top side connected through vias to silver conductor on bottom side.



Figure 5.40: View on double sided meander tracks: silver conductor overprinting leads to shorts between top and bottom conductor.

make sure they are not short-circuited.

5.12 Conclusions

An improved version of the technology presented in Chapter 4 has been discussed.

The use of polyimide as mechanical support for the stretchable conductors and flexible component islands is a major improvement in terms of processability and mechanical reliability of the stretchable electronic system. The photodefinable feature of the used polyimide allows us to define these supporting structures. In this way, more fluent transitions between rigid, flexible and stretchable parts can be defined, shifting the stresses to areas where measures are taken to cope with them. The first trials have been made to replace the photodefinable polyimide by screenprintable polyimides, the non-unavailability of suitable materials on the markets will make the development of this option longer. But, the first results seem to be promising. Some extensions on the technology have been presented: encapsulating the stretchable copper tracks by polyimide, on top and bottom. Furthermore, a technology for adding another conductor layer to the stack has been presented, allowing more complex and dense circuits. In Chapter 7, 2 demonstrators will be presented using the proposed technology for realizing functional, stretchable on-the-body applications. An infant respiratory monitor and a fitness activity monitor.

References

- [1] HD Microsystems. <http://www.hdmicrosystems.com>.
- [2] HD Microsystems. Technical datasheet - Product Information Pyralin PI 2730 series.
- [3] HD Microsystems. Technical datasheet - HD-4100 Series Polyimide.
- [4] Circuitfoil. <http://www.circuitfoil.com>.
- [5] UBE America Inc. Technical datasheet - U-VARNISH A.
- [6] F. Axisa, F. Bossuyt, T. Vervust, J. Vanfleteren. Laser based fast prototyping methodology of producing stretchable and conformable electronic systems. In *ESTC 2008: 2nd Electronics System-Integration Technology Conference, Vols 1 and 2, Proceedings*, pages 1387–1390, 345 E 47TH ST, NEW YORK, NY 10017 USA, 2008. Univ Greenwich; IEEE; CPMT; iMAPS, IEEE. 2nd Electronics System-Integration Technology Conference, Greenwich, ENGLAND, SEP 01-04, 2008.
- [7] UBE America Inc. Technical datasheet - Polyimide Base Copper Clad Laminate (Adhesiveless).

Chapter 6

Reliability evaluation of the technologies

Reliability results of the different technologies will be presented. The effects of different precautions in order to increase the lifetime of the system subjected to uniaxial elongations will be discussed.

6.1 Introduction

The obvious question concerns the reliability of the stretchable electronics technologies, more specifically the long-term performance of their stretchability and connectivity. Wearability will undoubtedly involve - depending on the application - large numbers of stretching cycles ranging from a few percent to a limited number of stretching cycles of about ten percent. As an example, an ECG-sensor implemented in such a technology for measuring the heartbeat several times per day, should be able to be stretched several times upto 10% during the moment of application on an arm or a leg of a patient and many thousand times during doing exercises requiring upto 3% elongation. If such sensor requires a lifetime of a year or more, one needs in the order of 10^4 cycles of 5-10% stretch and around 10^5 cycles of 1-3%. To qualify the presented technologies, reliability tests have been performed in order to be able to extrapolate these results to operational load cases. In this PhD-work, we mainly focused on the non-cyclic and cyclic endurance behavior of the stretchable interconnections and the interconnection with the interface of the non-stretchable islands. Other mechanical tests like compressing, bending, crumbling, washing... where out of the scope of this work and will be investigated in follow-up PhDs.

6.2 Physics-of-failure

A product's reliability is defined as 'the ability of the product to function according to specification, under specified loading conditions, during a specified period of time' [1]. This conduct has a statistical nature. Many handbooks deal in much detail with these issues. Here it suffices to emphasize the costs of reliability, or better the costs of unreliability. Although tests, analyses, and improvement cycles in the development process are time consuming and costly, they still form but a small part of the expenses when compared to the costs if - because of a reliability problem - one would have to intervene in the production lines. Therefore one is well advised to identify the possible failure modes of new products, technologies, and applications early in the development and to take appropriate measures. A suitable way of working to identify the potential failure modes and mechanisms in any product or application is the 'physics-of-failure' approach (PoF). In this section we will explain the different steps of physics-of-failure and try to fill in the parts that are known already. However, the topic of this PhD is a very special one that has hardly been treated before: stretchable substrates for electronic applications. Talking about failure mechanisms and failure modes it is good to first define these two notions that are quite often mixed up. A failure mode is any physically observable change caused by a failure mechanism. A failure mechanism is the process by which specific combinations of mechanical, electrical, chemical or physical stresses induce failure.

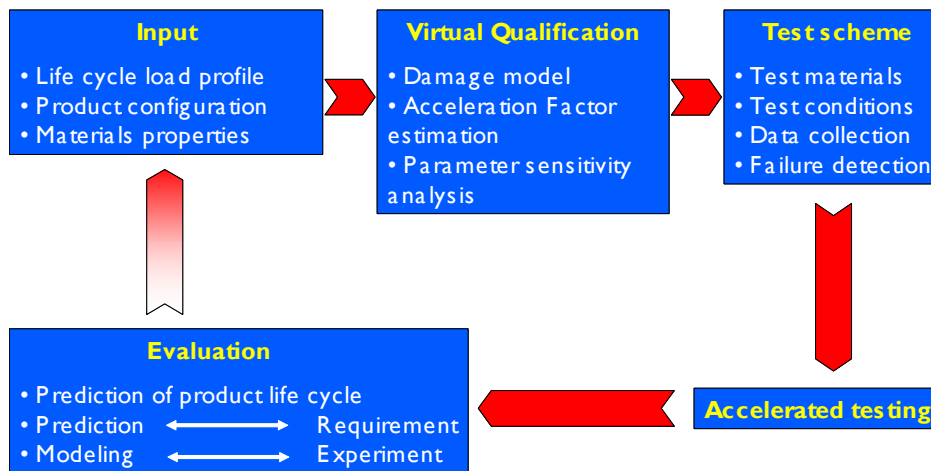


Figure 6.1: Schematic of physics-of-failure.

In Figure 6.1, one finds a schematic outline of the steps used in physics-of-failure. The most essential part is to gather input from a thorough inventory of the life

cycle load profile, the product configuration, and the materials' properties of the product in question. The life cycle load profile contains all stress loads exerted on the product during its useful lifetime, but should also include manufacturing, transportation and storage loads.

Secondly, one does a virtual qualification of the product in which a damage model is drafted physically describing when, how, and where a failure will occur. Tools to achieve this are manifold, like FMEA, brainstorming, etcetera. Further, acceleration factors and parameter sensitivity are estimated. This is meant to design accelerated tests.

In the third step the test scheme can be designed, comprising the choice of test materials, test conditions, but above all the definition of failure and the method to collect the data must be indicated. These latter two items are not trivial as sometimes failures are but difficult to detect. The actual test program is carried out in the fourth step, while finally the results are evaluated and compared to requirements and models that might be available. Much depends on the specifications for the products. A split can be made into various sets of specifications. These apply to the manufacturing processes, to transportation and storage, and the actual operation.

6.3 Performed reliability tests

A brief explanation of the many types of tests that exist is presented to forestall confusion as quite often these concepts are used together.

- verification and validation tests: verification is used to proof compliance to specification. Validation is used to investigate if the use requirements are covered by the specification.
- accelerated and aggravated tests: in an accelerated test non stressing time is taken out. In an aggravated test the severity of stressors exceeds the limits of field use.
- confidence tests or test-to-failure: confidence tests are usually part of a market release process. Test to failure is crucial to product improvement.
- general versus specific tests: general tests are used for confidence or validation, while specific tests apply to conceptualized failure modes: to see if the failure can occur or as a result of the named circumstances.

In this work, we will mainly focus on confidence tests or tests-to-failure. Due to the novelty of the technologies, we will mainly investigate the failure modes due to mechanical loading of the device. The most important feature of the presented technologies is the stretchability, therefore we have to characterize the stretchability of these technologies. Stretchability and electrical connectivity is the main

6.4 Mechanical reliability test setup

151

issue for the performed reliability tests. Results will be used in order to compare different technologies, different designs,.. this in order to further optimize the stretchable devices.

Endurance tests (or durability tests) should not lead to immediate failure. This happens either because of processing errors in which case one is actually testing the early-failure regime, or because the test load approaches the failure limit too closely. The application strains we are aiming for are situated in the 0-20% region. Therefore, samples will be fabricated and put to cyclic testing, this at a fraction of the failure load. For the presented technologies, large volume testing is not possible yet, so the results will only show the capability of the various technologies, in order to compare and improve them.

6.4 Mechanical reliability test setup

An Instron 5543 [2] electromechanical test system has been used for performing the cyclic stretch tests. These kind of systems are used to test a wide range of materials under tension and compression. Instron electromechanical load frames are designed to apply a load to a test specimen via the moving crosshead. The drive system moves the crosshead up to apply a tensile load on the specimen, or down to apply a compressive load on the specimen. A load transducer (load cell), mounted in series with the specimen, measures the applied load. The load cell converts the load into an electrical signal that the control system measures and displays. Control of the testing system happens via the dedicated software for setting test parameters, operating the system, collecting and analyzing test data. Our test system is shown in Figure 6.2 where also a sample loaded into a dedicated clamping tool is mounted on the machine.

The measurements were done by use of a four-point resistance measurement system, where typically 12.5 mA is applied per track. The end of lifetime was defined as the point where the conductivity goes to infinity.

6.5 Reliability tests of stretchable interconnects

We start our reliability study with testvehicles without interposer which means containing only stretchable interconnections and no component islands. Thus, we only focus on the meanders itself and not on the transition between the meanders and the rigid/flexible component islands. Different types of samples have been produced by use of similar layouts. The layouts consist of parallel meander tracks, embedded in Sylgard 186 by use of a casting procedure or by moulding by use of a dedicated mould. Connections to the outside have been made by spe-

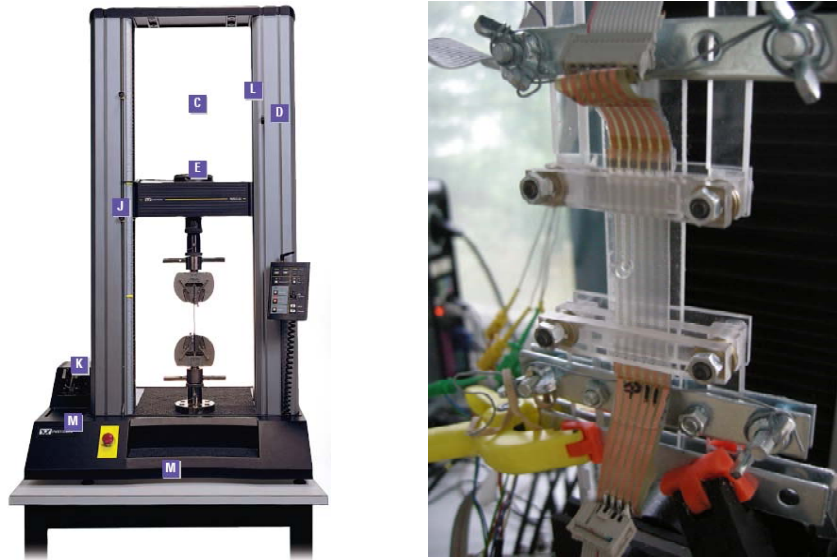


Figure 6.2: (Left) View on the electromechanical test system (Instron 5543). (Right) Sample mounted in a dedicated clamping tool.

cially designed flex connectors, which are soldered on the pads of the meanders. 2 designs have been used having both a $100\ \mu\text{m}$ track width but differing in meander angle and number of meanders per track. $100\ \mu\text{m}$ is taken being a common standard for minimal trackwidth in the PCB industry. Both designs are shown in Figure 6.3 and Figure 6.4. The parameters of both designs are depicted in Table 6.1, where in Figure 6.5 these parameters are indicated on a generic meander design.



Figure 6.3: Layout for single track using H45 ($\theta=45$) meander design, trackwidth= $100\ \mu\text{m}$.



Figure 6.4: Layout for single track using H30 ($\theta=30$) meander design, trackwidth= $100\ \mu\text{m}$.

A dedicated mold was used to have a smooth, stress releasing 'fillet' transition between the different thicknesses of the Sylgard 186 on top of the meanders and

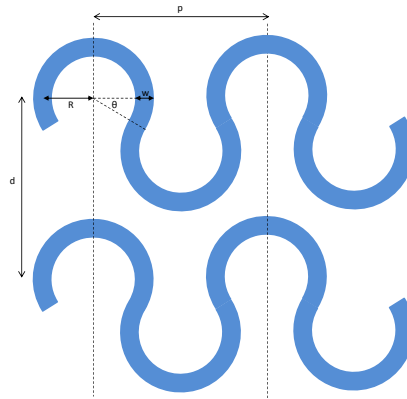


Figure 6.5: Generic design of meander-shaped conductor.

Parameter	H45 sample	H30 sample
Total length of sample	50 mm	74 mm
Total width of sample	18 mm	10 mm
Effective length for cyclic stretching	46 mm	25 mm
Amount of parallel stretchable tracks per sample	6	7
Parallel stretchable track pitch (d)	3 mm	10 mm
Amount of meanders per track	50	15
Meander track width (w)	0.1 mm	0.1 mm
Meander angle	45°	30°
Meander radius (R)	0.35 mm	0.325 mm
Meander period (p)	0.99 mm	2.60 mm
Embedding/support material	Sylgard 186	Sylgard 186
Embedding/support material thickness	1 mm	1 mm

Table 6.1: Characteristics of testsamples shown in Figure 6.3 and Figure 6.4. The geometrical parameters are defined in Figure 6.5.

at the connection pad. In mechanical engineering, a fillet is a concave easing of an interior corner of a part design. In Figure 6.6 the principle is shown, where in the situation without fillet, due to the small local area, the local stress is very high. When a fillet is introduced, the stress is distributed over a wider range. The introduction of a fillet also makes un moulding the parts easier, because of no vertical edges. The results are depicted in Figure 6.8

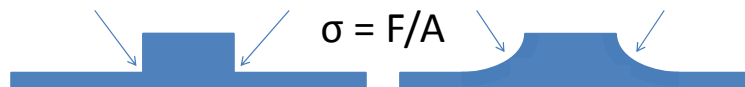


Figure 6.6: Local stress reduction by introduction of fillet.

A dedicated clamping tool was made in order to clamp the sample without having too much orthogonal force on the contact pads. This reduces the actual

stretchable length of the sample, because the sample is clamped at the contact pads. The stretching occurs parallel to the meander direction.

The testsamples realized in the different technologies using these designs, will be discussed in the following sections.

6.5.1 Peelable technology

H45 design, 18 μm TW-YE copper

Samples were made by use of 18 μm TW-YE copper foil (Circuitfoil) and Sylgard 186 (Dow Corning) as embedding material.

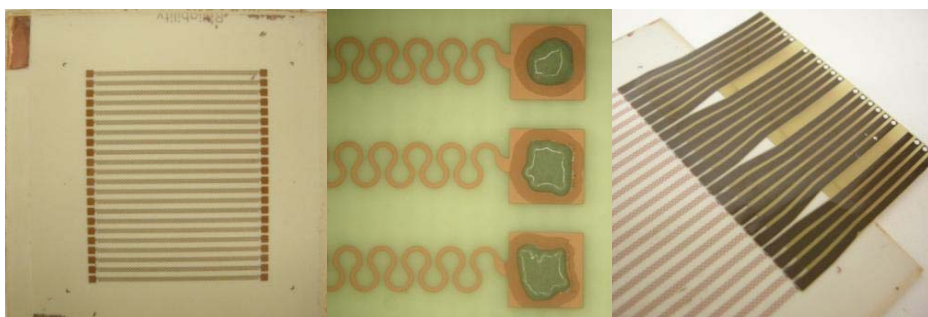


Figure 6.7: View on the fabrication of the testsamples before embedding: etched sample, sample with solderpaste applied, sample with flexible connector applied.

The fabrication of samples based on the H45 design, shown in Figure 6.3, is demonstrated in Figure 6.7.

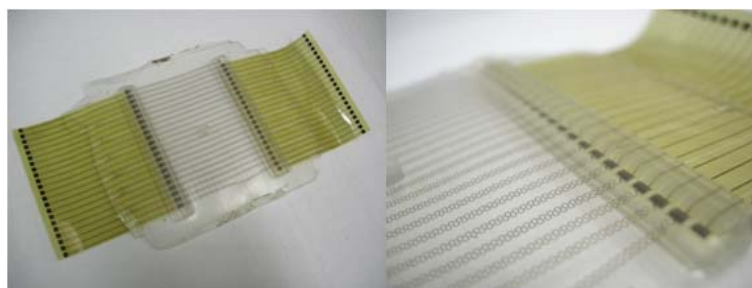


Figure 6.8: View on the fabrication of the testsamples after embedding: tapered, thicker silicone part at position of contact pads.

6.5 Reliability tests of stretchable interconnects

155

H45 design, 18 μm TW-YE copper with soldermask

The design and fabrication is the same as the previous sample, except that a layer of soldermask has been screenprinted on the meander tracks. The soldermask covering the meanders has the same dimensions as the defined copper tracks. We study the effect of having a soldermask cover on the copper. The screenprinted sample can be seen in Figure 6.9.

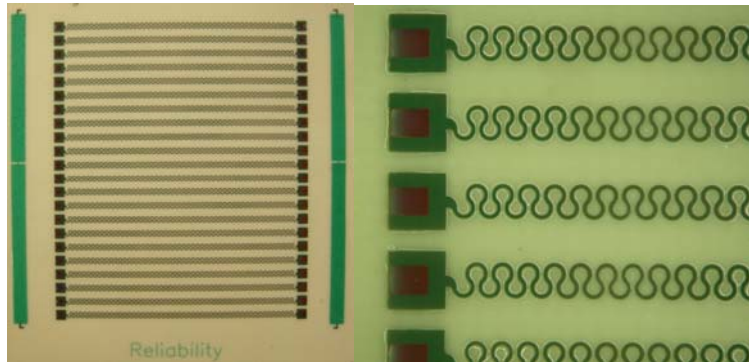


Figure 6.9: Testsample with 20 μm soldermask applied.

H45 design, 18 μm TW-YE copper with photodefinable polyimide

The design and fabrication is the same as the first described one, except that a layer of polyimide HD4100 is added below the copper, in the way described in Chapter 5. The shape and dimensions of the polyimide meanders are identical to the copper meanders. This in order to verify what the effect is of having a polymer supporting the copper. No picture is shown, because the polyimide can't be seen from above.

6.5.2 Stretchable substrate technology

H30 design, 18 μm TW-YE copper

Samples were made by use of 18 μm TW-YE copper foil (Circuitfoil) and Sylgard 186 (Dow Corning) as embedding material. The production method was based on the stretchable substrate technology, where a TW-YE foil is foreseen of adhesion promotor OS1200 and a 0.5 mm layer of Sylgard 186 casted using a doctor blade. After curing the PDMS, photolithography and wet chemical etching of the copper is done. Connectors are soldered and another 0.5 mm layer of PDMS is foreseen. The process flow is described in more detail in Chapter 3 and a realized sample is depicted in Figure 6.10.

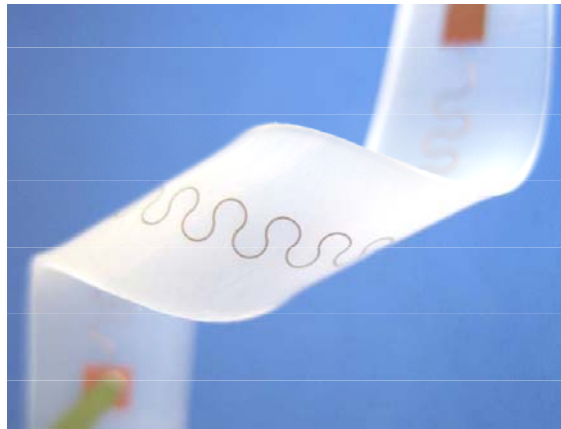


Figure 6.10: Testsample used for stretchable substrate reliability testing.

6.5.3 Double polyimide layer technology

H30 design, 9 μm copper

Samples were made starting from an Upisel SE1410 [3] copper-polyimide foil. The production method was based on the double polyimide layer technology described in Section 5.10. The H30 design is patterned on the copper by lithography and wet-etching. After the copper patterning, the foil is removed from the carrier and a layer of PI2611 polyimide is spincoated onto the substrate and hardbaked, this in order to cover the copper structures completely with a $\sim 25 \mu\text{m}$ polyimide layer. The realization of the testsample is demonstrated in Figure 6.11. The polyimide has the same H30 design, but has a track width of 300 μm .

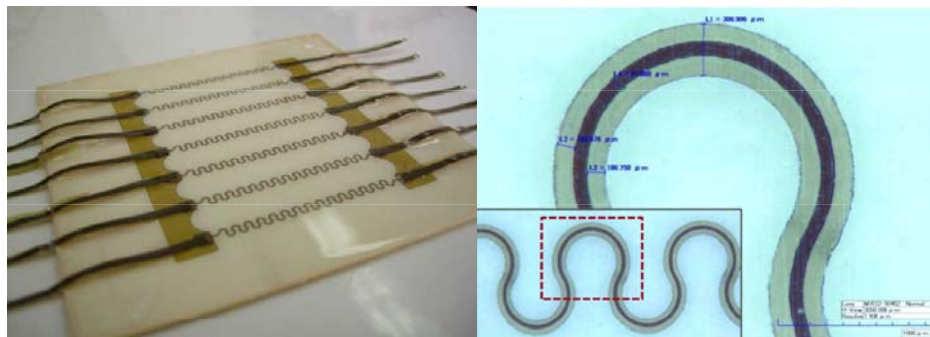


Figure 6.11: Double polyimide layer test sample using H30 design.

6.5.4 Cyclic endurance test results

Track resistance behavior

For all types of samples, the resistivity of the tracks showed no increase during mechanical loading. The average resistivity (depending on the meander shape, copper thickness,..) is a few ohms (2-10 Ω). Note that also the resistivity of the flexible, copper interconnects to the outside of the sample is included here.

Just before the moment of failure, a sudden increase of the resistivity is observed for the non-supported copper interconnects, leading to an interruption (Figure 6.12). For the photodefinable polyimide supported interconnects, the complete interruption is prolonged and spread over a big number of cycles. This is certainly due to the polyimide which reduces the speed of the crack propagation (Figure 6.13).

Lifetime data

A limited number of all types of samples has been tested, giving an indication of the lifetime of the different stretchable interconnects. In Figure 6.14, the average number of cycles before electrical failure is shown, for different applied strains (2.5%-20%) in case of 1% strainrate (s^{-1}) and for peelable and stretchable substrate technology.

The average numbers of cycles for the strains of 0-4%, 0-5%, 0-7.5%, 0-10%, 0-20% are respectively 105000, 17900, 3400, 2400, 200. The sample tested for 0-2.5% strain showed no failures even after 950000 cycles.

In order to determine if there's a difference in performance when the samples are subjected to different strainrates during the endurance tests, a set of samples

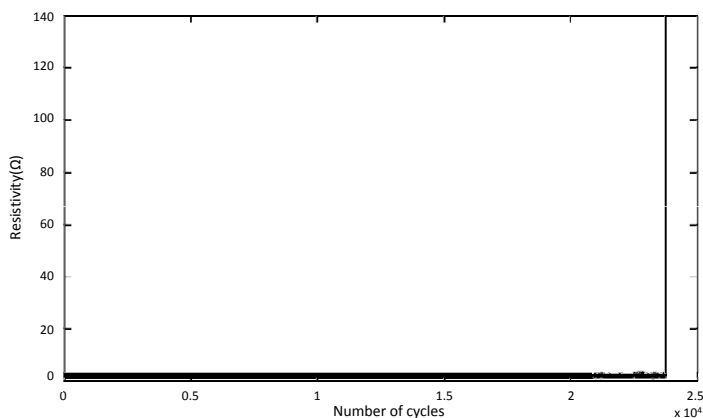


Figure 6.12: Resistance behavior of stretchable copper tracks without mechanical support layer during cyclic endurance tests (0-5% strain).

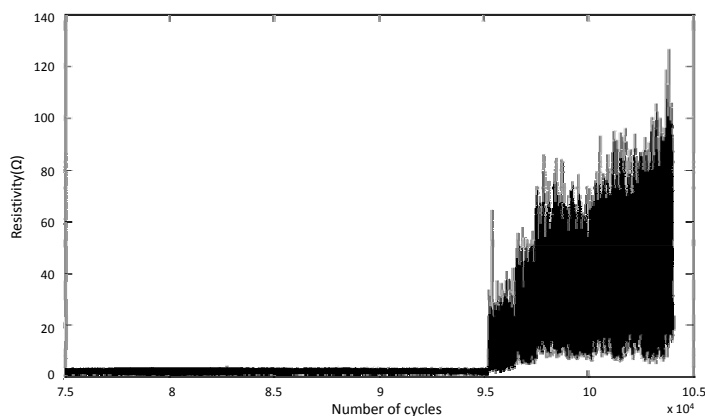


Figure 6.13: Resistance behavior of stretchable copper tracks with photodefinable polyimide support layer during cyclic endurance tests (0-5% strain).

was subjected to the same test conditions but at a higher strainrate of 10% (s^{-1}). The resistance behavior is the same as depicted in Figure 6.12. In Figure 6.15, the average number of cycles before electrical failure is shown, for different applied strains (2.5%-20%) in case of 10% strainrate (s^{-1}) compared to 1% strainrate (s^{-1}). The average numbers of cycles for the strains of 0-2.5%, 0-5%, 0-10%, 0-20% at 10% strainrate (s^{-1}) are respectively 1480800, 25200, 1330, 210. It can be observed that the differences fall within the error range of the test due to the limited number of tested samples. So we can conclude that there is no significant change in

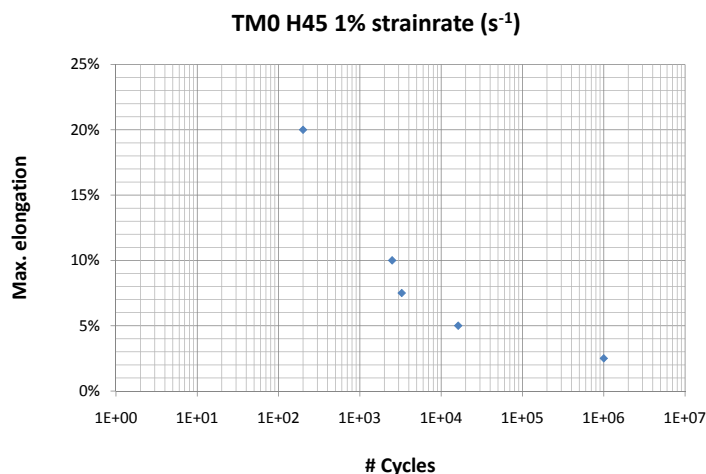


Figure 6.14: Cycles to failure for H45 horseshoe shape testvehicle and 1% strainrate for peelable technology.

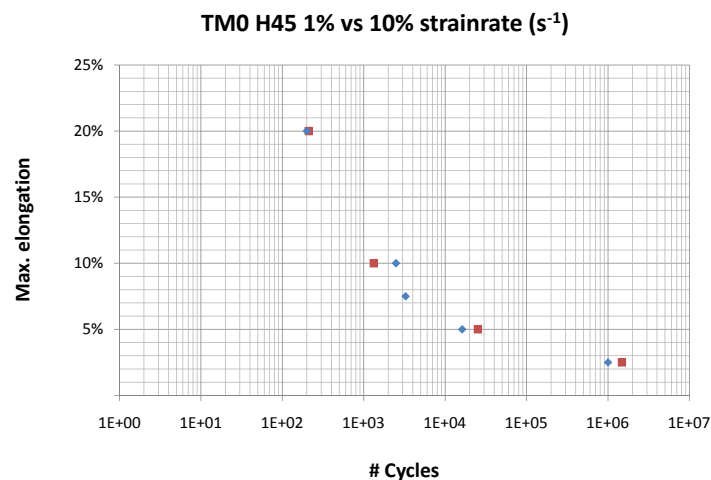


Figure 6.15: Cycles to failure for H45 horseshoe shape testvehicle for peelable technology. 1% (diamonds) and 10% strainrate (s^{-1}) (squares).

performance between 10% strainrate (s^{-1}) and 1% strainrate (s^{-1}).

In Figure 6.16, the results are shown of the cyclic endurance tests performed on peelable technology H45 samples foreseen of a 25 μm thick soldermask layer. The

results of the non soldermask covered samples are included for comparison.

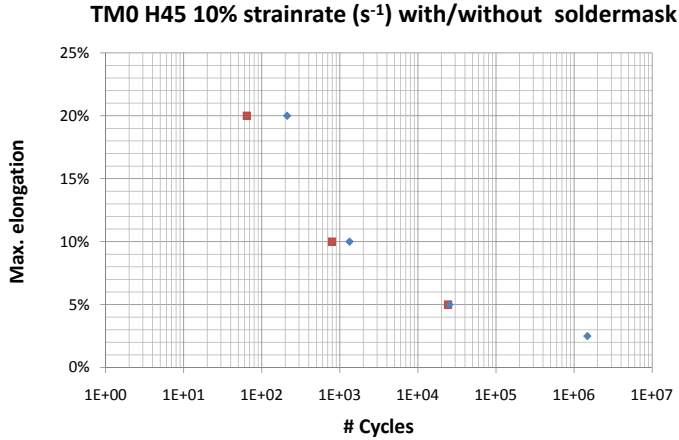


Figure 6.16: Cycles to failure for H45 horseshoe shape testvehicle, peelable technology covered with (squares) and without (diamonds) soldermask at 10% strainrate (s^{-1}).

The average numbers of cycles for the strains of 0-5%, 0-10%, 0-20% are respectively 24320, 800, 60. It can be observed that the differences fall within the error range of the test due to the limited number of tested samples. We can conclude that there is no significant change in performance when this type of soldermask is applied on top of the stretchable interconnects.

In Figure 6.17, the results are shown of the cyclic endurance tests performed on H45 samples foreseen of a $25 \mu m$ thick supporting layer of photodefinable polyimide HD4100 compared with non-supported peelable technology samples.

The average numbers of cycles for the strains of 0-5%, 0-10%, 0-20% are respectively 89000, 3420, 370. Immediately it can be observed that the photodefinable polyimide support has a positive effect on the lifetime of the interconnects. The average number of cycles for non-supported copper is 1330 at 10% strain, compared to 3417 for polyimide supported copper. For 5% strain, the average number of cycles for copper and supported copper is respectively 24320 and 89000. The effect seems more expressed for a lower applied strain of 5% (lifetime $\times \sim 3.6$) than for the higher applied strains (20%, 10%: lifetime $\times \sim 2$). This could have a physical reason but also be due to the fact that only a limited number of samples has been tested so the statistical relevance is low.

In Figure 6.18, the results are shown of the cyclic endurance tests performed on H30 samples made in the stretchable substrate technology as explained in Section 6.5.2.

6.5 Reliability tests of stretchable interconnects

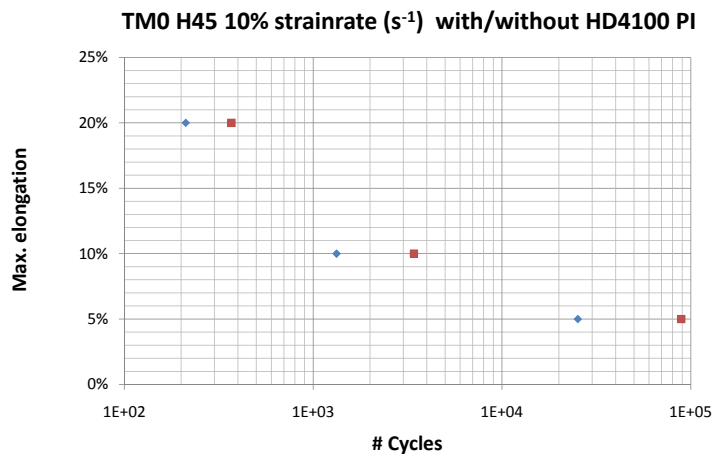


Figure 6.17: Cycles to failure for H45 horseshoe shape testvehicle supported by HD4100 photodefinable polyimide (squares) and 10% strainrate. Non-supported samples' results (diamonds) are included for comparison.

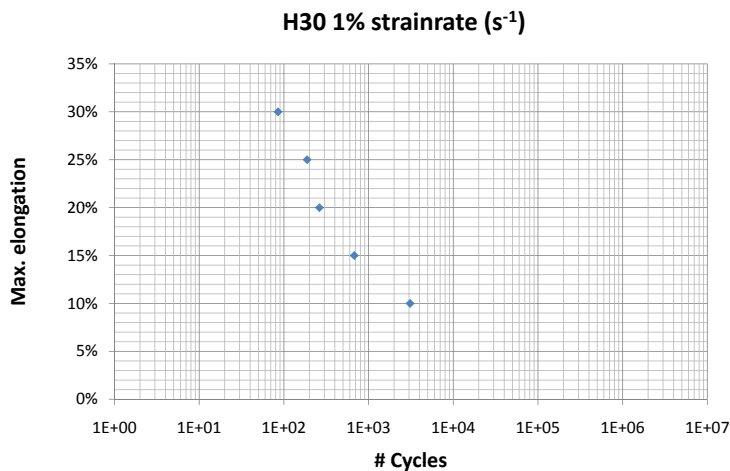


Figure 6.18: Cycles to failure for H30 testsample for 1% strainrate (s^{-1}).

The life test measurements were performed at higher strains, starting from 10%. These were performed by Hsu Yung Yu in the frame of his PhD study. The average numbers of cycles for the strains of 0-10%, 0-15%, 0-20%, 0-25%, 0-30% are respectively 3090, 680, 260, 190, 90. It's not done to compare this average value for 10% strain with the value obtained with the peelable technology samples

(2420 cycles). The meander design is different, the periodicity, the track spacing and number of meanders per track. It was expected that the lifetime would be better because a H30 design has less plastic strain deformation than a H45 design. Furthermore, the different tracks will affect each other less due to the higher track spacing. We cannot compare the technologies, but it is expected that for a same design, the lifetime will be in the same range. The failure mechanisms will be the same, only the way of production is different.

In Figure 6.18, the results are shown of the cyclic endurance tests performed on H30 samples made in the double polyimide layer technology as explained in Section 6.5.3.

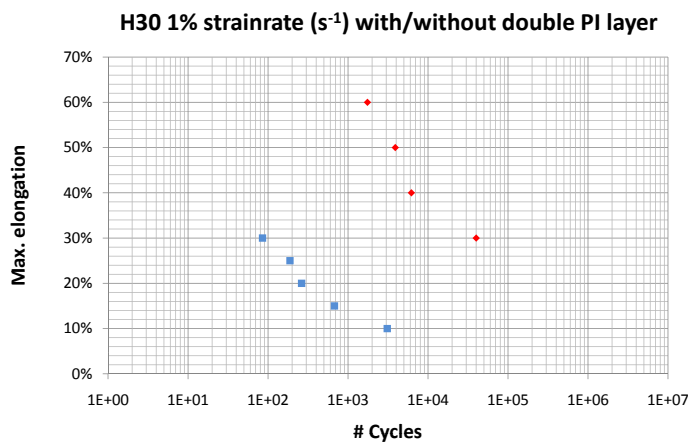


Figure 6.19: Cycles to failure for H30 testsample fabricated in double layer polyimide technology (blue) in comparison with non-supported H30 design (red).

The life test measurements were performed at even higher strains, starting from 30%. This is due to the fact that the lifetime was expected to be very high and it would take too much time to do the tests at lower strains. Again, these tests were performed by Hsu Yung Yu in the frame of his PhD study. The average numbers of cycles for the strains of 0-30%, 0-40%, 0-50%, 0-60% are respectively ~40000, ~6200, ~3900, ~1750. As can be observed, the lifetime has increased almost by a factor ~480 for 30% strain.

6.5 Reliability tests of stretchable interconnects

163

This high increase is a combination of the following factors:

- The supporting polyimide has been developed as support material for flexible electronic applications. The mechanical strength seemed to be higher compared to the photodefinable polyimide HD4100, which is mainly developed for chip passivation applications.
- The polyimide has been defined wider than the copper tracks. In this way, the strain on the copper when the meander opens during stretching, due to the buffer effect of the stiff surrounding polyimide.
- The copper is now on both sides protected by a polyimide layer. In this way, crack propagation on both sides will be prolonged. Furthermore, we have now a symmetrical buildup, the polyimide will act as a buffer for the stresses applied of the PDMS onto the copper.

6.5.5 Failure analysis

Optical microscopy was used to analyze the different types of samples after the tests. In Figure 6.20, a complete failure and a start of a failure of a non-supported copper trace is shown. In all other non-supported test samples, a similar failure mode was found. The copper interconnects break at the top of the meanders, the place where the highest accumulated plastic strain is present [4],[5].



Figure 6.20: Complete breakdown and observed microcracks at top of meanders in pure copper sample after stretching 0-5%. Trace width is 100 μm .

The start of the microcrack as seen in Figure 6.20 is not detected by the resistivity measurements due to the very low increase of the resistivity compared to the precision of the measurement system and its noise. Furthermore, the crack propagates during 1 or just a few cycles, leading to the sudden breakdown. In Figure 6.21, it can be observed that the crack originates at the bottom of the copper foil (Figure 6.21 A), due to its rough surface profile ($6\ \mu\text{m}$ - $8\ \mu\text{m}$). When strained 100 times at 30%, plastic deformation starts and crack is propagating to the surface (Figure 6.21 B). At the surface, it starts to propagate along the cross section of the meanders, leading to the failure (Figure 6.21 C). It seems that the crack propagates through the grains of the electrodeposited TW-YE copper (Figure 6.21 D).

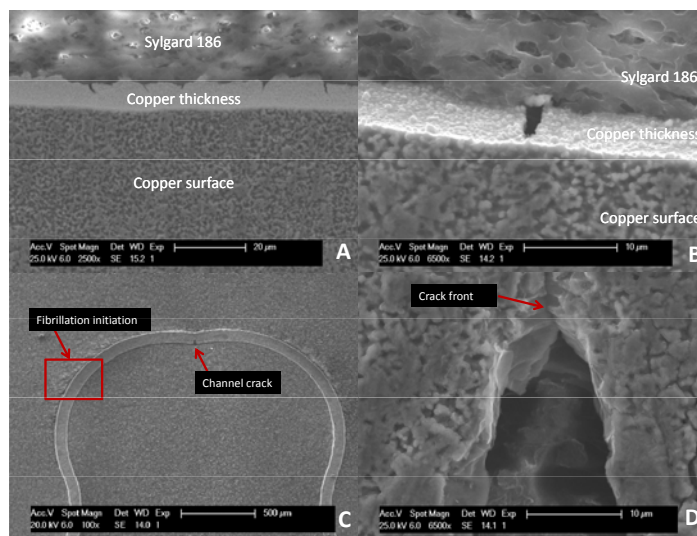


Figure 6.21: (A) Roughness of TW-YE copper ($6\ \mu\text{m}$ - $8\ \mu\text{m}$). (B) Crack growth at rough copper surface after 100 cycles stretching at 30% strain. (C) Crack propagation through cross-section of meander, fibrillation initiation observation at edges of meander. (D) Transgranular fracture through electrodeposited TW-YE copper.

Out-of-plane deformation has also been observed, having a positive effect on the lifetime of the copper meander due to reduced plastic strain. Depending on the stiffness of the embedding material, the plastic strain will be lower/higher if the meander can deform more/less out of plane [5]. But finally, the accumulated plastic strain leads to the observed failure, both for the peelable and the stretchable substrate technology.

In Figure 6.22, we can observe the same failure mechanism for the soldermask covered copper tracks: failure at the top of the meanders, due to fatigue coming from the accumulated plastic strain in the copper and polyimide. As can be ob-

6.5 Reliability tests of stretchable interconnects

165

served in the 3 pictures in Figure 6.23, the soldermask breaks easily and is not able to protect the copper from failure as was also indicated in Figure 6.16.



Figure 6.22: Complete breakdown and observed microcracks at top of meanders in soldermask covered copper interconnects after stretching 0-5%. Trace width is 100 μm .

In Figure 6.23, we can observe the same failure mechanism for the polyimide supported copper tracks: failure at the top of the meanders, due to fatigue coming from the accumulated plastic strain in the copper and polyimide. What we observe in these samples is that much more non-complete copper disruptions are present compared to the pure copper tracks. This clarifies the resistance behavior as shown in Figure 6.13: the delayed crack propagation due to the supporting polyimide can be observed by optical microscopy and the resistivity increase.

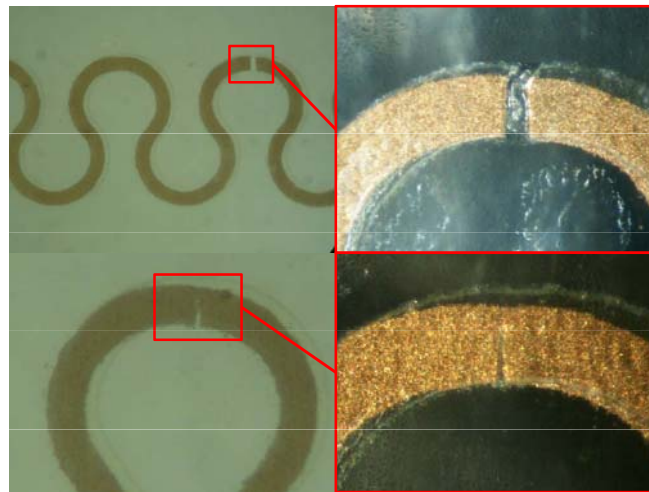


Figure 6.23: Complete breakdown and observed microcracks at top of meanders in photodefinable polyimide supported copper sample after stretching 0-5%. Trace width is 100 μm .

No failure analysis has been performed on the double layer polyimide H30 samples. This will be part of the PhD work of Hsu Yung Yu.

6.5.6 Discussion

In all types of test samples, the observed failure mechanism resembles fatigue. Manson mentions several fatigue regimes in his book on thermal stress and low-cycle fatigue [6]. Low-cycle fatigue occurs below about 10000 cycles and involves mainly plastic deformation. Very high-cycle fatigue with mainly elastic strain is found at low strain levels around and above one million cycles. A transition region is situated in a wide region around ten thousand cycles. Most of the strains ($> 2.5\%$) used in the experiments fall within the low-cycle fatigue region, leading to plastic deformation of the copper, covering soldermask and supporting polyimide. The improved performance of the supported photodefinable polyimide interconnects is due to the fact that the polyimide acts as a stress buffer between the copper and the encapsulant (PDMS). The polyimide is rather stiff (Young's modulus = 6.18 GPa) compared to the copper (Young's modulus = 120 MPa) and withholds the plastic deformation during strain application. Furthermore, it postpones crack propagation through the copper. For the double layer polyimide technology samples, the increased performance is mainly due to 3 factors: the use of a mechanical better polyimide, a wider polyimide acting as a strain buffer and covering both sides resulting to a more symmetrical buffer and crack propagation protection.

6.6 Reliability tests on testvehicle with embedded interposer

The purpose of this testvehicle is to study the effect of having a rigid/flexible interposer mounted in a stretchable substrate and to investigate the mechanical behavior especially at the transition of the rigid and stretchable parts, during uniaxial stretching. A first testvehicle has been made in the peelable technology. Also an improved version of this testvehicle has been designed and fabricated, in order to cope with the failure modes occurring during uniaxial stretching. Different compared to the previous section we first discuss the design, reliability tests and failure analysis of the first design. Then we will present the improved design including reliability test results and failure analysis.

6.6.1 Peelable technology: interposer testvehicle, 18 μm TW-YE copper

Samples were made by use of 18 μm TW-YE copper foil (Circuitfoil) and Sylgard 186 (Dow Corning) as embedding material. The sample consists of parallel meander tracks connected to a rigid interposer in the middle of the sample. Such a sample has been made by use of the peelable technology. By use of SAC solder-

6.6 Reliability tests on testvehicle with embedded interposer

paste, the interposer is mounted in the middle and special designed flex connectors are added to be able to measure the resistivity. In Figure 6.24, the design is shown where in Table 6.2, the dimensions are depicted.

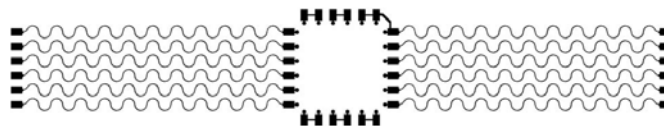


Figure 6.24: Design of copper mask used for embedded meander tracks with interposer testvehicle. Trackwidth= 100 μm.

Parameter	Value
Meander shape	H0
Length of meander line	2 x 32 mm
Meander pitch	1.8 mm
Copper thickness	18 μm
Width of tracks	100 (μm)
Meander period	3 mm
Amplitude	0.75 mm
Contact pads size	1.4 x 0.9 mm ²

Table 6.2: Characteristic dimensions of testsample.

In Figure 6.25, a realization is shown where the embedding has been done in a 2 step casting process by applying a 0.5 mm layer of Sylgard 186 on top and on the backside.

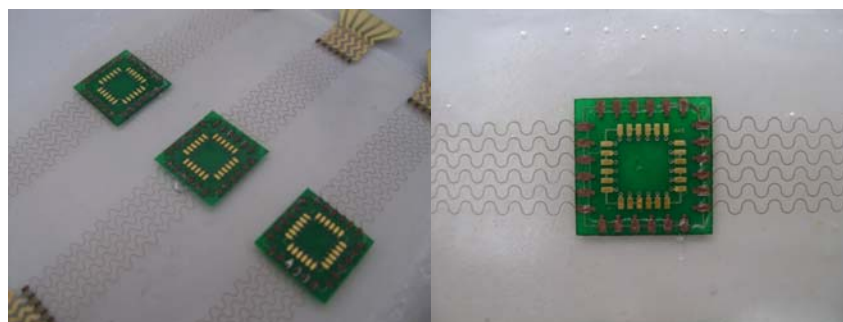


Figure 6.25: Embedded meander tracks with interposer: realization in peelable technology.

Cyclic endurance test results

First of all, the elongation till break has been determined for this testvehicle in order to determine the limits to perform the cyclic endurance tests. The average maximum elongation before break is around 60%. The strain profile used to determine this was stretching upto 20%, back to 0%, upto 40 %, back to 0%,.. in steps of 20%.

Cyclic endurance tests have been performed for a total elongation of 10% and at $1\% \text{ s}^{-1}$ strainrate. The samples only survived in average 400 cycles before the first failure occurred.

Failure analysis

After cyclic stretching, failures can be observed at the transition where the rigid interposer starts. Close to but not under the interposer many tracks were broken. Also, accros the meanders, failures are observed at the top of the meanders due to a high level of plastic strain (see Section 6.5.5). In Figure 6.26, these failures are shown. By means of observing the motion pictures in a couple of cases the order in which the failure modes occurred could be determined: most of the times the track broke loose from the solder pad first, then the traces close to the interposer failed, and finally the traces cracked elsewhere in the substrate.



Figure 6.26: Observed failures after cyclic stretching.

6.6.2 Peelable technology: improved interposer testvehicle, 18 μm TW-YE copper with photodefinable polyimide

In order to cope with the phenomenoms we've just observed, we adjusted the design in order to achieve a better reliability, especially at the interface between interposer and stretchable interconnections. The improved design was used in

6.6 Reliability tests on testvehicle with embedded interposer

169

Chapter 5 to demonstrate the feasibility of the technology and is shown once more in Figure 6.27.

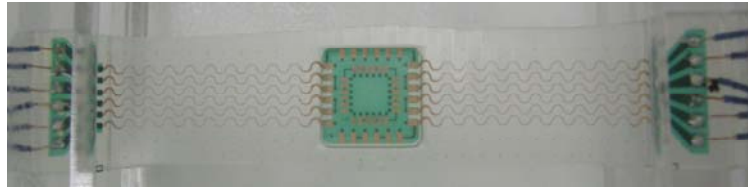


Figure 6.27: Improved interposer testvehicle.

The main improvements compared to the non-polyimide supported one are:

- the rigid interposer has been replaced by an integrated flexible interposer.
- rounded shaping of the polyimide of the flexible islands, to exclude sharp edges at the border.
- shaping of the polyimide of the flexible islands to form fingerlike structures at the connection with the stretchable parts in order to allow them to move separately in the 3 dimensions, especially out-of-plane.
- shaping of the polyimide at the interface between flex and stretch by tapering the polyimide from a wider track at the interposer to go fluently in a thinner track towards the metallic interconnection.
- shaping the copper at the interface between flex and stretch by tapering the copper from a wider track at the interposer to go fluently in a thinner track towards the metallic interconnection.
- use of moulding instead of casting in order to get smooth, fileted transitions between the thicker silicone parts and thinner silicone parts.

In Figure 6.28, the improvements compared to the previous design are illustrated. In the left pictures, it can be seen that the separate processed connectors are now implemented in the testvehicle by use of the supporting polyimide. Furthermore, the left pictures show the integration of the interposer itself and the moulding performed in order to obtain smooth, local stress reducing transitions.

Mechanical simulations have been done in order to compare the new situation with the previous situation.

Out of the simulations, it can be observed that the transition zone (critical region) is less deformed than the central region, where the maximum elongation is expected. Figure 6.29 depicts the maximum plastic strain after 20% effective

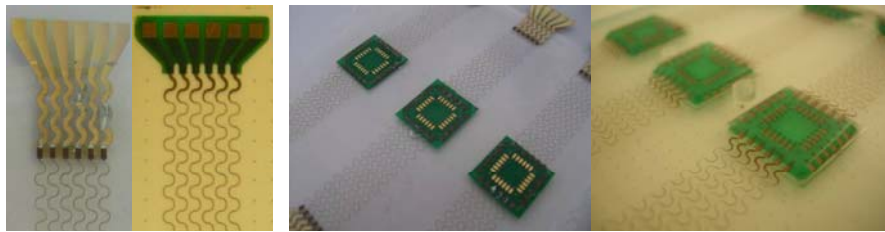


Figure 6.28: Comparison between pure peelable design and peelable with polyimide support: integration of connectors, integration of interposer and moulding.

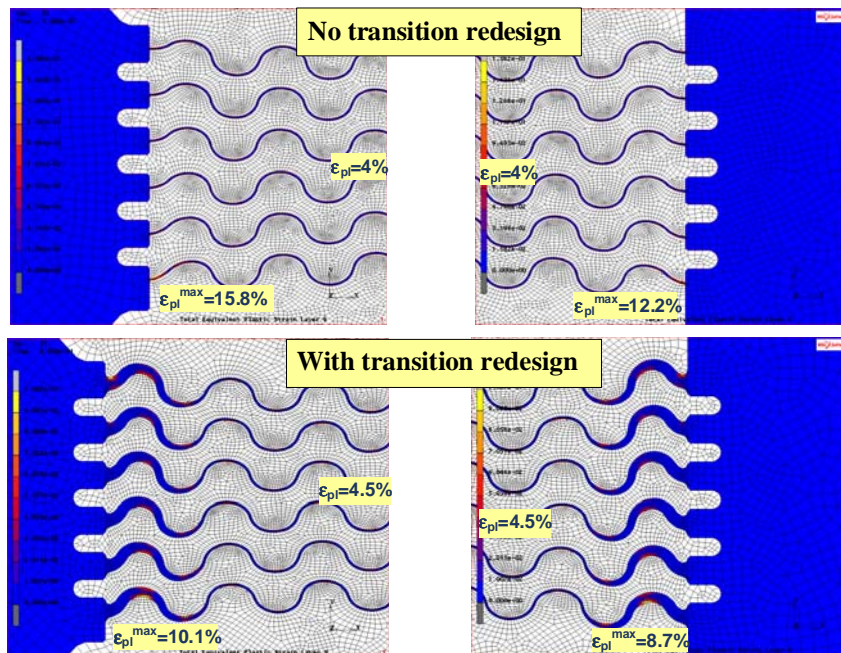


Figure 6.29: Modeling of interposer testvehicle before and after design optimization.

elongation. A clear reduction in the plastic strain is observed when the transition zone is reinforced with PI and the meander width is redesigned. Moreover, if a crack is initiated in the region where the copper is wider, then the final failure will take longer than the case of narrow copper tracks.

Cyclic endurance test results

In the same way as the non-polyimide enhanced sample, cyclic endurance tests have been performed for a total elongation of 10% and at 1%/sec strainrate. We observed an increase of the lifetime upto 2500 cycles. An increase of almost a factor 5 compared to the non-optimized samples.

Failure analysis

Again, due to plastic deformation in the copper, cracks originate from the bottom of the rough interface and propagate through the cross-section of the copper tracks. The places where the failures occur within the sample, are situated at the top of the meanders, base of the flexible interposer, thin and wide buckle at the flexible interposer. These positions are indicated in Figure 6.30.

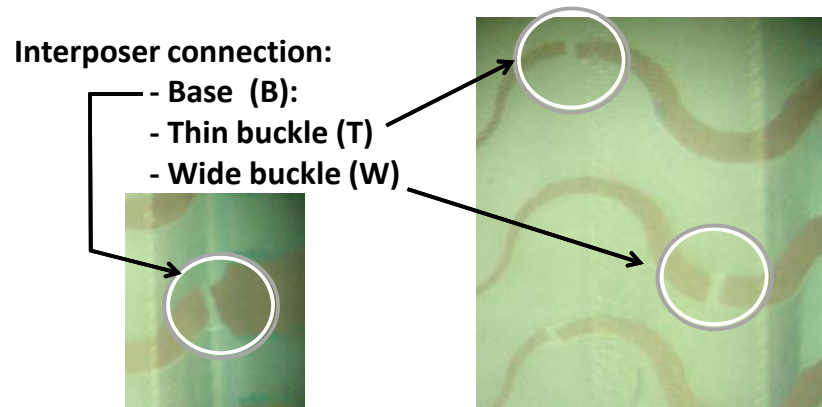


Figure 6.30: Failure modes at flex-stretch transition.

There was a random occurrence of these failure modes. It can not be said that the first failure occurs at the meanders or at the flex-stretch transition. We can conclude that we have optimized the whole design as such, but we don't have control yet to make sure the failure happens on the meanders site and not at the flex-stretch transition. More work is needed to improve the reliability of these transitions. This will be covered in follow-up PhDs.

6.7 Conclusions

We have given an overview of the status of the existing reliability tests in order to quantify the performance of a product during the research and development

phase. The technologies presented in this PhD work were subjected to cyclic endurance tests in the 0-20% strain range. The performance of 2 types of test-samples have been studied: designs containing only parallel meander tracks and designs containing parallel meander tracks and an interposer.

The resistivity behaviour of the parallel tracks during cyclic elongation has been observed, showing no significant increase during the lifetime of the track. The failure mode of the copper is due to accumulated plastic strain, leading to crack magnification at the rough side of the copper tracks, followed by a cross sectional crack propagation.

Copper, PDMS embedded meander tracks having a particular meander design, can be stretched upto more than a million cycles for 0-2.5% elongation. For higher strains, 0-5%, 0-10% and 0-20% the average number of cycles is around 17900, 2420 and 200 respectively.

No difference has been observed in the lifetime of the interconnects subjected to a strainrate of 1% (s^{-1}) and 10% (s^{-1}). Using a layer of 25 μm soldermask as coverlayer doesn't affect the lifetime. A layer of photodefinable polyimide HD4100 increases the lifetime by a factor $\sim 2-3.6$, depending on the applied strain. This due to the buffer effect of the stiff polyimide support and the crack propagation delay.

A huge increase in the lifetime has been observed by using the double layer polyimide technology (upto 480 times for 30% strain), due to 3 factors: the use of a mechanical better polyimide, a wider polyimide acting as a strain buffer and covering both sides resulting to a more symmetrical buffer and crack propagation protection.

Embedding of an interposer connected with the stretchable interconnects, leads to failures at the rigid-stretch transition. An improved version of this testvehicle has been proposed using photodefinable polyimide support. Mechanical simulation and experimental analysis have demonstrated the improved mechanical performance. This mainly due to the replacement of the rigid by a flexible interposer, optimizing the shape of the functional island and adjusting the mould design, an increase in lifetime from 400 upto 2500 cycles could be obtained for 10% strain. The failure modes occurred in a random way at different places, not only limited to the flex-stretch transition zone.

References

- [1] MIL-STD-721C. Military Standard, Definitions of Terms for Reliability and Maintainability.
- [2] INSTRON 5543. Reference Manual - Equipment.
- [3] UBE America Inc. Technical datasheet - Polyimide Base Copper Clad Laminate (Adhesiveless).
- [4] M. Gonzalez, F. Axisa, F. Bossuyt, Y. Hsu, B. Vandeveldel, J. Vanfleteren. Design and performance of metal conductors for stretchable electronic circuits. *Circuit World*, 35(1):22–29, 2009.
- [5] M. Gonzalez, F. Axisa, F. Bossuyt, Y. Hsu, B. Vandeveldel, J. Vanfleteren. Design and performance of metal conductors for stretchable electronic circuits. In *2008 2nd Electronics Systemintegration Technology Conference*, number vol.2, pages 371–6, 2008 2008.
- [6] S.S. Manson. *Thermal stress and low-cycle fatigue. Introduction*. McGraw-Hill, New York, 1966.

Chapter 7

Applications

In the previous chapters, we discussed several technologies to realize elastic microsystems. To prove the feasibility of the proposed technologies, we conclude this PhD study with an overview of realized, functional technology demonstrators.

7.1 Introduction

We will present here a whole range of demonstrators mainly for wearable applications, where conformability is a major improvement compared to the rigid version of the same device. There is a growing need, or at least a desire, to monitor human body functions during longer periods of time, not only while visiting a physician or therapist. This asks for sensors that can be placed close to or even on the skin, being able to communicate with a wireless node.

For this application area, we have developed a number of demonstrators including a stretchable temperature sensor, a stretchable heater, a stretchable respiration monitor and a fitness activity monitor. In order that these applications can function, power management and wireless communication are important aspects. We will cover these two aspects by demonstrating a wireless power circuit and stretchable high-frequency interconnects and antennas.

These are only a few applications the technologies could fit for, there are many many more..

7.2 Stretchable substrate technology demonstrators

7.2.1 Technology analysis samples

In this technology, we have mainly made test samples including parallel meander tracks for reliability testing, failure mode effect analysis,.. to study the behaviour of embedded stretchable tracks under strain. This because this technology is very suitable to make in a fast and reliable way such samples, due to its straightforward process. The mechanical behavior study in the publications [1], [2], [3] are all based on samples made in this technology.

7.2.2 Stretchable multi-electrode arrays

Very recently, a number of samples were made for use as a multi-electrode array for cell culturing, this in the frame of the PhD of Rik Verplancke. The study of the effect of stimulating cells with these kind of stretchable substrates including stretchable copper tracks is still in a development phase, we can already present here a few pictures of a realized cell cultivating device. In Figure 7.1, a view is given on the device. The stretchable substrate made of Sylgard 186 contains 8 stretchable interconnects starting with a contact pad and ending in an electrode. The interconnects are fully embedded, the contact pads and electrodes are made open by use of laser ablation. In this way, cells can be stimulated and wires can be soldered on the contact pads to drive the system.



Figure 7.1: Stretchable multi electrode array cell cultivating device.

The substrate is mounted on a pressure driven device consisting of 2 concentric rings realizing an uniaxial displacement in the electrode region due to an applied underpressure. The principle is depicted in Figure 7.2. So far, there aren't any measurements done of the functionality. We refer to the PhD of Rik Verplancke for more, elaborate results on this device.



Figure 7.2: Stretchable multi electrode array: uniaxial stretching is realized by creating underpressure in the device.

7.3 Peelable technology demonstrators

7.3.1 Temperature sensor demonstrator

We used a simple electronic design for temperature sensing, adopted in a layout for our stretchable electronic technology. It is based on the work described in [4] but the design has been adopted to this technology. The purpose is to integrate a temperature sensor for medical applications in our stretchable circuit technology. The temperature sensor should be placed on the front of the head of a patient by means of an extensible headband. In this way, the temperature of a patient can be monitored during a longer period of time without intervention of a nurse. The stretchable technology is perfectly suitable for such an application, where comfortness is of major importance. We use a LM92 digital thermometer IC that we will read out with a PC using the I²C protocol. The final design of the temperature sensor circuit includes a SMD LED, resistor, capacitor and a flexible flat connector (FFC). The LED is to show the voltage is applied to the IC; the capacitor is used as decoupling capacitor. The design is shown in Figure 7.3, the 4 meander tracks are used for reading out the data by use of the I²C protocol. The tracks are from top to bottom GND (ground), SDA (data signal), SCL (clock signal) and VCC (power).



Figure 7.3: Electronic design of stretchable temperature sensor: copper etch mask.

The different process steps are depicted in Figure 7.4 upto Figure 7.8. 18 μm TW-YE copper foil has been used in order to form the 100 μm wide meander copper tracks (Figure 7.4).

Soldermask has been defined in order to control the flow of the solder during vapour phase reflow soldering and in order to keep the copper meander tracks

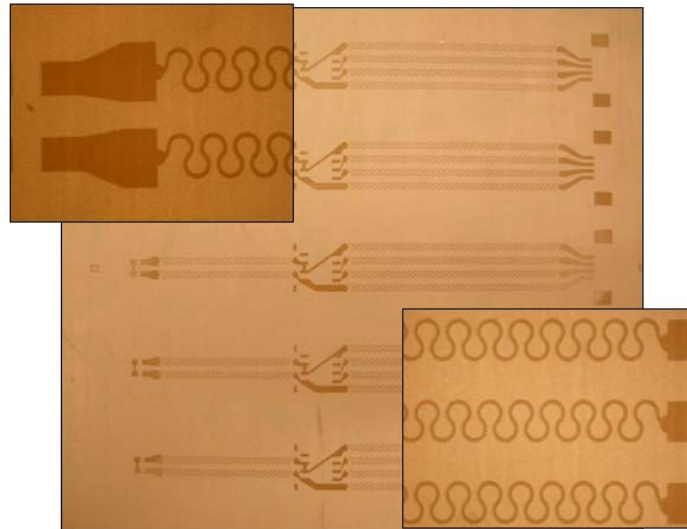


Figure 7.4: Production of stretchable temperature sensor: photodefined pattern on copper-wax-rigid carrier stack.

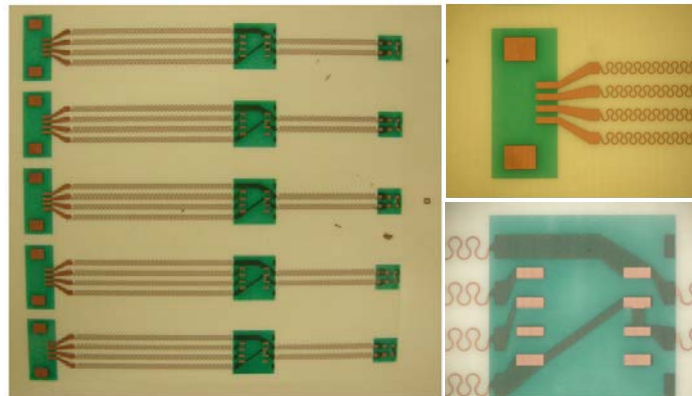


Figure 7.5: Production of stretchable temperature sensor: etched pattern on copper-wax-flexible carrier stack after soldermask application.

in place during vapour phase reflow soldering (Figure 7.5).

The mentioned components have successfully been soldered as can be seen in Figure 7.6. No flowing of the tracks or bad interconnections have been observed. Tombstoning of some components has been observed due to the manual, unbalanced application of the solderpaste.

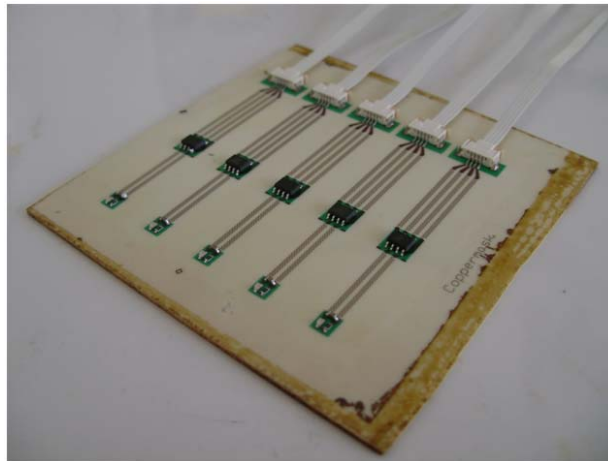


Figure 7.6: Production of stretchable temperature sensor: substrate after vapour phase soldering of components.

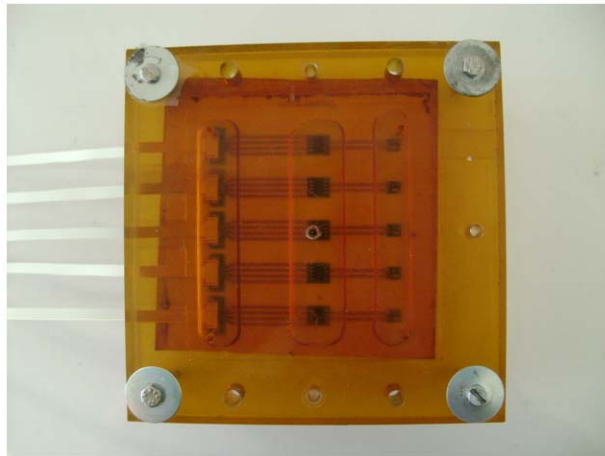


Figure 7.7: Production of stretchable temperature sensor: substrate placed in mold just before injection of Sylgard 186.

An adjusted mould design has been made in order to foresee the components with a thicker layer of Sylgard 186 (in order to limit the stretching here) compared to the stretchable meander parts. The mould has been made in ULTEM and fabricated by mechanical milling.

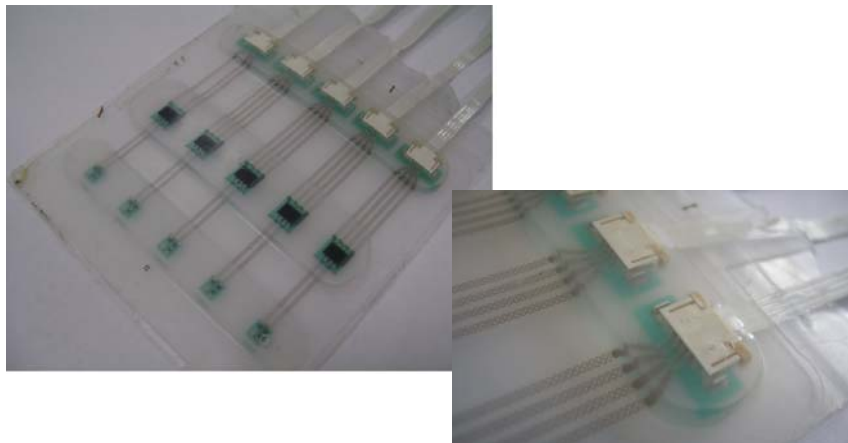


Figure 7.8: Production of stretchable temperature sensor: (Left) Completely embedded in Sylgard 186. (Right) Components are molded with a locally thicker layer of silicone in order to limit the stretching (components) and having a higher stretching in thinner silicone parts (stretchable interconnects).

In Figure 7.8, the result can be seen of a stretchable temperature sensor and in Figure 7.9, the application of the sensor in a textile on the forehead of a student can be seen.

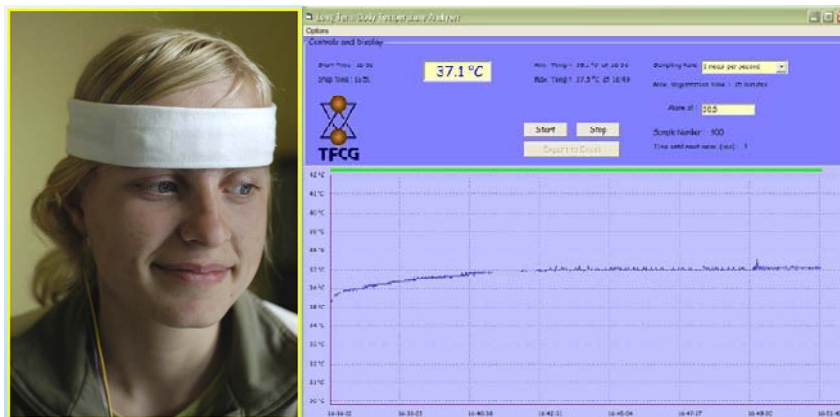


Figure 7.9: (Left) Stretchable temperature sensor implemented in a headband. (Right) Measurements of the body temperature demonstrating the functionality of the device.

7.3.2 Wireless power circuit

The purpose of this demonstrator is to show the feasibility of making a wireless charged electronic circuit. The degree of water resistance of such a fully, encapsulated circuit has been tested by water emersion tests. In this demonstrator, the power is wireless captured by an inductive coil. The used copper with a thickness of $70\ \mu\text{m}$ was selected due to resonance reasons: the silicone is a lossy substrate. This implies that it is difficult to have high quality factor coils unless using thicker lines. The demonstrator consists of an inductive power supply unit with a power conversion/regulation module and a LED. An external coil with its driver was used to generate a magnetic field inducing a current in the secondary tank. By modulating the carrier, data can be sent through the link together with the energy. In this case data were used to drive the blinking LED. The driving principle is shown in Figure 7.10. The design of the electronic circuit was done by MICAS-/ESAT KUL [5].

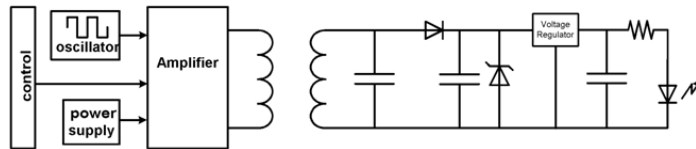


Figure 7.10: Driving scheme for wireless powering inductive coil.

In Figure 7.11(left), the electronic circuit is shown, built on a layer of wax on a flexible substrate, ready to be molded. In Figure 7.11(right), the electronic circuit is shown after embedding it in Sylgard 186 (Dow Corning). Figure 7.12 shows the feasibility of wireless transmitting power to feed the embedded LED, emersed in water. Such kind of circuit shows the possibility of embedding electronic circuits in textiles and feeding them wirelessly being to a certain degree waterproof.

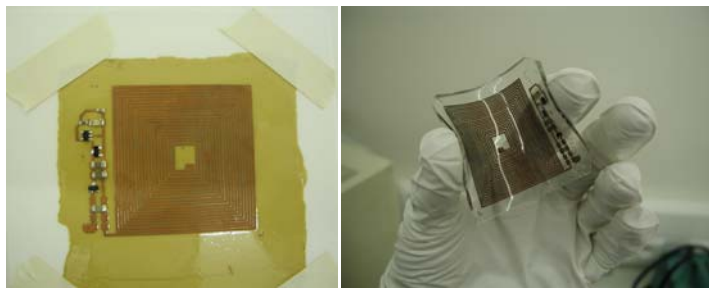


Figure 7.11: (Left) Realization of inductive link by use of $70\ \mu\text{m}$ copper before embedding. (Right) Same circuit after embedding in Sylgard 186.

Waterproof tests have been performed: only after one month of fully functional operation submerged in tap water, an increasing number of bubbles between the two silicone layers, copper oxidation and circuit failure were registered (Figure 7.13). A possible explanation could be the diffusion of water between the two layers and the consequent release of gas due to the copper oxidation.

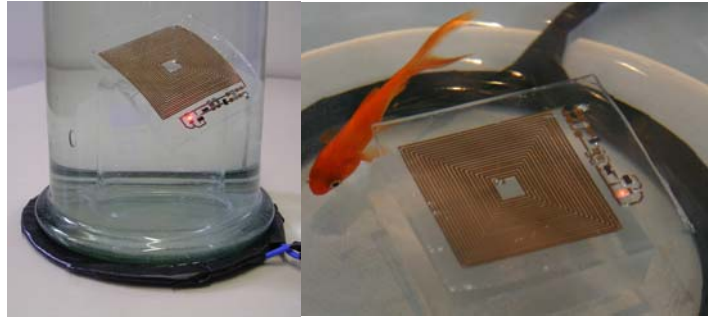


Figure 7.12: Inductive link in water environment.



Figure 7.13: Inductive link after 1 month emersion in water environment: increasing number of bubbles and oxidation of copper.

7.3.3 Stretchable high-frequency interconnects and antennas

The information generated by personal health systems, which monitor life signs such as e.g. heart pulsation, is mostly sent to an access point through a Wireless Body Area Network by using one of the multiple existing protocols operating in the 2.45 GHz ISM band. In the frame of a master thesis [6], stretchable transmission lines and antennas with an impedance-matched feedline were designed, for application in these personal health systems. The scope was to develop high-frequency interconnects, matched to a standard 50Ω impedance in order to serve as a feedline, functioning well under elongations upto approximately 15 to 20%. Several 2-dimensional stretchable antenna designs have been modeled, realized and characterized. In the frame of the thesis, 3 technologies have been used to realize these: a technology based on lasercutting stretchable interconnects out of

R	α	W	G	B
500 μm	30°	200 μm	50 μm	100 μm

Table 7.1: Transmission line horseshoe characteristics.

a polyimide-copper foil [7], the plating technology described in the beginning of Chapter 4 and the peelable technology. Only the results from the peelable technology will be discussed here. 9 μm copper has been used and Silastic MDX4-4210 [8] was chosen for its biocompatible properties as encapsulant.

Simulations and practical considerations have shown that a coplanar waveguide (CPW) topology with narrow reference conductors is to be preferred [6]. The cross-section of such a CPW embedded in silicone is shown in Figure 7.14a and the application for horseshoe structures is depicted in 7.14b.

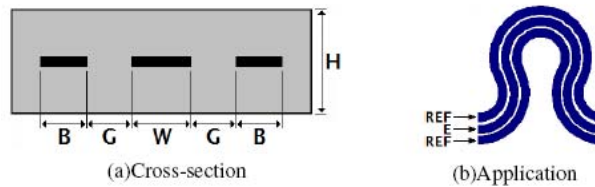


Figure 7.14: Coplanar waveguide with narrow reference conductors.

Based on field simulations with ADS Momentum from Agilent Technologies, the values for the parameters were chosen as listed in Table 7.1. In a lossless simulation, these transmission lines showed a minimal $|S(1, 2)|$ of -0.17 dB up to 10 GHz. This corresponds to 97% of the signal power and a characteristic impedance of 61.25 Ω . The peelable CPW consist of eight horseshoes. This brings the total length measured along the signal path of the peelable CPW 81.9 mm.

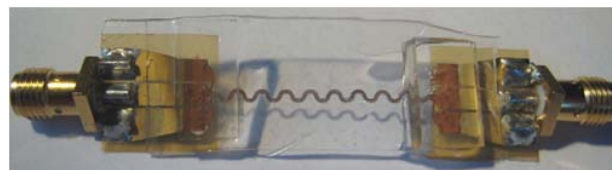


Figure 7.15: Transmission line realized in peelable technology by use of 9 μm copper.

In Figure 7.15, a realization of a transmission line is shown, produced in peelable technology.

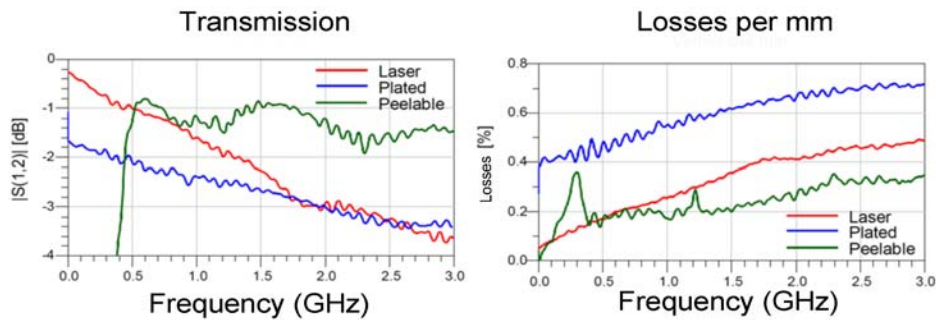


Figure 7.16: Transmission and loss characteristics of transmission lines realized in different technologies including peelable technology.

The measured fractions of insertion loss and transmission losses per mm of CPW are depicted in Figure 7.16. From 500 MHz to 3 GHz, the peelable CPW show a minimal $|S(1, 2)|$ of -2 dB and a maximum power loss of 0.35 % per mm. For the peelable technology, there were some small discontinuities in the conductors observed. However, they do not exclude high frequency transmission. The peelable CPW shows no transmission below 500 MHz, but once the frequency increases, this peelable CPW has the best characteristics compared to other technologies. Also, the influence of the horseshoe angle and size has been studied. It has been observed that these don't have an influence on the transmission characteristics. Losses increase in a linear way with the length of the signalpath.

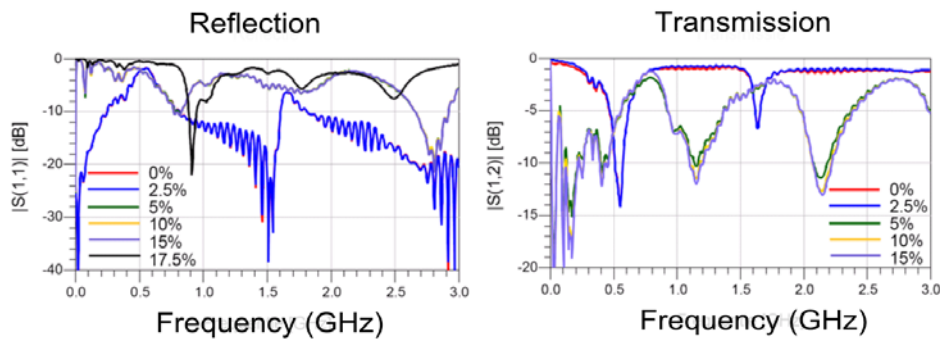


Figure 7.17: Reflection and transmission characteristics of stretched transmission lines realized in peelable technology.

In Figure 7.17, it can be observed that below 2.5% elongation, there is no sig-

nificant change on the transmission properties. Between 5% and 15%, discontinuities are introduced in the signalpath. Starting from 17.5% elongation, there is a permanent break in the transmission line. The peelable CPW has the best characteristics compared to other technologies, but shows reduced transmission once stretched.

In the frame of the same thesis [6], stretchable antennas have also been designed and realized, having following characteristics in mind:

- A coplanar waveguide will be used as feeding structure.
- The design should be stretchable in all directions, this means no solid groundplanes, straight or wide conductors.
- Under strain, the antenna needs to have good transmission characteristics. This means, having a wide bandwidth in order that the radiation characteristic is independent from the applied strain.

An antenna architecture fulfilling the first 2 needs is a slotdipole antenna. The design of a folded dipole antenna and the realization in peelable technology is shown in Figure 7.18. Because stretchability in all directions is needed, fractal patterns instead of meanders have been used.

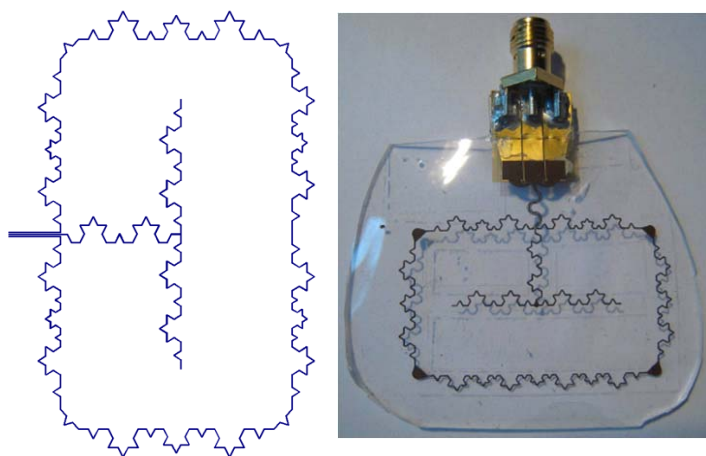


Figure 7.18: Design and realization in peelable technology of a fractal slot dipole antenna.

Such designs have been modeled, realized and characterized. The reflection characteristics are depicted in Figure 7.19.

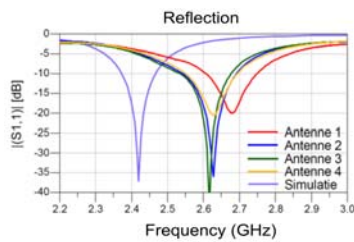


Figure 7.19: Reflection characteristics of realized fractal slot dipole antennas.

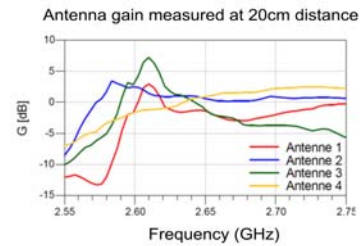


Figure 7.20: Antenna gain at 20 cm distance of realized fractal slot dipole antennas.

Compared to the simulation, there is a shift in the resonance peak observed. The bandwidth of the designed antenna is 145 MHz.

The feasibility of the design of 2 dimensional, stretchable slot dipole antennas has been demonstrated. Single- and double slot dipole antennas with radiation and gain in the 2.45 GHz have been realized. Small adjustments are needed to be able to use the antennas for personal health applications.

7.3.4 Stretchable heater with built-in flexible display

In the frame of another master thesis [9], a stretchable heater has been realized with a uniform heat distribution for use in medical applications (wound healing, skin treatment,..). It is based on the fact that due to resistivity losses, a conductor generates heat when a current flows through it. The heat distribution will be in direct relation to the current distribution. Resistor networks have been designed, simulations were performed in Spice and the results achieved with real prototypes have been compared with these simulations. The dimensioning of the resistor network has been optimized to avoid hot spots. The lay-out of the heater is shown in Figure 7.21. This figure also shows the power distribution: the power generation is almost uniform, only around the LM92 digital temperature sensor (National Semiconductors [10]), the power generation is a lot higher than on the rest of the heater.

This design has been realized in the stretchable technology by use of a thermal conductive silicone Dow Corning 3-1818 [11] as encapsulation material. It has been found that the use of this thermal conductive silicone has a positive effect on the heat distribution. An IR picture of the heater is shown in Figure 7.22. The picture isn't symmetrical, because during the production a short-circuit was introduced in the circuit due to bad etching process, so only the right half of the heater is working correctly. The heater reaches a temperature within an interval between 33°C and 39°C. If the hot spot is not taken into account, the temperature

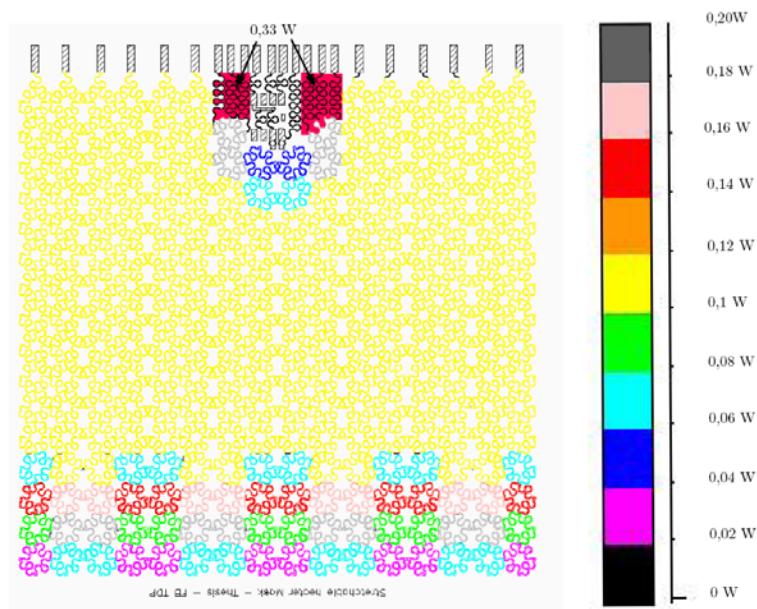


Figure 7.21: Stretchable heater: (Left) Detail of stretchable connections. (Right) Realization by use of Sylgard 184.

interval is between 33°C and 36°C , which is a difference of 3°C . The hot spot takes only 10% of the surface, which means that 90% of the heater is in a temperature range of 3°C . A picture of the realized heater is shown in Figure 7.23.

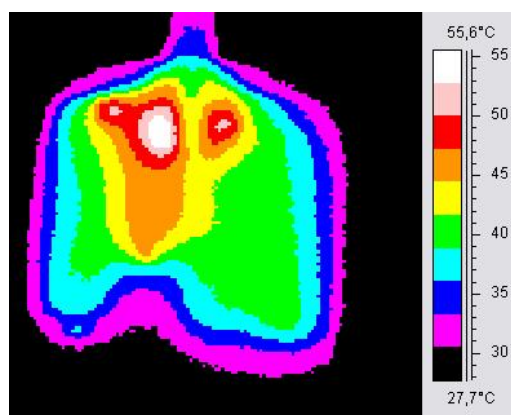


Figure 7.22: IR picture of heater when 3 A is applied.



Figure 7.23: Stretchable heater: detail of stretchable connections.

Also the effect of the heater on the skin was tested, after being heated with the heater. An IR picture of the skin is shown in Figure 7.24 . It shows that the skin, with a normal temperature of 32°C, can be heated to a temperature upto 39°C. The hot spot around the temperature sensor is still visible, but less dominant as the skin distributes the heat and produces as such a more uniform heat distribution.

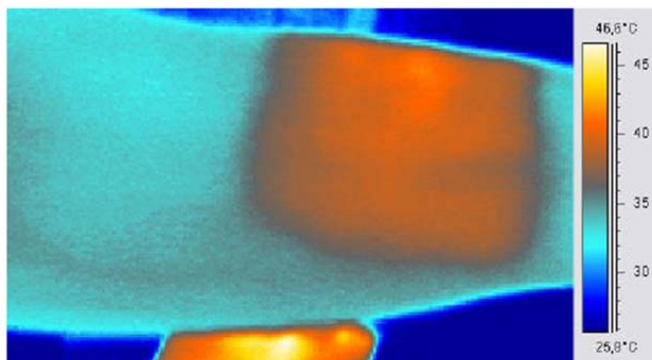


Figure 7.24: Stretchable heater: IR picture of heat distribution when applied to the human skin.

7.4 Peelable technology with local polyimide support demonstrators

7.4.1 Baby respiration monitor

In cooperation with Verhaert in the frame of the STELLA project, a demonstrator for a baby respiration monitor was designed and built with the presented single layer peelable polyimide supported technology. The baby respiration monitor measures elongation by movement of the chest and the abdomen. This elongation is measured by 2 capacitive sensors, the rubbery rulers, done at two locations to enhance the detection reliability of the system. The signals produced by the sensors are read and evaluated by a battery operated measuring unit that operates fully autonomous. This unit contains the necessary electronics to run an algorithm to process the capacitive signal for verification whether there is breathing activity or not. The device is produced in a stretchable format, containing rubbery rulers, embedded in silicone. The encapsulated system is attached on a cloth that can be clipped onto a fitted pyjama. The pyjamas are thus exchangeable and washable, while the electronic system can be removed. The cloth with electronics is self contained and apart from clipping the cloth onto the pyjamas, no other setup is required.

Sensors: Rubbery rulers

2 sensors are used to measure respiration effort at both abdomen and chest. The rubbery ruler (Figure 7.25), developed by the University of Melbourne, has been selected for this purpose. It is a capacitive sensor where the change of capacity is directly related to elongation. The sensor contains a double helix of a conductive wire embedded in a silicone tube. The sensitivity of the used ruler is shown in Table 7.2 and Figure 7.26.



Figure 7.25: Rubbery ruler: capacitive sensor changing capacitance during elongation.

Absolute (mm)	Elongation (mm)	Elongation (%)	Capacity (pF)	Frequency (KHz)
0	70	0.00	136.00	105.04
3	73	4.29	128.80	110.91
6	76	8.57	122.40	116.71
9	79	12.86	117.60	121.47

Table 7.2: Rubbery ruler characteristics.

7.4 Peelable technology with local polyimide support demonstrators 189

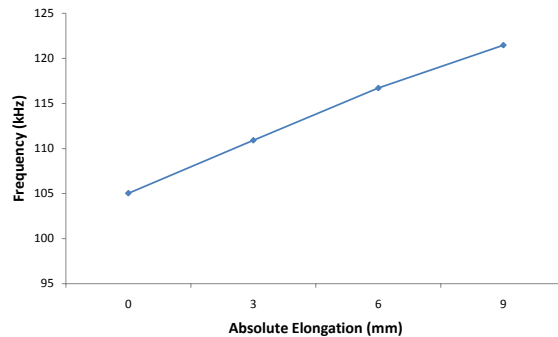


Figure 7.26: Sensitivity of the rubbery ruler sensors.

Signal processing electronics

This block enables the transformation of a change of capacity in the rubbery ruler into a useful signal, by digitizing the analogue signal from the sensors. This is done by providing power to the sensor, providing an oscillation signal to drive the sensor and conditioning the signal of the sensor.

The signal processing is done by use of a microcontroller chip, chosen in order to be low power, highly integrated and small. The MSP430-range covers the performance needs and low power characteristics. This range is also often used in medical applications. For the rigid testboard, a MSP430F149IPM was selected, for the stretchable circuit, the MSP430F149IRTDT is more suitable. After evaluation of the software, a cheaper compatible microcontroller might be chosen if the software requires less memory and processing capabilities to reduce the cost of a high volume consumer product.

The microcontroller implements the following functionalities:

- Read out the 2 sensor interfaces.
- Contains algorithm to process the sensor signals and produce an alarm signal output.
- Manages the user interfaces (leds, buzzer).
- Performs calibration and self-test.
- Permanently checks system integrity (are sensors connected/working).
- In charge of power management to reduce the power consumption to a minimum.
- Monitors battery.

Besides the microcontroller, the circuit still contains the following items:

- 2 Leds are foreseen to indicate the condition of the device. A red LED indicating low battery, alarm and malfunction. An orange LED indicating that the unit is switched on and working in normal operation. These features remain, since it is still a prototype demonstrator and thus a handy tool for detecting faulty situations.
- A buzzer: in case an alarm is generated, the buzzer gives an acoustic feedback.
- JTAG interface connector: for development, evaluation and (re)programming, an interface connector is foreseen. Of course, this connector will not be part of the final product.
- Battery pack with on/off switch: in the prototype demonstrator, the power is supplied by 2 standard non-rechargeable AAA batteries. The external batteries are connected to the circuit with wires. They are part of a battery pack with an on/off switch. This straightforward power supply facilitates measurements on location. After evaluation of the power consumption, a more suitable power supply for the final demonstrator can be selected.
- Protection diode: This to protect the circuit from incorrect connection of the batteries. Optional a LDO can be mounted.

Realization

During the realization, different prototypes have been made with different designs. The final design of the demonstrator has been fixed containing 2 islands of electronic components connected with each other by stretchable interconnections. This design is shown in Figure 7.27, showing the supporting polyimide mask, the copper mask and the soldermask. Pictures of the realization in the peelable technology with local polyimide support are shown in Figure 7.28, 7.29 and 7.30. Trials were done to realize this demonstrator in the peelable technology with no polyimide support, but due to the complexity of the circuit, this didn't worked out. The polyimide is really necessary to prevent tracks from floating and to improve the reliability of the circuit.

Dedicated moulds have been made in order to encapsulate the system. Not only the electronic circuit had to be encapsulated, also the rubbery rulers and the buzzer. This in a way that the system is still stretchable enough in order that the rubbery rulers can function. In Figure 7.31, pictures are shown of the mould design indicating the positions of the rubbery rulers and the buzzer. Outlets are foreseen for the battery pack. In Figure 7.32, the dimensions of the final moulded

7.4 Peelable technology with local polyimide support demonstrators 191

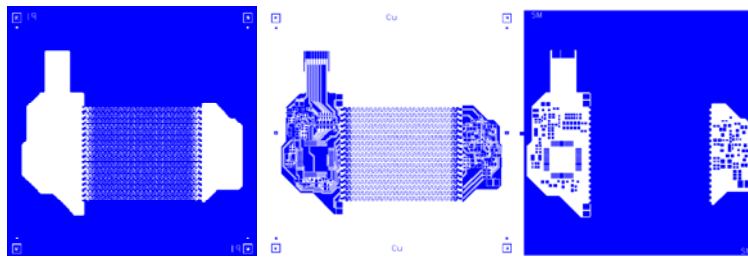


Figure 7.27: Stretchable respiratory monitor production: polyimide mask, copper mask and soldermask.

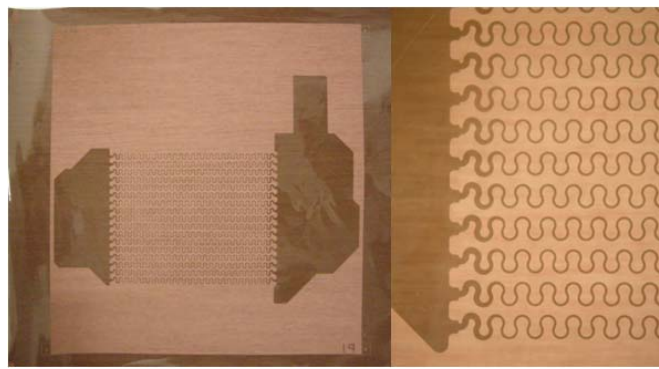


Figure 7.28: Stretchable respiratory monitor production: HD4100 polyimide support defined on copper.

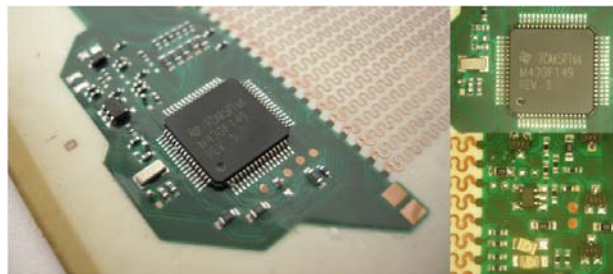


Figure 7.29: Stretchable respiratory monitor production: after vapour phase soldering of components.

device are shown. The thickness of the middle part, where the stretchable interconnections are, has been chosen to be very thin (0.1 mm) in order to not decrease the stretchability of the rubbery rulers.

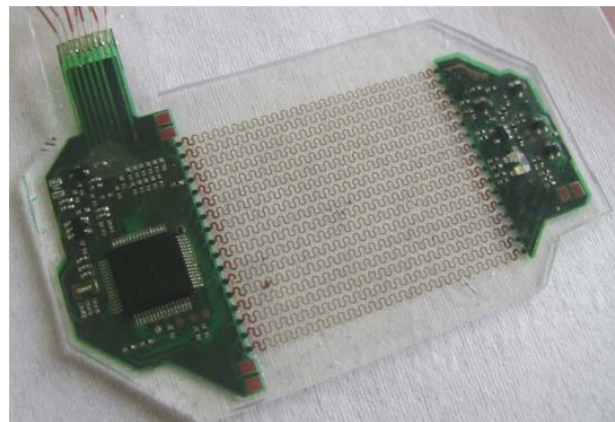


Figure 7.30: Stretchable respiratory monitor production: encapsulated by casting Sylgard 186.

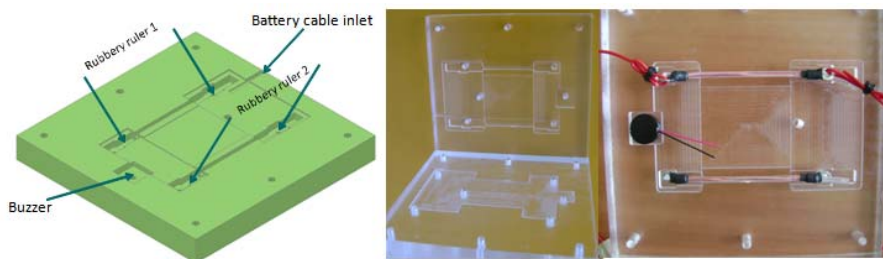


Figure 7.31: Stretchable respiratory monitor production: dedicated moulds used for encapsulation indicating placement of rubbery rulers, buzzer and external connection (battery).

The final moulded device is shown in Figure 7.33. In Figure 7.34, the same device is attached to a textile and implemented in a baby suit.

In Figure 7.35, the mechanical model of the baby is shown used to test the functionality of the demonstrator. The mechanical model mimics breathing activity of a baby, thus stretching the rubbery rulers of the attached baby monitor. Experiments have shown that the system monitors and doesn't give an alarm during normal breathing activity. When the motor of the mechanical is stopped and the breathing stops, the frequency of the indicator LED increases resulting in an alarm by the buzzer after some predefined time. The device is still far from a commercial product but the functionality of the technology and the device has been successfully demonstrated.

7.4 Peelable technology with local polyimide support demonstrators 193

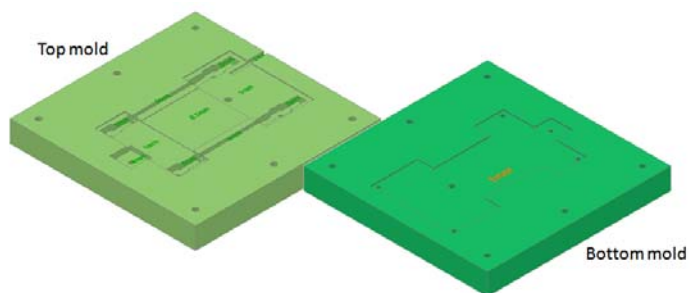


Figure 7.32: Stretchable respiratory monitor production: view on the dimensions of the dedicated moulds.

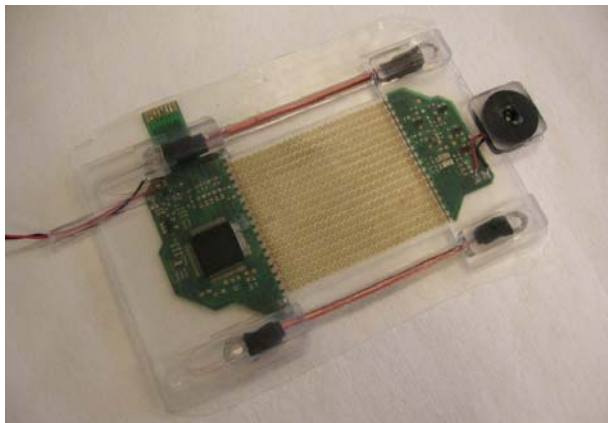


Figure 7.33: Stretchable respiratory monitor production: moulded Verhaert demonstrator using Sylgard 186.



Figure 7.34: Stretchable respiratory monitor production: moulded demonstrator attached to different textiles.

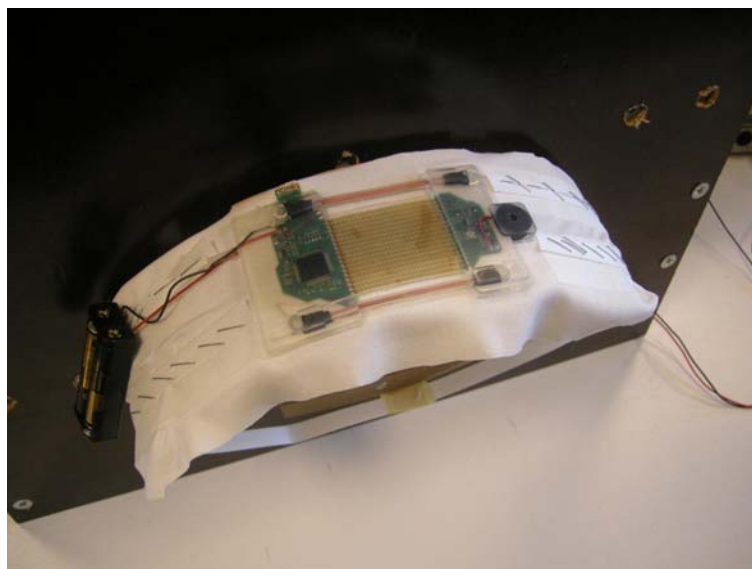


Figure 7.35: Stretchable respiratory monitor: mechanical baby model used for testing functionality of the demonstrator.

Reliability

To have a good idea of the lifetime fatigue stretch of the demonstrator, a special test substrate has been made. This substrate had the same design as the final demonstrator. In this test we mainly focus on the weakest and mechanical most stressed points, the meanders. In order to perform the measurements, a connector is placed on both sides instead of the signal processing electronics. Figure 7.36 shows the lifetime fatigue test setup. The data logger is able to test only 4 channels and we need to test 16 tracks. Therefore a resistor network has been made which gives us the ability to check 4 tracks on one channel. This test will give some reliability figures of the whole demonstrator setup (all meanders) and not from separately tested meanders. Picture 7.37 shows a typical example of the resistance behaviour of the stretchable interconnects during the endurance test. The chosen test parameters are 10% elongation and a strain rate of 1% per second. After ~2000 cycles the first meander is broken. Other broken meanders will follow after some more cycles, being seen in the picture as a sudden resistivity increase in the measurements.

7.4 Peelable technology with local polyimide support demonstrators 195

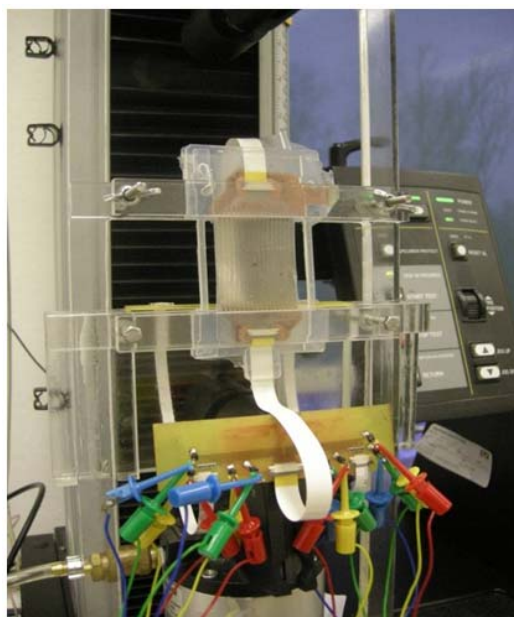


Figure 7.36: Stretchable respiratory monitor: reliability test sample mounted on Instron 5543 for uni-axial testing.

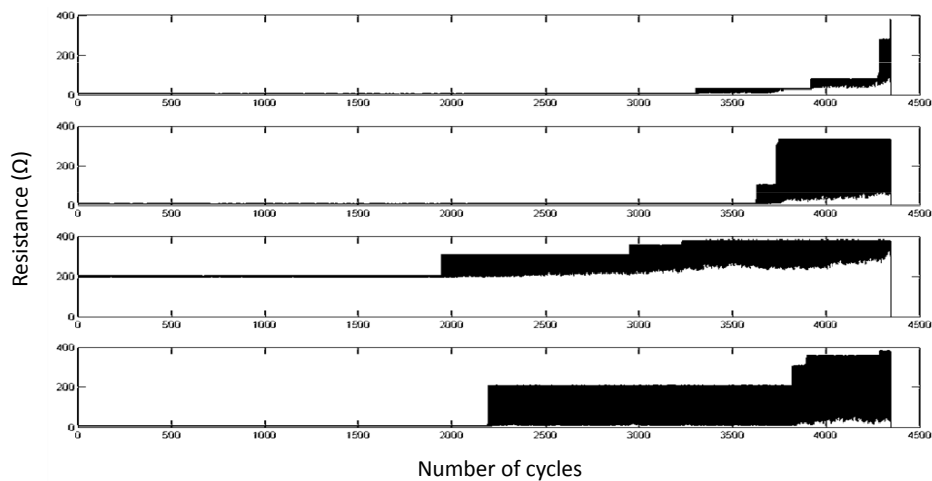


Figure 7.37: Stretchable respiratory monitor: reliability test results.

7.4.2 Fitness activity monitor

Also within the frame of the European Stella project and in cooperation with Philips, a fitness monitor has been developed. The device should be worn on the body during fitness activities. For the demonstrator, its sensor-functions are focused on energy consumption/weight management of the sportsman. For optimal comfort, a compromise has to be made between size and stretchability: a small, low-weight device enhances comfort but means that the substrate surface area is low, resulting in a low effective stretchable area.

The demonstrator includes the following basic functions:

1. Sensor module with two sensors: acceleration (3D) and magnetic field (2D)
2. Processor (Coolflux from NXP)
3. Radio module for wireless data communication
4. Memory (Flash)
5. Power module
6. Power cell (battery)

The partitioning of the system over 5 interposer boards is shown in Figure 7.38 and Figure 7.39.

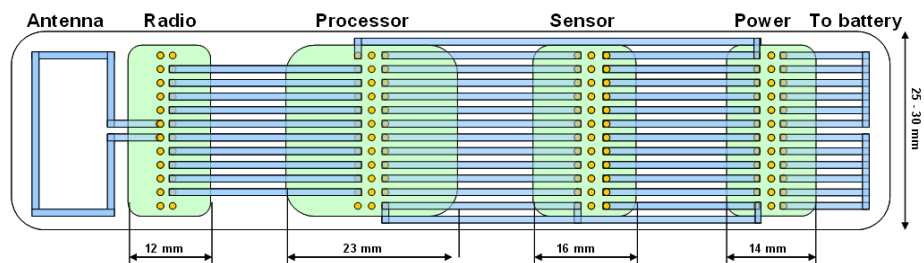


Figure 7.38: Scheme of the Philips Fitness monitor.

7.4 Peelable technology with local polyimide support demonstrators 197

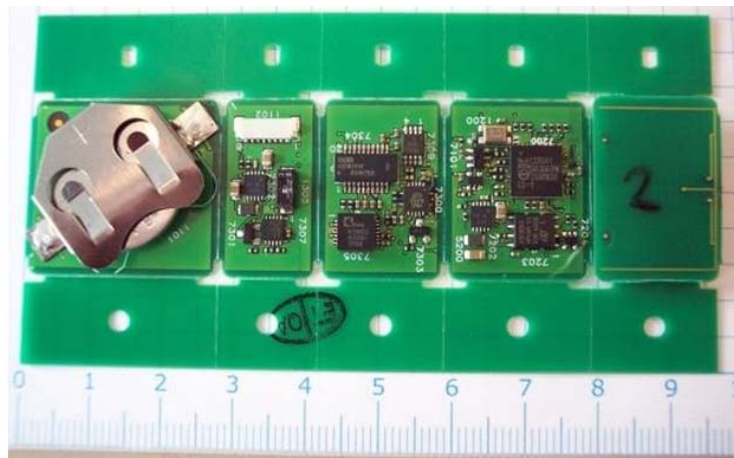


Figure 7.39: Interposer boards used in the Philips Fitness monitor.

Movement sensors

The demonstrator is an example of a wireless body monitor, which is part of a smart wearable system architecture. The wireless activity monitor transmits rough 3-axial acceleration data, which are converted locally in e.g. acceleration graphs or energy consumption. The sensors in the activity monitor are commercially available SMD sensors. As they are soldered on an interposer board, the sensor choice is not related to the stretchable technology. The acceleration is measured in each of the three dimensions in a range of ± 2 g (optional ± 6 g) and with an accuracy of at least 2% (Kionix, KXM52-1050 [12]). The resolution is 1 mG which corresponds to a 13-14 bit data length. This accuracy should be reached for measurements performed at a sampling frequency up to 1 - 1.5 kHz.

The Magnetometer (Honeywell, HMC6052 [13]) has an accuracy of 5% in a range ± 2 gauss and a resolution of 2 mGauss (11 bit). It is used to measure orientation related to the earth magnetic field.

Due to the maximum substrate processing size of 10 cm by 10 cm, an adapted design has been made to show the feasibility of the process by realizing this demonstrator. For the application, the demonstrator should have a straight design in the final version but due to the space restrictions, an U-shape design has been made, fitting on the substrate. The design with the different layers is shown in Figure 7.40. It consists of the polyimide supporting layer, the copper and soldermask layer. The feasibility of the process has first been tested by use of non-functional interposer boards, in order to check the connection between the interposers and the stretchable substrate.

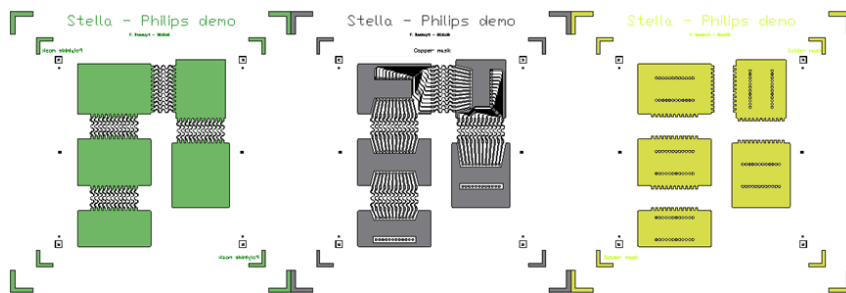


Figure 7.40: Fitness activity monitor: polyimide mask, copper mask and solder mask.

Tests showed that the copper should be well cleaned before soldering. Pictures of the realization of the demonstrator are shown in Figure 7.41, Figure 7.42, Figure 7.43 and Figure 7.45.

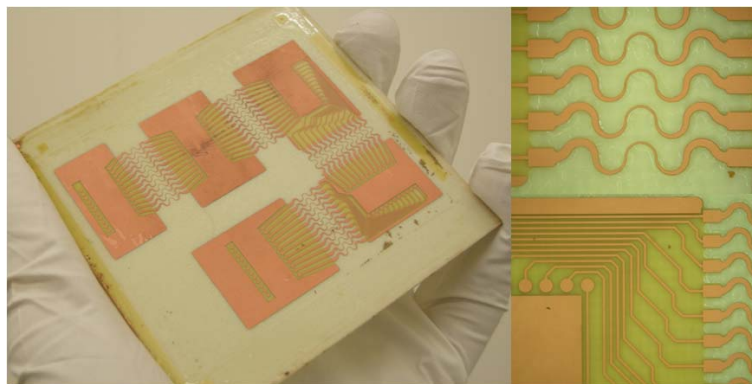


Figure 7.41: Production of fitness activity monitor: after polyimide definition, lamination and copper definition.

The functionality of the system has been demonstrated. Data was wirelessly received giving numbers about the 3 dimensional acceleration and the magnetic field observed. The device is still far from a commercial product but the functionality of the technology and the device has been successfully demonstrated.

7.4 Peelable technology with local polyimide support demonstrators 199

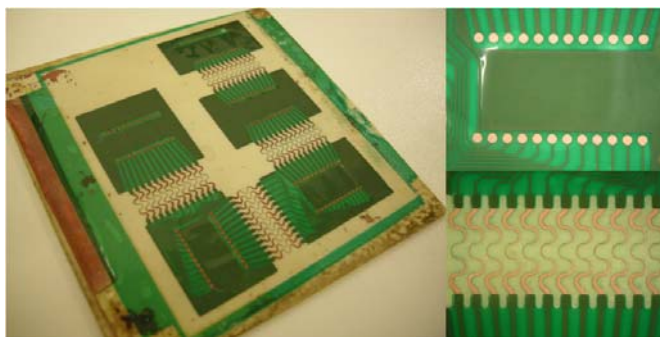


Figure 7.42: Production of fitness activity monitor: after soldermask definition.

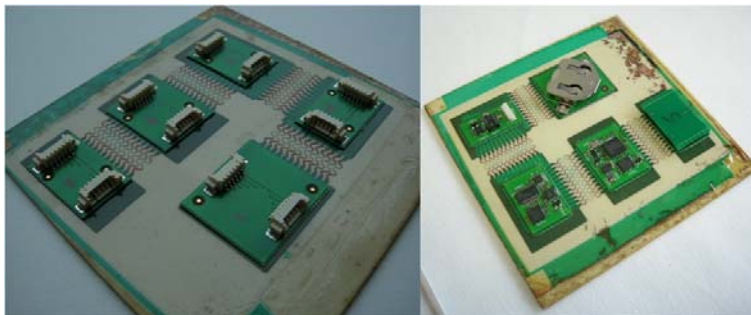


Figure 7.43: Production of fitness activity monitor: after soldering test interposers (left) and functional boards (right).

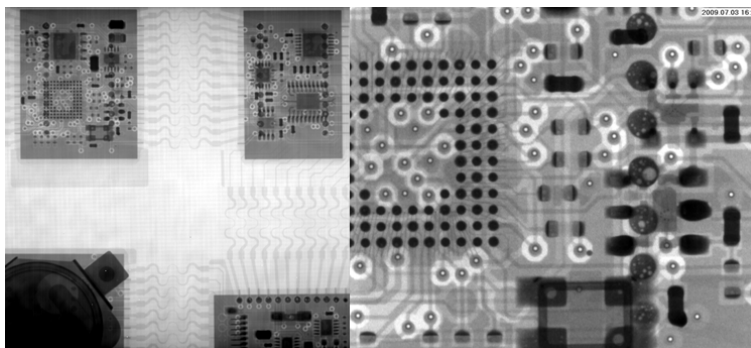


Figure 7.44: Philips activity monitor: X-Ray measurement after vapour phase soldering functional boards. Voids in the solderballs can be observed.



Figure 7.45: Production of fitness activity monitor: after moulding into Sylgard 186.

7.5 Conclusions

Based on the developed technologies covered in this PhD work, we have developed a number of demonstrators for wearable applications including a stretchable temperature sensor, a stretchable heater, a stretchable respiration monitor and a fitness activity monitor. Furthermore, we demonstrated the feasibility of having a fully encapsulated, to a certain degree water resistant, wireless power circuit. Stretchable high-frequency interconnects and antennas for wireless communication have been realized. The first steps in the realization of a stretchable multi-electrode array have been done.

These are only a few applications the technologies could fit for, there are many many more, this is only the beginning..

References

- [1] Y. Hsu, M. Gonzalez, F. Bossuyt, F. Axisa, J. Vanfleteren, I. De Wolf. In situ observations on deformation behavior and stretching-induced failure of fine pitch stretchable interconnect. *Journal of Materials Research*, 24(12):3573–3582, DEC 2009.
- [2] Y. Hsu, M. Gonzalez, F. Bossuyt, F. Axisa, J. Vanfleteren, B. Vandeveld, I. de Wolf. Design and analysis of a novel fine pitch and highly stretchable interconnect. *Microelectronics International*, 27(1):33–38, 2010.
- [3] Y. Hsu, M. Gonzalez, F. Bossuyt, F. Axisa, J. Vanfleteren, I. DeWolf. The effect of pitch on deformation behavior and the stretching-induced failure of a polymer-encapsulated stretchable circuit. *Journal of Micromechanics and Microengineering*, 20(7), JUL 2010.
- [4] I. Backers. Ontwerp en realisatie van een temperatuursensor in geavanceerde uitrekbare integratietechnologie. Master's thesis, Katholieke Hogeschool Brugge-Oostende, 2005-2006.
- [5] MICAS/ESAT KU LEUVEN. <http://www.esat.kuleuven.be/micas/>.
- [6] B. Huyghe. Ontwerp en realisatie van rekbare flexibele hoogfrequent structuren voor personal health toepassingen. Master's thesis, Ghent University, 2006-2007.
- [7] F. Axisa, F. Bossuyt, T. Vervust, J. Vanfleteren. Laser based fast prototyping methodology of producing stretchable and conformable electronic systems. In *2008 2nd Electronics Systemintegration Technology Conference*, number vol.2, pages 1387–90, 2008 2008.
- [8] Dow Corning. Technical datasheet - Silastic MDX4-4210 Biomedical grade elastomer with catalyst.
- [9] T. De Prycker. Elastisch verwarmingselement met ingebouwd flexibel display. Master's thesis, Ghent University, 2006-2007.

- [10] National Semiconductors. Technical datasheet - LM92 digital temperature sensor.
- [11] Dow Corning. Technical datasheet - Dow Corning 3-1818 Thermally Conductive Adhesive.
- [12] Kionix. <http://www.kionix.com>.
- [13] Honeywell. <http://www.honeywell.com>.

Chapter 8

Conclusions and outlook

This chapter presents an overview of the main achievements within this PhD work and a brief look into the opportunities of future work.

8.1 Main achievements

The main objective of this PhD was the development of elastic microsystems technologies for large area applications for use in health care, functional clothes and for integrated electronics in stretchable parts and products. This included the development of a new stretchable substrate with stretchable conductors, assembly technology adapted for stretchable substrates, integration methods for stretchable electronics in elastomeric parts and manufacturing methods for such systems. This based on the use of standard printed circuit board fabrication technologies, in order to make it as close as possible to conventional industry adapted processing techniques.

Different developed technology approaches have been presented, leading to the most suitable technology approach described in Chapter 5. In order to make an electronic circuit stretchable, the system is subdivided in functional islands connected with each other through stretchable interconnections. The stretchable electronic circuit is fabricated on a rigid carrier being attached to it by use of a temporary adhesive. Islands and interconnections are supported by a polyimide layer, copper sheets are used to form the conductive traces and the fabrication method is close to standard PCB fabrication technology. After definition of the circuit, pre-assembly and assembly steps including the mounting of electronic components, the circuit is transferred into a stretchable polymer. This by means of a 2-step injection moulding process by use of a dedicated mould.

Reliability tests have been performed on the stretchable interconnects made by different fabrication methods and stack buildups (polyimide support, soldermask covering,...). Also, the reliability of the interconnects to an embedded interposer has been tested.

Pure copper, PDMS embedded meander tracks having a particular meander design, can be stretched upto more than a million cycles for 0-2.5% elongation. For higher strains, 0-5%, 0-10% and 0-20% the average number of cycles is around 17900, 2420 and 200 respectively. There is no increase of resistance during cyclic loading, a sudden breakdown is observed after a number of cycles. The effect of strainrate has been studied showing no significant difference between 1 and 10% strainrate (s^{-1}). The effect of having a soldermask layer on the interconnects has been determined, resulting in a non significant improvement of the lifetime. Furthermore, polyimide as supporting layer showed a big increase in lifetime by a factor $\sim 2-3.6$ depending on the total applied strain. The supporting polyimide acts as a buffer between encapsulant and copper, and prevents crack propagation through the copper. For 0-5% strains, the lifetime increases upto ~ 90000 .

For all samples, the observed failure mechanism is fatigue due to accumulated plastic strain at the top of the meanders. The accumulated strain in the copper leads to breakdown but can be prolonged by the use of the polyimide.

A number of cyclic endurance tests have been performed on samples containing stretchable interconnects and a functional island, in order to study the behaviour at the rigid-flex-stretch transition. 2 types of samples have been made, a pure copper and a polyimide enhanced type of sample. The latter showed a lifetime improvement by a factor 3 for cyclic endurance tests for 0-10% elongation.

The development of the technologies has been supported by modeling activities, in order to determine the effect of certain technology steps (addition of polyimide). Pre-knowledge has been used in order to make the first versions of the technologies. Modeling and analytical work has been performed on fabricated samples in the different technologies.

Several sidesteps have been investigated in order to improve or extend the technology. This in order to increase the reliability performance and the functionality that can be implemented in the basic technology. The effect of adding polyimide has been studied, below and above the conductors. The first steps in finding other ways to apply the supporting polyimide were explored. Screenprinting tests of non-photodefinable polyimide have been performed.

We presented an extension of this technology by adding an extra conductor layer, screenprinted silverpaste, reducing the need of zero-ohm resistors in order to realize cross-overs and increasing the possible complexity of such a system.

A huge number of functional demonstrators have been presented, made in the

various technologies: a stretchable temperature sensor, a wireless power circuit, stretchable waveguides, a stretchable heating element, a baby respiratory monitor, a fitness activity monitor,...

8.2 Future work

The technology, as presented in this PhD, had actually no special dedicated application in mind during its development; however in the meantime, many potential applications have become apparent. Since its development, the technology mainly has been used for wearable electronics.

In general one can say that applications for stretchable circuits are situated in those areas where there is need for conformability (on or in the body):

- When the circuit is too large so that a single rigid or flexible component island is uncomfortable and thus the circuit has to be partitioned in smaller parts, interconnected by stretchable interconnects.
- When the desired functionality requires a large area with distributed components, which have to be electrically interconnected. Examples are large area pressure sensor matrices e.g. for robotics or artificial skin, LED display matrices, the implementation of a distant electrode in an ECG monitor, etc.

The research presented, forms the base for a wide variety of further activities, trying to solve remaining problems or extending the technologies and applications:

- Work is going on for medical (up to implantable) and biomedical applications. Therefore, a thin film version based on the same principles (circuit production before embedding) is being developed within the PhD of Rik Verplancke. More dense circuitry, chip embedding and the use of more biocompatible metals like Au, Pt are the main features of this technology.
- Application of the developed technologies to textiles, especially the washability feature of the technologies and the combination with textile elements like e.g. textile antennas and conductive yarns for interconnection is under investigation within different projects (BELSPO-SWEET project, FP7-Place-It project and FP7-PASTA project) and in the PhD of Thomas Vervust.
- Further improvement of the lifetime of the stretchable devices by optimization of the flex-stretch transitions, meander and island support technology is planned. Reliability and washability of these stretchable circuits for daily use still needs to be proven.

- Making certain process steps more cost effective and still more PCB fab compatible (e.g. screenprinting of meander and functional island support instead of spinning and photopatterning).

However, the developed technologies have reached sufficient maturity so that transfer to industry and real applications are under development:

- The developed processes are compatible with industrial PCB fabrication and assembly processes. Contacts with local industry for effectively verifying that certain process sequences can run in an industrial fab are ongoing.
- Evolution from small substrates until now (10 cm x 10 cm) to larger area and replacement of lab type processing to fab type processes: planned purchase and installation of number of machines at CMST facilities capable of handling larger formats (9 inch by 12 inch, exactly a quarter of standard minimal PCB format).